Superconducting Wind Turbine Generators

Pan Yunying, Gu Danzhen
Shanghai University of Electric Power

***Abstract*—Wind energy is well known as a renewable energy because its clean and less polluted characteristic, which is the foundation of development modern wind electricity. To find more efficient wind turbine is the focus of scientists around the world. Compared from conventional wind turbines, superconducting wind turbine generators have advantages at zero resistance, smaller size and lighter weight. Superconducting wind turbine will inevitably become the main trends in this area. This paper intends to introduce the basic concept and principle of superconductivity, and compare form traditional wind turbine to obtain superiority, then to summary three proposed machine concept.While superconductivity have difficulty in modern technology and we also have proposed some challenges in achieving superconducting wind turbine finally.**

***Index Terms*—superconducting, wind turbines, torque, types**

I. INTRODUCTION

A. The background of wind turbine generator

Wind power generation technology originated in Europe, Dan Wheat, Holland, Germany and other countries where have proposed it more than 20 years. The United States, Canada and other countries also focus on wind power in recent years.

With the development of the global economy, the wind power market also develops rapidly. In the past 5 years, the world wind power market annual growth at the rate of 40%. And the cost of wind power decrease increasingly. European Wind Energy Association estimated that until 2020, the cost of wind power generation will decrease to 3cent/KWh.

On the end of 2006, the world wind power installed capacity was 74 WG, while, until 2010, the value have reached 150GW. Global wind power installed capacity in 2020 will reach 12.31 million kilowatts, which will account for the global power generation of 12%. Therefore, wind power will be the mainstream for generation and become mature technology and emerging industries.

Wind power is a clean, renewable energy to generate the electricity. Although its reliability is not very well, wind turbine market has been growing rapidly. While, due to the interference of surrounding residents and low wind speed, the number of the wind power sites development are limited. On the contrary, the off shore wind power has high speeds and low interference. Therefore, it is more competitive. Nowadays, 1000MW wind power is under development.

The key of wind power is the wind turbine generator. Currently, the common used wind turbine generators are Double-Fed Induction Generator (DFIG) and Direct-driven Wind Turbine Generator. DFIG is most common in the market. The generators consist of the motor and the cooling system. The motor is mainly composed by the stator, rotor and bearing system. Stator winding is directly connected to the grid, the rotor windings are connected to the grid through a converter. The frequency, voltage, amplitude and phase of rotor windings' power are adjusted by the inverter according to operational requirements automatically. The unit can achieve constant-frequency generation at different speed to meeting the electricity grid and load requirements. Compared with DFIG, Direct-driven Wind Turbine Generator has no gearbox. It is a generator that direct driven by wind, also known as the wind turbine generator with no gearbox. It uses a multi-pole motor directly connected with the impeller to drive, replacing the traditional parts of the gear box. [1]

The conventional wind turbine generators have some drawbacks such as the low capacity and low economy. There are two methods to improve the wind turbine generator technology, one is improving the capacity, the other is using superconductors. Therefore the scientists put forward an idea about superconducting wind turbine generators to overcome the problems on the conventional wind turbine generators.

B. Superconductor and its superconductivity

Superconductivity is a character of certain substances that are reduced to zero at a certain temperature (generally low temperature). In 1911 Dutch physicist Heike Kamerlingh Onnes found that the mercury will suddenly be a new state when the temperature down to 4.2K and its resistance is too low to measure. He called this new state of mercury as the superconducting state. And later, he found that many other metals also have superconductivity. A substance that occurs at a temperature below a certain temperature is called a superconductor.

The direct current resistivity of the superconductor is suddenly disappeared at a certain low temperature, and is called the zero resistance effect. Conductor had no resistance, current flows through the superconductor has no heat losses, therefore the current can be without resistance in a wire to form a strong current and generating a strong magnetic field. Superconducting materials and superconducting technologies have a broad application prospect. Due to the characteristics of the superconducting, more and more scientists try to applicate it in the turbine in order to improve the efficiency and advantage

of wind power.[2]

C. Merits of superconducting wind turbine generators

The emergence of superconducting technology and its rapid development make the large-scale offshore become possible.

The characteristic of the superconducting wind turbine generators is that the power generation efficiency is high, the volume is small and the lightweight.

The low resistance and even zero resistance of HTS materials can effectively improve the power generation efficiency. In theory, the weight of the high temperature superconducting generators can be decreased to 1 / 2-1 / 3 of the conventional motor with the same capacity, which greatly reduce wind power construction and installation cost when the high power generators placed to high meters. If the size and the weight of the generator is maintained, the capacity of the high-temperature superconducting generator can be increased several times, effectively reduce the cost of wind power generation.[2]The reason is that superconducting wind turbine generators air gap magnetic field intensity is 2 times more than the traditional permanent magnet wind turbine air gap magnetic field intensity. Improving the power density by increasing the magnetic flux density, thus the capacity of wind turbine generators can improve.[3]

Additionally, the superconducting wind turbine generators also have the advantages of low synchronous impedance, low noise, low harmonic content, simple maintenance and so on.

II. SUPERCONDUCTING WIND TURBINE GENERATORS

A. The introduction of superconducting wind turbine

The wind turbines rely on the input of mechanical energy. It is a machine improving gas pressure to guide the gas flow. And it is a driven fluid machine. The working principle of wind turbine is the same as the working principle of the turbine compressor. Because of the low gas flow rate and the pressure has little change, it is unnecessary to consider the changes in the specific volume of gas, so handling the gas as incompressible fluid[3].

High temperature superconducting and its application technology were developing from 1986 which has been a mature technology. Generally speaking, high temperature superconducting generators use high temperature superconducting magnets instead of ordinary copper wire coil as the excitation winding of the generators. Due to the high current carrying capacity of HTS materials (100-200 times as the carrying capacity of the same section of the copper conducting wire). Additionally, HTS wind turbine generators allow cancelling total or part of the magnetic circuit of the generators. The effective work magnetic field of the generators can reach a few T or more which is conducive to design a more compact, smaller generators.

The geometry of superconducting wind turbine generators depend on the comparison of operational magnetic field strength B_r and saturation field strength of the magnet steel in the generator. The generator with B_r lower than the saturation limit is similar to the traditional wind turbines, where the magnetic flux path is shaped by the magnetic teeth in rotor and stator. However, the effect of steel is reduced above the saturation limit and resulting the sever hysteretic losses in the steel. Therefore, when designing the superconducting wind turbine generators operating at field strength above the saturation limit of the steel, it is necessary to remove the steel in the rotor and the stator. For the magnetic field of the stator will rotate synchronously with the superconducting rotor coils, which ideally experience the time of magnetic field is constant and therefore only suffer from DC loss, so the superconducting wind turbine generators is operated as a synchronous machine[4].

B. The structure of superconducting wind turbine generators

The most common topology of a superconducting wind turbine generator is illustrated in Fig.1,which showing a multi-pole rotor based on superconducting race track coils[5].

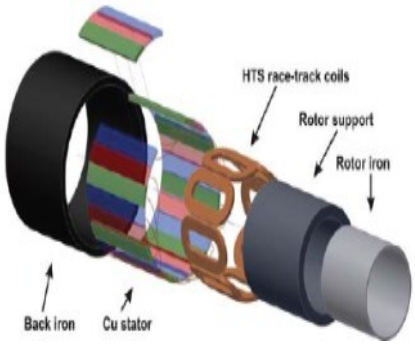

Fig.1 A superconducting multi-pole generator. Reproduced from Courtesy of Converteam.

It is a direct-drive High Temperature Superconducting Wind Turbine Generator system with low speed. The machine consists of the stator back iron, stator copper winding, HTS field coils, rotor core, rotor support structure, rotor cooling system, cryostat and external refrigerator, electromagnetic shield and damper, bearing, shaft and housing. The key of these all components is the arrangement of stator, rotor, cooling and gearbox.

The stator back iron is holding the three phase stator Cu winding. The coils are mounted on the rotor support structure, might holding an inner steel tube to confine the magnetic flux between the rotor and the stator and transfer the torque to the turbine shaft at room temperature.

The rotor generally contains steel laminate, concentrating the magnetic flux to the air gap and a cryostat to maintain the good thermal insulation of the superconducting coils.

C. Design of superconducting wind turbine generators

Conventional wind turbine has resistive windings and the iron cores are highly-multipolar machines. But, in general, the superconducting wind turbine is different. Superconducting machines requires thermal insulation between the very low temperature components and the room-temperature components. Thus, it is inevitable produce a large air gap between the superconducting field coils and air-gap armature windings. And need a pole-pitch larger than the traditional

machines. If the pole pitch is very small, the magnetic field generated by superconducting field magnets can not reach the armature windings sufficiently.

Here introducing a size and design of superconducting wind turbine generator introduced in [2].

Fig. 2 displays a wind turbine generator designed from the Finite Element Method analysis of the magnetic field. The rotor has 12 superconducting field coils generating 12-pole magnetic field. The coils have a simple racetrack shape with a rectangular cross-section. The stator has air-gap armature windings, which are double layer, distributed three-phase windings.

Fig 3 shows the outer and inner diameters of the armature windings which is 4.32 m and 3.84 m and the outer diameter of the superconducting field coil set is about 3.6 m. The racetrack superconducting coil is as large as 1.8 m (length)× 0.8 m (width) and its cross section is 0.18 m × 0.18 m as shown in Fig. 4.

(a) Armature and field coils

Fig.2A wind turbine generator designed from the Finite Element Method Analysis of the Magnetic Field. Reproduced from reference [2]

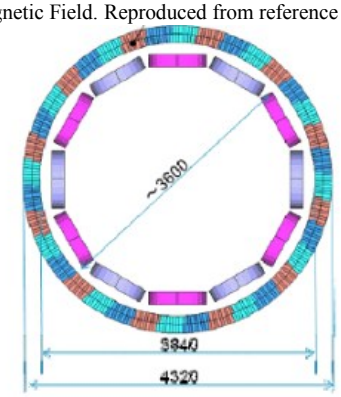

Fig.3 Dimensions of the designed superconducting wind turbine generators. Reproduced from reference [2]

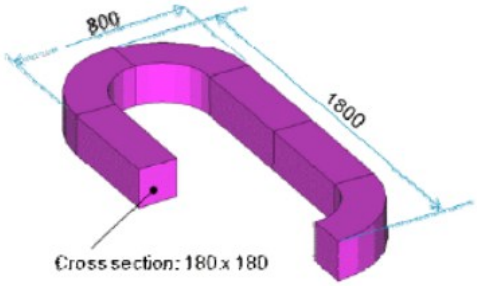

Fig.4 Superconducting racetrack coil for field magnets. Reproduced from reference[2]

D. torque of synchronous superconducting generator

The torque T of the superconducting generators can be determined by integrating the force F acting on each stator wire at air gap radius R, $dT \sim R \times F$ .Moreover, the Lorentz force on each wire $F \sim I_S \times B$ .In addition, assuming the magnetic flux density in the air gap is harmonic,

$$B(\theta) = B_0 \cos(p\theta) \tag{1}$$

B_0 is the peak flux density and p is the pole number. Assuming a harmonic current distribution of the stator in the coordinate system of the rotor,

$$I_S = A_S \cos(p(\theta + \gamma)) \tag{2}$$

γ is the angular displacement of the current distribution relative to the rotor field distribution and A_S is the rms armature loading in the units of [A/m]Therefore, we can get the torque that

$$T \propto B_0 A_S R^2 l \cos(p\gamma) \tag{3}$$

l is the length of the machine.[1]

III. Different Types

A. Wind turbine with superconducting field windings

Recently, the most common superconducting wind turbine generator is the generator with superconducting field winding

Two concepts of superconducting wind turbine generator have been proposed. First is that only field windings are superconducting. Second is that both field windings and armature windings are superconducting. Fig.5 shows the axial-radial cross-section of superconducting synchronous generators, in which the field winding is superconducting and the armature winding is copper. The superconductor is thermal insulated from ambient and cold section is equipped with torque transfer element, which can not only insulate but also transfer the torque from cold area to warm area.[1]

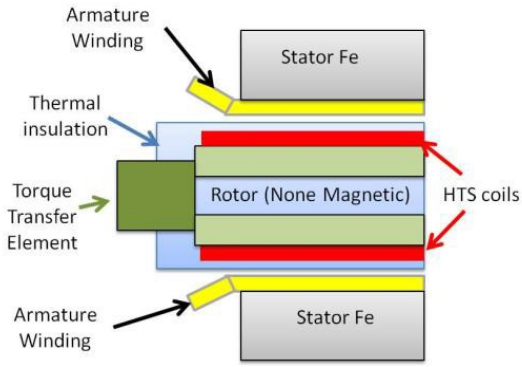

Fig.5 Axial-radial cross section of a superconducting synchronous machine. Reproduced from reference [1]

B. *Fully superconducting wind turbine generators*

Fully superconducting wind turbine generators can be divided into two types. One is using LTS which used widely. The other is using HTS that only little projects use it.[1]. Compared to conventional superconducting wind turbine, the merits of fully superconducting generator is that the air gap flux density and the electric loading is increased.

Moreover, if both armature and field windings operate at the same temperature, the air gap can be much smaller. Because there is no thermal insulation between these two, the whole magnetic design of the machine can be more efficient [1]. However, the biggest problem of this concept is the AC losses that generated in the armature windings. Nowadays, because of the poor cooling efficiency, the amount of AC losses in high field AC application is considered as prohibitive.

C. *High Temperature Superconducting Wind Turbine Generators (HTSWTG)*

In the past, using Low Temperature Superconductors (LTS) to improve the traditional design of electric machines had been tried in many projects. And all these have shown the successful and advantages of superconducting wind turbine generators. However, there are still some challenges such as the cost of the refrigeration system and the temperature control of 2K-4K of LTS.

Nowadays, with the development and discovery of HIT materials, superconducting machines become more competitive from the commercial view. The temperature rang of HTS is 30K-80K which is much higher than LTS. Moreover, a device that using HTS has a wider temperature window, which has profound influences on the refrigeration complexity and efficiency, as shown by Fig.6.By using HTS, the refrigeration system and thermal insulation is more simple and efficiency than using LTS and MgB2.

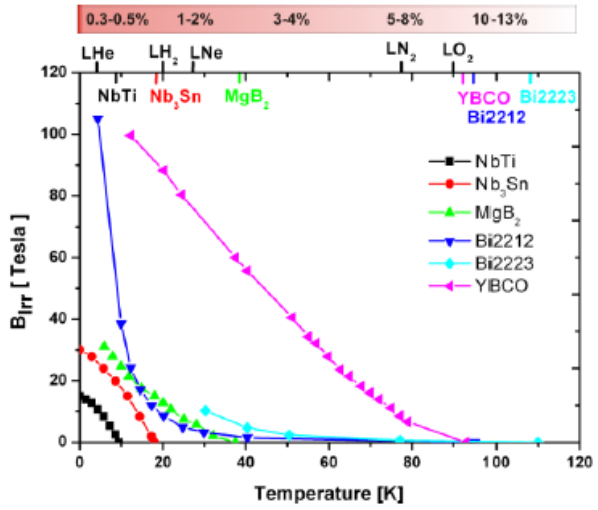

Fig.6 Operation boundaries of different superconductors, where the critical current vanishes. The top bar indicated the typical efficiency of a cryogenic cooling system. Reproduced from[6]and[7]

Actually, superconductors are rarely used in the stator because of the AC losses and it is difficult to build stator winding by HTS coils. Therefore, a radical design of a superconducting arrangement is not realistic. As a result, the HTSWTG is a synchronous generator consists of copper stator and superconductor rotor.

HTS machines can be divided to four different types[8]:

Type1. Conventional stator and HTS rotor with magnetic pole bodies.

Type2. Conventional stator and HTS rotor with non-magnetic pole bodies

Type3. Airgap stator winding and HTS rotor with magnetic pole bodies

Type4. Airgap stator winding and HTS rotor with non-magnetic pole bodies

Different types of the machines have different merits and characteristics. Due to the minimized rotor loss and does not offer substantial reduction in weight and dimension,Type1 has high efficiency. And type 2 can also get high efficiency but it needs more HTS wires to build necessary flux density. Compared with conventional stator,type3 has higher flux density at the airgap which reduce the mass and size of machine. However, the efficiency is reduced due to the rotor iron can operate highly saturated.Type4 allows significant reduction in weight and dimension, and also minimizes potential high cost cold magnetic materials. But it requires more HTS wires in use.

Wind power is a cost sensitive market and the capital cost is important in producing large machines. For offshore wind turbines, saving cost is more important than size reduction. Therefore, the actual compromise is made between the low cost, low mass and high efficiency. For the direct-drive wind turbine generator, types 3 and 4 both can offer the lowest mass. Type 4 may be a more cost-effective module for iron and 2G HTS wires. Converteam use type4 to design an 8MW 12rpm High Temperature Superconducting Wind Turbine Generators.

IV. Produced Wind Turbine Generators

A. *AMSC——Seatitan*

Several machines were constructed in projects led by American Superconductor (AMSC). Currently, AMSC announced intentions to construct a direct drive wind turbine generator under the brand named SeaTitan. Based on the ship propulsion motor technology and superconducting technology of United States Navy projects, the output power of SeaTitan from AMSC can be double than the largest wind turbine generator, up to 10MW.The key to get success is the high temperature superconducting direct drive engine with a diameter of 5m and the weight is 160t.In contrast, the diameter of a permanent magnet direct drive motor that producing the same output will reach 10m and weight is also more than 200t.Moreover,the power density of superconducting wind turbine generators can achieve high power output and high economic.Fig.7 shows 10MW Seatitan offered by AMSC.

Fig.7 10MW Seatitan offered by AMSC. Reproduced from[1]

AMSC also claims that, although the focus is on the 10MW Seatitan system, but it is also feasible to design 20MW wind turbine generator with the high temperature superconducting technology.

B. EcoSwing

Last year, EcoSwing superconducting wind turbine generators produced by Envision and funded 1 billion yuan by EU and its member state. Significantly different from the other superconducting technologies, the power of superconducting wind turbine generator is only 3.6MW. The purpose of EcoSwing is not the large capacity, but to promote the reduction of the cost of wind power.

Compared with the traditional wind turbine generator, the advantage of EcoSwing is that under the same torque, the weight can reduce more than 40% which can reduce the entire cabin weight 25%.And the weight of other materials can reduce in proportion. At the same time, the use of rare earth will be reduced the amount of at least two orders of magnitude. Due to the advantages of EcoSwing in torque density, the economy of wind power generation will be greatly improved by the EcoSwing superconducting wind turbine generator. According to the prospect of global innovation center, the use of EcoSwing superconducting wind turbine technology are expected to decline the wind power cost by at least 30% or more. In order to make the technique applied successfully, EcoSwing project team will carry out comprehensive risk research and evaluation. After the laboratory test for EcoSwing, Envision plans to use it on the large megawatt wind turbine generators in Denmark at least one year and maintain it regularly.

"A lightweight and highly competitive superconducting wind turbine has a very exciting development potential." Anders Rebsdorf, the president of Envision in Denmark global innovation center said that EcoSwing superconducting wind turbine will be an important progress in the way of pursuit of reducing the cost of renewable energy."

Anders Rebsdorf also said that EcoSwing superconducting wind turbine technology can reduce the cost of wind power more than 30%. And Envision hopes to use their own top technology to make the wind and solar power become the mainstream energy of the global.Fig.8 The concept of EcoSwing.[9]

Fig.8 The concept of EcoSwing. Reproduced from [9]

C. SUPRAPOWER

On 20th April 2015, SUPRAPOWER held a workshop about high power electric generators for cost reduction of offshore wind. The workshop included presentations about trends on high power generators and about new developments of superconducting machines. SUPRAPOWER is funded by the European Union (EU) and it is a project that aims to a high power, lightweight and reliable superconducting generator for large offshore wind turbines. The goal is using superconductor to develop the wind power. There are nine industrial and scientific partners participate in this project. The technical physics research of university KIT will build rotating cryostat for this project. By pure heat conduction, the superconducting coil cooled to -253.15 ℃. At this temperature, the superconductor does not appear the resistance phenomenon. Therefore it can realize the lossless conduction. A generator with a superconductor can be increased to 10 MW, reducing the volume and weight as well. In addition, compared to the current wide use of permanent magnet wind turbine, the superconducting wind turbine generators only need less than 1% of the rare earth. Therefore superconductors can make the wind turbine higher, more stable, simpler, saving a great deal of raw materials and reduce the construction, operation and maintenance costs, improving the service life of the turbine.[10]

Other companies also have designed different superconducting generators. However, comparing these enterprises, Sway started earliest. And the advantage of American Superconductor is that they have the core technology. Tecnalia cooperate with KIT to make the product better. Superconducting wind turbine generator is superior than permanent magnet generator. Although Sway started earliest, its development is slow and in wrong direction. American and Tecnalia & KIT have advanced technologies. While, their technologies in wind power still need to explore. Otherwise the design and manufacture of the large-scale wind turbine generator still have some difficulties. The 3.6MW superconducting wind turbine generator produced by Envision is improved by the basis of 3MW wind turbine generator. Therefore, the design and production are easier. Each company has its own preponderance, the key to success is the new technology.

V. CHALLENGES

Superconducting wind turbine generator is only a concept now. The application of superconducting technology in other areas has been realized. But the application in the wind turbine generators is not quite feasible currently. Maybe there will be 5-10 years to produce a prototype or make a major technical breakthrough. For the large-scale commercial production, it is possible require 30-50 years.

A. The materials of HTS wires

The material is the key to manufacture the superconducting wind turbine. Currently, most of use is called first generation (1G) wires. The ceramic superconductor is BSCCO. This kind of wires can bear the rang of the current from 100A to 180A with the cross-section of 4mm*0.3mm.The manufacture process is very complex, therefore the cost is too high for application.

Recently, the second generation (2G) wires are also available. The ceramic superconductor is YBCO. Compared with BSCCO, its price is lower and have more merits.

However these materials still have some problems like the supply and the price. Whether these can be in use widely is the main to consider.[13]

B. The maintenance of superconducting wind turbine generators

There will be high vibration when the superconducting wind turbine generators in operation. And with different wind speeds, the frequency resonant is different. Therefore, the requirement of sealing is very high. The interior of superconducting wind turbine generator is liquid nitrogen refrigeration. Once it leak, it will cause the irreparable fault on other device. On the other hand, thunder and lightning may cause the wires of wind turbine some faults. Once a failure occurs, the maintenance cost is very high because of the high technology used in the superconducting wind turbine generators. Additionally, the general staff may cannot do it for its complexity. It will affect the utilization.

C. Excitation system

The coils have negligible Ohmic resistance. Under normal operation, there will be a high current with a low voltage. However, when ramping the HTS coils, a large excitation voltage is required. The rang of the excitation voltage is 100V or higher to achieve the field current changes within an acceptable periods of time. Therefore, a control scheme using excitation current is required. And the system must be able to operate in merely inductive load. On the other hand, HTS can not disperse the energy stored in the rotor inductance. Thus, the exciter is the key of superconducting wires protection.

Currently, two methods are in use. First is using brushes and slip rings to transfer the current. The other one is that via rotating transfer to achieve brushless excitation. This require a complex control and protection system. The first one is widely used in synchronous generators. However, the maintenance requirement is high and normally hard to tolerate. In addition, the second solution is a complex and high requirement system. Its design is difficult. Although there have been some designed HTS, the utilization is not common.

In conclusion, the excitation system of superconducting wind turbine generators still have a lot to improve and develop. [13]

D. Refrigeration for rotor cooling system

Refrigeration for rotor cooling system is an important part of superconducting power equipment. The refrigeration to cryogenic temperature for HTS is different with conventional wind turbine generator. The temperature of HTS is 30K in normal operation and requiring a few hundred of Watt refrigeration power. Recently, there have been no commercial applications that close to those parameters.

The best fit refrigeration is GM (Gifford-McMahon), which is regenerative refrigeration, generally developed from the cooling thermal shield of LTS MRI system, which reduce the boiloff of fluid Helium. GM used widely and many industrially established technologies provide very attractive price. However, those parameters have been designed and the operation condition is a little rough now. GM refrigerator has several drawbacks:[19]

1) GM refrigerator relies on the rotary valve to control the air flow to the cold head or return to the low pressure side of the compressor. Air flow through the valve will produce pressure head loss. Therefore, the efficiency of GM is relatively low.
2) The compressor of GM pressure is relatively stable and it can use the activated carbon to remove oil. Therefore, using commercial oil-lubricated compressor, which is reliable and having lower cost. But the compressor is large and requiring maintenance annually.
3) In addition, the cooling head includes a moving device, also need to maintain. Currently, refrigeration power of models with the temperature of 25K and 100W is limited. Thus, GMs have to be operated in parallel. The operation of a conventional oil-lubricated compressor depends on the orientation with respect to gravity. Thus, in some applications, it also requires other techniques.
4) Pulse Tube refrigerator is also regenerative refrigeration. In large-scale cooling capacity, the actual efficiency is low, especially cooling capacity of pulse tube refrigerators are met the problem of flow angle distribution is not uniform and interior of heat exchanger flow unsteadily, which leads to lower efficiency. And it has not been widely used in the field of superconducting machines.

The refrigerator has its own advantages and disadvantages, also affect the development of HTS. Its technology, defects and manufacturing conditions are the key factors that result the slow development of HTS.

E. Stator cooling

Effective stator cooling is the basic to achieve the effective current density of stator winding. To realize a more compact generator, a more intensive stator cooling method is required. Recently, two cooling schemes are in use. The first one is

air-cooled stator which is more conservative. The other one is fluid-cooled stator and it is more innovative. The stator winding is completely immersed in the dielectric insulating oil. This method has been used commonly in large power generators.[13]

F. Manufacturing Processes and Acceptance Tests

Nowadays, the acceptance tests for superconducting generators have been produced as products. To reduce the production costs, developing a standardized manufacture is necessary. Compared with conventional generators, the factory acceptance tests need to be modified. Special tests are designed for special components of superconducting generators. However, this kind of tests and manufacturing process still need to be improved and develop.

VI. CONCLUSION

. In recently years, due to more environment pollution and high carbon emission, the implementation of clean energy become popular and wind power has been the dominant position. However, conventional wind turbine generators still have some drawbacks, such as high cost and low efficiency. Therefore, many companies began to implement the superconducting wind turbine. Superconducting wind turbine generators have the advantages of high efficiency, lighter and volume is smaller. This greatly improves the preponderance of wind power. However, there are still many challenges and problems to overcome in superconducting wind turbines such as design and capacity. When these problems are overcome, it is believed that the use of superconducting wind turbine generators will become more and more common, and become a mainstream.

REFERENCES

[1] Bogi B. Jensen, Nenad Mijatovic, Asger B. Abrahamsen: "Development of Superconducting Wind Turbine Generators", Journal of Renewable and Sustainable Energy, 2013, 5(2):347-355

[2] Hiroyuki Ohsaki, Yutaka Terao, Rashidul M. Quddes, Masaki Sekino, "Electromagnetic Characteristics of 10 MW Class Superconducting Wind Turbine Generators", International Conference on Electrical Machines and Systems, 2010:1303-1306

[3] Introduction of wind turbine. [Online]. Available: http://www.baike.baidu.com/link?url=WCmY4GUXTAUt_anNpo5mwCA1uij05gAV9ZtZ7p6OfvO6mZjyZIiz8GaezIvmYnskkKGg7avge---owast-KUZa

[4] A.B.Abrahamsen, N. mijatovic, E. Seiler, T. Zirngibl, C. Traeholt "Superconducting wind turbine generators" Superconductor Science and Technology, vol. 23, no. 3, 2010

[5] A.B.Abtahamsen, N.Magnusson,B.B.Jensen and M.Runde "Large superconducting wind turbine generators" Energy Procedia 2012, 24(24): 60-67

[6] H. Rogalla and P.H .Kes, "100years of superconductivity", CRC press, 2012, 24(Suppl 1):S147-S148

[7] J.Bray, "Superconductor in Application; Some Practical Aspects." IEEE Transactions on Applied Superconductivity,vol.19,no.3,pp.2533-2539,2009.

[8] Wenping Cao, High-Temperature Superconducting Wind Turbine Generators, [Online]. Available: http://www.intechopen.com

[9] Da Keke (2015,Step), What is EcoSwing, [Online]. Available: http://www.china-nengyuan.com/news/83418.html

[10] Suprapower, [Online]. Avaliable: http://www.suprapower-fp7.eu/

[11] G. Snitchler, B. Gamble, S.S. Kalsi, "The performance of a 5 MW high temperature superconductor ship propulsion motor", IEEE Transactions on Applied Superconductivity, 2005, 15(2): 2206-2209

[12] H. Ohsaki, M. Sekino, T. Suzuki, and Y. Terao, "Design Study of Wind Turbine Generators using Superconducting Coils and Bulks", International Conference on Clean Electrical Power, 2009, 234(3): 479-484

[13] J. Frauen hofer, J. Grundmann, G. Klaus, W. Nick. "Basic concepts, status, opportunities ,and challenges of electrical machines utilizing High-Temperature Superconducting (HTS) windings", 8th European Conference on Applied Superconductivity, 2008, 97(1): 182-189

[14] Zhang Hongjie, Sun Jianfeng. "Application prospect of high temperature superconducting generator in wind power generation". New material industry, 2008, preface (5): 55-59

[15]]Zheng Hailu, Jin Jianxun. "Development and research status of high temperature superconducting generators", Journal of Electronic Science and Technology University, 2007, 1673(6530):1-6

[16] Zhu Yingna (2015,April), Analysis of 10MW superconducting generator connected to grid. [Online]. Available: http://xueshu.baidu.com/s?wd=paperuri%3A%280946fa26130bcaa877647c268ee6b6c1%29&filter=sc_long_sign&tn=SE_xueshusource_2kduw22v&sc_vurl=http%3A%2F%2Fcdmd.cnki.com.cn%2FArticle%2FCDMD-10614-1015714516.htm&ie=utf-8&sc_us=8883208649839666566

[17] [Clive Lewis, Jens Muller. "A Direct Drive Wind Turbine HTS Generators".Wind power Monthly magazine, 2005, 13(2): pp 53-60

[18] Xu Hongling, Wang Huiling, Wang Jian, Shi Ling, Rao Rongshui, Chen Jin, Tang Yuejin, "Low temperature technology in high temperature superconducting system", Cryogenics, 2003, 2:20-24
Bi Yanfang, Hong Hui, Xin Ying, "Cryogenic cooling system and refrigerating machine for high temperature superconducting", Science China Press, 2013, 42(10):pp1001-1111

Pan Yunying was born in Shanghai, China, in 1992. She received the B.S. degrees in Power Engineering from Shanghai University of Electric Power in 2014. And now, she is a double M.S. student in Shanghai University of Electricity Power and Brandenburg University of Technology.

Gu Danzhen is an associate professor in Shanghai University of Electric Power. She mainly engaged in modeling and simulation of power system, power market and so on.
She has participated in the study of Baosteel power grid energy management system, the transient stability study of 500kV Yangcheng--Huaiyin after its in operation, the research of large impact load of Jiangsu power grid and its influence and so on. She has also participated in the major program of the National Natural Science Foundation of China, such as wide area modeling and simulation theory and methods of dynamic security analysis of power system (Project No. 50595412).
She has published more than 10 papers in the Chinese Journal of electrical engineering, power grid technology, and other journals and conferences.

Optimization of Distribution System Reliability

L. Zemite, J. Gerhards, M. Gorobetz, A. Levchenkov

***Abstract*— reliability analysis of distribution systems has been attracting increasing attention. A special concern pertains to the distribution networks on which most failures occurs. The optimization of distribution system of breakers and power switches is a possible strategy to improve reliability. The paper describes development procedure for modelling restoring after a fault and calculating associated reliability indices and customers' outage costs. The developed model of the network and reliability and outage costs calculating algorithm is suitable for multi-criteria analysis of the network. Proposed reliability and outage costs calculation algorithm is based on Monte Carlo simulation and genetic algorithm.**

***Index Terms*— distribution network, simulation, power supply reliability.**

I. Introduction

With the development of economy and mankind the electric distribution networks and technical and technological solutions of the equipment connected to them are also changing resulting in the changes of its application opportunities and requirements to quality of the supplied energy.

Taking into account the conditions of the free market and increasing demands of the customers in an uninterrupted electric power supply the effectiveness of capital investments are expected to be determined as well as losses resulted from the supply interruptions and electric supply reliability should be calculated.

The basic task of an electric supply network operator is to provide a customer with energy supply of a necessary level of reliability and quality with as low financial expenses as possible.

The evaluation of interruptions risks of an electric supply system requires to know structure of the network, its load and customers data [1].

II. Methods for Calculation of the Losses Resulted from the Electric Supply Interruptions

The losses resulted from the electric supply interruptions that have economic and social influence on the society can be divided into direct and indirect losses.

Direct losses are connected with undelivered electric energy. Indirect losses are not connected with the interruptions themselves but with their consequences.

Different types of losses calculations depend on different durations of interruptions, distribution of the customers' groups, methods of results calculations, methods of data obtaining, etc. [2, 3].

According to the calculation types the methods of losses calculation can be divided into three subgroups – analytical, simulation and methods of customers' interview [2, 3].

After choice of methods – analytical, simulation or interview, the direct and indirect losses resulted from interruptions should be analyzed and calculated.

The factors influencing the reliability can be divided into subgroups according to the customers of electric energy, undelivered energy or power, duration of interruptions, frequency as well as combining these subgroups in different ways.

The customers groups are divided taking into account equal electric energy consumption and equal interruption losses (Fig.1.) [4].

Methodology of calculation of electric supply losses from interruptions The values of the electric supply reliability and losses resulted from the interruptions are calculated with the accounting of the following factors: structure of electric supply

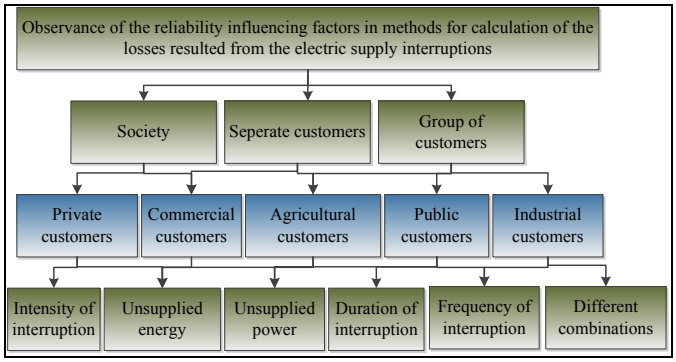

Fig. 1. Factors influencing the losses from electric supply interruptions.

network, undelivered electric energy, distribution functions of the interruptions durations probabilities, the duration of electric supply system interruptions elimination for reserved, unreserved and auxiliary elements as well as the losses of the network, society and customers resulted from the interruption [5, 6, 7].

The purpose of the calculations is to consider different scenarios as well as to calculate the losses form the interruptions.

For the calculation of the losses the following tasks are

defined:

- to model the network and select the criteria for reliability and from interruptions resulted losses;
- to provide an opportunity to calculate the losses resulted from the electric supply interruptions;
- to develop the methods for calculations of losses resulted from the interruptions for different periods of time and models of network taking into account consumption of electric energy, loading factor, length of the line, structure of the network, number of the customers, expenses for the interruptions elimination and capital investments, etc. and analyze the obtained results.

In the calculations of total losses for different scenarios for the analysis of capital investments scenario the several factors considered in the multi-criteria analysis are taken into account (Fig.2.) [4, 8].

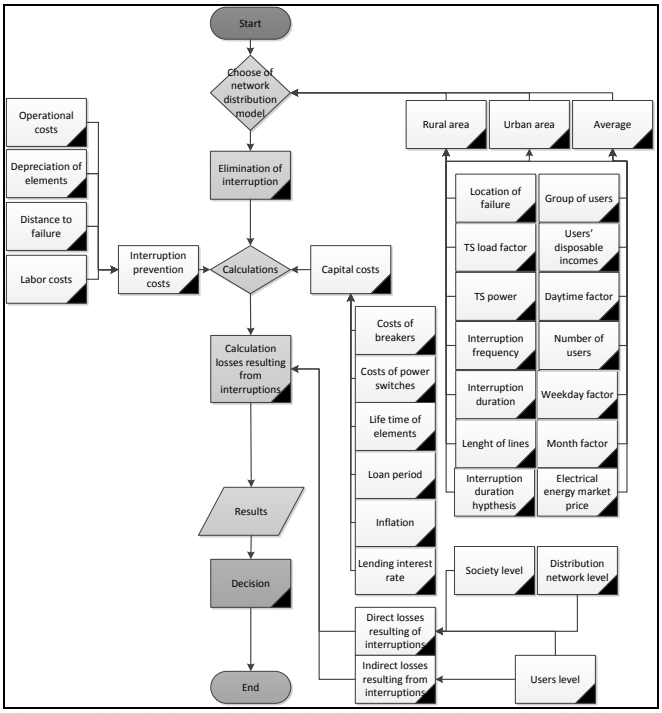

Fig. 2. Multi–criteria analysis of calculation of electric supply reliability and losses resulted from interruptions.

20kV distribution network of Latvia is analyzed in details and calculated. It resulted in a developed model of network the data determined below (Fig.3.).

The reservation of electric supply is possible along the connecting line for supply sources A2, A3 and A4.

In normal regime the power switches QF1, QF5, QF3 are in on condition.

In normal regime power switches QF4 and QF2 are in off condition. Points 16, QF4 and QF5 are distribution places.

In general case for a particular group of customers the losses resulted from the interruptions depend on the number of customers (N), on the month fm(t), on the day of a week fn(t), and time of a day fh(t). Thus the average incomes of the correspondent customers C(d) (€/year) and td – duration of interruptions, h (1) [3]

$$ECOST(t,N,d) = N \cdot f_m(t) \cdot f_n(t) \cdot f_h(t) \cdot C(d) \cdot t_d \quad (1)$$

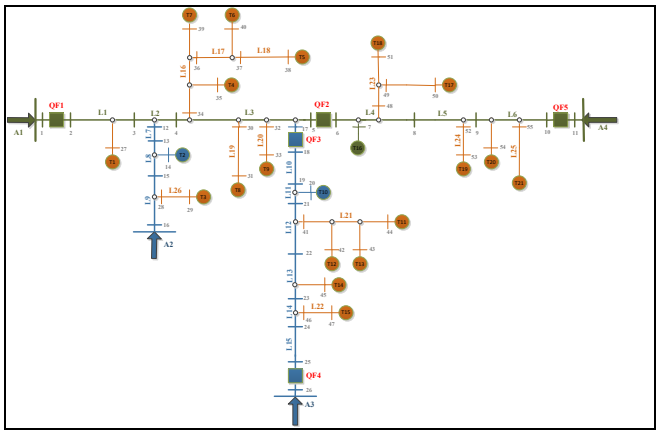

main line, connecting lines, branch line, A – supply source, A1, A4 – supply source of main line, A2, A3 – supply source of connecting lines, L1 – L26 – lines, QF1 – QF5 – power switch, T1–T21 – transformer substations (TS), T16 – transformer substation connected to main line, T2, T10 – transformer substation connected to connecting line, 1, 2, 3,…, 55 – breakers, QF4, QF5, 16 – places of distributing

Fig. 3. Model of distribution system.

For the determining of the efficiency of the planned capital investments in the network with several possible solutions that can change the model of the network, the economic calculations are required.

While calculating the level of the losses from interruptions and capital investments the capital investments expenses, ageing of the elements and the expenses for the elimination of the supply system interruptions.

The expenses are formed from (2), where C – losses from interruptions during the calculation period, €/year, Cki – capital investments expenses, €/year, CANi – interruptions elimination expenses, €/year, CEUi – direct and indirect losses of the customers, €/year, n – number of new elements, m – number of customers [8]

$$C = \sum_{i=1}^{n} C_{ki} + \sum_{i=1}^{m} C_{EUi} + C_{AN} \rightarrow \min \cdot \quad (2)$$

III. DESCRIPTIONS OF CALCULATION OF ELECTRIC SUPPLY RELIABILITY AND LOSSES FROM INTERRUPTIONS

A – Star algorithm is a heuristic method for the way search in given graph. The algorithm detects whether there way from the starting point to the end point.

There are developed algorithm modifications, which are intended for checking whether the customer is connected to a power source. In the algorithm modifications there are taken into account in additional restrictions – the reserve source searching in the case of network element interruption in accordance with network node positions [9].

If to take into account the features of the network structure according to a particular customer it is possible to obtain a more accurate duration of the interruptions and frequency for each customer.

Reservation the elements of electric supply can be divided into 3 basic groups – unreserved, reserved and auxiliary.

Reservation the elements of electric supply can be divided into 3 basic groups – unreserved, reserved and auxiliary.

Unreserved elements are those which in case of interruptions customers cannot be provided with electric supply along the lines or from other sides.

Reserved elements are those which in the case of interruptions customers can be supplied from other sides.

Auxiliary elements are the elements that in case of interruptions for customers can restore electric supply for the element under consideration, as soon as interrupted element is interrupted [9].

The frequency of the elements interruptions regarding to the considered transformer substations (TS) can be found as (3), where $\omega N[x]$ – frequency of failures of unreserved elements, $\omega_{TA}[x]$ – frequency of failures of unreserved TS, $\omega N_{lin}[x]$ – frequency of failures of unreserved lines, $\omega N_{AT}[x]$ – frequency of failures of unreserved breakers, $\omega N_{JS}[x]$ – frequency of failures of unreserved power switches, $\omega R[x]$ – frequency of failures of reserved elements, $\omega R_{lin}[x]$ – frequency of failures of reserved lines, $\omega R_{AT}[x]$ – frequency of failures of reserved breakers, $\omega R_{JS}[x]$ – frequency of failures of reserved power switches, $\omega P[x]$ – frequency of failures of auxiliary elements, $\omega P_{lin}[x]$ – frequency of failures of auxiliary lines, $\omega P_{AT}[x]$ – frequency of failures of auxiliary breakers, $\omega P_{JS}[x]$ – frequency of failures of auxiliary power switches:

$$\begin{cases} \omega N[x] = \omega_{TA}[x] + \omega N_{lin}[x] + \omega N_{AT}[x] + \omega N_{JS}[x], \\ \omega R[x] = \omega R_{lin}[x] + \omega R_{AT}[x] + \omega R_{JS}[x], \\ \omega P[x] = +\omega P_{lin}[x] + \omega P_{AT}[x] + \omega P_{JS}[x]. \end{cases} \quad (3)$$

The total frequency of failures of the elements interruptions is calculated with (4)

$$\omega[x] = \omega N[x] + \omega R[x] + \omega P[x]. \quad (4)$$

The total frequency of the elements interruptions $a[x]$ can be calculated as (5), where $aN[x]$ – number unreserved elements, $aR[x]$ – number reserved elements, $aP[x]$ – number of auxiliary elements

$$a[x] = aN[x] + aR[x] + aP[x]. \quad (5)$$

The total duration of the elements interruptions $\tau[x]$ is (6), where tN – duration of interruption of unreserved elements, tR – duration of interruption of reserved elements, tP – duration of interruption of auxiliary elements

$$\tau[x] = aN[x] \cdot tN + aR[x] \cdot tR + aP[x] \cdot tP. \quad (6)$$

A. Calculations of interrupted energy assessment rate

The statistical data of several countries were compared, the calculated interrupted energy assessment rate (IEAR) was determined for all groups of customers; the values of maximum and minimum undelivered electric energy were calculated [10].

B. Calculations of losses from interruptions by Monte Carlo method

The electric supply reliability and the losses resulted from the electric supply interruption for the models with additional manually indicated localizations of power switches are calculated on the basis of Monte Carlo modelling method.

The calculations take into account the analysis of the factors influencing the reliability for the urban and rural areas electric supply network models as well as for the average model with the purpose to calculate the expected duration of the interruptions without the analysis of previous power switches localizations [8, 11].

C. Calculations of losses from interruptions by genetic algorithm with optimized numbers and localizations of power switches

The optimization of the number and localization of the power switches is realized with the help of genetic algorithm (GA), taking into account capital expenses and the expenses of elimination of supply system interruption [8, 10, 12].

The calculation of losses from interruptions according to the number and localization of additionally placed power switches in main lines and connection lines is realized with the aim to define an optimal number and localization of power switches taking into account the capital investments for power switches [10].

D. Calculations of losses from interruptions by genetic algorithm with optimized numbers and localizations of breakers

The criteria of the optimization of the power switches resulted in the decision to optimize the breakers in the main lines and connecting lines, taking into account the expenses of the capital investments and interruptions elimination.

The optimization of the number and localization of breakers in main and connecting lines is realized with the help of genetic algorithm for the electric supply network models of rural area, urban area and average type.

Capital investments and expenses for the interruptions elimination without loan, for the loan period of 10 years and for the loan period of 25 years.

IV. RESULTS OF CALCULATIONS OF ELECTRIC SUPPLY LOSSES RESULTED FROM INTERRUPTIONS

A. A. Results of interrupted energy assessment rate

IEAR calculated for an average electric supply network model is demonstrated in Fig. 4.

IEAR calculated for an electric supply network model in rural areas is demonstrated in Fig. 5.

IEAR calculated for an urban electric supply network model is demonstrated in Fig. 6.

The summarized data show that the losses from the

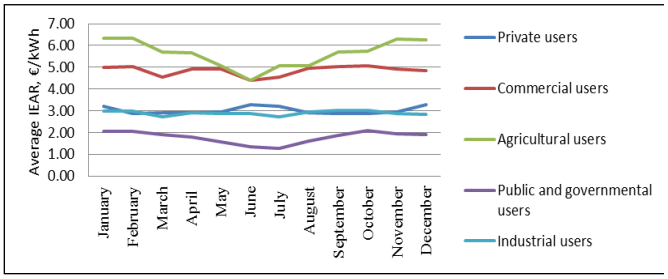

Fig. 4. Average IEAR.

interruptions in 20 kV electric supply network in Latvia are equivalent to those in Finland, Norway, the Netherlands, USA

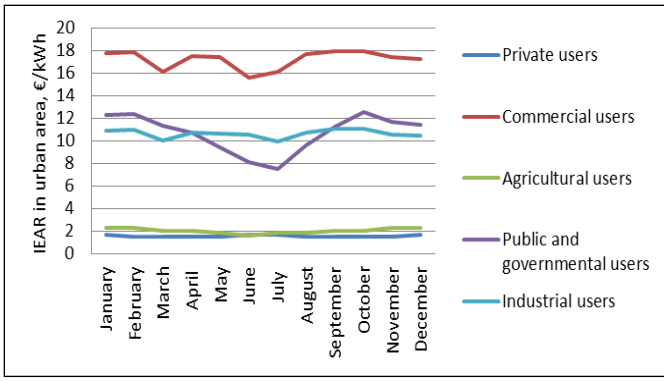

Fig. 5. IEAR in a rural area.

and Sweden [4, 11, 13].

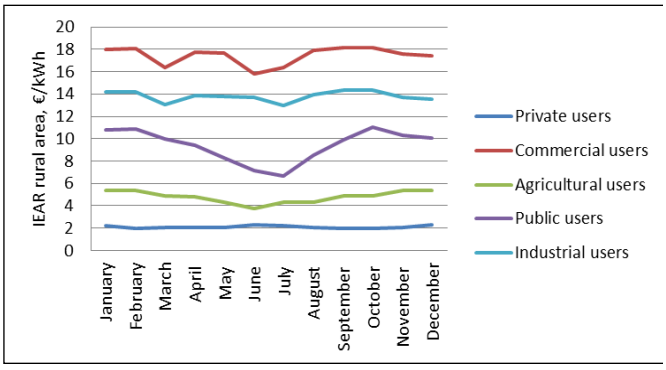

Fig. 6. IEAR in a urban area.

B. Results of calculations of losses from interruptions by Monte Carlo method

The purpose is to calculate the parameters of reliability and losses resulted from the interruptions. Application of Monte Carlo method gives an opportunity to obtained more accurate results using distribution of probabilities and reducing the number of assumptions. For an average electric supply model with one additional manually indicated power switch the total losses resulted from the interruptions are reduced for 14 %, for the models of rural areas – for 1.6 %, urban areas – for 19 %.

For an average electric supply model with two additional manually indicated power switches the total losses resulted from the interruptions are reduced for 19 %, for the models of rural areas – for 3.2 %, urban areas – for 19 %.

For an average electric supply model with three additional manually indicated power switches the total losses resulted from the interruptions are reduced for 22 %, for the models of rural areas – for 21 %, urban areas – for 22.8 % (Fig. 7).

The optimal localization of the power switches in the network is a significant factor for improving of electric supply reliability and, therefore, decreasing of the losses from interruptions.

The absence of the optimal localization of sectioning

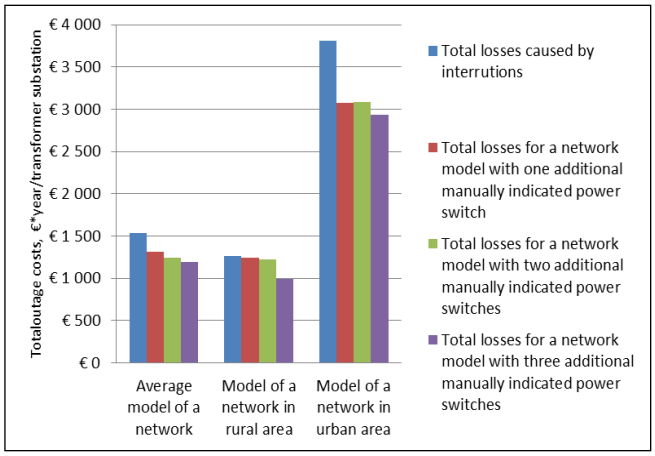

Fig. 7. The total losses resulting from interruptions.

elements in the network can cause an increasing or insignificant decreasing of the losses resulted from the interruptions as well as the manually indicated localizations of the sectioning elements do not give an opportunity to calculate the efficiency of capital investments for the reliability level increasing [8].

The reducing of the losses from interruptions are directly proportional to TS power, number of customers, consumption of electric energy and incomes of the customers.

C. Results of calculations of losses from interruptions by genetic algorithm with optimized numbers and localizations of power switches

The optimization of the number and localization of power switches in main and connecting lines is realized with the help of genetic algorithm for the electric supply network models of rural area, urban area and average type.

The total losses of the distribution network, society and customers resulted from the interruptions after the optimization of the number and localization of power switches and for different loan periods are given in Fig.8.

After the optimization of the number and localization of power switches for the case of no loan the losses resulted from the interruptions for the average network model are reduced for 14 %, for the model of rural area electric supply network – for 12.6 %, and for the urban area model – for 33.6 %.

Total losses from interruptions for the loan period of 10 years in the model of average network are reduced for 8 %, in the model of rural area network – for 7 %, and in the model of urban area – for 30 %.

Total losses from interruptions for the loan period of 25 years in the model of average network are reduced for 5.8 %, in the model of rural area network – for 11 %, and in the model of urban area – for 20 %.

Summarizing the results we can conclude that for the models of average and rural areas electric supply networks the capital investments for the purchasing of power switches are proportionally decreased.

The total losses resulted from the interruptions are significantly decreased as a result of sectioning for the model

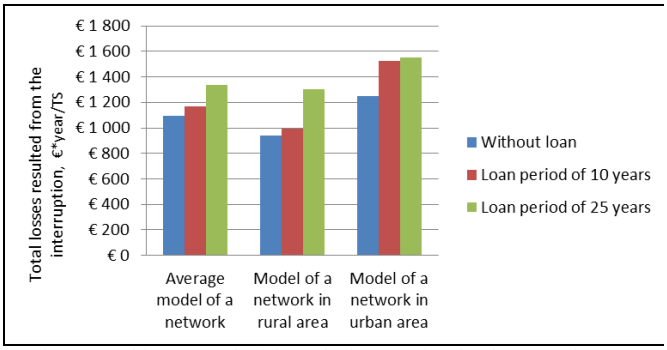

Fig. 8. Total losses resulted from the interruption for the case of power switches optimization.

of urban area electric supply network.

This is connected with higher consumption of electric energy in the urban regions and higher incomes of the customers [8].

Taking into account the total losses from the interruptions the additional connection of power switches can be considered from the smart grids development and maintaining easy point of view.

D. Results of calculations of losses from interruptions by genetic algorithm with optimized numbers and localizations of breakers

Note that the optimization of the number and localization of the breakers does not give an opportunity to achieve a minimum level of the losses resulting from the interruptions.

Besides, the correspondence of the optimal number of the breakers to that of the power switches, the breakers cannot provide the operation of the network without the interruptions that is why the minimized expenses include the customers' losses from the interruptions.

Fig.9. represents the total losses of the distribution network, customers and society for an optimal number of breakers for the loan period of 10years, 25 years and without the loan.

After the optimization of the number and localization of breakers for the case of no loan the losses resulted from the interruptions for the average network model are reduced for 2 %, for the model of rural area electric supply network – for 1%, and for the urban area model – for 9%.

Total losses from interruptions for the loan period of 10 years in the model of average network are reduced for 6 %, in the model of rural area network – for 3 %, and in the model of urban area – for 9 %.

Total losses from interruptions for the loan period of 25 years in the model of average network are reduced for 8 %, in the model of rural area network – for 3 %, and in the model of urban area – for 7 % (Fig. 9).

Taking into account the total losses from the interruptions, the additional connection of breakers can be considered from the perspective of smart grid development and easy maintenance.

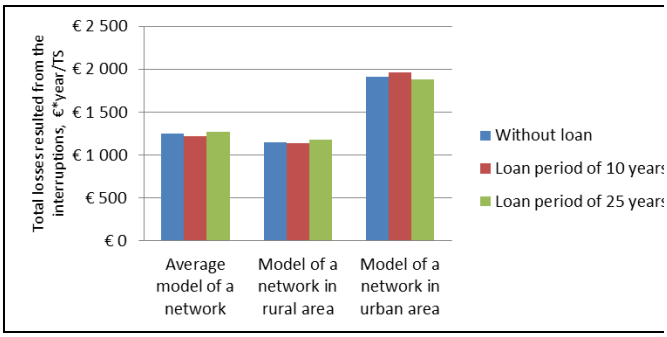

Fig. 9. Total losses resulted from the interruption for the case of breakers optimization.

V. CONCLUSIONS

The proposed methods can be applied for the calculations of the interruption risks of the customers and compensation of the losses resulted from the interruptions.

The possible future modifications of the proposed methods are applicable in the solutions of different problems related to the analysis of electric supply interruptions.

The overview, analysis and systematization of the methods of distribution networks reliability calculation, optimization methods of reliability improvement, the alternative of the reliability improvement and the losses resulted from the electric supply interruptions give an opportunity to search for the solutions of capital investments on the level of distribution networks, customers and society taking into account the tendencies of development and perspective technologies.

Optimization of the number of power switches and localization completed with the help of genetic algorithm, in accordance with the loan term and properties of the network model, allows reducing the losses from interruptions from 5.8 % to 33.6 %.

Optimization of the number of breakers and localization completed with the help of genetic algorithm, in accordance with the loan term and properties of the network model, allows reducing the losses from interruptions from 1 % to 9 %.

The risks, losses, planning and advantages of the electric supply network should be analyzed in accordance with economic, environment, electric supply quality, probability of interruptions, the risks of the changes in legislation, etc.

Estimating the solutions of the electric supply reliability improvement most of the attention should be turned to the selection of optimal number and localization of the sectioning elements that provides an immediate improvement of the electric supply reliability.

Taking into account the total losses from the interruptions the additional connection of power switches and /or breakers can be considered from the smart grids development and easy maintenance point of view, but not from the losses decreasing

point of view.

The volume of the possible losses resulted from interruptions can be variable with the increasing of electric energy consumption and/or changing of the customer properties.

ACKNOWLEDGEMENT

This research work has been supported by Latvian Council of Science (Project No. 673/2014). L. Zemite, J. Gerhards, M. Gorobetz, A. Levchenkov, Riga Technical University Faculty of Electrical and Power engineering, Riga, Latvia.

REFERENCES

[1] Brown R. E. Electric Power Distribution Reliability. – Marcel Dekker, New York, 2002. – p. 365.

[2] Alevehag K. Impact of Dependencies in Risk Assessments of Power Distribution Systems. – Licentiate Thesis, Royal Institute of Technology, School of Electrical Engineering, Electric Power Systems, Stockholm: Sweden, 2008. – p. 155.

[3] Helseth A. Modeling Reliability of Supply and Infrastructural Dependency in Energy Distribution Systems. – Thesis for the degree of philosophy doctor, Trondheim, Norwegian University of Science and Technology, 2008. – p. 132.

[4] Chayakulkheeree K. Economy of Power System Reliability. – A Training Workshop on Power System Economics and Planning, Asian Institute of Technology, 2006. – p. 68.

[5] Kjølle G. H., Samdal K., Singh B., Kvitastein O. A. Customer Costs Related to Interruptions and Voltage Problems: Methodology and Results. – Power Systems, IEEE Transactions on, vol.23, no.3, Aug. 2008. – pp. 1030. – 1038.

[6] Billinton R. Reliability of power supplies. In Electronics and Power , vol.24, no.4, , April 1978. – pp. 307. – 310.

[7] Theil A., Theil M. Medium Voltage network reliability: efficiency oriented supply restoration strategies. – 15th PSCC, Session 8, Paper 5, Liege, 2005. – pp. 1–6.

[8] Distribuzione C. N. Optimal Placement of Automation Devices in Enel Distribution Network. – in Electricity Distribution – Part 1, 2009. CIRED 2009. 20th International Conference and Exhibition, 8–11 June 2009. – pp. 1. – 4.

[9] Haghifam M. R. Optimal allocation of tie points in radial distribution systems using a genetic algorithm.– Eur. Trans. Elect. Power, vol. 14, no. 2, 2004. – pp. 85. – 96.

[10] Zemīte L., Gerhards J., Gorobecs M., Ļevčenkovs A. Optimization of Switch Allocation in Power Distribution Systems – International Workshop on Deregulated Electricity Market Issues (DEMSEE 2015), Ungārija, Budapešta, 2014.. – pp.166. – 173.

[11] Sljivac D., Nikolovski S., Kovac Z. Distribution Network Restoration Using Sequential Monte Carlo Approch. – The 9th International Conference on Probabilistic Methods Applied to Power Systems, June 11–15, 2006. – p. 6.

Laila Zemite is graduated PhD in 2016, assistant professor of Riga Technical University Institute of Power and Electrical Engineering. Results of research activity are published in various international scientific proceedings and journals in fields of distribution system reliability, power system development, planning and control. She is leader of various national projects and international projects.

Janis Gerhards is PhD professor, Riga Technical University, Institute of Institute of Power and Electrical Engineering. His fields of interests are optimization theory, reliability research in free electricity market conditions, distribution system reliability, automatization, power system development, planning and control. He was leading various national and international projects, author of many patents, books and publications.

Mikhail Gorobetz is graduated PhD. in 2008, assistant professor and leading researcher of Riga Technical University Institute of Industrial Electronics and Electrical Engineering. Results of research activity are published in various international scientific proceedings and journals in fields of adaptive control, neural networks, genetic algorithms, modelling and simulation of dynamic processes. He is leader of various national projects and international projects. He is author of many study books and patented inventions.

Anatoly Levchenkov, PhD professor, Riga Technical University, Institute of Industrial Electronics and Electrical Engineering, Institute of Railway Transport. He got engineer diploma in electrical engineering in 1969, PhD degree in 1978. His fields of interests are optimization theory, group decision support systems, negotiation support systems, scheduling, logistics, intelligent transport systems, evolutionary algorithms for embedded systems. He was leading various national and international projects, author of many patents, books and publications.

Design and realization of a tactile switches module with capacitive sensing method implemented with a microcontroller

Lorenzo Capineri

Department of Information Engineering
University of Florence

Abstract— **The aim of this research project is the architecture and the design of an electronic system for controlling domestic tactile switches to be integrated into a home automation system based on the KNX standard. All the steps that led to the fulfillment of the finished prototype are reported, from the study and design of the capacitive tactile sensors and the electronic control board according to the specifications imposed by KNX standard. The touch event detection is reached as a trade-off with the footprint requirements of the switch. Experimental results of the fabricated prototype are presented to demonstrate the feasibility of this device.**

Index Terms— **Industrial electronics, capacitive switch, home automation, KNX standard**

I. INTRODUCTION

THE home automation industry is going through a phase of strong growth overall in Europe, mainly thanks to the knowledge gained by users on potential of this technological approach in terms of greater safety, comfort, energy savings and ease of use. Even the building designers show a greater interest in home automation, as an added value of dwelling and contributing factor to the increase in competitiveness of the offer. In parallel with the advancement of home automation solutions in recent years the offer of advanced functionalities and increasing levels of integration is enhanced. To this is added the modern conception of logic in living styles requiring housing with greater flexibility to match the changing needs of users in connection with new technologies. The home automation market manifests a growing interest especially for use in new or renovated houses with particular interest to the issue of security and the energy saving. From the users' side the main requirements for new home automation devices are:

- Ease of use: you must ensure easily accessible information preferring intuitive interfaces and the use of touch-screen.
- Solutions based on open standards: that there must be the possibility for the user to replace the entire system or change a service without requiring a redesign of the facilities.
- The reliability of continued operation: can be obtained by providing flexible and easily programmable systems to suit the needs of customization of each user and an efficient maintenance service.

The purpose of this work is to describe the research and development phase of an electronic system for controlling domestic tactile switches to be integrated into a home automation system based on the KNX standard.

The device designed tries to respond to the major needs of end-users of a home automation system, preferring a tactile technology to the control elements and using KNX it is at present the open standard for home automation widespread in Europe.

As for the use of capacitive touch acquisition of control, it should be noted that in recent years, this technology has matured enough to provide greater robustness, reliability and greater user satisfaction compared to traditional switches mechanical.

The main advantages of the proposed solution are:

- Greater durability and reliability due to the absence of moving parts, which is due to the mechanical switches of the device wear. Moreover, the absence of openings they make it possible to use in harsh environments where dust and moisture could penetrate the device.
- A sleek design that allows switches to be integrated perfectly into the home.
- The multi-functionality: hardly feasible with mechanical switches, it becomes possible with tactile technology that can implement different functions starting from a single control element.
- Feedback to the user: the apparent lack of tactile switches do not provide the user with clear evidence of the activation, is instead resolved by providing the ability to have different types of feedback as the lighting of a LED, a sound or one of the key vibration and differentiate them according to the function performed.

The work presented in this paper is organized into the following sections:

1. The study of the state of the tactile capacitive acquisition techniques and solutions used in home automation systems;
2. The design of the sensors, the electronic control board and

the software according to the specifications;

4. Description of the realization and implementation of the electronics and the firmware;

5. Experimental results obtained with a full operational prototype.

II. STUDY OF TACTILE CAPACITIVE ACQUISITION TECHNIQUES

A simplified model to understand the principle on which is based the capacitive acquisition considers the electrode as one of the faces of a capacitor, while the second is represented by the environment in which it is located (forming the parasitic capacitance C_0) or, in addition, by another conductive object such as a finger (forming a C_T capacitance).

The overall capacitance is connected to a measuring circuit that periodically acquires the value of the electrode capacity. This model shown in Figure 1 neglects the detrimental effects due to the interaction of the finger with the scattered fields generated by the coupling between the electrode and the underlying ground plane.

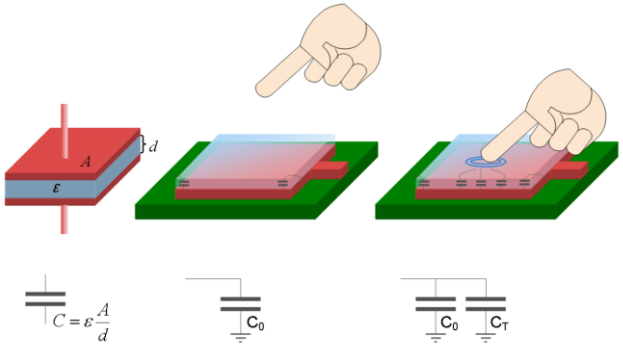

Fig. 1. Simplified model of change of capacitance from the value C_0 to C_0+C_T when a finger is touching the dielectric layer top surface.

To analyze how occurs the change in capacity from the physical point of view, we make reference to Figure 2.

The coupling between the copper electrode on the upper surface of the printed circuit board (PCB) and the underlying ground plane generates a parasitic capacitance, usually of the order of 10 pF to 300pF. The charge distributions on the two capacitor plates determine an electric field: most of the energy will be concentrated directly between the two conducting surfaces but a part protrudes in the external area and gives rise to the electric field lines denominated "fringing fields".

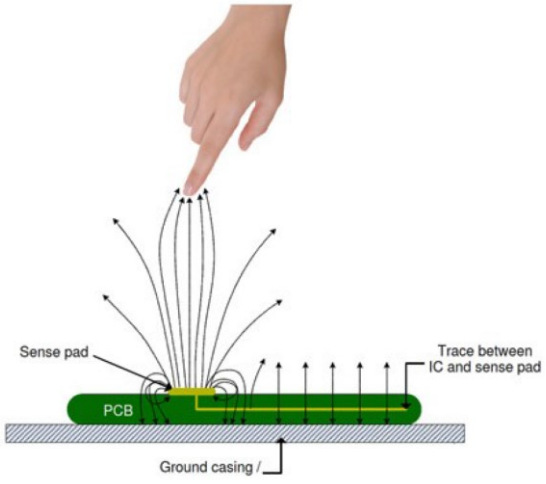

Fig. 2. Effects of electrical field fringes.

According to the general characteristics explained above, it is important to indicate the main parameters sizing of the electrodes and the choices done in this project:

- Presence of a double interface: the sensors consist of a double interface, the first made by the copper layer on the surface of the touch board and the plastic cover, the second by the plastic cover and the outer cover made of steel. At these will go to addition, in case of touch, the contact surface between the metal cover external and finger.
- Material and thickness of casing: polycarbonate, 1 mm
- Geometry: rectangular with rounded corners
- Dimensions: ratio of coverage and thickness of the electrode side at least 1: 4
- Distance between the electrodes: ratio between the distance and longer side of electrode 1: 8 and use of adjacent key suppression (AKS) method available for microcontroller implementation.
- Inserting a ground plane: reduces sensitivity.

A. *Techniques of capacitive touch sensing*

After understanding the physical principle underlying the change in capacity determined by the contact of the electrode fingers, it must explain how this change can be detected and converted into a useful signal. There are numerous methods to detect the capacity increase caused by the proximity or contact of a conductor from: variation of the resonance frequency, frequency modulation or amplitude, the measurement of the charge/discharge, delay measurement time in reaching a threshold or duty cycle [1][2][3].

Most of these methods require analog circuits inheriting the related problems as crosstalk and sensitivity to noise [4], this may be preferable for a digital approach that guarantees smaller dimensions and lower power consumption than analog solutions. Some of the most commonly used acquisition techniques are described in the following paragraphs, divided on the basis of the expected degree of integration. In fact we can distinguish two main categories of implementation: software-based solutions, using microcontrollers for general use, and specialized controllers for capacitive acquisition.

Of course are also possible other solutions such as custom microcontrollers for interfacing capacitive sensors whose architecture include modules dedicated to scanning arrays of capacitive sensors and are easy to implement. In tactile sensing the recent trend is to prefer the use of custom microcontrollers or otherwise use microcontrollers already tailored for capacitive acquisition. Each class of solutions, however, has its strengths and weaknesses and then depending on the application requirements, the designer must select the best approach.

In this section are compared the two approaches based on dedicated microcontrollers and the other based on the use of a

general purpose microprocessor requiring the programming of software for touch detection.

B. Solutions based on the use of dedicated controllers

Several off the shelf solutions have been analyzed and compared for the design of the final prototype:

1) FUJITSU FMA1127

The FMA1127 is a controller for capacitive sensors, which converts the capacitance generated by the interaction between the human body and the electrode only in digital data without any analog signal processing.

Moreover, this solution increases the flexibility of design, provides good performance in terms of power consumption and stability. In Figure 3 is shown the acquisition scheme adopted for this case.

This scheme has two R-C delay lines: one connected to a reference capacity CR and the other one connected to the "sensing" capacity CM, that is, the electrode, subjected to the same environmental conditions. Both are controlled by the same clock (CLK) signal, which frequency can be programmed up to 20 kHz to ensure fast response times and no negative impact on the system's susceptibility to the EMI. The leading

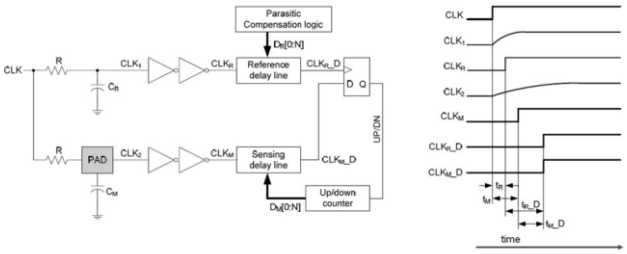

Fig. 3. Diagram of the acquisition technique blocks used for FUJITSU FMA1127 and the timing signals for the touch event detection.

front of the clock increases more slowly because the larger charging time due to increased capacitance in the case of the touch event. In Figure 3 can be observed that CLK2 rises more slowly than CLK1, and then reaches a threshold value considered "high", with a delay.

Therefore the two logic signals CLKR and CLKM generated by CLK1 and CLK2 respectively, have two rising edges with different delays with respect to CLK signal. These two rising edges, however, arrive in phase to the flip-flop thanks to the parasitic compensation logic obtained with DR digital values DR[0: N], the digital delay DM [0: N] values are adjusted by a feedback control with an Up/Down counter until CLKR_D and CLKM_D are in phase. The CM of the measured capacitance value can then be derived from the difference between the digital values DR [0: N] and DM [0: N]. The CM capacity, as well as the difference between the delays of the two clocks on the lines, will be proportional to the difference DR [0: N] - DM [0: N].

In a capacitive sensor, the value of the CM capacity changes depending on whether or not a finger is present on the conductive plate, while the CR capacity has small variations due to environmental conditions (e.g. Temperature changes). During a touch event, CM varies rapidly from a minimum value (CM1 = C0) to greater (CM2 = C0 + CT), and this change must cause a signal variation to reach a threshold.

In the reference delay line the value of DR[0: N] is configured during the initialization phase to a value slightly lower than that of DM1[0: N], which indicates the absence of a touch. So the difference DR[0: N] - DM1[0: N] will give a negative delay value. The presence of the finger is detected when the difference (DR[0: N] - DM2[0: N]) becomes positive, in fact DM2[0: N], related to the case CM2 = C0 + CT, will be less than the digital value DR [0: N].

2) QTOUCH® IN AT42QT1070 CONTROLLER

QTouch® is a technology for the tactile acquisition developed and patented by Atmel that employs both controllers dedicated to this type of detection is the use, for these purposes, the processors of the AT-MEGA family (see Figure 4).

In this work the acquisition technique was initially estimated by the evaluation-board Qtouch Xplained. This card supports four capacitive touch interfaces acquisition: slider, wheel and two touch-buttons and provide the connection to a dedicated card containing the ATxmega128A1 processor. In Figure 4 the two blue circles represent two planar electrodes, each of which is connected to the GPIO pin of the processor by means of a number of capacities and resistances visible in the lower part of the PCB which allow the detection of the capacity variation

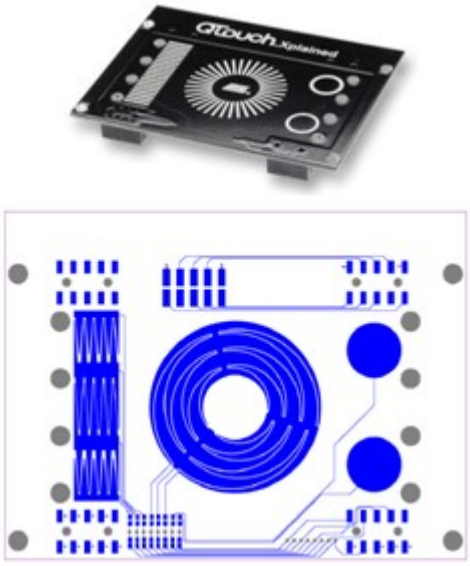

Fig. 4. Tactile capacity sensor card Qtouch Xplained (Atmel).

electrode. In this study the technique was deepened with the AT42QT1070 controller tests and reproducing the operating diagram with discrete components using NXP LPC 1227 processor, as will be detailed below.

The QTouch® technique is based on charge transfer from the electrode capacity of acquisition to a higher value. In the first phase the Cx electrode, having unknown capacitance because its value will be different depending on whether the touch occurred or not, is charged to a known potential. The charge is then transferred to a measurement capacitor Cs (see Figure 5), the latter has a fixed value and greater than about one order of magnitude compared to Cx.

We can assume that the sensing electrode capacity is of the order of pF and the design for Cs value is fixed in the range 12-22nF. The charge transfer cycle is repeated until the voltage at the terminals of Cs reaches a threshold voltage of Vih. The level of the signal of interest is given by the number of charge transfer cycles from the capacity Cx to Cs taken to reach this voltage. Placing a finger on the touch surface introduces an external capacity that increases the amount of charge transferred in each cycle (because it increases Cx), thus reducing the total number of cycles necessary for Cs to reach the threshold voltage. When the number of cycles falls below the aforementioned threshold, then the sensor is again placed in the touch detection phase.

Cx and Cs are currently connected with a certain number of resistors Rs in series. Some of these series resistors are inserted in this design to enhance the performance of the system to EMI and ESD, the number and the value of these resistors must be chosen on the basis of the Cx value, a total value of resistance is usually considered appropriate 10kΩ; the presence of additional resistance is due to the resistivity of the tracks that connect the capacitive sensor and to that of the electrode constituent material itself.

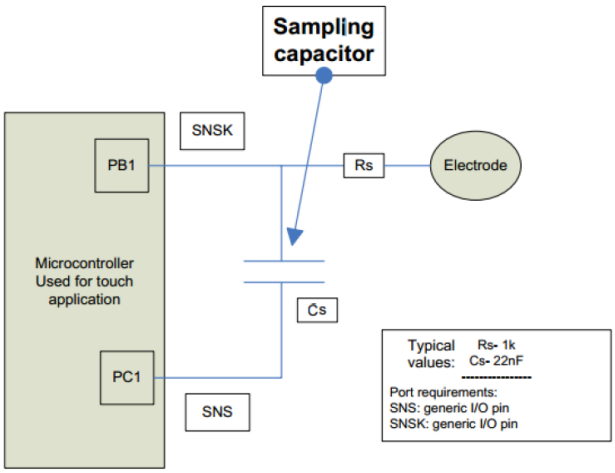

Fig. 5. Illustration of Atmel solution for capacitive acquisition based on the charge transfer. Electrode capacitance is Cx..

The RC time constants that are determined tend to slow down the acquisition process, therefore it is important to measure the settling time relative to the individual pulses of the charge transfer in order to have fronts of the more rectangular as possible while ensuring reliable detection. A simple test may be performed with the oscilloscope by placing the tip of the probe on a coin resting on the surface of the sensor cover.

C. Experimental evaluation of two solutions for capacitive tactile switches

After the general analysis reported in the previous sections, two possible solutions have been evaluated with experimental board and switches prototypes and their descriptions as follow.

1) Microprocessor and custom software programming

This solution was carried out in microprocessor and software configuration, employing at first the electrodes of the evaluation-board Qtouch Xplained Atmel and subsequently two

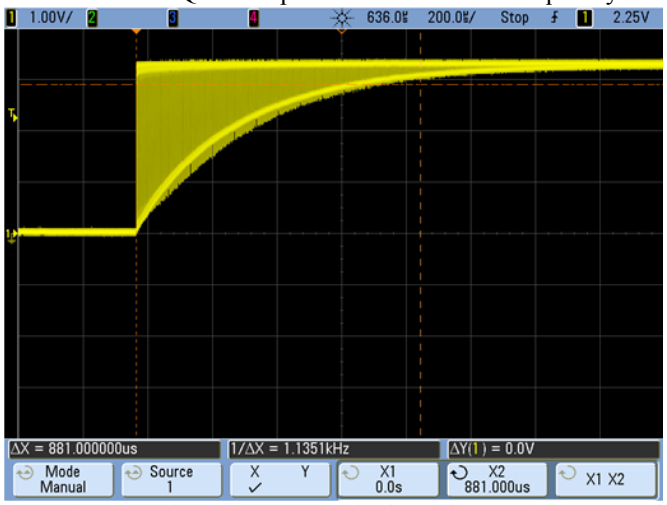

Fig. 6. Charge transfer cycle of 0,881 ms for the touch case, where is assumed for Cx=5-10 pF and Cs=12nF.

copper electrodes of the same type as the final touch card, realized on the surface of the PCB and having a central hole for the signaling LED, with area1.6 cm x 1.5 cm. The processor is mounted on the NXP LPC1227 Evaluation Board IAR KICKSTART KIT. The software was developed in the environment IAR Embedded Workbench. With this setup have been measured the duration of the charge transfer cycle for the touch and no-touch cases, that are 0,881ms and 1,784 ms

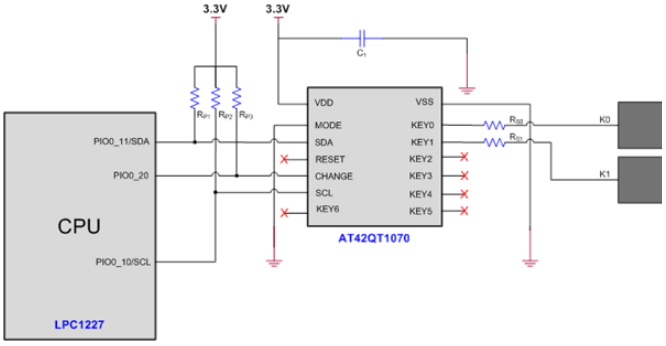

Fig. 7. Tactile interface solution with dedicated microcontroller and two tactile switch keys (K0 and K1).

respectively. An illustration of the waveforms recorded for the touch case is reported in Figure 6.

2) ATMEL custom microcontroller AT42QT1070

The second solution was based on the AT42QT1070 controller ATMEL, configured Comms Mode and employing six channels of detection. The unused channels can be disabled by setting to zero the Averaging Factor parameter. The schematic of the electronic circuit is shown in Figure 7.

The CPU of this LPC1227 IAR Kickstart Kit, communicates with the microcontroller via I2C line. The event of variation of the state of one of the buttons involves the transition of the CHANGE line from logic high to a low level that is signaled to the microprocessor via an interrupt allowing the savings of otherwise necessary resources for the periodic reading of the registers of the controller. With reference to Figure 8; we can observe that the reading of the registers occurs only to the interruption, after which the CHANGE line returns high again.

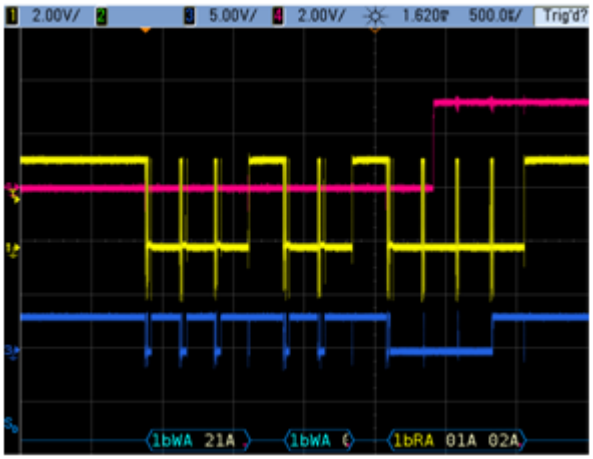

Fig. 8. Signals on lines SDA, SCL and CHANGE in case touch on Key 1

The CHANGE line (red color) goes from low level to high

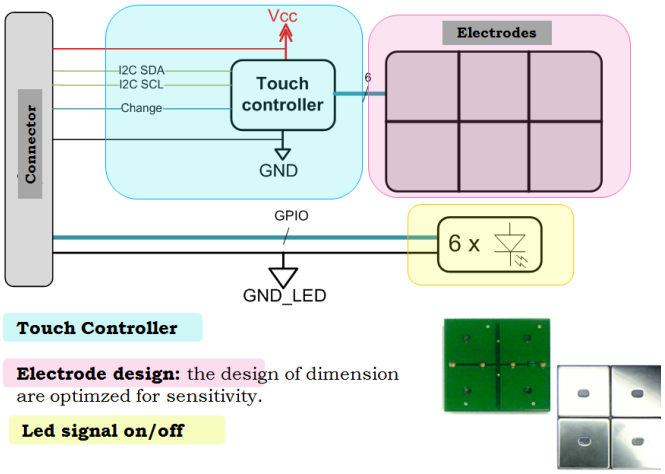

Fig. 9. Block scheme of the designed Touch detection board for up to 6 capacitive tactile sensors. On the bottom right the prototype with 4 electrodes with the front metal panel and the PCB for reference electrodes

following the reading of first register, blue and yellow lines are reported respectively for the I2C clock and data lines and show the I2C standard reading protocol.

The outcome of the comparison of these solutions, led to prefer the use of a custom microcontroller for the following reasons:

- Simplified management of multiple electrodes,
- Touch event capture rate
- Increased reliability of detection
- Saving microprocessor resources
- Fewer GPIO pins and links
- Greater flexibility of use

III. ELECTRONIC HARDWARE DESIGN AND IMPLEMENTATION

The system design consists of two main logical sections that

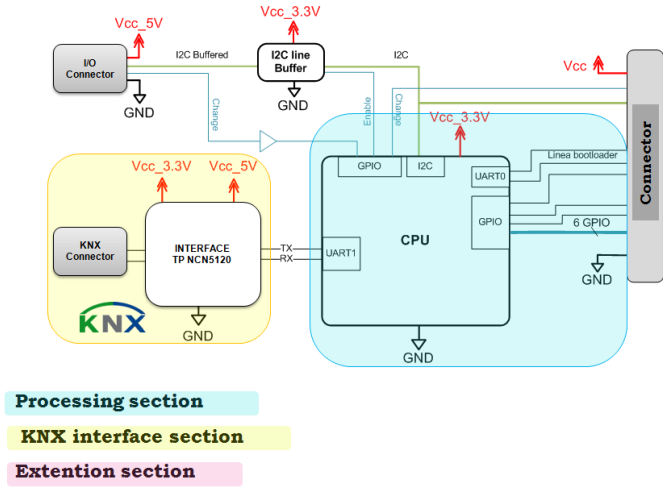

Fig. 10. Block scheme of the designed control board

correspond to implementation with two PCBs: the touch board realizes the acquisition of the touch (see Figure 9); the control card implements the control section and the interface with the KNX bus and the external expansion.

The control board is composed of three main sections: the processing consisting of the microprocessor which communicates with the acquisition section via the I2C line and the mezzanine type connector (see Figure 10).

The system communicates with the KNX bus through NCN5120 transceiver. Besides allowing interfacing with the KNX bus system on twisted pair networks, the device integrates two programmable DC/DC converters that allow to change the input voltage available from the KNX bus line, to the voltage levels needed to power the integrated circuit. The extension section shown in Figure 10 has been introduced to interface the CPU with other external devices, for example temperature sensors. The I2C line buffer is useful to perform a level shift for the communication with devices powered at different voltage levels.

IV. SOFTWARE DESIGN AND IMPLEMENTATION

In this section is briefly reported the software design. System management software covers both the acquisition of the user commands by the touch controller is communicating with the KNX bus. To minimize the software development time has

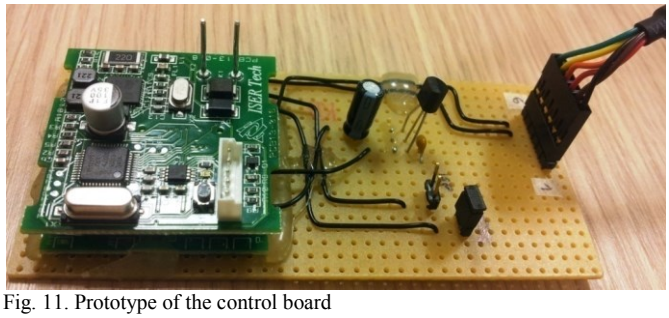

Fig. 11. Prototype of the control board

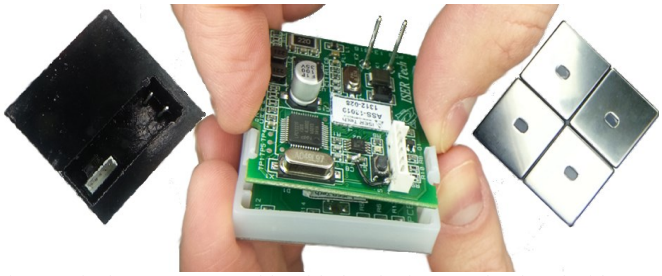

Fig. 12. Final prototype assembly with the plastic cases developed with a 3D printer. On the right the four tactile metal switches.

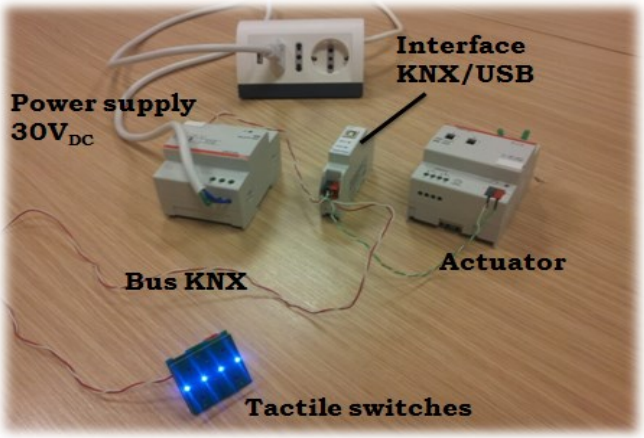

Fig. 13. Final demonstration system.

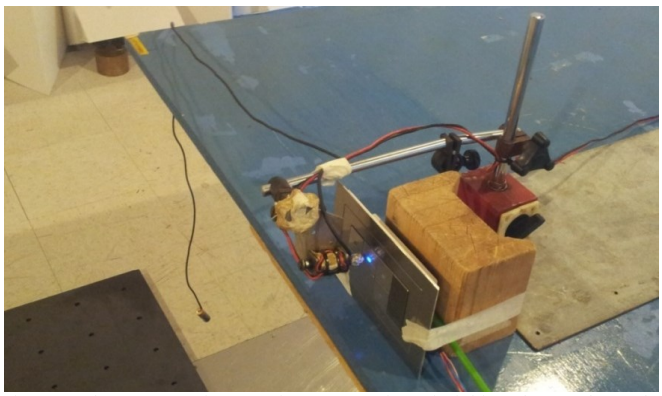

Fig. 14. Electromagnetic actuation system for mimicking the touch on the metal switch with an aluminum rounded tip connected to a 1.5 V battery for the electrostatic stimulus. The assembly was installed in the anechoic chamber during EMC tests.

been decided to use Communication Stack SW already certified for KNX bus. The communication stack assigns different functions to the tactile switches, for example typical configurable functions required by domotic houses are:

- Remote relays
- Switch ON / OFF
- Lighting control
- Window with sliding curtains

V. PROTOTYPE REALIZATION AND FIRMWARE TESTING

The prototypes of the control board and the integrated touch board with capacitive touch sensors have been realized also considering the possible problems arising from the possible certifications EMI. After installing the firmware on the control card (see Figure 11) through the UART port of the microprocessor and the PC on which is installed the boards of the programming tool, a series of electrical tests on the prototype were carried out. The complete device was assembled by using a 3D printing for the plastic case of the electronics and sealed connectors and the 4 tactile metal switches (see Figure 12).

In Figure 13 is shown the final set-up with the power supply, the four tactile switches board with LED signaling, the KNX interface and electromechanical actuator (relay).

A. Power consumption analysis.

A preliminary estimation of the power consumption of the prototype was done during the electronic design phase.

The following list reports the estimate of power consumption of the main electronic components of the system:

- Microprocessor: 13mW (operating freq. 4,9152MHz, Configuration Active mode, peripherals all active)
- Touch controller : 3mW (parameter LP mode = 0)
- Transceiver: 150 mW (normal operating mode, no load, both DC/DC activated)
- 6 LEDs: 79mW

Adding up all these value the total is ≈ 245 mW. The measurements on the final prototype results in:

- Current = 3.8mA @30V for KNX bus: 114mW
- 6 LEDs ON: 79mW

The total power consumption for these two components is 193 mW that is in good agreement with the preliminary estimate and it is acceptable for a domotic plant.

VI. PRELIMINARY CERTIFICATION TESTS

In order to submit a product on the European market it is necessary to verify compliance with the applicable EU directives, in our case the RoHS (Restriction of hazardous substances) and EMC (Electro Magnetic Compatibility). Evidence of radiated and conducted emission has been measured at a test laboratory.

The product has passed all tests except EMC immunity to conducted interference, therefore, is necessary to improve the design of the prototype. For carrying out immunity tests it was necessary to study a mechanical equipment that can reproduce the touch: it is proposed a piston controlled via PC actuated by a magnetic coil that was moved at regular intervals for pressing one of the buttons, the plunger tip is aluminum covered and connected to a battery 1.5V to simulate the touch (see Figure 14).

The KNX certification covers both the hardware part of the product software, checking the requirements imposed by the standard; choosing the hardware interface (NCN5120) and the Communication Stack already KNX certified simplifies the procedure by reducing time and costs for the obtaining of the brand.

VII. Conclusions

The study of the architecture of an integrated system with tactile capacitive switches and a KNX interface is presented with explanation of the design criteria. After the fabrication of a prototype with 4 tactile capacitive switches, a series of tests have been carried out to verify the correct operation of the of capacitive tactile signal acquisition which shown an excellent sensitivity and a good KNX communication reliability. The total power consumption of the device is about 245 mW that is rather low for a domotic plan device. Foreseen the industrialization of the prototype, preliminary tests have been developed according to EMI and ESD standards. This new device is useful for domotic plants to save energy consumption thanks to the versatile use of tactile switches function with limited additional cost for installation due to simple cabled connection of KNX.

Acknowledgment

The author wishes to acknowledge the contribution of ATMEL University program with Industrial Electronics Laboratory at PIN (Prato, Italy).

References

[1] A. Ożadowicz, "Communication Reliability in the Intelligent Building Systems, " white paper, http://www.knx.org/fileadmin/downloads

[2] Atmel – AT42QT1070 Seven channel QTouch® Touch Sensor IC Datasheet. http://www.atmel.com

[3] M. Lee, "The art of capacitive touch sensing" by Cypress , http://www.cypress.com/file/72881/download

[4] S. Kim, W. Choi, W. Rim, Y. Chun "A Highly Sensitive Capacitive Touch Sensor Integrated on a Thin-Film-Encapsulated Active-Matrix OLED for Ultrathin Displays," IEEE Transactions on Electron Devices, Vol. 58 , pp. 3609 - 3615, Aug. 2011

[5] Directive 2011/65/EU of the European Parliament and of the Council of 8 June 2011 on the restriction of the use of certain hazardous substances in electrical and electronic equipment Text with EEA relevance

[6] Directive 2004/108/EC of the European Parliament and of the Council relating to electromagnetic compatibility.

[7] CEI EN 50491-5-2 standard.

[8] CEI EN 61000-6-3 standard.

Lorenzo Capineri (M'83–SM'07) was born in Florence, Italy, in 1962. He received the M.S. degree in electronic engineering, in 1988, the doctorate degree in nondestructive testing, in 1993, and post-doctorate in advanced processing method for ground penetrating radar systems from the University of Florence, in 1994.In 1995, he became an Associate Researcher and an Associate Professor of Electronics with the Department of Information Engineering (formerly Department of Electronics and Telecommunications) with the University of Florence, in 2004. He has worked on several research projects in collaboration with national and international companies, the Italian Research Council (CNR), the Italian Space Agency (ASI), and the European Space Agency (ESA), AEA Technology and UKAEA, England, International Science and Technology Centre (ISTC), Moscow, Russia, Thales Alenia Space Italia (TASI), Texas Instruments, USA, General Electric (UK) , Joint Research Centre (European Commission), and NATO. He has coauthored six Italian patents, three book chapters, and around 200 scientific and technical papers. His research interests include the design of ultrasonic guided waves devices, buried objects detection with seismo-acoustic methods, and holographic radar.

Can we use IEC 61850 for safety related functions?

Micaela Caserza Magro, Paolo Pinceti, Luca Rocca
Department DITEN
University of Genova
Genova, Italy
paolo.pinceti@unige.it

***Abstract*—Safety is an essential issue for processes that present high risk for human beings and environment. An acceptable level of risk is obtained both with actions on the process itself (risk reduction) and with the use of special safety systems that switch the process into safe mode when a fault or an abnormal operation mode happens. These safety systems are today based on digital devices that communicate through digital networks. The IEC 61508 series specifies the safety requirements of all the devices that are involved in a safety function, including the communication network. Also electrical generation and distribution systems are processes that may have a significant level of risk, so the criteria stated by the IEC 61508 applies.**

Starting from this consideration, the paper analyzes the safety requirement for the communication network and compare them with the services of the communication protocol IEC 61850 that represents the most used protocol for automation of electrical plants. The goal of this job is to demonstrate that, from the technical point of view, IEC 61850 can be used for implementing safety-related functions, even if a formal safety certification is still missing.

Keywords—communication protocols, fieldbus, functional safety, IEC 61508, IEC 61850

I. Introduction

The automation system of an electrical generation or distribution system is today based on intelligent electronic devices (IED) connected through a digital network. Each intelligent device controls, protects, supervises, measures a section of the plant. In medium voltage switchgears we normally have an intelligent device per cubicle, in high voltage substations one or more per bay.

All the status signals, interlocks, closing or tripping commands are transmitted through the communication network. Some general purpose protocols can be used for communicating with intelligent devices (e.g. Modbus RTU, Ethernet TCP/IP and others), but also specific protocols for electrical plants exist, like the series IEC 60870 and DNP3. All these protocols can be effectively used for the configuration and the interrogation of the IEDs, and support all the functions that are typical of a SCADA (Supervisory, Control, And Data Acquisition). On the other hand, none of these protocols supports real-time functions, so they cannot be used for commands or interlocks. The only protocol that supports all the functions required for the substation automation is the more recent IEC 61850. It has services both for SCADA and for real time functions. With the use of IEC 61850, protection logic, safety interlocks, commands from real time functions (e.g. load-shedding) are transmitted digitally. Fig. 1 shows a typical architecture of the automation system in a substation, with different protocols used for different functions:

- IEC 61850 for real-time control
- IEC 61870 for remote control
- TCP/IP for remote maintenance
- USB for local set-up and commissioning

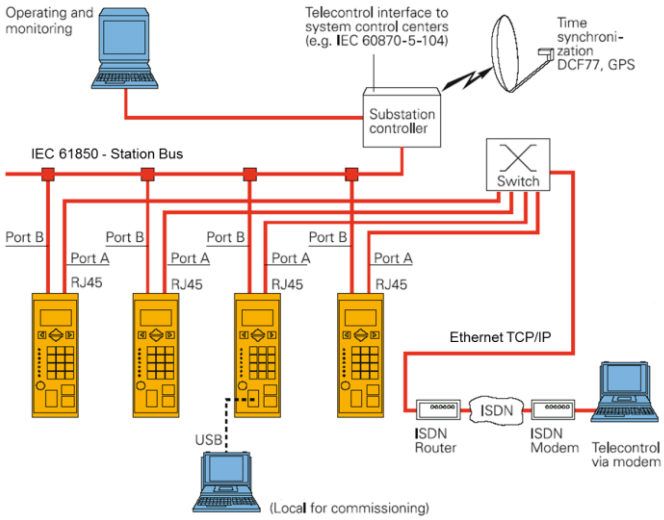

Fig. 1. Typical architecture for substation automation

With a full-digital architecture, also the commands related to safety functions are transmitted through the communication protocol. In electrical plants most safety commands lead to the de-energization of a circuit or a machinery (e.g. the emergency stop of a motor, fire alarm, etc.). In some cases, the safety electrical command is related to a risk of the process and requires the energization of a circuit (e.g. starting a ventilation fan in a tunnel, starting an emergency generator, switching from one source to another, etc.).

Fig. 2 shows an example of interaction between an emergency stop push button and the trip of one or more circuit breakers. When the button is pushed, the safety PLC receives the status through the safety fieldbus and sends a trip command to the station control unit on the IEC 61850 network. Then the trip command is sent on the IEC 61850 bus, normally via GOOSE message, to the IEDs that command the relevant circuit breakers.

The paper analyses the requirements of communication protocols when used for carrying out safety functions, with reference to the international standards series IEC 61508. The transmission mechanisms of IEC 61850 are then considered to check if it can be used for safety related functions.

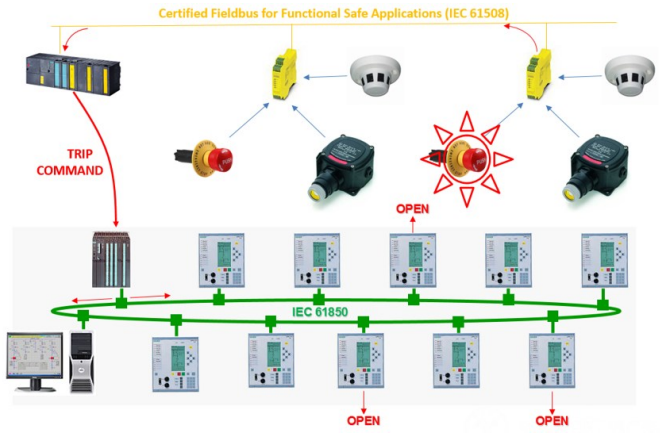

Fig. 2. Example of safety system interaction with IEC 61850

II. FUNCTIONAL SAFETY CONCEPTS

Safety is a concept dealing with the reduction of the risk of physical injury or of the damage to the people/environment health. The overall risk must be below the so-called acceptable risk. There are several concepts of safety, and this paper focuses on the functional safety, which involves the operation of the industrial processes or machineries.

Functional safety [1] is a part of the overall safety, and it is based on the principle that a system or equipment operates correctly in response to its inputs. Functional safety cannot be determined without considering the system as a whole and the environment with which it interacts.

A process or a machinery has an intrinsic level of risk. The risk is the probability of happening of a fault multiplied by the consequences of the fault, in terms of damages to people or to the environment. If the risk of a certain fault or malfunction is above the acceptable risk, it is necessary to introduce a safety related function to reduce it. Such a function has the role to intervene for avoiding the fault or for reducing the consequences of the fault; in other words, for reducing the risk below the level of acceptable risk. The safety related systems can be implemented using any technology, but there is the constraint to respect some requirement of integrity. This means that it is mandatory that any safety related system has an adequate integrity level for assuring the proper operation. Integrity is here intended as the probability that a specific function/system is properly working when requested. The required safety integrity level (SIL) of a safety function must be adequate to the risk of the process/machine malfunctioning. The higher the risk of a fault the higher the required SIL.

Today, most safety related functions use electrical and/or electronic and/or programmable electronic (E/E/PE) technologies. E/E/PE safety functions are regulated by the IEC 61508 series [2].

One of the concept within the IEC 61508 is the definition of safety function as the coordinated operation of some basic elements, like in Fig. 3:

- Sensors, that are responsible for measuring or detecting the abnormal operation,
- Analogic/digital conversion, if needed,
- Logic solver, within one Programmable Logic Controller PLC, that may be programmable or not. It is responsible for implementing the safety logic according to the inputs coming from the sensors,
- Analogic/digital conversion, if needed,
- Actuators, that are responsible for acting on the process to drive the overall system in a safe condition.

The concept and performance of SIL applies to the overall safety function, thus the Probability of Failure on Demand (PFD) of each component should be compliant to the requirements identified to achieve the requested PFD of the complete safety function. The IEC 61508 defines four level of SIL: from 1 to 4. The higher the SIL the lower the PFD for the safety function and the higher the reduction of the risk. Note that PFD is a value that indicates the probability of a system failing to respond to a demand. The average probability of a system failing to respond to a demand in a specified time interval is referred as PFDavg.

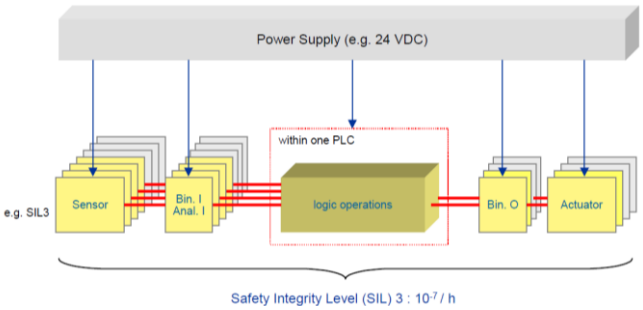

Fig. 3. Example of a safety function

TABLE I. VALUES OF PFD ACCORDING TO THE SIL VALUE

Safety integrity level (SIL)	Average probability of a dangerous failure on demand of the safety function (PFD_{avg})
4	$\geq 10^{-5}$ to $< 10^{-4}$
3	$\geq 10^{-4}$ to $< 10^{-3}$
2	$\geq 10^{-3}$ to $< 10^{-2}$
1	$\geq 10^{-2}$ to $< 10^{-1}$

Safety concepts are applied both to the hardware and to the software related to safety functions. This means that also the software should comply with the required PFD. The software is both the firmware and the specific application software. This is an important aspect also for the operation and the connections between the components of the safety function.

Traditionally, the connection between the field devices and the logic solver uses copper cables for transmitting ON/OFF or

4/20 mA signals. Today, with the wide use of digital communication networks there is the need of using digital communication protocols even for safety functions.

A communication system contains a hardware part (cables and communication chips) and a firmware part, responsible for the definition of the telegram, the technique for accessing the medium, the mechanism for transmitting, and so on. For safety applications, it is necessary that also the communication protocol comply with integrity requirements. IEC 61508 allows the use of digital communication protocol for safety functions, but it requires that methods are implemented to detect transmission errors. In a quantitative way, IEC 61508 requires that the communication system use no more than the 1% of the budget PFD for the safety function (see **Błąd! Nie można odnaleźć źródła odwołania.**).

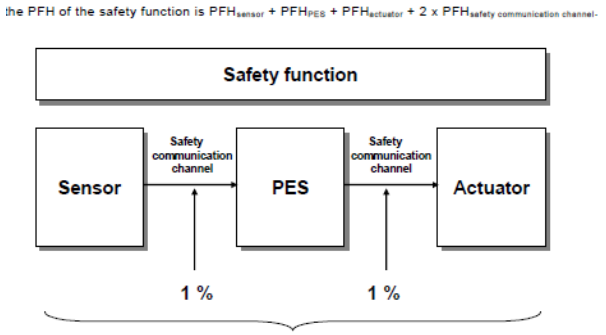

Fig. 4. Safety communication as a part of safety function

III. IEC 61850 BASICS

IEC 61850 is an Ethernet based protocol typical of electrical automation systems. Its main goal is to exploit the ability of IEDs from different manufacturers to exchange information used for protection, control and monitoring of an electrical substation. The standard defines this feature as interoperability [5].

The IEC 61850 series consists of ten parts that specify all the various aspects of communication into details. Section 7 is the core of the standard's innovative concepts. The standard defines all the devices and functions that exist in a substation, and it organizes them into a set of Logical Nodes. A LN has a four letters standardized name in which the first letter defines the class the LN belongs, i.e. protection, control or monitoring. LNs are the interface between the automation functions and the real world: the IED's manufacturer, following its own engineering practices, implements the function while the structure of data and data exchange are standardized.

Section 7.2 defines the information models and the information exchange service models (ACSI Abstract communication service interface). The information model consists on the definition of four elementary classes that can model any type of logic device [6]:

- **Server** – it represents the visible behavior of the device from the outside. A server's role is to manage communication with the client and send information to the other servers,
- **Logical Device (LD)** – it contains information managed and shared between different applications hosted in the same device. Homogeneous info are grouped into Logical Nodes,
- **Logical Node (LN)** – it contains the elementary data necessary for implementing the function the logical node refers to (i.e. overcurrent protection, measuring, breaker command, etc.),
- **Data** – it represents the value of interest with all the attributes that are used to describe it.

The ACSI comprises also the information exchange models needed to operate on data, which are:

- **Data sets** – used to group data,
- **Substitution** – supports replacement of a process value by another value,
- **Setting group control block** - permits to switch from one set of setting values to another one,
- **Report control block** - describes the model used to exchange information between a LN and a client. Report generation can be triggered by a change of a process data value,
- **Control blocks for generic substation event (GSE)** - describes the exchange of hard real-time information. It is used for information changing sporadically and it provides simultaneous delivery of the same message to multiple devices using multicast/broadcast frames. The principal information exchange model for time critical information like tripping function or interlocking is called Generic Object Oriented Substation Event (GOOSE),
- **Control blocks for transmission of sampled values** - used by measuring devices to send fast and cyclically analog sampled values,
- **Control** - describes the services that a client use to control an IED,
- **Time and time synchronization** - provides the time base to the substation automation system,
- **File transfer** - provides the exchange of large data.

IV. REMEDIAL MEASURES TO DETECT ERRORS AND FAILURES OF A COMMUNICATION SYSTEM

If used in a safety function, the communication system must implement specific measures to detect communication errors and failures [3]. This is mandatory in order to avoid that any error or fault compromises the proper operation of the safety function.

While IEC 61508 does not restrict the use of communication technologies, IEC 61784-3 [3] focuses on the use of fieldbus based functional safety communication systems. When using IEC 61158 [4] based fieldbus structures without modifications in the definition of each communication layer, all the measures necessary to implement transmission of safety data in accordance with the requirements of IEC 61508 shall be supported by an additional "safety communication layer".

Fig. 5 describes the so-called "black channel" approach. The communication protocol of the selected fieldbus is not affected by any additional safety service. All the safety functions are in an additional layer, the safety layer, which is above the 7th layer (application) of the protocol. The safety messages are embedded within the standard protocol.

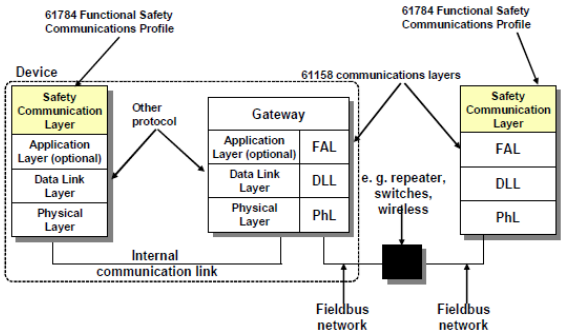

Fig. 5. Implementation of a safety layer over a standard fieldbus communication system

The role of the safety profile or layer is to detect all the possible errors that may lead to the loss or the corruption of the packets.

The safety data must satisfy the following requirements:

- Trusted data, the safety data must be correct,
- Correct receiver, the receiver of the data must be correct,
- Just in time, the data must receive the destination at a proper time.

The first step is to consider what are the possible errors in a digital communication system, as in IEC 61784:

- **Corruption**: Messages may be corrupted due to errors within a bus participant, due to errors on the transmission medium, or due to message interference,
- **Unintended repetition**: Due to an error, fault or interference, old not updated messages are repeated at an incorrect point in time,
- **Incorrect sequence**: Due to an error, fault or interference, the predefined sequence (for example natural numbers, time references) associated with messages from a particular source is incorrect,
- **Loss**: Due to an error, fault or interference, a message is not received or not acknowledged,
- **Unacceptable delay**: Messages may be delayed beyond their permitted arrival time window, for example due to errors in the transmission medium, congested transmission lines, interference, or due to bus participants sending messages in such a manner that services are delayed or denied,
- **Insertion**: Due to a fault or interference, a message is inserted that relates to an unexpected or unknown source entity,
- **Masquerade**: Due to a fault or interference, a message is inserted that relates to an apparently valid source entity, so a safety relevant participant, which then treats it as safety relevant, may receive a non-safety relevant message,
- **Addressing**: Due to a fault or interference, a safety relevant message is sent to the wrong safety relevant participant, which then treats reception as correct.

Starting from the list of the possible errors in the communication system, the IEC 61784 defines the measures that can be implemented in the communication stack in order to detect the errors and to set the system into a safe condition.

Proposed remedial measures are:

- **Sequence number**: A sequence number is integrated into messages exchanged between message source and message sink,
- **Time stamp**: In most cases the content of a message is only valid at a particular point in time. The time stamp may be a time, or time and date, included in a message by the sender,
- **Time expectation**: During the transmission of a message, the message sink checks whether the delay between two consecutively received messages exceeds a predetermined value. In this case, an error has to be assumed,
- **Connection authentication**: Messages may have a unique source and/or destination identifier that describes the logical address of the safety relevant participant,
- **Feedback message**: The message sink returns a feedback message to the source to confirm reception of the original message. This feedback message has to be processed by the safety communication layers,
- **Data integrity assurance**: The safety-related application process shall not trust the data integrity assurance methods if they are not designed from the point of view of functional safety. Therefore, redundant data is included in a message to permit data corruptions to be detected by redundancy checks,
- **Redundancy with cross checking**: In safety-related fieldbus applications, the safety data may be sent twice, within one or two separate messages, using identical or different integrity measures, independent from the underlying fieldbus. In addition to this, the transmitted safety data is cross-checked for validity over the fieldbus or over a separate connection source/sink unit. If a difference is detected, an error shall have taken place during the transmission, in the processing unit of the source or the processing unit of the sink.

In a safety communication profile errors must be detected and the methods for doing so are those described above. It is not mandatory to implement all the protection measures, since it is necessary to implement only the measures that can avoid all the possible errors.

IEC 61784-3 defines the correlation between the errors and the possible detection methods (Fig. 6).

Communication errors	Safety measures							
	Sequence number (see 5.4.2)	Time stamp (see 5.4.3)	Time expectation (see 5.4.4)	Connection authentication (see 5.4.5)	Feedback message (see 5.4.6)	Data integrity assurance (see 5.4.7)	Redundancy with cross checking (see 5.4.8)	Different data integrity assurance systems (see 5.4.9)
Corruption (see 5.3.2)					X [d]	X	Only for serial bus [c]	
Unintended repetition (see 5.3.3)	X	X					X	
Incorrect sequence (see 5.3.4)	X	X					X	
Loss (see 5.3.5)	X				X		X	
Unacceptable delay (see 5.3.6)		X	X [b]					
Insertion (see 5.3.7)	X			X [a]	X		X	
Masquerade (see 5.3.8)				X	X			X
Addressing (see 5.3.9)				X				

Fig. 6. Overview of the effectiveness of the various measures on the possible errors

Even when the messages are arriving in a correct (deterministic) manner the safety data still may be corrupted. Thus data integrity assurance is a fundamental component of the safety communication layer to reach a required safety integrity level. Suitable hash functions like parity bits, cyclic redundancy check (CRC), message repetition, and similar forms of message redundancy shall be applied.

Generally, the communication channel shall not use the same hash function the superimposed safety communication layer uses. The safety code shall be functionally independent from the transmission code.

The residual error rate is calculated from the residual error probability of the superimposed (safety) data integrity assurance mechanism and the transmission rate of safety messages. The number of destination sinks has to be considered for this calculation.

The value of admissible residual error is related to the SIL level of the safety function, like TABLE II. shows.

TABLE II. RELATIONSHIP OF RESIDUAL ERROR RATE TO SIL LEVEL

Applicable for safety functions up to SIL	Probability of a dangerous failure per hour for the functional safety communication system	Maximum permissible residual error rate for the functional safety communication system
4	$< 10^{-10}$ / h	$\Lambda < 10^{-10}$ / h
3	$< 10^{-9}$ / h	$\Lambda < 10^{-9}$ / h
2	$< 10^{-8}$ / h	$\Lambda < 10^{-8}$ / h
1	$< 10^{-7}$ / h	$\Lambda < 10^{-7}$ / h

NOTE Values in this table are based on the assumption that the functional safety communication system contributes no more than 1 % of the total failures of the safety function.

V. SAFETY ANALYSIS OF IEC 61850'S COMMUNICATION SERVICES

Protection and interlocking functions are the main applications that may require a functional safe communication system. These functions use the GOOSE model to exchange information.

GOOSE is based on a publisher/subscriber mechanism, and it uses a multicast transmission of data. If the value of one or more data configured in the GOOSE application changes, one IED (the publisher) sends a message to a group of IEDs (the subscribers) simultaneously within a single GOOSE message. In addition to the data, a GOOSE frame contains a set of parameters that describe the message itself (see Fig. 7).

IEC 61850-7-2 parameter		Parameter name
Attribute Name	Attribute Type	Argument
		Destination address
DatSet	ObjectReference	datSet
GoID	VISIBLE STRING	goID
GoCBRef	ObjectReference	gocbRef
T	TimeStamp	T
StNum	INT32U	stNum
SqNum	INT32U	sqNum
timeAllowedtoLive	INT32U	timeAllowedtoLive
Simulation	Boolean	simulation
ConfRev	INT32U	confRev
NdsCom	Boolean	ndsCom
GOOSEData	INT16U	numDatSetEntries
	Type depends on the number and types of the members in DatSet.	allData

Fig. 7. GOOSE service parameter mapping

In particular, GOOSE messages implement a time stamp parameter that contains the time at which one value configured in the data set has changed. At the same time, the parameter "state number" is incremented. This parameter represents a counter that increments each time a value change is detected within the data set, and a GOOSE message has been sent. The frame contains also a sequence number that increment each time a GOOSE message is sent. Time stamp, state number and sequence number are remedial measures against unintended repetition, incorrect sequence, loss, unacceptable delay, insertion errors as defined in section IV.

GOOSE data exchange allows the use of VLANs and priority tagging as defined in IEEE 802.1 Q. The use of VLANs permits defining the set of IEDs that shall receive the GOOSE message. This feature prevents a safety relevant information to be delivered to the wrong device and to cause unintended events or errors: it is a remedial measure against masquerade and addressing errors defined in [3].

The GOOSE message frame is terminated with a Frame Check Sequence. FCS field contains a number calculated from the data in the frame. The receiver calculates autonomously this number, and compares it with the number in the FCS field. If the numbers are different, the receiver knows that an error in the communication is occurred and it discards the corrupted frame.

Furthermore, GOOSE messages use a specific scheme of re-transmission to achieve the appropriate level of reliability (Fig. 8). When an event occurs, the GOOSE server generates a SendGOOSEMessage request and the current data set values are encoded in a GOOSE message. The GOOSE message is transmitted immediately and then retransmitted with a variable time interval (T_1, T_2, T_3) not defined by the standard and

gradually increasing the parameter "sequence number". An effective scheme of retransmission is based on an exponential increment of the time between the frames. The time interval increments until it reaches the retransmission stable time T_0 defined in the configuration of the GOOSE application as T_{max}. T_0 can be shortened by the event ((T_0) in Fig. 8). Each message in the retransmission sequence contains a timeAllowedToLive parameter that represents the time the receiver waits before the next retransmission. If the timeAllowedToLive expires, the receiver reports a communication problem, and the system should be switched in a safe mode. The retransmission mechanism explained can be used as a time expectation measure defined in section IV.

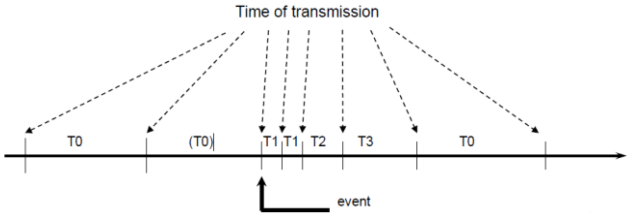

Fig. 8. Transmission time for events

VI. Conclusion

All the safety buses existing today use the "black channel" approach to detect communication errors. IEC 61850 does not implement any form of safety communication channel (black channel) as required by IEC 61784-3. However, the analysis made in section V reveals that the standard natively implements a bunch of remedial measures to detect all the communication errors defined by IEC 61784 [3]. The problem is that the standard does not define what must be done when a communication error is detected. If the communication between two IEDs fails, the system has to switch in a safe condition. It is reasonable to think that, for electrical plants, the safe state is considered a circuit de-energized. A possible solution is to implement in the 61850 stack the functions energize-to-trip and de-energize-to-trip. Another possible solution is to configure the IED to switch the system in safe mode when a communication error is detected using the IED's configuration tool. The two solutions present a significant difference considering a hypothetical safe certification process. Implementing functions in the 61850 stack means that the stack should be certified compliant to the IEC 61508 standard; on the other hand, if a configuration software is used to program one or more safety function in a device, the software itself should be certified.

While this work focuses on IEC 61850 communication protocol, it is also important to remember that SIL's concepts applies to all the hardware and the software that compose the safety system. This means that not only the communication protocol should be certified, but also all the IEDs and circuit breakers that compose the safety chain.

Further analysis will be made on a typical safety function that uses IEC 61850 as communication protocol. This will be useful to understand if IEC 61850 can satisfy the requirement of IEC 61508 about the maximum use of 1% of the budget PFD for a typical safety function and to estimate what is the maximum possible Safety Integrity Level of a safety system that uses a communication network based on IEC 61850.

References

[1] IEC 61508-0 "Functional safety of electrical/electronic/programmable electronic safety-related systems – Part 0: Functional safety and IEC 61508", 2010

[2] IEC 61508-1 "Functional safety of electrical/electronic/programmable electronic safety-related systems – Part 1: General requirements", 2010

[3] IEC 61784 "Industrial communication networks – Profiles – Part 3: Functional safety fieldbuses – General rules and profile definitions"

[4] IEC 61158 series "Industrial communication networks – Fieldbus specifications", 2014

[5] IEC 61850-1 "Communication networks and systems for power utility automation – Part 1 Introduction and overview", 2013

[6] IEC 61850-7-2 "Communication networks and systems for power utility automation – Part 7-2: Basic communication structure – Abstract communication service interface (ACSI)", 2010

[7] IEC 61850-8-1 "Communication networks and systems for power utility automation – Part 8-1: Specific communication service mapping (SCSM) – Mappings to MMS (ISO 9506-1 and ISO 9506-2) and to ISO/IEC 8802-3"

[8] K-P Brand, M.Ostertag, "Safety related, distributed functions in substations and the standard IEC 61850", 2003 Bologna Power Tech Conference, June 23th-26th, Bologna, Italy

[9] J. Hoyos, M. Dehus and T. X. Brown, "Exploiting the GOOSE Protocol: A Practical Attack on Cyber-infrastructure", Proc. 2012 IEEE Globecom Workshops, pp. 1508-1513

Modification of Duval Triangle for Diagnostic Transformer Fault through a Procedure of Dissolved Gases Analysis

Sobhy S. Dessouky [A], Ahmed E.Kalas [B], R.A.Abd El-Aal [C], Abdel Moneim M. Hassan [D]
[A, B, C] Electrical Engineering Dept. Faculty of Engineering, Port-Said University. Port Said, Egypt
[D] Abo-Sultan Steam Power Plant, Ismailia. Egypt

Abstract— **Dissolved gas-in-oil analysis (DGA) is a sensitive and dependable technique for the detection of incipient fault condition within oil-immersed transformers. When the mineral oil is subjected to high thermal or/and electrical stresses, it decomposes and, as a result, gases are generated.**

This paper presents modification of Duval triangle DGA diagnostic graph to numerical method that is easy to use for diagnosing and a Matlab program. To study such as the following evaluation. This evaluation is carried out on DGA data obtained from three different groups of transformers each group are two identical transformers. A Matlab program was developed to automate the evaluation of Duval Triangle graph to numerical modification, Also the fault gases can be generated due to oil decomposing effected by transformer over excitation which increasing the transformer exciting current lead to rising the temperature inside transformer core beside the other causes.

Index Terms— **Dissolved Gas Analysis (DGA), mineral oil, decomposition, degradation, and transformer condition**.

I. Introduction

Dissolved gas analysis (DGA) is a popular diagnostic technique that is used to detect incipient faults in oil-filled power transformers [1]. By using DGA data, transformer criticality can be identified with proposing the proper maintenance action [2].

Several methods were proposed to diagnose incipient faults based on DGA. These methods are key gas method, Rogers's ratio methods, Duval triangle method, Doernenburg Ratio method, Basic Gas Ratio, and artificial intelligence based methods.

The key gas method identifies the key gas for each type of fault and uses the percent of this gas to diagnose the fault as suggested by IEEE standard C57.104 [3]. The percent amount of gas is obtained in terms of the total combustible gases (TCG). The main disadvantage of this method is that the interpretation by the individual gases is difficult in practice since each incipient fault produces traces of other gases in addition to the key gas of such fault. The ratio methods for fault diagnosis use certain ratios of dissolved gas concentrations according to combinations of codes [4, 5]. An incipient fault is detected when a code combination matches with the code pattern of the fault. The most widely used ratio methods are the Doernenburg Ratio Method, Rogers Ratio Method, and IEC standard. Six gas ratios have been used by different methods. The major drawback of ratio methods is the "no decision" problem associated with some cases that lie out of the specified codes.

In recent years, many researchers have studied the application of artificial intelligence based techniques for transformer fault diagnosis. These techniques include expert systems, fuzzy logic, artificial neural networks or mixed techniques [6, 7]. However, these methods are too complicated to be implemented practically on a wide range.

This paper investigates the new aspects, accuracy and consistency of these methods in interpreting the transformer condition.

II. DGA TO DIAGNOSE TRANSFORMER FAULTS

When an incipient fault occurs, either thermal or/and electrical, a number of gases are generated and dissolved into the oil. These gases are mainly H_2, CH_4, C_2H_2, C_2H_4 and C_2H_6. In addition CO and CO_2 will exist if cellulose degradation is involved, based on the type and amount of generated gases [1, 8-9].

A. Duval Triangle (DGA) Diagnostic Graph Method

M. Duval. Proposed another diagnostic method to overcome this limitation, well known as Duval triangle. This method is based on a triangle graphical representation to visualize the different cases for oil-insulated high-voltage equipment (mainly transformers), Fig. (I) provides a graphical method of identifying a fault. It uses a three-axis coordinate

Sobhy S. Dessouky, Electrical Engineering Dept. Faculty of Engineering, Port-Said University. Port Said, Egypt (e-mail: sobhyserry@yahoo.com).
Ahmed E.Kalas , Electrical Engineering Dept. Faculty of Engineering, Port-Said University. Port Said, Egypt (e-mail: kalas_14@yahoo.com).
R.A.Abd El-Aal, Electrical Engineering Dept. Faculty of Engineering, Port-Said University. Port Said, Egypt (e-mail: ramadanhv@yahoo.com).
Abdel Moneim M. Hassan, Abo-Sultan Steam Power Plant, Ismailia. Egypt (e-mail: abdelmoname333@yahoo.com).

system, where concentrations of CH_4, C_2H_4 and C_2H_2 are used as coordinates, and the likely fault falls within one of the fault regions of the triangle. The various regions within the Duval Triangle are given in Table (I) [10-13].

For example if C_2H_2 = 0.07, CH_4 = 0.2 and C_2H_4 = 0.73. The fault diagnostic is T3 (Thermal fault t > 700 °C), and if C_2H_2 = 0.36, CH_4 = 0.32 and C_2H_4 = 0.32, the fault diagnostic is D2 (High-energy electrical discharge), as shown in fig (I).

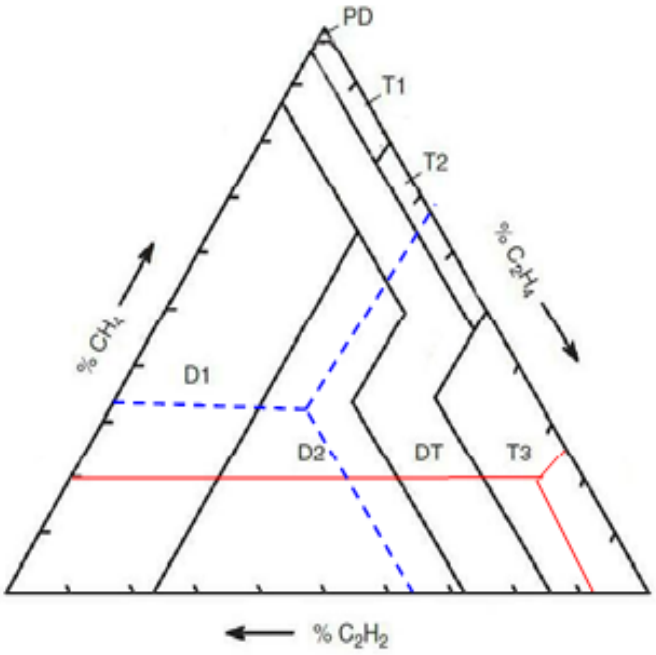

Fig. 1. Duval Triangle

TABLE I. FAULT CODE

PD	Partial discharge
T1	Low-range thermal fault (below 300 °C)
T2	Medium-range thermal fault (300-700 °C)
T3	High-range thermal fault (above 700 °C)
D1	Low-energy electrical discharge
D2	High-energy electrical discharge
DT	Indeterminate - thermal fault or electrical discharge.

A. Duval Triangle Graph to Numerical Method

In this paper, we developed A Matlab program to automate the evaluation of Duval Triangle graph to numerical modification. Table (II) shows the Modification of Duval triangle DGA diagnostic graph to numerical method.

For example if C_2H_2 = 0.1, CH_4 = 0.3 and C_2H_4 = 0.6. We can use table (II) easy to determine the fault Diagnostic (Thermal fault t > 700 °C), and if C_2H_2 = 0.36, CH_4 = 0.32 and C_2H_4 = 0.32, the fault diagnostic is (High-energy electrical discharge), the same results as in the previous example.

TABLE II. MODIFICATION OF DUVAL TRIANGLE (DGA) DIAGNOSTIC GRAPH TO NUMERICAL METHOD

C2H2%	CH4%	C2H4%	Fault
0.00 - 0.02	0.98 - 1.00	0.00 - 0.02	Partial discharge (electrical fault)
0.00 - 0.04	0.46 - 0.80	0.20 - 0.50	Thermal fault 300 < t < 700 °C
	0.76 - 0.98	0.02 - 0.20	thermal fault t < 300 °C
0.00 - 0.15	0.00 - 0.50	0.50 - 1.00	Thermal fault t > 700 °C
0.04 - 0.13	0.47 - 0.96	0.00 - 0.40	Mixtures of thermal and electrical faults
0.13 - 0.29	0.21 - 0.56	0.40 - 0.50	
0.15 - 0.29	0.00 - 0.35	0.50 - 0.85	
0.13 - 0.29	0.31 - 0.64	0.23 - 0.40	Discharge of high energy (electrical fault)
0.29 - 0.77	0.00 - 0.48	0.23 - 0.71	

III. CASE STUDY DISSOLVED GAS ANALYSIS

The case study carried out from three different groups of transformers each group are identical in Abu-Sultan steam power plant. Fig. (2) Shows the schematic diagram configuration for transformers under testing. The first group of transformers are three single phase 192 MVA, 15/220 KV, Off L.T.C. The Second group of transformers are three phase 16 MVA, 220/6.3KV, ON.L.T.C, and the third group of transformers are three phase 16 MVA, 15/6.3/6.3 KV, ON.L.T.C. The rating and (DGA) testing results for the above-mentioned Power Transformer are shown in tables (III, IV).

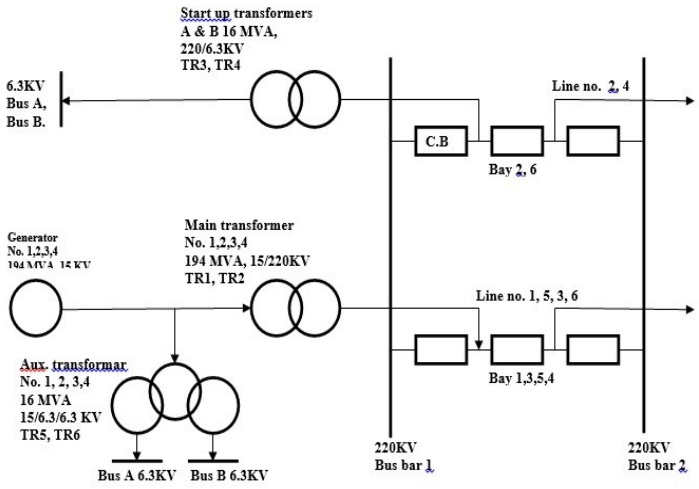

Fig. 2. Schematic Diagram for Transformers under Evaluation

TABLE III.
RATING OF POWER TRANSFORMER UNDER TESTING

Transformer Name	Operating Date	Rated Power MVA	Rated Voltage KV	Number Of Phases	Oil Type
Main transformer Unit no. 1 (TR_1)	19/3/1983	192	15/220	3 single Phase	Mineral Oil Naphthenic
Main transformer Unit no. 2 (TR_2)	15/8/1983				
Start Up transformer A (TR_3)	19/3/1983	16	220/6.3	3- Phases	
Start Up transformer B (TR_4)	15/10/1984				
Aux. transformer unit no. 1 (TR_5)	19/3/1983	16	15/6.3/6.3	3- Phases	
Aux. transformer Unit no. 2 (TR_6)	15/8/1983				

IV. DIAGNOSTIC METHOD USED BY MODIFICATION SYSTEM.

The diagnostic methods for DGA are used by a numerical method, The Matlab program diagnoses output for the under testing transformers. Table (V) shows application of the faults diagnosed by various methods, which indicate that all transformers are thermal faults.

V. RESULTS AND DISCUSSION

Comparison of various methods as shown in the table (V), a thermal fault in oil within all transformers is diagnosed for all five methods. Where winding temperature do not exceed 95°C and oil temperature do not exceed 85°C for all transformers during normal operation. Moreover, the possible collapse of cooling system during operation in this case is too small and there is no increase in the viscosity of the oil, as it is clear in the results of chemical analysis of samples oil and no wax materials. However, there is an important factor is the increased over excitation due to reduction of generator speed when some of the generating units from the network goes out during normal operation or the frequency disturbances that occur when large loads are connected to the electrical network system.

Over-excitation or/and under frequency protection may be or may be not operate depends on the response of power system control. The under frequency relay operate at 47.5 Hz with time lag 0.5 sec and over excitation relay operate at V/Hz = 1.1pu for 45 sec time lag or V/Hz =1.18 pu for 2 sec time lag at generators.

TABLE IV.
(DGA) TESTING RESULTS

Transformer & Samples date			Main transformer unit no. 1 ph (B) from 08/05//2013 to 27/11/2013	Main transformer unit no. 2 ph (B) from 08/05/2013 to 05/11/2014	Start Up transformer A from 08/05/2013 to 06/05/2014	Start Up transformer B from 07/04/2013 to 27/11/2013	Aux. transformer unit no. 1 from 08/05/2013 to 29/03/2015	Aux. transformer unit no. 2 From 07/04/2013 to 02/04/2014
Total combustible gases (T.C.G) without C3H6 & C3H8			274 477	164 592	98 249	219 426	246 429	193 400
Hydrogen	Combustible gases	H_2	9 7	3 16	1 19	5 6	14 28	7 35
Hydrocarbons		CH_4	25 48	15 37	2 4	19 61	48 49	9 12
		C_2H_2	0 0	0 0	0 0	0 0	0 0	0 0
		C_2H_4	5 2	1 12	2 8	5 6	3 10	2 3
		C_2H_6	12 29	10 50	1 3	57 142	28 45	2 3
		C_3H_6 & C_3H_8	14 26	5 -	2 3	30 81	14 -	2 3
Carbon Oxides		CO	223 392	135 477	91 215	132 212	154 297	173 348
	Non-Combustible gases	CO_2	2877 6052	775 4854	482 1324	848 1772	1632 3787	439 2581
Non-fault or atmospheric gases		O_2	2042 2664	1633 3758	3432 5766	991 1911	1420 13615	1118 3300
		N_2	31551 38801	45633 90526	39302 56161	74493 88856	82762 137375	\ 30606 119152

TABLE V.
APPLICATION OF THE FAULT DIAGNOSED BY VARIOUS METHODS

Transformer no.	Duval's triangle numerical modified P(96/4)	Basic gas ratio P(77/8)	Doernenburg ratio P(71/3)	Rogers Ratio P(62/5)	Kay gas P(42/58)
TR1	thermal fault t < 300°C	thermal fault t < 300°C	thermal decomposition	slight overheating t <150 °C	pyrolysis in cellulose
TR2	Thermal fault 300 < t < 700 °C	thermal fault t < 300°C	thermal decomposition	slight overheating 150-200 °C	pyrolysis in cellulose
TR3	Thermal fault t > 700 °C	thermal fault of low temperature t <150°C	Cannot be applicable	general conductor overheating	pyrolysis in cellulose
TR4	thermal fault t < 300 °C	thermal fault t < 300°C	thermal decomposition	slight overheating 150-200 °C	pyrolysis in cellulose
TR5	Thermal fault t > 700 °C	thermal fault t < 300°C	thermal decomposition	Cannot be applicable	pyrolysis in cellulose
TR6	Thermal fault 300 < t < 700 °C	Cannot be applicable	Cannot be applicable	general conductor overheating	pyrolysis in cellulose

If frequency decreases and the voltage is constant, the transformer core is heated. Fig. (3) Shown voltage, current and frequency of generating unit transformer number one at Abu-sultan steam power plant from 17/5/2015 to18/5/2015, which indicate that frequency, reduced to 49.2 Hz at voltage 14.85. KV.

The rated generator voltage and frequency is 15 KV and 50Hz respectively. So generator is over excitation =1.0061 Pu. At unit, start up the voltage may be built to 15KV at generator frequency 48 Hz then 1.042 Pu over-excitations. Disturbance in frequency is repeated from 18/5/2015 to 20/5/2015 in power system as shown in Fig. (4) and affect all network transformers in this moment and there is an instantaneous decrease in power system frequency to 45.36 Hz without operate under frequency or/and over-excitation relays because disturbance duration less than 0.5 sec as shown in Fig. (5).

Transformers require an internal magnetic field to operate. The core of a transformer is designed to provide the magnetic flux Necessary for rated load.

An over-excitation condition occurs when this equipment is operated such that flux levels exceed design values. The voltage output of a transformer is a function of the rate of change of the flux and the number of turns in the output winding. $e = N\, d\varphi/dt$ during normal power system operation.

The voltage is sinusoidal and the rate of change is determined by the frequency, which is in turn determined by generator speed [14].

The equation shows core flux to be directly proportional to voltage and inversely proportional to frequency $\varphi \alpha V/f$. The actual magnitude of flux in transformer core is can be quantified in terms of per unit volts / Hertz.

A generator or transformer operating at no load with rated voltage and frequency would have one per unit excitation. The same equipment operating at rated voltage and 95% frequency would have 1.0/0.95 = 1.05 Pu flux or 1.05 Pu excitation.

Over-excitation will result from high voltage at rated frequency and from rated voltage with low frequency.

Because over excitation is a function of voltage and frequency, it can occur without notice. Transformers and generators can be subject to repeated over excitation by inappropriate operating.

The practices or operator error without a disruption to operations. The resulting thermal faults lead to oil decomposing to generate fault gases H_2, CH_4 at temperature 120°C, C_2H_6 at temperature 150°C, C_2H_4 at temperature 300°C, and C_2H_2 at temperature 700°C.

In addition, degradation of insulating material is cumulative. A transformer or generator that survives a serious over excitation event or many small events may fail because of a moderate event during normal service as all transformers under study.

In addition, if voltage increased, at rated frequency, the exciting current increases, as shown in Fig. (6). So Tr_1 through Tr_6 are effected by over excitation due to network normal operation but Tr_1, Tr_2,Tr_5, Tr_6 are effected by Over excitation damage usually occurs during periods of off-frequency operation such as start up or shut down for unit transformer as shown in Fig.(2) and table (VI).

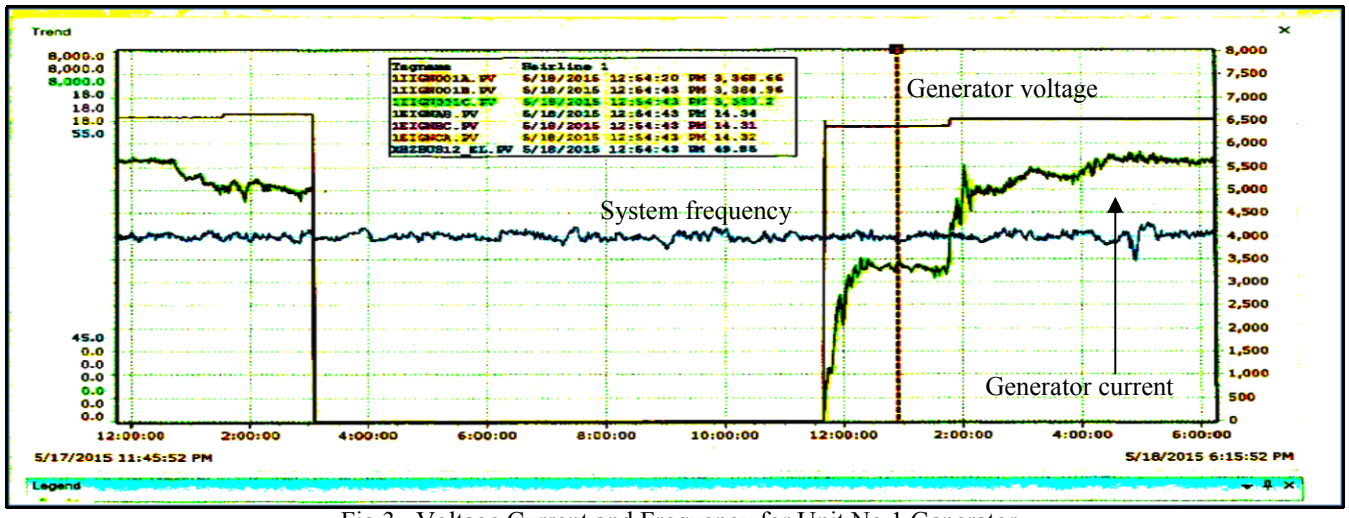

Fig 3. Voltage Current and Frequency for Unit No.1 Generator

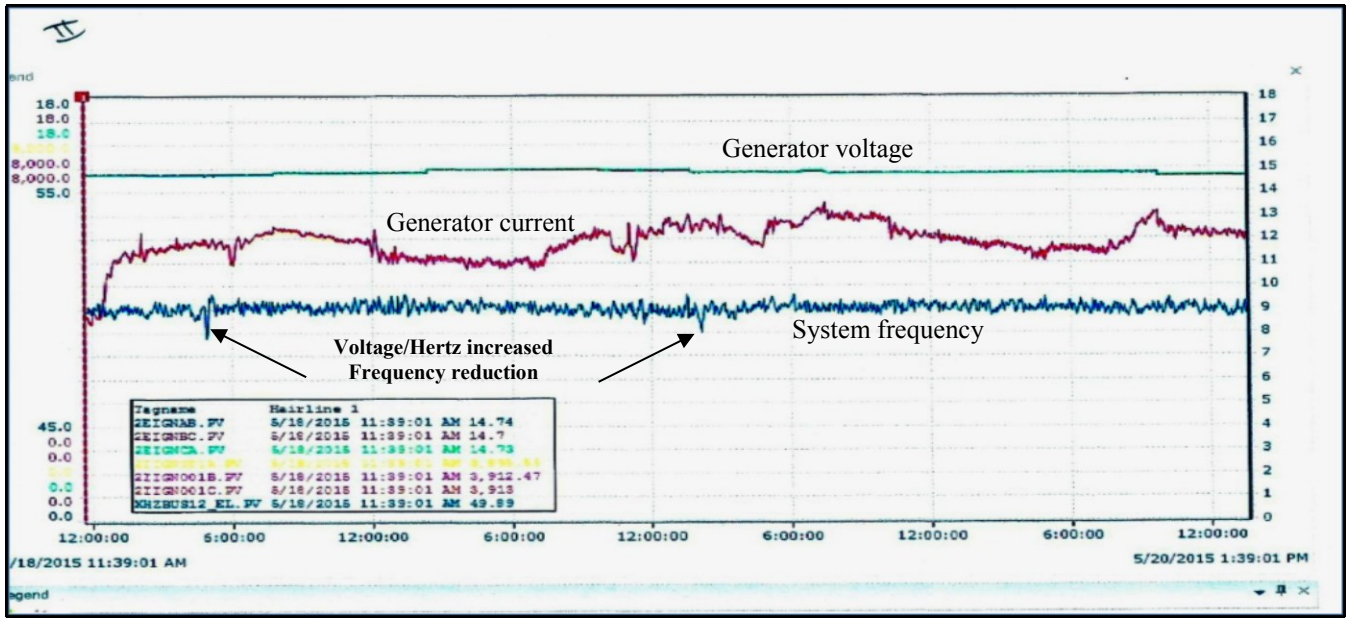

Fig 4. Repeating Disturbances in Power System Frequency

Fig 5. Instantaneous Decrease in Power System Frequency

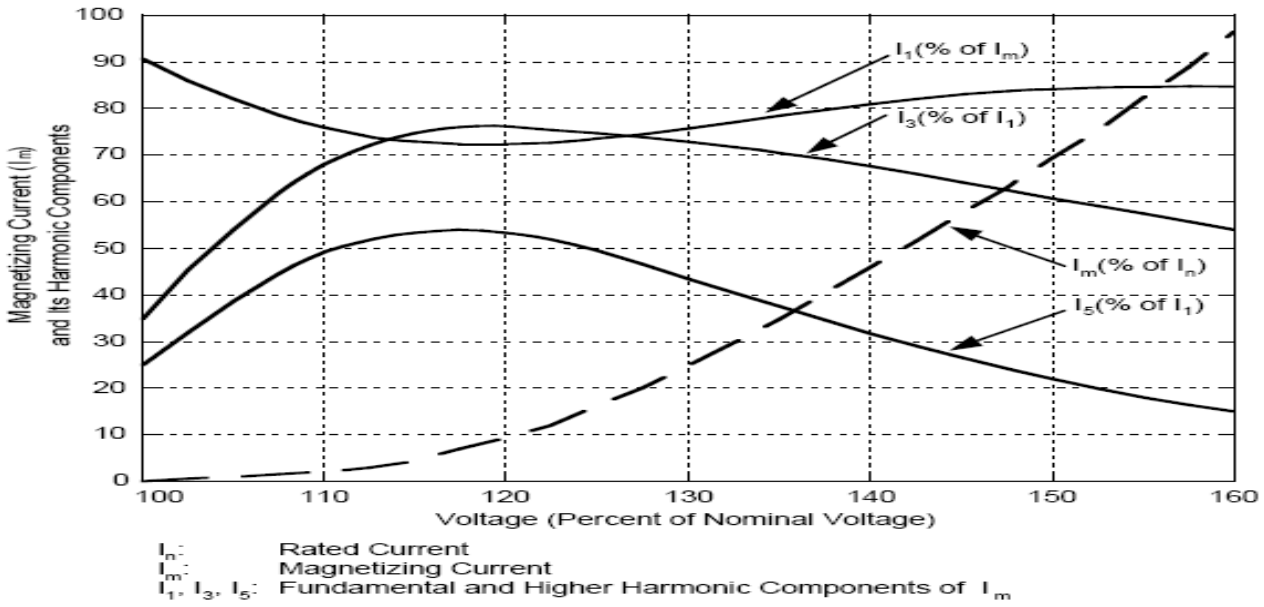

Fig 6. Voltage Increased, at Rated Frequency Exciting Current Increase

TABLE VI.
CAUSES OF THERMAL FAULTS, NORMAL AND ACCELERATED AGING

				Tr1	Tr2	Tr3	Tr4	Tr5	Tr6
Normal aging due to dynamic load cycle	Over Temperature	Fault currents							
		Overload &Unbalanced load							
		Cooling system failure							
		Increased Oil viscosity							
	Over excitation	Unit startup	maintain the set point voltage at low frequency	X	X			X	X
		Unit shutdown	field breaker fails to open when the generator trips	X	X			X	X
		Over Voltage At rated frequency	The charging current for a high-voltage transmission line.	X	X	X	X	X	X
		Power system disturbance	Loss of some units During operation or suddenly heavy load	X	X	X	X	X	X
Accelerating aging	normal operating Temperature 80 - 120 °C.	Moisture	Oxidation of the insulation and oils forms acids, Acid attacks cellulose and accelerates insulation degradation, with moisture (PD) Electrical stress can occur and more insulation degradation						X
		Oxygen							X
		Acidity							X

VI. CONCLUSION.

Modification of Duval triangle DGA diagnostic graph to numerical method is easy to use for diagnoses and a Matlab program. Transformer thermal faults during dynamic load cycle due to temperature increase from over load, cooling system failure or trouble, fault currents and /or over excitation condition.

Over excitation, damage usually occurs during periods of off-frequency operation such as start up or shut down for unit transformer. In addition, the fault gases can be generated due to oil decomposing effected by transformer over excitation.

Transformers and generators can be subject to repeated over excitation by inappropriate operating practices or operator error without a disruption to operations. It's can be concluded also, the resulting thermal faults lead to oil decomposing to generate fault gases H2, CH4 at temperature 120°C, C2H6 at temperature 150°C, C2H4 at temperature 300°C, and C2H2 at temperature 700°C.

The gas type and gas quantity depends on the intensity and duration of Over-excitation. Transformer diagnostic thereby results depends on the events inside evaluation interval or before evaluation time.

REFERENCES

[1] T. K. Saha, "Review of modern diagnostic techniques for assessing insulation condition in aged transformers", IEEE Transactions on Dielectrics and Electrical Insulation, Vol. 10, pp. 903-917, 2003.

[2] A. Abu-Siada and S. Islam, "A new approach to identify power transformer criticality and asset management decision based on dissolved gas-in-oil analysis", IEEE Transactions on Dielectrics and Electrical Insulation, Vol. 19, pp. 1007-1012, 2012.

[3] "IEEE guide for the interpretation of gases generated in oil-immersed transformers", IEEE Standard C57.104-2008, 2009.

[4] M. J. Heathcote, the J & P Transformer Book, Twelfth Edition, Reed Educational and Professional Publishing Ltd, 1998.

[5] S. M. Islam, T. Wu and G. Ledwich, "A novel fuzzy logic approach to transformer fault diagnosis", IEEE Transactions on Dielectrics and Electrical Insulation, Vol. 7, pp. 177-186, 2000.

[6] M. A. Izzularab, G. E. M. Aly and D. A. Mansour, "On-line diagnosis of incipient faults and cellulose degradation based on artificial intelligence methods", IEEE International Conference on Solid Dielectrics (ICSD), pp. 767-770, 2004.

[7] Md Umar Farooque, Shufali Awani,Shakeb akan "Artificial neural network (ANN) based implementation of Duval pentagon"2015 International Conference on condition assesment techniques in electrical systems (CATCON) pp 46-50, 2015.

[8] Diaa-ELdin A.Monsour "-Development of a new graphical technique for dissolved gas analysis in power transformers based on the five combustible gases"IEEE Transactions on Dielectrics and Electrical Insulation, Vol. 22, pp. 2507 - 2512, 2015.

[9] Alamuru Vani and Pessapaty Sree Rama Chandra Murthy" Hybrid diagnosing techniques for analyzing dissolved gases in power transformers " ISSN 2006 - 9790, pp 33-34, 2015.

[10] M. Duval, "A review of faults detectable by gas-in-oil analysis in transformers", IEEE Electrical Insulation Magazine, Vol. 18, pp. 8-17, 2002.

[11] Nitin K. Dhote1 and Jagdish B. Helonde" Fuzzy Algorithm for Power Transformer Diagnostics" Academic Editor: M. Onder Efe, pp 1-2, 2013.

[12] Stefan Tenbohlen , Sebastian Coenen , Mohammad Djamali " Andreas Müller Diagnostic Measurements for Power Transformers" Academic Editor: Issouf Fofana, Energies, pp 2, 2016.

[13] Sherif S.M.Ghoneim , Ibrahim B.M.Taha , Nagy I.Elkalashy "Integrated ANN-Based Proactive Fault Diagnostic Scheme for Power Transformers Using Dissolved Gas Analysis" IEEE Transactions on Dielectrics and Electrical Insulation, Vol.23,No 3 , pp1838-1845, 2016

[14] L.G Hewitson "Protective Relaying for Power Generation Systems" Book Taylor & Francis Group, Publishing Ltd 2006.

Sobhy Serry Dessouky was born in Dakahlie of Egypt in 1946. He received the B.Sc. degree (1970) and M.Sc. (1977) in electrical engineering from Suez Canal University in Helwan University respectively. Dr. Dessouky received the Ph. D. degree from TU, Dresden, German in 1982. From Oct. 1970 to 1975, he was Joined Faculty of Engineering, Suez Canal University, as Demonstrator. He worked as Demonstrator from 1975-1977 in Faculty of Engineering, Helwan University. In 1977, he worked as lecturer assistant in Electrical Engineering Department, Faculty of Engineering, Suez Canal University. From 1983 to 1987, he worked as Assistant Professor (Lecturer), in Electrical Engineering Department, faculty of Engineering, Suez Canal University, Port Said Campus. In 1987, he promoted as Associate Professor in the same Department. In 1991, Dr. Dessouky became a full Professor of Electrical power and H.V Engineering. He was a member in IEEE from 1996. In parallel, he worked as a department chair, Vice Dean for Community Affairs and Environment, and Director of Engineering Research Center for Developing and Technological Planning in Suez Canal University.

Ahmed E.Kalas received the B.Sc. degree in electrical engineering from the Suez Canal University with honor first rank in EGYPT 1982, M.Sc. degree (Power electronic and electrical Drives), from the Suez canal university, EGYPT 1987, ph. D. degree (Power electronic and electrical Drives) from Gdansk university, POLAND 1994 From 1994 up to 2010 he worked as a lecture in electrical engineering at Suez canal university, from 2010 up to now he worked as a lecture in electrical engineering at port said university research contributions, as well as his on-going efforts/investigations in the area of AC drives and power electronics, can be classified into the following topics:

Control of electric machines; Vector control, nonlinear control, adaptive control, model predictive control, double feed induction motors ,DTC -Power electronic converters, two-level and multilevel, matrix converter, ZS-Artificial Intelligence in machines and power electronics control, Fuzzy logic, neural networks -Renewable energy conversion for PV and wind systems, maximum power point tracking -Fault detection Diagnosis in electrical machines and drives.

R.A.Abd El-Aal was born in Egypt, 1971. He received the B.Sc. degree (1996) and M.Sc. (2002) in electrical engineering from Suez Canal University. He received the Ph. D. degree in H.V Engineering from Port Said University in 2008. He works as lecture in electrical engineering Dept., Port Said University, Egypt. His research interests are H.V Engineering and power system protection.

Abdel Moneim M. Hassan. was born in Ismailia of Egypt in 1963. He received the B.Sc. degree (1986) in electrical engineering from Helwan University. He works as General Manager in Abu Sultan steam power plant 4*150 MW, from 1988 to 1998, He worked in operation department as operation engineer in Abu Sultan power plant, from 1998 to 2014, He worked as electrical maintenance, measuring and protection engineer in the same plant.

A Review of LCC-HVDC and VSC-HVDC Technologies and Applications

Oluwafemi E. Oni, Kamati I. Mbangula, and Innocent E. Davidson

***Abstract*—High Voltage Direct Current (HVDC) systems has been an alternative method of transmitting electric power from one location to another with some inherent advantages over AC transmission systems. The efficiency and rated power carrying capacity of direct current transmission lines highly depends on the converter used in transforming the current from one form to another (AC to DC and vice versa). A well-configured converter reduces harmonics, increases power transfer capabilities, and reliability in that it offers high tolerance to fault along the line. Different HVDC converter topologies have been proposed, built and utilised all over the world. The two dominant types are the line commutated converter LCC and the voltage source converter VSC. This review paper evaluates these two types of converters, their operational characteristics, power rating capability, control capability and losses. The balance of the paper addresses their applications, advantages, limitations and latest developments with these technologies.**

***Index Terms*—Commutation failure, HVDC, line commutated converter, modular multilevel converter, voltage source converter.**

I. INTRODUCTION

The first electric generator was DC machine, as well as the first electric power transmission system by Thomas Edison [1, 2]. In the last few decades, High Voltage Direct Current (HVDC) technology has been used, due to some of its inherent benefits in long distance transmission application. It is widely used all over the world for bulk power delivery over long distances, interconnections of asynchronous systems, stability of AC lines, power control, long submarine transmission and renewable energy integration. Reduction in the right of way (ROW) is another edge over AC systems [3].

HVDC transmission system involve the use of converter for the conversion of AC to DC (rectifier) at the transmitting end, and converting the DC back to AC at the receiving end (inverter), [4]. This converter usually has a 12-pulse arrangement, of valves connected in a star-delta, star-star formation to the AC networks. A reactor, dc capacitor and AC filters are also part of the converter circuitry. The two ends of the converters are connected via DC transmission lines which can be either overhead cable or submarine cable or directly in the same location as in the case of back-to-back configuration. Continuous progress in HVDC systems is linked to advances in the power electronics technologies for the fabrication of highly efficient semiconductor devices for HVDC converter topology [5].

There are two dominant methods used in converting AC to DC and vice versa. These methods are the Line commutated converter LCC and the voltage source converter VSC. The success of these two technologies became possible with the development of power electronics devices [6, 7]. Before the power electronics was the transverter, electrolytic and the atmospheric converter, all these are part of the several attempts made for AC/DC conversion. These entire attempts failed due to some technical reasons and safety measures inherent in using them [8].

The invention of mercury-arc valves brought temporary success to AC/DC conversion which later became outdated. The mercury arc valve which operated then have either been scrapped or upgraded to semiconductor converter technology [9]. Semiconductors devices have been in used since 1970s and are still a growing technology because of the high switching capacity and ability to withstand high current rating. Examples are the diode, diac, triac, thyristors, MOS-controlled thyristors (MCTs) [10], insulated-gate bipolar transistors (IGBT) and integrated gate-commutated thyristors (IGCTs) etc. [11].

This paper looks critically into the two dominant HVDC converter technologies taking into consideration their operational characteristic and their output AC waveform when subjected to three-phase short circuit as well as dc line fault. The simulation is carried out on DigSILENT Powerfactory and the results of each technology are compared alongside each other.

II. CONVERTER CONFIGURATION AND TOPOLOGY

HVDC interconnections can be configured in different forms to suit different desired performance and operational

This paper was submitted for review on July 28, 2016 and accepted on September, 9, 2016. This work was supported by Eskom Power Plant Engineering Institute, Eskom Centre of Excellence in University of KwaZulu-Natal. Westville campus, South Africa.

O. E Oni is with Electrical Engineering Department, University of KwaZulu-Natal. Durban 4041, South Africa (e-mail: maxiphem@yahoo.com).

K. N. I. Mbangula was with Department Electrical Engineering, University of KwaZulu-Natal. Durban 4041, South Africa. He is now with the Department of Electrical Engineering, University of Namibia. Ongwediva 3624, Namibia (e-mail: imbangula@unam.na).

I. E. Davidson was with Department of Electrical Engineering, University of KwaZulu-Natal. Durban 4041, South Africa. He is now with the Department of Electrical Power Engineering, Durban University of Technology. Durban 4001, South Africa (e-mail: InnocentD@dut.ac.za).

requirements, namely:

1) *Back to back connection*
   This has both the inverter and the rectifier in the same location, and the valves are normally in the same building. It therefore has a short dc line of few meters located inside the same environment.
2) *Monopolar connection*
   This has both converters separated by a single dc pole line, either positive or negative voltage. The ground is used as a current return path. Most submarine cable connections use monopolar systems.
3) *Homopolar connection*
   This has two or more dc line of the same polarity connected to the converters. Negate polarity is normally used for less corona and reactive power loss. Ground is used as the return path. It works as a monopole when one pole develop a fault. The disadvantage of high cost make it unpopular and seldom used.
4) *Bipolar connection*
   This is the most popular method in HVDC interconnection of converters. It is similar to the homopolar connection, but it has different polarities. Each pole is independent, that is, it can operate with a single pole with ground used as return path [3].
5) *Multi-terminal connection*
   This has more than two sets of converters operating independently. Each converters can operate as a rectifier or an inverter [12].

B. COMPONENTS OF A CONVERTER STATION

HVDC converter stations comprises of different interconnected system working together for efficient power transmission. Predominantly, any HVDC converter station comprises of the converter circuits itself, then the converter transformer, smoothening reactors, harmonics filters, and other peripherals devices. Few definitions of the most important parts are explained below.

1) *Converter transformer*
   LCC HVDC uses special type of transformer different from the AC transformer in that it has special features such as on load tap changes and follow different configuration. For example, the 12-pulse converter can follow six single-phase two windings, three single-phase three winding or two three-phase two windings configuration to suit specification and operational performance [13, 14]. But the VSC HVDC uses same transformer as the normal AC transformer.
2) *Smoothing Reactors*
   This is used for removal of ripples of the DC current. It is also used to limit the rate of rise of the fault current on the DC line.
3) *Harmonic filters*
   These are connected to the converter terminals to provide a low impedance path to ground for removal of harmonics current. Filter used also provide the AC line with the reactive power compensation.

III. LINE COMMUTATED CONVERTER (LCC-HVDC)

LCC, also known as a current source converter CSC uses a thyristors base technology for its converter. The thyristors are silicon semiconductor devices with four layers of N and P type material acting as bi-stable switches, triggered on with a gate pulse and stayed in that on condition until the next current zero crossing. In other for LCC to commutate, the converters require a very high synchronous voltage source, thereby hindering it use for a black start operation. With LCC current rating reaching up to 6250A and blocking voltage of 10KV, this make LCC to have the highest voltage and power rating level of all the HVDC converter technologies [15-17].

LCC achieves its control by regulating the firing angle $\bar{\alpha}$ on both rectifier and inverting side. It has an approach that utilizes a uni-directional line commutated flow of DC current which is inject into a receiving AC network, thereby termed CSC because the output current is kept at a constant level [18].

TABLE I
RECENT LCC –HVDC PROJECTS

PROJECT NAME	LOCATION	CHARACTERISTIC			
		(MW)	(KV)	Year	(km)
UK - Netherlands		1000	±400	2011	260
Jinpin – Sunan	China	7200	±800	2012	2093
Mundra – Haryana	India	2500	±500	2012	960
Rio – Madeira	Brazil	800	100	2012	B-B
Rio – Madeira	Brazil	2x3150	±600	2013	2375
Xiluodu – Guangdong	China	6400	±500	2013	1251
Nuozhadu – Guangdong	China	5000	±800	2013	1451
Southern Hami – Zhengzhou	China	8000	±800	2014	2200
Biswanath – Agra	India	6000	±800	2014	1728
Xiluodu-Zhejiang	China	8000	±800	2014	1688
Zhundong – Sichuan*	**China**	**10000**	**±1100**	**2015**	**2600**

Power reversal from one station to another is carried out by inverting the DC voltage polarity in both stations but the current direction remains constant. The technology operates with good reliability and minimal maintenance. It is the most suitable way of transmitting bulk power using high voltage transmission lines. These features make LCC technology the most popular among HVDC schemes [19].

Table 1 shows few of the recent LCC-based HVDC around the globe. Zhundong-Sichuan scheme has the highest voltage and power, and the longest distance, project in China [20].

IV. VOLTAGE SOURCE CONVERTER (VSC-HVDC)

Voltage source converter uses insulated gate bipolar transistor IGBT technology. The current in this technology can both be switched on and off at any time independent of the AC voltage, that is, it creates its own AC voltages in case of blackstart [21]. Its converters operate at a high frequency with

pulse width modulation PWM which allows simultaneous adjustment of the amplitude and phase angle of converter while keeping the voltage constant [22]. VSC has high degree of flexibility with inbuilt capability to control both its active and reactive power as shown in fig. 1, which makes it more useful in urban power network area [23].

This technology was develop in the 1990's with the first project commissioned by ABB, 1997 [9]. But due to its capacity limits, VSC-HVDC has not been able to make much edge over its contemporary LCC scheme due to low device rating, high power losses and high dielectric stress on equipment insulation. Its application is approaching 1800MW, 500KV. An example is the 1400MW, ±525KV Nordlink that interconnect the grid of Statnett in Norway and TenneT in Germany over a distance of 623km [24]. A lot of research is ongoing to override this limitation [25] and to have the ability to ride through fault [26]. Ref. [27] explain VSC control, modelling, simulation and stability analysis in power systems.

The basic building block of VSC-HVDC topology start with two-level converter [28, 29]. It is like a six-pulse bridge in which IGBT with inverse-parallel diodes replaced the thyristors, and the dc smoothing reactor of LCC is replaced by DC capacitor as shown in fig. 2. It derives its name from the fact that it has a switching device which are complementarily operated to generate two levels of voltage (+Vdc/2 and –Vdc/2) at the ac output terminal of the converter. This complementary operation only allows one switching devices to operate at a time, and the other is turned off. Simultaneous turning on of both two switching devices will lead to short circuit of the capacitor across the dc link which may destroy the converter switches due to over-current. With this topology, each semiconductors switch withstands the full voltage stress that is flowing in the link [30].

Prevention of the dc voltage from changing polarity is done by the diode that is connected in parallel to the IGBT, since the diode can only conduct when forward biased, thereby discharging the dc circuits. But the current flows in both direction, passing through either the IGBT or the diode [31].

It adopt the pulse width modulation (PWM) techniques to control the gate switching frequency of the IGBT, and to reduce the harmonic distortion generated by the converter. Due to high switching losses in the IGBTs as a result of the PWM which is switched on and off many times in a cycles, the overall transmission efficiency of a two-level converter is very poor compared to the LCC converter. Another major setback is that a high level of electromagnetic interference occur when two-level converter is used for high voltage DC systems [32].

An attempt to reduce the poor harmonic distortion and to have a high efficient VSC converter brings about the multi-level converter (MMC, which start from the three-level converter with three discrete voltage level).

It synthesizes more than two voltage level at the AC terminal of each phase as shown in fig. 3. Several types of multilevel converter have been mention and analyzed in the literature [33-35], such as the diode clamped, where diodes are used as clamped and the dc output is subdivided into switches by a capacitors.

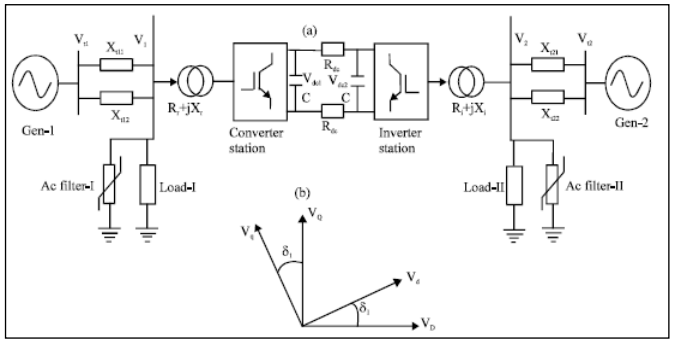

Fig. 1. VSC-HVDC scheme design

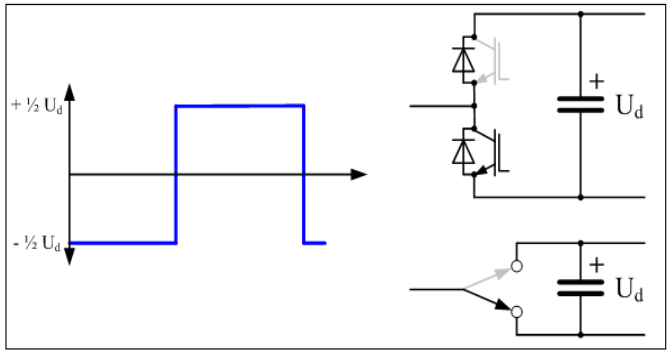

Fig. 2. Block diagram of a two-level VSC-HVDC

With n-levels, there will be n+1 capacitors, and n-1 switch pair are required to work in a complementary manner to generate the output dc voltage. High efficiency for switching at fundamental frequency, low cost and a lesser number of components are some of its merits. However it suffer setback as its less attractive for high voltage transmission due to difficulty in charging and discharging of its dc capacitor, lack of modular index and large inductance stray in the clamping path which have effect on the converter switching characteristics [33, 34]. Flying capacitors multilevel converter is another type which made use of a pre-charged capacitor. Unlike the diode clamped, two or more switch can synthesize an output voltage at the ac output terminal of the converter, and has a phase redundancies which allows specific choice of capacitor to be charge or discharged for voltage balancing across different levels. It has the ability to control real and reactive power flow, and to ride through fault and voltage sag because of its large number of capacitors [35]. Nevertheless, as the level increases, so does the size of the capacitors, as it becomes bulky. Also, the control to track the voltage for all the capacitor becomes complicated, as it requires high frequency switches. The single-phase full bridge is the building block for the cascaded H-bridge multilevel link. It has four switches connected to an isolated capacitor (separate dc source). Each H-link generate three voltage levels. Easy modularized layout package for the series H-bridge, makes it cheap and quickly to fabricate. It also have more possible output voltage-levels than the dc source. Good for reactive power compensation. With good voltage balancing capability through adaptive control action. However, cascaded H-bridge conversion is not suitable for HVDC application because it H-bridge requires the use of many isolated DC sources in series [36].

Recently, a new alternative of VSC-HVDC circuits was

proposed in 2003, at the University of Bundeswehr in Munich, Germany, by Prof. Rainer Marquardt [37, 38]. These converter topologies is based on series-connection of several sub-modules of two semiconductor switches and a capacitor. This topology is known as modular multilevel converter (MMC or M2C) as shown in the (fig 3). The converter can either adopt the half bridge cascaded or full-bridge connections for the arrangement of each sub modules. The half-bridge modular multilevel (HB-MMC) addresses some of the limitation encountered in the convectional VSC converter. Namely; the reduction in the magnitude of the transient dc fault current, converter scalable to the highest transmission voltage through addition of more levels, great reduction in the harmonic content and elimination of low-order harmonics which usually requires large filters, and losses reduced to approximately 1% per converter. All these features made HB-MMC to be widely adopted in recent years. But the HB-MMC freewheeling diodes is unable to stop AC grid contribution to the dc fault current which makes it in need of fast acting dc circuit breaker, else the excessive current stresses may damage the freewheeling diode. The recent technology that overrides the overcurrent fault condition of the HB-MMC is the full bridge multilevel converter (FB-MMC). Though, this technology increases semiconductor losses but the important feature of dc fault reverse blocking capability was achieved by the converter by blocking current flow in the converter switches during dc faults, thereby disallowing both active and reactive power exchange that may want to occur between the dc systems and the ac grid [39, 40].

Other recent HVDC converter topologies with intrinsic dc fault ride-through capabilities are alternative arm modular multilevel (AA-MMC) converters and hybrid cascaded multilevel converter with ac side H-bridge cells. These converters achieve dc fault reverse blocking capability in order to eliminate ac grid contribution to dc side faults, but has little footprint and conversion losses compared to the H-bridge modular multilevel converter [39-41].

Independent control of power at each converter is possible, with one converter controlling the DC voltage at the link to match the nominal level and the other converter sets the amount of active power through the link. With the help of the phase reactor from the series inductance between the converter and the AC grid (fig 4), active and reactive power control was achieved as depict in (1) and (2).

$$P = \frac{U_{ac}U_{conv}\sin\delta}{X} \quad (1)$$

$$Q = \frac{U_{conv}(U_{conv} - U_{ac}\sin\delta)}{X} \quad (2)$$

X-represent the series reactance of the phase reactor and the transformer in the converter station.

Ability of VSC-HVDC to absorb and inject active and reactive power is shown in the P-Q-capability chart below (fig 4). This P-Q capability chart characteristic can be termed to a circle with a radius equal to the maximum MVA rating of the converters. Available reactive power depends on the active power transmitted which directly fall between the operating ranges of the converter MVA rating. The converters are restricted by the power electronics switches current rating and the capability circles. Vac is raised above the AC grid voltage to inject reactive power. The converter voltage however suffers restriction to the maximum rating of the power electronics which limit the capability chart for higher AC voltage.

Nevertheless, VSC remains the most suitable choice in transmitting renewable energy (such as wind power and solar power) either offshore or onshore systems. Table II shows some existing VSC-HVDC installations.

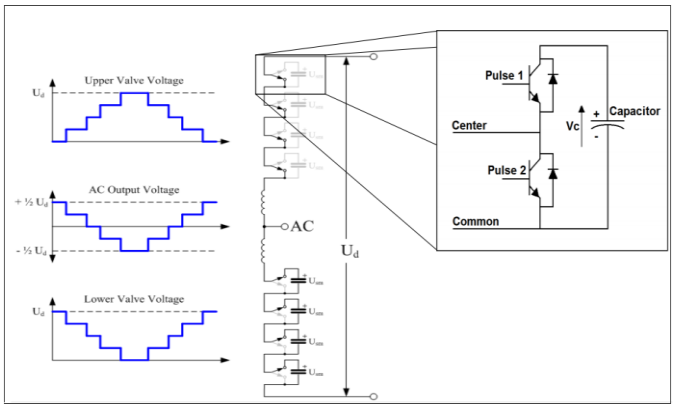

Fig. 3. Modular multilevel converter topology

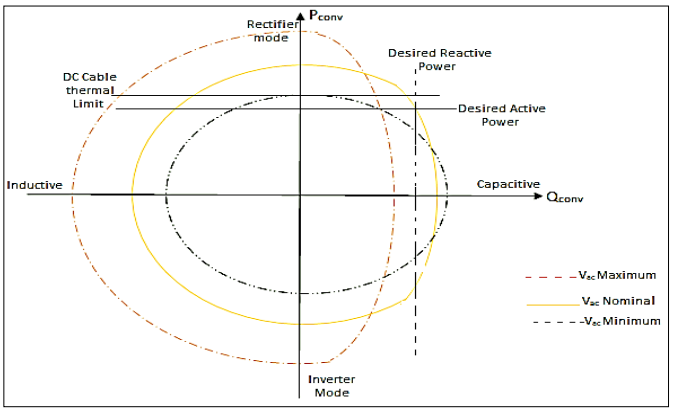

Fig. 4. Simplified PQ characteristic of a VSC HVDC terminal [42]

TABLE II
SOME VSC-HVDC INSTALLATIONS

PROJECT NAME	LOCATION	CHARACTERISTICS			
		(KV)	Year	(MW)	(Km)
Borwin 1	Germany	±150	2009	400	200
Caprivi link	Namibia	±350	2010	300	951
Transbay	USA	±200	2010	400	85
EWIC	UK	±200	2012	500	261
Inelfe	France	±320	2013	1000	65
Skagerrak 4	Norway	±500	2014	700	244

TABLE III
A COMPARISON OF LCC AND VSC SCHEMES

LCC	VSC
Thyristor base technology	IGBT base technology
The semiconductor can with-stand voltage in either polarity	Withstand current in either direction
Constant current direction	Current direction changes with power
Energy is stored inductively	Store energy capacitively

Turned on by a gate pulse but rely on external circuit for its turn off High power capability	Both turn on and off is carried out without the help of an external circuit Lower power capability
Good overload capability	Has weak overload capability
Requires stronger AC systems for excellent performance	Operate well in a weak AC systems
Requires additional equipment for black start operation	Possesses black start capability
Requires AC and DC harmonic filters for removal of distortion and harmonics	Requires no filter because it generates an insignificant level of harmonics
Poor in reactive power control	Good reactive power control
Large site area, dominated by harmonic filters	A more compact site area
Requires converter transformer	Conventional transformer is used
Lower station losses	Higher station losses
More mature technology	Still at its infancy
Reversal of power is done by reversing the voltage polarity	Power is reverse by changing the current direction
Higher voltage capability of over 1000KV	Lower voltage capability of almost 600KV
Mostly used to transmit bulk power for a long distance	Used for transmitting power from remote area with renewable energy
Suffers commutation failures as a result of a sudden drop in the amplitude or phase shift in the AC voltage, which result in dc temporal over-current Though, the effect has no significant impact on the AC systems as it's a self-clearing effect within a few power frequency cycles.	Ability to turn on as well to be turned off makes it immune to any voltage dips or transient AC disturbance; therefore, it does not suffer commutation failure.
Commutation failures, need for change in dc polarity when converter want to change from rectifier to inverter mode make LCC HVDC more problematic to adopt in a multi-terminal HVDC system. Reason for low number of LCC base technology for multi-terminal HVDC.	Suitable for multi-terminal HVDC systems because it does suffer from commutation failures, has independent, multidirectional power flow, and operate with the same voltage polarity.
During short circuits on the dc line, control of the firing angle of the thyristors valves stops the increase of dc fault current. This converter control and protections reduces the damage caused by the fault current. Incased of overhead lines fault, power transmission is stopped for arc de-ionization, after which power transmission resumed.	Continuous conduction in the diode will cause an increase in dc fault current even when the IGBTs are turned off. The ac circuit breakers at both VSC HVDC ends must be opened to stop the diode conduction. The converter link must be re-started after fault has been removed.

TABLE IV
A COMPARISON OF THYRISTOR AND IGBT

FEATURES	THYRISTORS	IGBT
Max. Voltage rating (V)	8000	1700
Voltage blocking	Sync/Async	Async.
Voltage blocking	Sync/Async	Async.
Gating	Pulse	Voltage
Conduction drop (V)	1.2	3
Switching frequency (KHz)	1	20
Development target maximum voltage rating (KV)	10	3.5
Development target maximum current rating (KA)	8	2

Fig. 5 shows an overview of HVDC projects around the world and fig. 6 depict HVDC available ratings for different transmission medium.

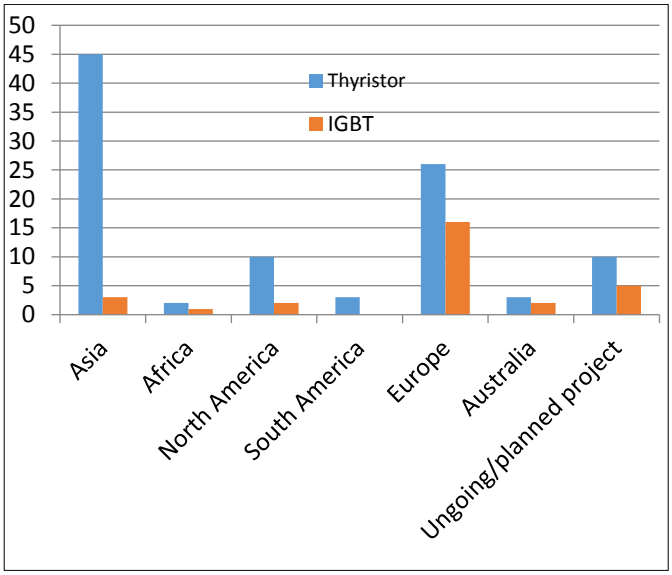

Fig. 5. Overview of HVDC projects around the world

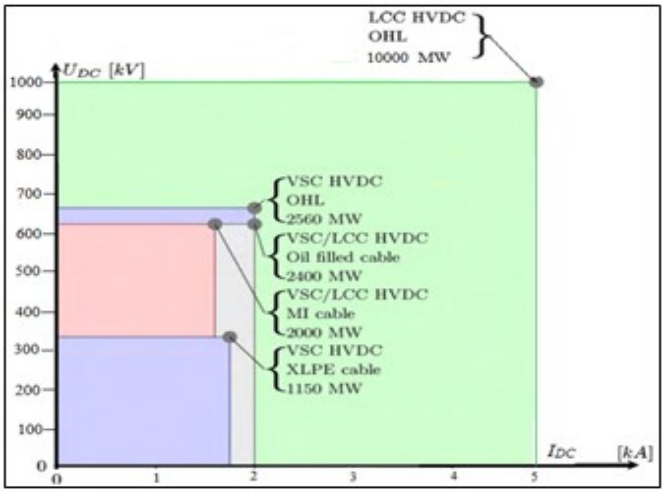

Fig. 6. Available ratings of HVDC systems (U_{DC} refers to voltage per pole, and I_{DC} is the current rating, in a bipolar setup, $P=2U_{DC}\ I_{DC}$)[13]

V. FAULT CHARACTERISTIC OF LCC AND VSC

DigSILENT PowerFactory was used for the modelling of both technologies. This is to explain briefly the transient response of LCC and VSC HVDC to faults in the AC network on the two side of the converters' end.

Fig 7 show the LCC HVDC setup. It is a bipolar HVDC system, each pole consisting of twelve-pulse thyristors on both the inverter and rectifier side, with 1000MW of power at ±600KV transmitted per pole via 1000km overhead dc lines. An external grid is connected at both the rectifier and inverter end of the converter station to serves as power generation and load respectively at both ends.

VSC HVDC setup is modelled as shown in Fig. 8. Each converter rated at 1000MW, 600KV via 1000km overhead lines.

To study these responses, the AC busbar at the inverter side is subjected to a three-phase short circuit of 10Ω fault impedance for 200ms using the time domain simulation (EMT).

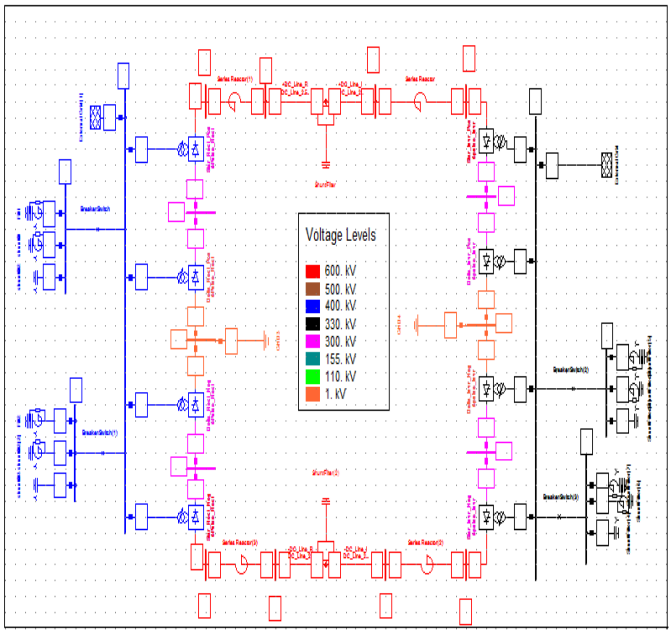

Fig. 7. LCC modelling on DigSILENT

During EMT simulation of both the LCC and VSC model, fig. 9 shows the graphic subplots for the current waveforms for LCC HVDC converter scheme. During the fault period, each converter controller helps in alleviating the effect of the fault on the converter. Like in the case of LCC, the voltage current order limiter (VDCOL) in the rectifier controller help to reduce the dc current, which in turn aid the inverter side to regain fast from commutation problem.

Fig. 10 shows subplot for VSC HVDC, during three-phase AC fault on the inverter busbar with little or no impact of the AC fault on the converter operation. This subplot shows that VSC HVDC system is immune to AC fault

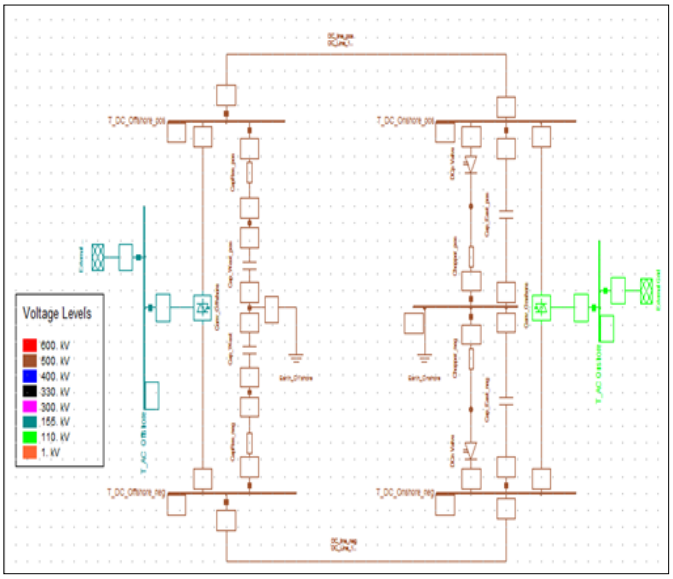

Fig. 8. VSC HVDC model on DigSILENT

Different fault analysis which has been carried out on both two technologies on ability to reduce switching surge overvoltage and power systems restoration after blackout was discussed in [43]. The use of LCC-HVDC for different purposes, such as to improved voltage stability, transient and rotor angle stability was discussed in [44-47], while [48-50] talks on the new hybrid multi-level converter (alternate-Arm multi-level) with half-bridge multi-level benefit of low distortion, losses and full H-bridge converter benefit of DC-side fault blocking capability. The alternate-Arm multi-level discussed also have the ability to supply reactive during severe abnormal operation. This makes it more useful for AC grid during fault since it can provide reactive power support during voltage instability

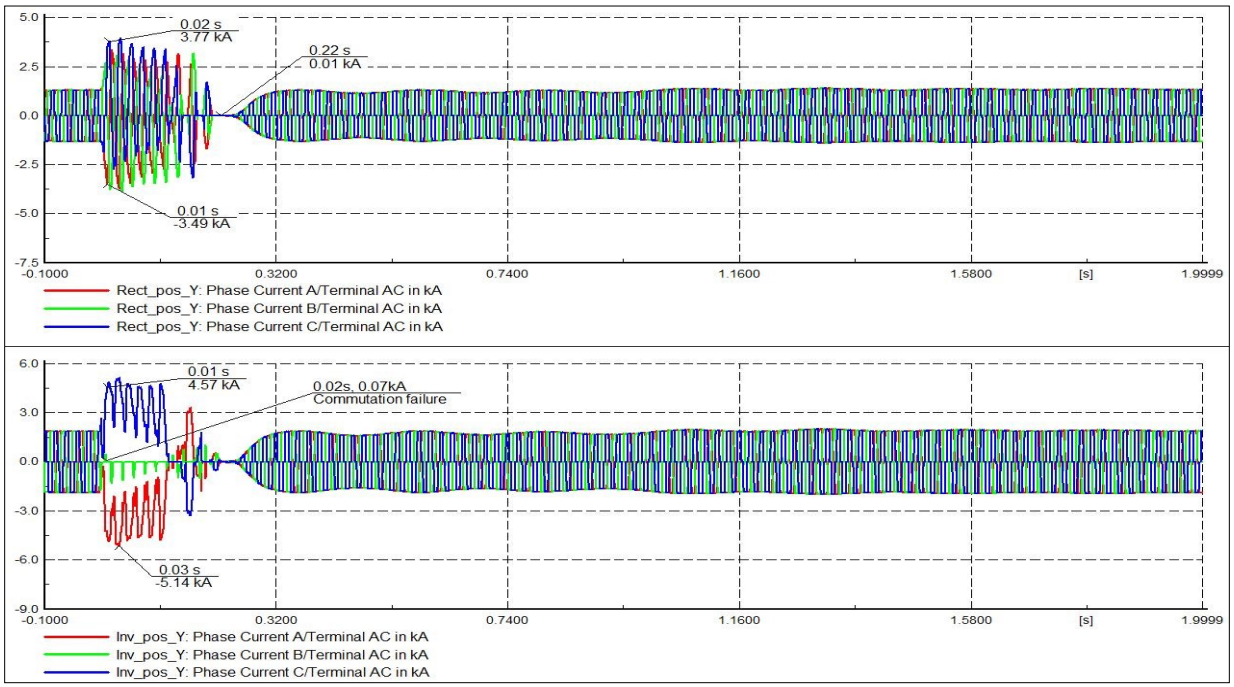

Fig. 9. LCC HVDC converter current during fault.

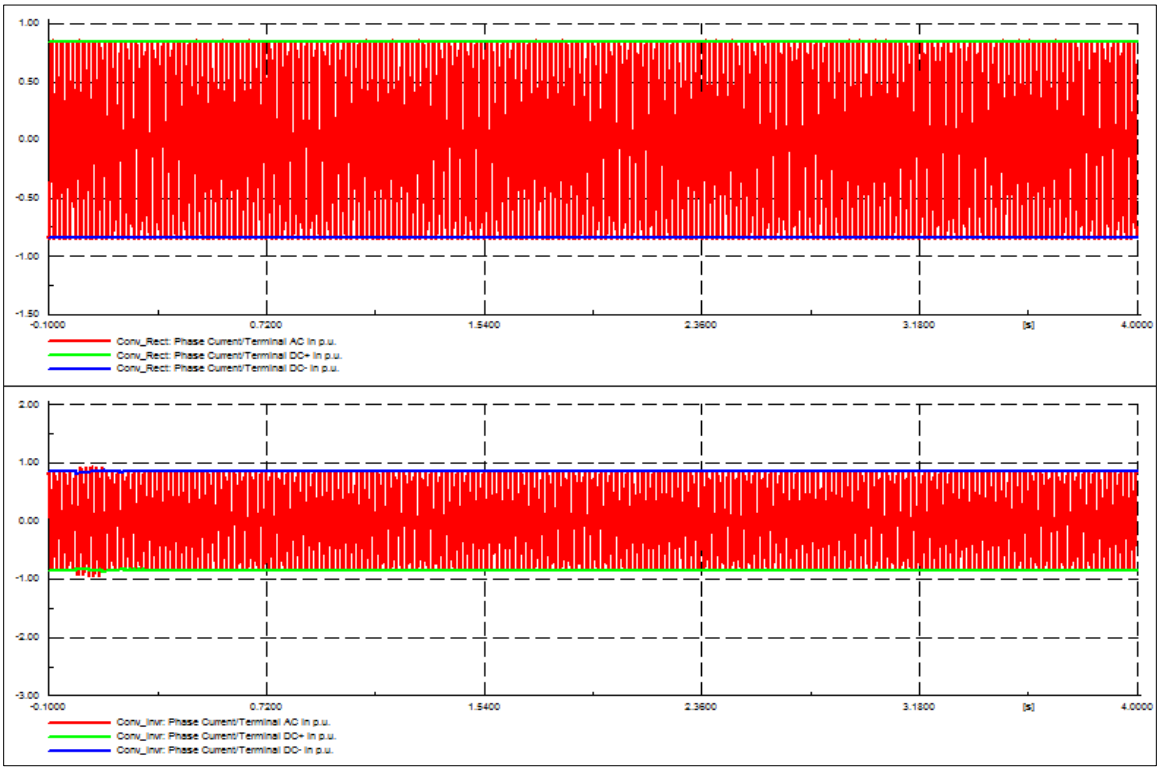

Fig. 10. Monopolar HVDC model.

VI. FUTURE TREND

VSC HVDC has more technical advantages than the contemporary LCC HVDC being a new method of HVDC transmission technology. The future trend in the development of this technology is likely to lead to a more efficient and cheaper use of VSC-HVDC. With an ongoing, never ceasing improvement, research and development on VSC-HVDC technology, especially in the area of converter design and topology, such breakthrough will surely contribute to the spread of VSC-HVDC transmission systems with overhead lines and accelerate the practical realization of HVDC networks that use VSC technology.

Future trends also include the manufacturing of better power cable with higher voltage rating for VSC HVDC transmission. 320XLPE HVDC are still the maximum rating in service. But with ongoing research on power cables with high power rating and reduced cost, this will bring about more attraction to VSC-HVDC technology.

The use of VSC HVDC will continue to increase and apply to different power system interconnections at higher dc voltage and power rating.

Fig. 11 shows the earlier stage of VSC based HVDC converter technology with much power losses. But due to the development in the converter and control technology, the present VSC-based HVDC technology is of lower magnitude. But with the introduction of the multi-level VSC configuration, this has significantly narrow the gap between LCC and VSC HVDC schemes.

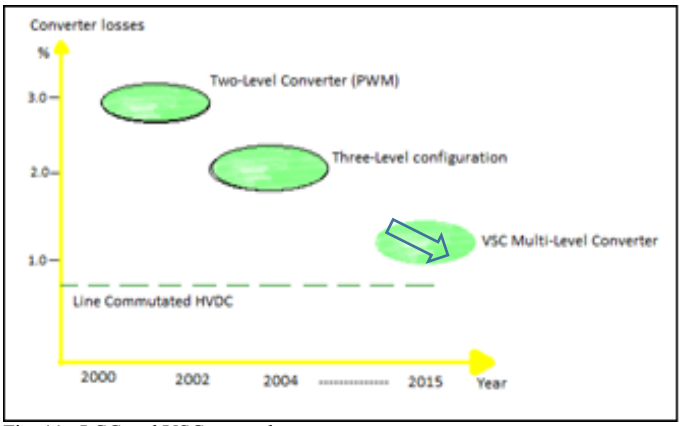

Fig. 11. LCC and VSC power loss

VII. CONCLUSION

The two dominant HVDC transmitting technology have been reviewed in this paper. Power electronics being the building block of any converter station, and the efficiency of these two technologies depend in the converter topology and the switches (semiconductors) used in fabricating them. LCC has the highest power rating and can sustain better during faults. However, for power control, flexibility and high converter efficiency, the VSC is superior. Though with this trend, LCC may remain the more utilized of these technologies in the near future due to its high reliability and well-established thyristors base technology that it utilizes. However, with the improvement in VSC technology and the advantages which it offers over LCC, VSC is bound to grow, and gain more recognition and market share, especially with the large-scale renewable energy integration into traditional AC power grids going on worldwide.

REFERENCES

[1] S. Shah, R. Hassan, and S. Jian, "HVDC transmission system architectures and control - A review," in Control and Modeling for Power Electronics, 2013 IEEE 14th Workshop on, 2013, pp. 1-8.

[2] N. M. Kirby, "HVDC system solutions," in Transmission and Distribution Conference and Exposition T&D, IEEE PES, 2012, pp. 1-3.

[3] M. H. Okba, M. H. Saied, M. Z. Mostafa, and T. M. Abdel-Moneim, "High voltage direct current transmission - A review, part I," in Energytech, 2012 IEEE, 2012, pp. 1-7.

[4] R. Radzuan, M. A. A. Raop, M. K. M. Salleh, M. K. Hamzah, and R. A. Zawawi, "The designs of low power AC-DC converter for power electronics system applications," in Computer Applications and Industrial Electronics, IEEE Symposium on, 2012, pp. 113-117.

[5] N. Flourentzou, V. G. Agelidis, and G. D. Demetriades, "VSC-Based HVDC Power Transmission Systems: An Overview," Power Electronics, IEEE Transactions on, vol. 24, pp. 592-602, 2009.

[6] M. P. Bahrman, "HVDC transmission overview," in Transmission and Distribution Conference and Exposition, 2008; IEEE/PES, 2008, pp. 1-7.

[7] H. K. Müller, S. S. Torbaghan, M. Gibescu, M. M. Roggenkamp, and M. A. M. M. van der Meijden, "The need for a common standard for voltage levels of HVDC VSC technology," Energy Policy, vol. 63, pp. 244-251, 12// 2013.

[8] L. de Andrade and T. P. de Leao, "A brief history of direct current in electrical power systems," in HISTory of ELectro-technology CONference (HISTELCON), 2012 Third IEEE, 2012, pp. 1-6.

[9] S. M. Yousuf and M. S. Subramaniyan, "HVDC and Facts in Power System," International Journal of Science and Research, vol. 2, 2013.

[10] B. K. Bose, "Evaluation of modern power semiconductor devices and future trends of converters," Industry Applications, IEEE Transactions on, vol. 28, pp. 403-413, 1992.

[11] S. Tamai, "High power converter technologies for saving and sustaining energy," in Power Semiconductor Devices & IC's (ISPSD), 2014 IEEE 26th International Symposium on, 2014, pp. 12-18.

[12] E. Kontos, R. T. Pinto, S. Rodrigues, and P. Bauer, "Impact of HVDC Transmission System Topology on Multiterminal DC Network Faults," Power Delivery, IEEE Transactions on, vol. 30, pp. 844-852, 2015.

[13] M. Jafar and M. Molinas, "A transformerless series reactive/harmonic compensator for line-commutated HVDC for grid integration of offshore wind power," Industrial Electronics, IEEE Transactions on, vol. 60, pp. 2410-2419, 2013.

[14] T. N. Tran, L. Luo, J. Xu, S. Dong, Z. Zhang, Z. Zhao, et al., "Analysis of the characteristics of the new converter transformer based on the matrix model," Power Delivery, IEEE Transactions on, vol. 27, pp. 821-830, 2012.

[15] J. Vobecky, "The current status of power semiconductors," Facta Universitatis, Series: Electronics and Energetics, vol. 28, pp. 193-203, 2015.

[16] M. Schenk, J. Przybilla, U. Kellner-Werdehausen, R. Barthelmess, J. Dorn, G. Sachs, et al., "State of the Art of Bipolar Semiconductors for Very High Power Applications,"; Proceedings of International Exhibition and Conference for Power Electronics, Intelligent Motion, Renewable Energy and Energy Management;, Europe 2015, pp. 1-8.

[17] J. Vobecky, V. Botan, K. Stiegler, U. Meier, and M. Bellini, "A novel ultra-low loss four inch thyristor for UHVDC," in Power Semiconductor Devices & IC's,IEEE 27th International Symposium, 2015, pp. 413-416.

[18] C. Guo, Y. Liu, C. Zhao, X. Wei, and W. Xu, "Power Component Fault Detection Method and Improved Current Order Limiter Control for

[19] H. Jingbo, L. Mingjie, Y. Jun, C. Qing, X. Tao, and Y. Zhao, "Research on dynamic characteristics and countermeasures of AC-DC hybrid power system with large scale HVDC transmission," in Power System Technology (POWERCON), 2014 International Conference on, 2014, pp. 799-805.

[20] Anonymous, "HVDC Projest List," Prepared for HVDC and Flexible AC transmission subcommitted of the IEEE Treansmission and Distribution Committee, March 2012.

[21] Y. Jiang-Hafner, H. Duchen, M. Karlsson, L. Ronstrom, and B. Abrahamsson, "HVDC with voltage source converters-a powerful standby black start facility," in Transmission and Distribution Conference and Exposition, 2008; D. IEEE/PES, 2008, pp. 1-9.

[22] K. Friedrich, "Modern HVDC PLUS application of VSC in Modular Multilevel Converter topology," in Industrial Electronics (ISIE), 2010 IEEE International Symposium on, 2010, pp. 3807-3810.

[23] J. Luo, J. Yao, D. Wu, C. Wen, S. Yang, and J. Liu, "Application research on VSC-HVDC in urban power network," in Power Engineering and Automation Conference (PEAM), 2011 IEEE, 2011, pp. 115-119.

[24] M. Callavik, P. Lundberg, and O. Hansson, "NORDLINK Pioneering VSC-HVDC interconnector between Norway and Germany," March 2015.

[25] V. Gelman, "Insulated-Gate Bipolar Transistor Rectifiers: Why They Are Not Used in Traction Power Substations," Vehicular Technology Magazine, IEEE, vol. 9, pp. 86-93, 2014.

[26] O. Abarrategui, D. Larruskain, I. Zamora, V. Valverde, G. Buigues, and A. Iturregi, "VSC-based HVDC System Capability to Ride Through Faults," International Conference on Renewable Energy and Power Quality, 2015.

[27] F. Shewarega and I. Erlich, "Simplified Modeling of VSC-HVDC in Power System Stability Studies," International Federation of Automatic Control, Cape Town, South Africa, 2014.

[28] C. C. Davidson and D. Trainer, "Innovative concepts for hybrid multi-level converters for HVDC power transmission," in AC and DC Power Transmission. 9th IET International Conference on, 2010, pp. 1-5.

[29] R. Marquardt, "Modular Multilevel Converter: An universal concept for HVDC-Networks and extended DC-Bus-applications," in Power Electronics Conference (IPEC), 2010 International, 2010, pp. 502-507.

[30] T. Guangfu, H. Zhiyuan, and P. Hui, "R&D and application of voltage sourced converter based high voltage direct current engineering technology in China," Journal of Modern Power Systems and Clean Energy, vol. 2, pp. 1-15, 2014.

[31] P. Hurtuk, R. Radvan, and M. Frivaldský, "Investigation of possibilities to increasing efficiency of full bridge converter designed for low output voltage and high output current applications," in ELEKTRO, 2012, 2012, pp. 129-132.

[32] R. Marquardt, "Modular Multilevel Converter topologies with DC-Short circuit current limitation," in Power Electronics and ECCE Asia, 2011 IEEE 8th International Conference on, 2011, pp. 1425-1431.

[33] H. Abu-Rub, J. Holtz, J. Rodriguez, and G. Baoming, "Medium-voltage multilevel converters—State of the art, challenges, and requirements in industrial applications," Industrial Electronics, IEEE Transactions on, vol. 57, pp. 2581-2596, 2010.

[34] G. P. Adam, S. J. Finney, A. M. Massoud, and B. W. Williams, "Capacitor balance issues of the diode-clamped multilevel inverter operated in a quasi two-state mode," Ieee Transactions on Industrial Electronics, vol. 55, pp. 3088-3099, Aug 2008.

[35] E. Najafi and A. H. M. Yatim, "Design and implementation of a new multilevel inverter topology," Industrial Electronics, IEEE Transactions on, vol. 59, pp. 4148-4154, 2012.

[36] Y. Zhang, G. P. Adam, T. C. Lim, S. J. Finney, and B. W. Williams, "Analysis of modular multilevel converter capacitor voltage balancing based on phase voltage redundant states," Iet Power Electronics, vol. 5, pp. 726-738, 2012.

[37] M. Glinka and R. Marquardt, "A new AC/AC multilevel converter family," *Industrial Electronics, IEEE Transactions on,* vol. 52, pp. 662-669, 2005.

[38] A. Lesnicar and R. Marquardt, "An innovative modular multilevel converter topology suitable for a wide power range," in Power Tech Conference Proceedings, 2003, p. 6.

[39] G. P. Adam, O. Anaya-Lara, G. M. Burt, D. Telford, B. W. Williams, and J. R. McDonald, "Modular multilevel inverter: pulse width modulation and capacitor balancing technique," IET Power Electronics, vol. 3, pp. 702-715, 2010.

[40] G. Adam and I. Davidson, "Robust and Generic Control of Full-Bridge Modular Multilevel Converter High-Voltage DC Transmission Systems," in IEEE Power electronic transaction, 2015.

[41] S. Qiang, L. Wenhua, L. Xiaoqian, R. Hong, X. Shukai, and L. Licheng, "A Steady-State Analysis Method for a Modular Multilevel Converter," Power Electronics, IEEE Transactions on, vol. 28, pp. 3702-3713, 2013.M. Glinka and R. Marquardt, "A new AC/AC multilevel converter family," Industrial Electronics, IEEE Transactions on, vol. 52, pp. 662-669, 2005.

[42] Eskom, HVDC Power Transmission: Basic Principles, Planning and Converter Technology (Part 1): Crown Publication cc., 2012.

[43] G. P. Adam, S. Finney, K. Bell, and B. Williams, "Transient capability assessments of HVDC voltage source converters," in Power and Energy Conference at Illinois (PECI), 2012 IEEE, 2012, pp. 1-8.

[44] K N I Mbangula, O. E. Oni and I E Davidson, "The Impact of HVDC Schemes on Network Transient Rotor Angle Stability," 24th Southern

African Universities Power Engineering Conference, South Africa January 2016.
[45] O. E. Oni, K N I Mbangula, and I. E Davidson "Voltage Stability Improvement of a Multi-Machine System using HVDC", in press, IEEE power system conference, USA, March 2016.
[46] K N I Mbangula and I E Davidson, "Detailed power system transient stability analysis using expert system concepts and stability improvement of a large multi-machine HVAC network using HVDC technologies," Proceedings of the 23rd South African Universities Power Engineering Conference, South Africa, January 2015.
[47] K N I Mbangula, I E Davidson and R Tiako, "Improving Power System Stability of South Africa's HVAC Network Using Strategic Placement of HVDC Links". Proceedings of the CIGRE International Symposium 2015 Development of Electricity Infrastructures for Sub-Saharan Africa, Cape Town, South Africa, October 26-30, 2015.
[48] M. Merlin, T. Green, P. D. Mitcheson, D. Trainer, D. Critchley, and R. Crookes, "A new hybrid multi-level voltage-source converter with DC fault blocking capability," in AC and DC Power Transmission, 2010. ACDC. 9th IET International Conference on, 2010, pp. 1-5.
[49] G. P. Adam, K. H. Ahmed, S. J. Finney, K. Bell, and B. W. Williams, "New Breed of Network Fault-Tolerant Voltage-Source-Converter HVDC Transmission System," IEEE Transactions on Power Systems, vol. 28, pp. 335-346, Feb 2013.
[50] N. Nayak, S. K. Routray, and P. K. Rout, "A robust control strategies to improve transient stability in VSC-HVDC based interconnected power systems," in Energy, Automation, and Signal (ICEAS), 2011 International Conference on, 2011, pp. 1-8.

Oluwafemi E. Oni was born in Nigeria on 17 September 1988. He received his BSc (Honours) Degree in Electrical and electronic engineering from Ekiti State University, Ado Ekiti, Nigeria, in 2013. He then proceed to University of KwaZulu-Natal, Durban, South Africa in 2015 for his MSc degree in electrical engineering (currently handed in his Thesis for examination).

He was a system and maintenance engineer at Egbin Power Thermal Plant, Lagos, Nigeria, in 2012 and Omotosho Power plant, Ore, Nigeria, in 2013/2014. He is currently a Research Assistance with Department of Electrical Engineering, University of KwaZulu-Natal. His research includes power systems stability analysis using High Voltage Direct Current transmission scheme, integration of renewable energy into the grid using multi-terminal HVDC scheme, and smart grid systems using FACTs.

Mr. Oni's award and honors include MTN foundation scholarships, ETISALAT scholarship and Ekiti state scholarship.

Kamati N.I. Mbangula was born in Namibia on 20 August 1989. He graduated with a BSc. (Honours) Degree in Electrical Engineering from the University of Namibia (UNAM). He pursued his postgraduate studies in South Africa at the University of KwaZulu-Natal (RSA), and carried out his research at the Eskom Centre of Excellence in High Voltage Direct Current (HVDC). His work experience includes working as a Staff Development Fellow at UNAM, and working as a research assistant and lab technician at the Eskom centre of excellence in HVDC. He is currently employed as a lecturer at UNAM. His fields of interests include power systems stability analysis, and low voltage reticulation systems design and analysis.

Innocent E. Davidson (M'92–SM'02) received the BSc (Hons) and MSc degrees in Electrical Engineering from University of Ilorin in 1984, and 1987 respectively. PhD in electrical engineering from the University of Cape Town, Rondebosch, South Africa1998; and Postgraduate Diploma in business management from the University of KwaZulu-Natal, South Africa, 2004; Associate Certificate, sustainable energy management, British Columbia Institute of Technology, Burnaby, Canada, 2011.

From 1994-1995, he was Engineering Inspector, Rainbow Energy Project at EASIGAS (Pty) Ltd, Cape Town; Senior Lecturer, University of Pretoria (1999-2001); Senior Lecturer, Department of Electrical Engineering, University of KwaZulu-Natal (UKZN), 2001–2006; Part-time Instructor, Graduate Engineering Program (Power & Energy), UKZN High Voltage DC Centre (2000-2008) a program co-offered by UKZN and Eskom - South Africa's Electric Utility. From 2005–2006, he was a Visiting Professor, Powertech Labs Inc., Surrey, BC, a world leading consortium in clean energy technologies, independent testing services, power system solutions and smart utility services. From 2007-2011 he was Energy Consultant in Surrey, BC, implementing energy efficiency (electricity/gas) measures, British Columbia provincial government's mandate on Climate Change. He has been an invited guest writer for the IEEE Power and Energy technical magazine as an Expert on Africa: "Energizing Africa's Emerging Economy", IEEE Power and Energy, Vol. 3, No 4, July/August 2005. He was Associate Professor of Electrical Engineering and Research Coordinator, University of Namibia (2012-2014); Director, Eskom Centre of Excellence in HVDC Engineering, UKZN (2014-2016). Currently, he is a Full Professor of Electrical Engineering, Durban University of Technology, South Africa. He is the author/co-author of over 150-refereed journal and conference papers. His research focus is on Grid integration of renewable energy using Smart Technologies and Innovation for Smart Cities.

Prof Davidson is a member, Western Canada Group of Chartered Engineers (WCGCE); the Institute of Engineering and Technology (IET Canada) British Columbia Chapter; a Chartered Engineer, C.Eng. United Kingdom. He is a Fellow of the South African Institute of Electrical Engineers and a registered professional engineer, P. Eng. (ECSA), South Africa.

Dynamic Voltage Stability Studies using a Modified IEEE 30-Bus System

Oluwafemi E. Oni, Kamati I. Mbangula, and Innocent E. Davidson

***Abstract*—Power System stability is an essential study in the planning and operation of an efficient, economic, reliable and secure electric power system because it encompasses all the facet of power systems operations, from planning, to conceptual design stages of the project as well as during the systems operating life span. This paper presents different scenario of power system stability studies on a modified IEEE 30-bus system which is subjected to different faults conditions. A scenario whereby the longest high voltage alternating current (HVAC) line is replaced with a high voltage direct current (HVDC) line was implemented. The results obtained show that the HVDC line enhances system stability more compared to the contemporary HVAC line. Dynamic analysis using RMS simulation tool was used on DigSILENT PowerFactory.**

***Index Terms*—CCT, Commutation failure, Dynamic Voltage stability, HVDC, Steady state analysis.**

I. INTRODUCTION

RESTRICTION in transmission network expansion due to reduced right of way (ROW) brings about long distance bulk power transfer. A minor fault on a heavily loaded line may result in cascading problem which can eventually lead to systems collapse if proper preventive measures are not taken. Increase in heavy system load in major urban centre is another major concern. This now goes to the fact that proper systems planning and predictions goes a long way for stable and quality power transfer to major areas that are prone to load increase. AC lines have been the most commonly means of power transmission from one area to another especially in African countries. But with the inherent problems associated with AC lines such as stability problem, cascading effect, corona loss, synchronism problem, and the situation whereby the generating stations are located far away from load centres. AC lines are not suitable for such transmission being that it requires different compensating devices for a specific distance interval. Solving these problems brings about usage of HVDC lines to transfer bulk power over long distance which also tends to improve the stability margin of the systems.

Power systems fault such as loss of synchronization of a large power plant, tripping of a load and/or sudden disturbance on a transmission line, most times result in interconnecting systems to enter voltage instability state by not meeting active/reactive power demanded and acceptable voltage at each systems bus. This state can further lead to voltage collapse when all the voltage profile after disturbance is below acceptable limits in an important part of the power systems such that the different part of the systems controllers are stressed beyond their operational limit. Thus, ability of the systems to remain practically intact and regain a state of operating equilibrium makes the system voltage stable.

Much research has been done on voltage stability analysis [1] , [2]. Improvement through the use of FACT devices was discussed in [3]-[5]. The effect of the automatic voltage regulator (AVR), on-load tap changers and power systems stabilizer (PSS) on voltage stability was discussed in [6] and [7], while [8] and [12] extensively discusses the impact of HVDC links on power system stability analysis and improvement.

HVDC transmission became favorable when HVDC converter problems were reduced by the introduction of thyristor based switches. Still a lot of improvement has been made in this area of interest, from HVDC cables, converter transformer, converter technology and topology, etc. and there is still a lot of ongoing research being conducted in this area.

This paper presents an investigation into the impact of HVDC links on power systems operation by considering the line loadings and voltage profile. Also, a dynamic approach with the use of real time simulation RMS tools was also considered in analyzing the critical clearing time with and without HVDC line. The obtained results were compared to determine the extent to which the HVDC system helps in improving voltage stability of the network

II. VOLTAGE STABILITY ANALYSIS

Voltage stability is the ability of a power system to be able to maintain an acceptable voltage profile at all buses in the power network when operated under healthy conditions or when

This paper was submitted for review on August 1, 2016. This work was supported by Eskom Power Plant Engineering Institute, Eskom Centre of Excellence in University of KwaZulu-Natal. Westville campus, South Africa.

O. E Oni is with Electrical Engineering Department, University of KwaZulu-Natal. Durban 4041, South Africa (e-mail: maxiphem@yahoo.com).

K. N. I. Mbangula was with Department Electrical Engineering, University of KwaZulu-Natal. Durban 4041, South Africa. He is now with the Department of Electrical Engineering, University of Namibia. Ongwediva 3624, Namibia (e-mail: imbangula@unam.na).

I. E. Davidson was with Department of Electrical Engineering, University of KwaZulu-Natal. Durban 4041, South Africa. He is now with the Department of Electrical Power Engineering, Durban University of Technology. Durban 4001, South Africa (e-mail: InnocentD@dut.ac.za).

subjected to systems disturbance. Fig. 1 shows effect of load increase on voltage profile. More increase in load demand beyond the critical point can result in system collapse [1], [10], [13].

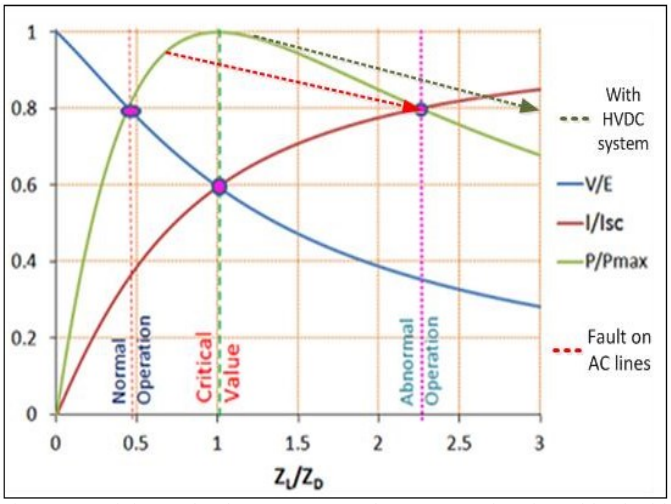

Fig. 1. Receiving end voltage, current and power as a function of load with HVDC line.

A. Static Analysis

Static analysis of voltage stability involves the use of PV curves to investigate the maximum power that can be transmitted through a transmission line to a load considering the voltage profile of the load bus and the, reactive power needed for the load at specific load power. It can also made use of reduced Jacobian matrix in (1)-(4) to analyse the voltage sensitivity of a particular bus to change in reactive power in that bus while the active power is kept constant [1], [10].

$$\begin{bmatrix}\Delta P\\ \Delta Q\end{bmatrix}=\begin{bmatrix}J_{P\theta} & J_{PV}\\ J_{Q\theta} & J_{QV}\end{bmatrix}\begin{bmatrix}\Delta\theta\\ \Delta V\end{bmatrix} \quad (1)$$

Let ΔP=0, then,

$$\Delta Q=\left[J_{QV}-J_{Q\theta}J_{P\theta}^{-1}J_{PV}\right][\Delta V] \quad (2)$$

$$\Delta Q=J_R\Delta V \quad (3)$$

$$\Delta V=J_R^{-1}\Delta Q \quad (4)$$

Where; ΔP - Incremental change in bus real power
ΔQ - Incremental change in bus Reactive Power
Δθ - Incremental change in bus Voltage phase angle
ΔV - Incremental change in bus voltage magnitude

J_R^{-1} is called the V-Q sensitivity as it value determines how stable the system is. A positive value indicates a stable system, while a negative value indicates an unstable system. For a positive value, the smaller the sensitivity value, the more stable the system becomes, meaning as load increases, the value tends towards infinity signifying an unstable system condition.

For the modal analysis that explains different snapshot of voltage sensitivity to reactive power, this is given by (5)-(9).

$$J_R=\xi\Lambda \quad (5)$$

$$J_R^{-1}=\xi\Lambda^{-1}\eta \quad (6)$$

$$\Delta V=\xi\Lambda^{-1}\eta.\Delta Q \quad (7)$$

Since $\xi^{-1}=\eta$, i.e. an identity matrix.

Therefore,

$$\eta\Delta V=\Lambda^{-1}\eta.\Delta Q \quad (8)$$

$$v=\Lambda^{-1}q \quad (9)$$

($v=\eta\cdot\Delta V$) is the vector for the modal voltage variations and ($q=\eta\cdot\Delta Q$) is the modal of reactive power variations.

B. Dynamic Analysis

Critical Clearing time (CCT) is one of the method used in analyzing the transient rotor angle stability of a power system. This involves the use of real time dynamic analysis to calculate, for a given defined fault, the maximum allowable clearing time in which the system remains transiently stable. This time frame gives the allowance to which the fault must be cleared or isolated from the rest of the system for the power system to remain in a stable state of operation. If the fault clearing time is longer than the CCT, the power system will definitely become unstable [14], [15].

Dynamic voltage stability model comprises of first order differential equations as shown in (10)-(12). 'x' connotes the state vector of the system and 'y' represent the network variable like bus voltage. Eq. 10 becomes linear during the case of small disturbance around a steady state equilibrium point (x_o, y_o) and further eliminated to give (12). Static bifurcation, capable of causing voltage collapse will occur when D is zero. Thus an assumption of D≠0 is always made for dynamic bifurcation studies.

$$\dot{x}=f(x,y) \quad (10)$$

$$0=g(x,y) \quad (11)$$

$$\frac{d\Delta x}{dt}=(A-BD^{-1}C)=A'\Delta x \quad (12)$$

Dynamic voltage stability can then be performed by analyzing the eigenvalues of A'. (A, B, C and D are appropriate dimensioned matrices) [1], [16], [17].

III. METHODOLOGY

A modified IEEE 30 bus test network was used for this study. Modified in the sense that the IEEE 30 Bus test network is a representation of a portion of the American Electric power system (in the Midwestern US) as of December, 1961. Fig. 2 shows the modified IEEE 30 bus test network as setup on DigSILENT PowerFactory. The modified network consist of 30 buses, 8 generators, 20 loads, 40 lines, 11 transformers, 1 shunt capacitor, and 1 shunt reactor. The main voltage level of the network is 400kV (nominal voltage) with nominal transmitting frequency of 50Hz. The 132kV of bus 19, bus 20 and bus 21, and the 11kV of bus 15 and bus 18 was assumed on power factory for this study.

A. Model Parameters

The model parameters were based on calculations and use of standard IEEE models, due to the fact that most data unit were not specified by different online sources for the IEEE 30 bus systems.

1) Load model

The loads are modelled to be voltage dependent with constant active and reactive power demand for load flow calculation and for stability analysis according to (13). The value of kp is set to be 1 for active power (constant current behaviour) and 2 for the reactive power (constant impedance) [18].

$$P + jQ = P_0\left(\frac{U}{U_0}\right)^{kp} + Q_0\left(\frac{U}{U_0}\right)^{kp} \quad (13)$$

2) Generator model

All the generators are connected via a transformer. SM (synchronous machine) was used on PowerFactory to name all the generators. Table I shows the generator parameter as used on DigSILENT. SM 1.1 with 0^0 voltage angle and 1.00pu voltage set-point was used as the reference machine because it is connected to the bus with the highest fault level. All generator were set to be in voltage control mode.

Two generator type were used as shown in Table II, first is the 16.5KV, 500MVA used by SM 3, 5 and 6 and the other synchronous machine uses the 20KV, 800MVA type. Transformer parameter used is shown in Table III.

TABLE I
GENERATOR PARAMETER

SM	MW	Mvar	SM	MW	Mvar
1.1	Slack	5	***4.1***	720	*5*
1.2	700	0	***4.2***	720	*0*
2	320	0	***5***	390	*0*
3	*407*	*0*	***6***	*385*	*5*

TABLE II
SYNCHRONOUS MACHINE TYPE DATA

SM	MVA	kv	xd (pu)	xl (pu)	xq (pu)	Td´ (s)	Tq´ (s)
Typ1	800	20	2.2	0.3	2.2	2.1	0.28
Typ2	500	16.5	1.3	0.15	2.0	1.0	1.0

TABLE III
TRANSFORMER TYPE DATA

	Sn MVA	KV	uk & uk0	Vector. group	ULTC
Trf 1	400	11/400	12.6	YNd1	-5 to 5
Trf 2	600	16.5/400	14.88	YNd1	-4 to 4
Trf 3	850	20/400	14.44	YNd1	-5 to 5
Trf 4	400	132/400	11.82	YNyn	-3 to 3

All generators are rated for realistic inertial time constant and modelled using the IEEE controller model on PowerFactory for the automatic voltage regulator, governor control as well as the power systems stabilizer (but the PSS for all the generator are disable due to set point error).

3) HVDC model

The HVDC network is modelled as depicted in Fig. 3 with the parameter on Table 1V. The 1350MW monopolar with 600KV operating voltage transmits power over a distance of 700km. The reliability of the HVDC network was put to test using a three phase fault at the inverter terminal (fault reactance of 10Ω for 200ms. Result shows a commutation failure at the inverter side of the converter which the voltage dependent current order limiter (VDCOL) was activated as a result of reduction in DC voltage. The commutation failure was resolved when the rectifier controller reduces the DC current to allow minimum power across the link during fault conditions. With this, most of the DC faults are self-clearing with the help of a well-equipped controller.

Equations (14) and (15) show the fundamental law governing the HVDC systems. HVDC equivalent circuits' equation is given by (16).

$$V_{dI} = \frac{3\sqrt{2}\alpha_I V_{tI}\cos\gamma_I - 3X_C I_D}{\pi} \quad (14)$$

$$V_{dR} = \frac{3\sqrt{2}\alpha_R V_{tR}\cos\alpha_R - 3X_C I_d}{\pi} \quad (15)$$

$$I_d = \frac{V_{dor}\cos\alpha - V_{doi}\cos\beta\cos\gamma}{R_{cr} + R_L \pm R_{ci}} \quad (16)$$

HVDC control as set up on DigSILENT PowerFactory software can be divided into two hierarchical levels: inverter control and rectifier control. A block definition that defines the transfer function in the form of graphical block diagrams and equation is first created for each of the controllers, and then a composite block frame is created for the overall control. This consists of the entire overview diagram showing all the slots interconnections and which object should be assign to a slot. After a common model is created from the block definition, they are then added into the composite model. Fig. 4 and 5 from [19] give a simple overview diagram of the controller as connected to the converter.

TABLE IV
HVDC DATA

	Rectifier	Inverter
AC Voltage (KV)	400	400
Firing angle control	Current control	Voltage control
Commutation Reactance	13.445Ω	13.445Ω
Tap changer control	α-control	γ-control
Actual winding ratio	0.97	0.97

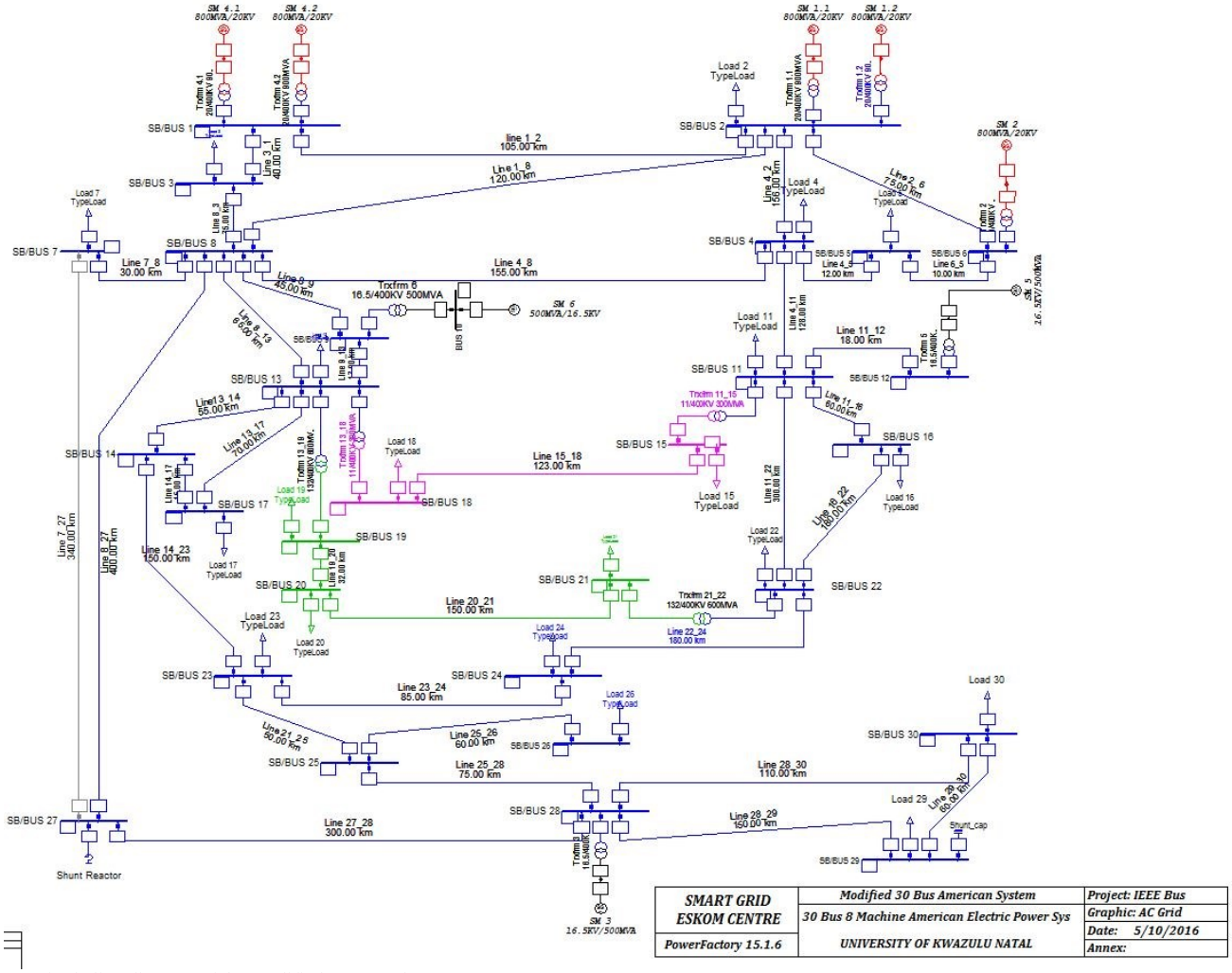

Fig. 2. Single line diagram of the modified IEEE 30 bus system.

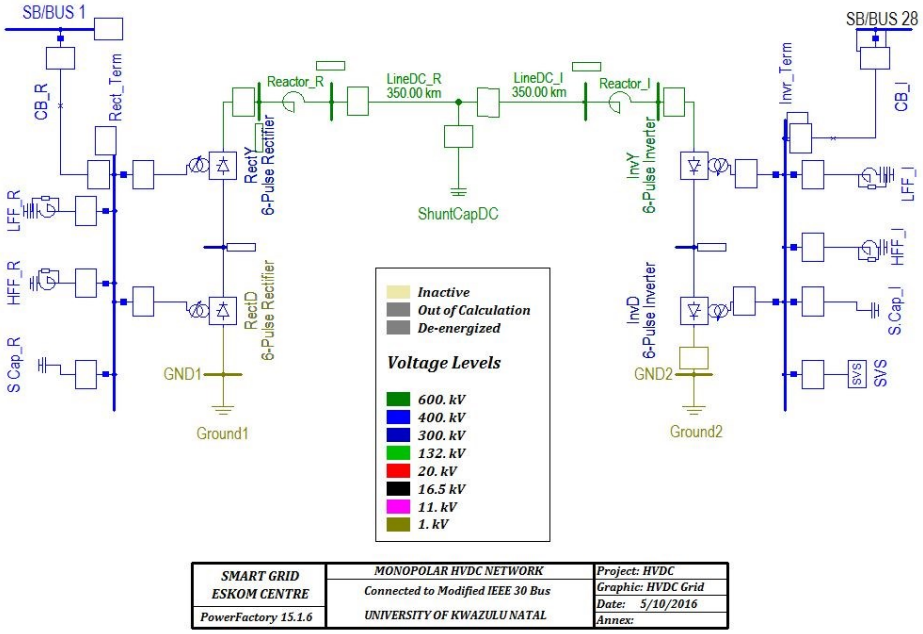

Fig. 3. Monopolar HVDC model.

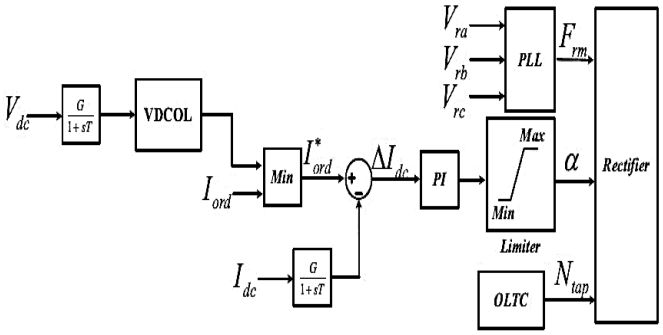

Fig. 4. Rectifier Controller.

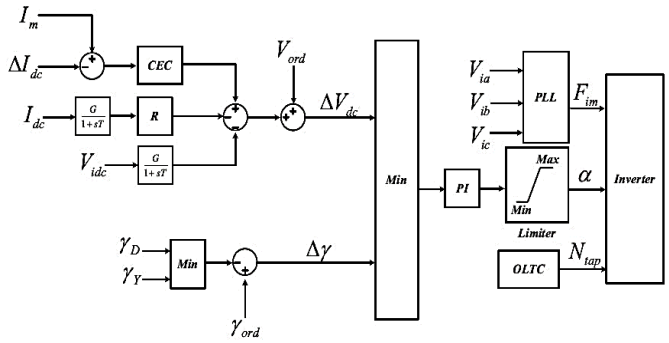

Fig. 5. Inverter Controller.

IV. Simulation Result

The results consist of both the steady state power flow results which are depicted in bar graphs and transient stability analysis results which are configured using the real time RMS simulation.

A. Steady-State Load Flow

The steady state load flow results follows the Newton Raphson iterative equation for power flow calculation. Fig. 4 to 8 show the steady load flow presented in a bar diagram format for the bus voltage magnitudes, the line loading, and load active and reactive power respectively. From the line loading diagram, the transmission line connecting bus 3 and 1, and the line connecting bus 8 and 3 is already overloaded beyond their ratings, even transmission line connecting bus 9 to bus 13. However, the HVDC line is out of service, so as to know the systems condition when only AC lines is in operation (meaning HVDC system is out of service). Fig. 8 present active load demand in the IEEE 30-bus system.

B. Time-Domain Stability Simulation

Two operational scenarios were considered in this study. The first scenario is when the power is being transmitted using AC lines only, and the second scenario is when an existing longest AC line is replaced with an HVDC line and the results are depicted on a graph. Bus voltage and generator excitation current are the main object of focus for this study.

For the bus voltage magnitude graph, specific busbar that are prone to voltage instability was selected rather than use all the 30 buses of the network.

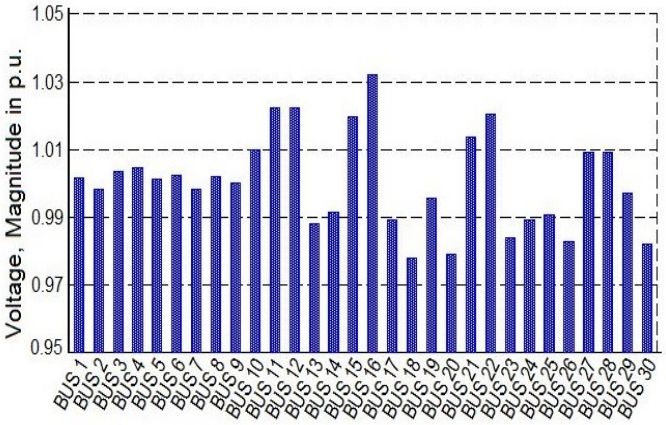

Fig. 6. Busbar voltage magnitudes.

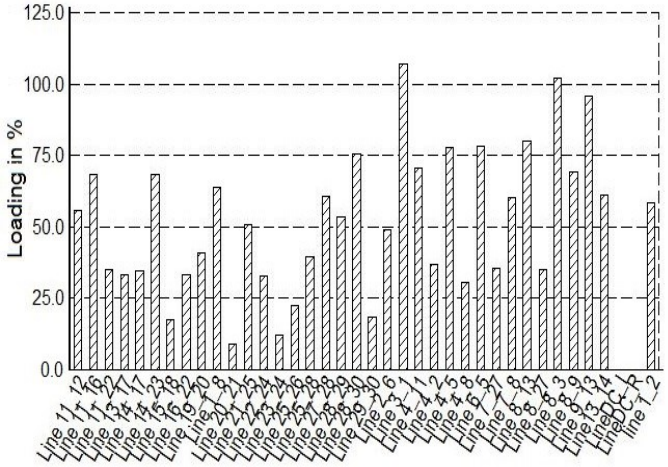

Fig. 7. Line loading (AC Lines only).

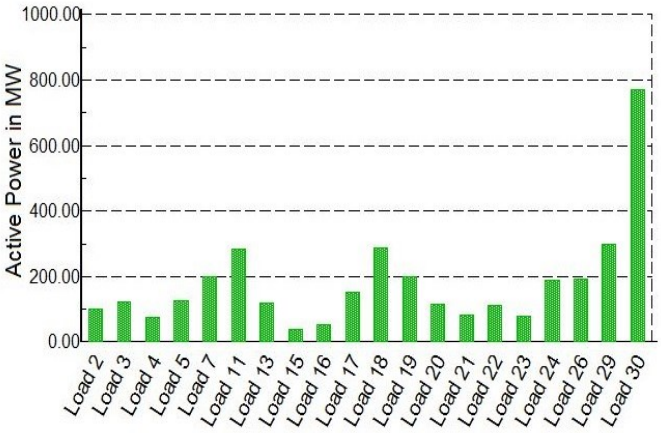

Fig. 8. Load active power.

1) First scenario (without HVDC)

Different study cases was carried out while using the time domain simulation to investigate the weakest area of the network. This involve the use of critical clearing time to observe the maximum time a fault can stay on each of the element on the network (busbar and lines). Three phase short circuit fault was placed on each of the busbar once at a time and their CCT was estimated. It was observed that bus 8 has the least critical time. The same process was also carried out on the line (placing the fault at the beginning of the line) and cleared

by switching off the line.

Fig. 9-11 show the bus voltage magnitude, generator rotor angle and its excitation current when a three phase fault placed at the beginning of 'line 1_3' was simulated and the fault cleared by switching the line off after 100ms. This is the maximum allowable time the fault can stay on the line for the system to be stable when using only AC lines to transmit power from one region to another. During the fault, the bus voltage dips down to about 0.11pu, but the generator exciter helps to restore the system back to stability by increasing the field current winding of the synchronous generator. Thereby automatically adjust the field current to maintain the required terminal voltage.

Fig. 12-14 shows a situation whereby the fault stay more than expected time before the circuit breaker of the line was opened (120ms). This caused the generator to have yielded all its excitation limit and the systems enter instability when the voltage profile of all the buses cannot be met again. This causes the generator angle to swing 360^0 off from the reference machine, a situation caused when the generator pole slipped.

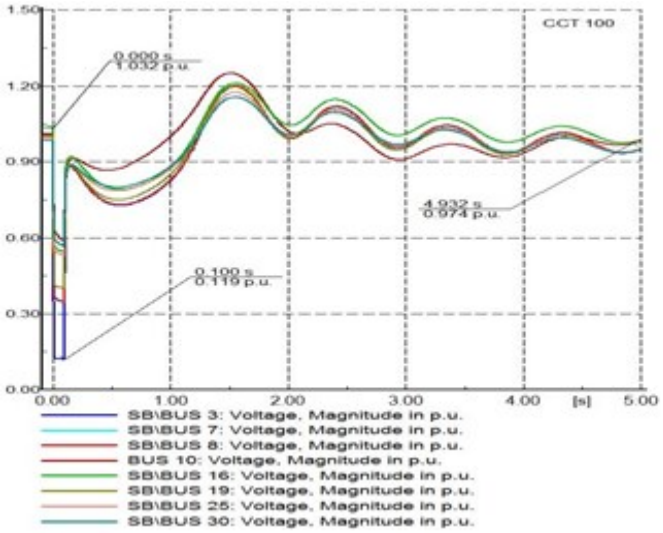

Fig. 9. Voltage Plot during fault on 'Line 3_1', cleared by switching off the line after 100ms. (Without HVDC line).

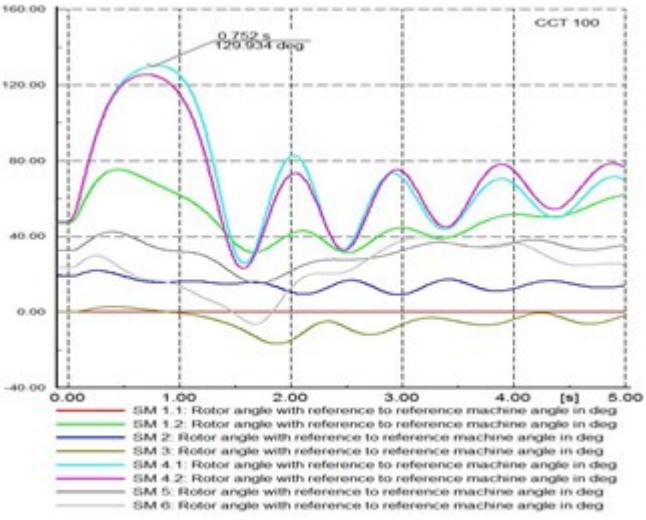

Fig. 10. Generators rotor angle (Without HVDC line).

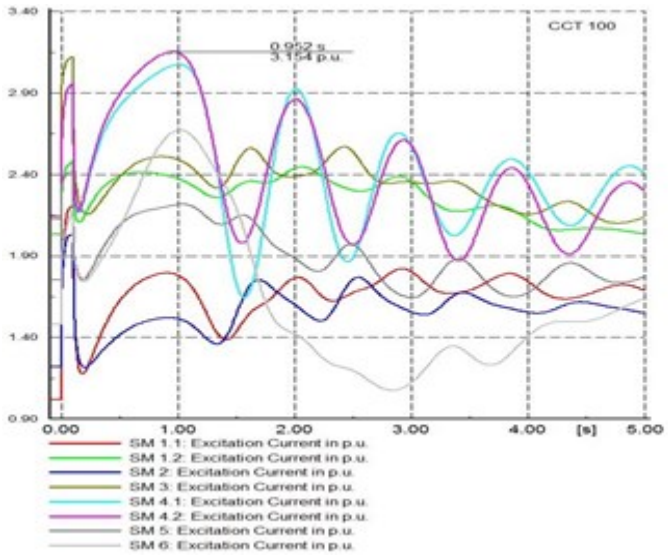

Fig. 11. Generator excitation current (Without HVDC line).

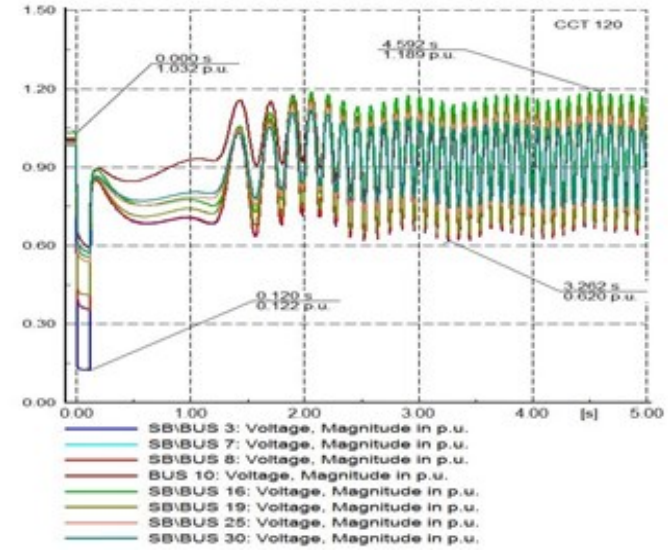

Fig. 12. Voltage Plot during fault on 'Line 1_3', cleared by switching off the line after 120ms. (Without HVDC line)

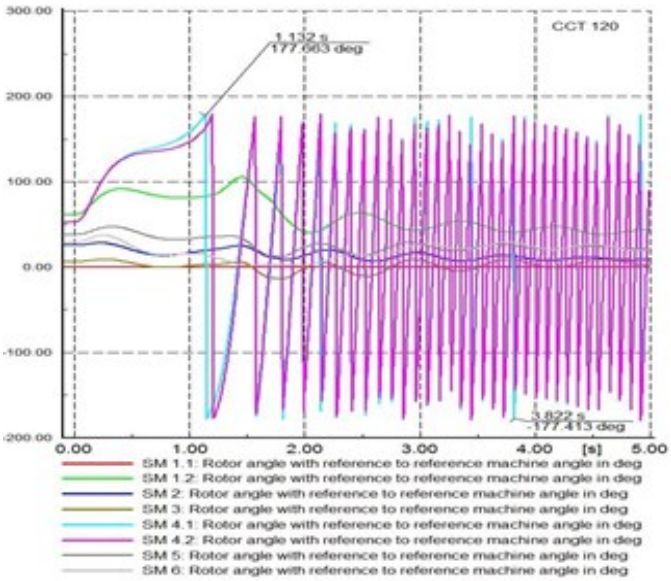

Fig. 13. Generator Rotor angle fault (Without HVDC line)

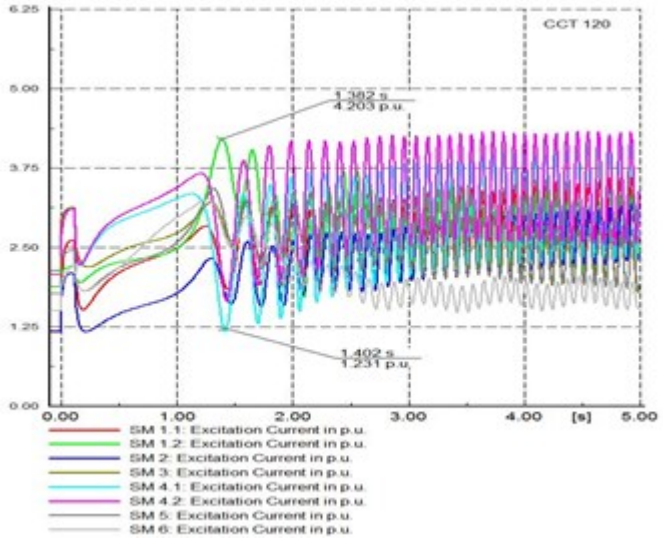

Fig. 14. Generator Excitation current (Without HVDC line)

2) Second scenario (With HVDC line).

When existing AC 'line 8_27' was replaced with a monopolar HVDC system as shown in fig. 3, the load flow result for the lines loading are shown below in Fig. 15, with all lines loading within acceptable range.

The same three phase fault scenario was carried out on 'Line 3_1' and the fault cleared by isolating the line after 120ms while using HVDC line to interconnect 'bus 1' to 'bus 28', it was found out that the system was stable even until it reaches a maximum time of 150ms. Further increase of fault clearing duration beyond this limit resorted in convergence error. Fig. 16-18 shows the bus voltage magnitude, generator rotor angle and excitation current respectively.

A case of commutation failure occur at the inverter side of the HVDC link during fault period, but with the help of the converter selection mode by blocking the fault current from transferring into the HVDC link, the systems was able to maintain stability. HVDC systems thus help to increase the time duration a fault can stay on the line before being isolated from the systems. All different study cases carried out on the systems prove the efficacy of HVDC link in power systems stability and control during system disturbance.

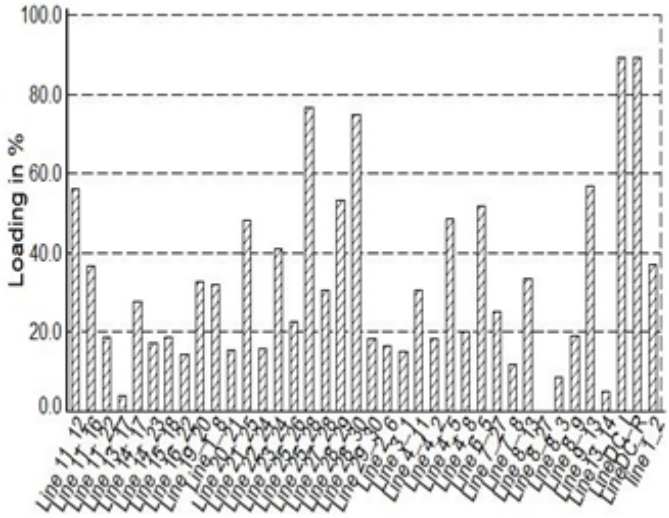

Fig. 15. Line loading (with HVDC line).

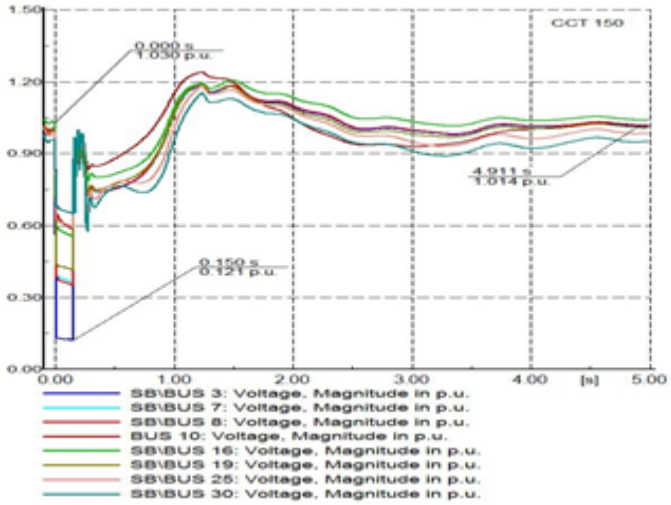

Fig. 16. Voltage Plot during fault on 'Line 3_1', cleared by switching off the line after 150ms. (With HVDC line).

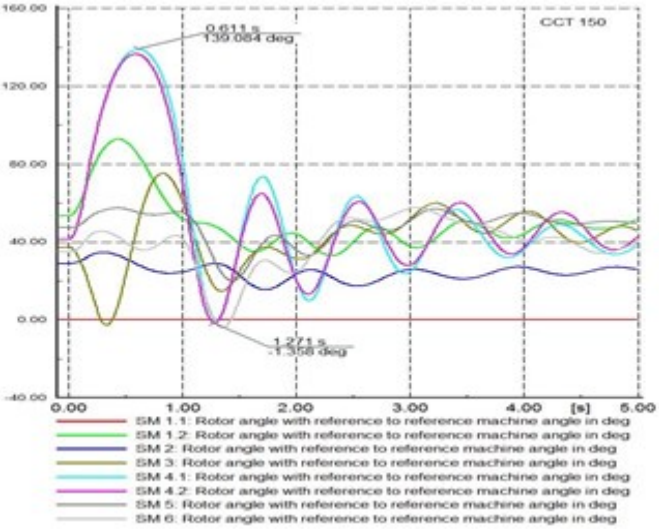

Fig. 17. Generators rotor angle (With HVDC line).

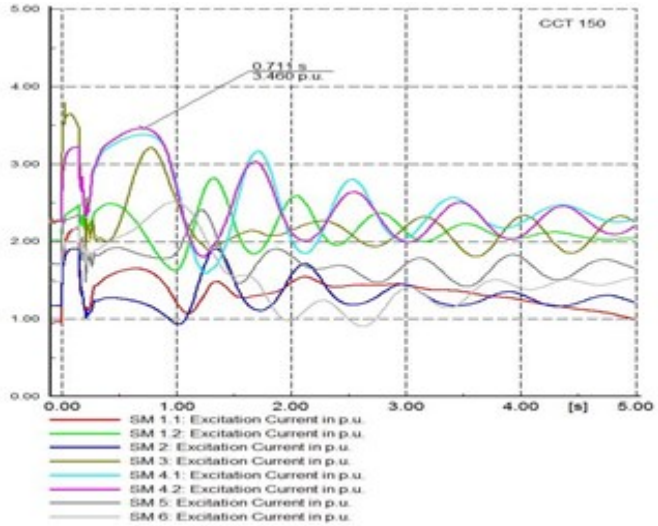

Fig. 18. Excitation current. (With HVDC line).

V. CONCLUSION

Impact of HVDC scheme on AC systems short term voltage stability study was investigated in this study, and based on this study; it was found out that HVDC systems helps in enhancing voltage stability than the AC line, in that it helps to improve the critical clearing/ isolating time for disturbances on the systems. The effect of VDCOL in HVDC link during systems disturbance was also analyzed. The strategies for improving voltage stability are thus proposed; that HVDC lines improve dynamic voltage stability of power systems.

Although, different FACTs devises and a well modelled generator controller helps in enhancing voltage stability of a system. However, this cannot be compared to the benefit which HVDC systems offers, namely; little line losses, long distance bulk power transfer, immunity to cascading effect, bi-direction power transfer, small right of way, asynchronous interconnection etc. Initial cost of constructing converter station can be a little expensive, but the cost saved by transmission line construction with associated losses in DC systems outweigh the latter. And with the emergence of new power electronic converter and well rugged controller, HVDC system will be the best mode to transmit bulk power due to high efficiency and economics of transmission that it offers.

VI. REFERENCES

[1] G. Morison, B. Gao, and P. Kundur, "Voltage stability analysis using static and dynamic approaches," IEEE Transactions on Power Systems, , vol. 8, pp. 1159-1171, 1993.

[2] T. Van Cutsem and C. Vournas, Voltage stability of electric power systems vol. 441: Springer Science & Business Media, 1998.

[3] M. Noroozian, L. Ängquist, M. Ghandhari, and G. Andersson, "Improving Power System Dynamics by Series-Connected FACTS Devices," IEEE Transactions on Power Delivery, , vol. 12, pp. 1635-1641, 1997.

[4] Y.-H. Song and A. Johns, Flexible AC Transmission Systems (FACTS): IET, 1999.

[5] S. Gasperic and R. Mihalic, "The Impact of Serial Controllable FACTS Devices on Voltage Stability," International Journal of Electrical Power & Energy Systems, vol. 64, pp. 1040-1048, 2015.

[6] C. Vournas and M. Karystianos, "Load Tap Changers in Emergency and Preventive Voltage Stability Control," Transactions on Power Systems, IEEE, vol. 19, pp. 492-498, 2004.

[7] Y. Wang, D. J. Hill, R. H. Middleton, and L. Gao, "Transient Stability Enhancement and Voltage Regulation of Power Systems," IEEE Transactions on Power Systems, , vol. 8, pp. 620-627, 1993.

[8] D. L. H. Aik and G. Andersson, "Power Stability Analysis of Multi-Infeed HVDC Systems," IEEE Transactions on Power Delivery, , vol. 13, pp. 923-931, 1998.

[9] Hammad, "Stability and Control of HVDC and AC Transmissions in Parallel," IEEE Transactions on Power Delivery, vol. 14, pp. 1545-1554, 1999.

[10] O. E. Oni, K.N.I. Mbangula and I.E. Davidson, "Voltage Stability Improvement of a Multi-Machine System using HVDC," Proceedings of the Clemson University Power Systems Conference (PSC), March 8-11, 2016, Clemson University, Clemson, SC, USA.

[11] K. N. I. Mbangula, I. E. Davidson and R. Tiako, "Improving Power System Stability of South Africa's HVAC Network Using Strategic Placement of HVDC Links", CIGRE Science & Engineering Journal (CSE), Vol. 5, June 2016, pp. 71-78.

[12] K.N.I. Mbangula, O.E. Oni and I.E. Davidson, "The Impact of HVDC Schemes on Network Transient Rotor Angle Stability". In Proceedings of the 24th South African Universities Power Engineering Conference, 26-28 January 2016, Vereeniging, South Africa, pp. 461 – 466, ISBN 978-1-77012-386.

[13] DigSILENT PowerFactory: Power System Stability Seminar DigSILENT Buyisa (Pty) Ltd.

[14] W. A. Oyekanmi, G. Radman, A. A. Babalola, and T. O. Ajewole, "Effects of STATCOM on the Critical Clearing Time of Faults in Multi-Machine Power Systems During Transient Stability Analysis Studies," in 2014 IEEE 6th International Conference on Adaptive Science & Technology (ICAST), 2014, pp. 1-6.

[15] R. Kamdar, M. Kumar, and G. Agnihotri, "Transient Stability Analysis and Enhancement of IEEE-9 Bus System. Electrical & Computer Engineering: An International Journal (ECIJ) Volume 3, Number 2, June 2014"

[16] J. Chow and A. Gebreselassie, "Dynamic Voltage Stability Analysis of a Single Machine Constant Power Load System," in Proceedings of the 29th IEEE Conference on Decision and Control, 1990, pp. 3057-3062.

[17] B. H. Lee and K. Y. Lee, "Dynamic and Static Voltage Stability Enhancement of Power Systems," IEEE Transactions on Power Systems, , vol. 8, pp. 231-238, 1993.

[18] DigSILENT PowerFactory: Technical Reference Documentation - General Load, Gomaringen, Germany, 2013.

[19] D. Kong, "Advanced HVDC Systems for Renewable Energy Integration and Power Transmission: Modelling and Control for Power System Transient Stability," Doctor of Philosophy, School of Electronic, Electrical and Computer Engineering, University of Birmingham, Birmingham, 2013.

Oluwafemi E. Oni was born in Nigeria on 17 September 1988. He received his BSc (honours) Degree in Electrical and electronic engineering from Ekiti State University, Ado Ekiti, Nigeria, in 2013. He then proceed to University of KwaZulu-Natal, Durban, South Africa in 2015 for his MSc degree in electrical engineering (currently handed in his Thesis for examination).

He was a system and maintenance engineer at Egbin Power Thermal Plant, Lagos, Nigeria, in 2012 and Omotosho Power plant, Ore, Nigeria, in 2013/2014. He is currently a Research Assistance with Department of Electrical Engineering, University of KwaZulu-Natal. His research includes power systems stability analysis using High Voltage Direct Current transmission scheme, integration of renewable energy into the grid using multi-terminal HVDC scheme, and smart grid systems using FACTs.

Mr. Oni's award and honors include MTN foundation scholarships, ETISALAT scholarship and Ekiti state scholarship.

Kamati N.I. Mbangula was born in Namibia on 20 August 1989. He graduated with a BSc. (Honours) Degree in Electrical Engineering from the University of Namibia (UNAM). He pursued his postgraduate studies in South Africa at the University of KwaZulu-Natal (RSA), and carried out his research at the Eskom Centre of Excellence in High Voltage Direct Current (HVDC). His work experience includes working as a Staff Development Fellow at UNAM, and working as a research assistant and lab technician at the Eskom centre of excellence in HVDC. He is currently employed as a lecturer at UNAM. His fields of interests include power systems stability analysis, and low voltage reticulation systems design and analysis.

Innocent E. Davidson (M'92–SM'02) received the BSc (Hons) and MSc degrees in Electrical Engineering from University of Ilorin in 1984, and 1987 respectively. PhD in electrical engineering from the University of Cape Town, Rondebosch, South Africa1998; and Postgraduate Diploma in business management from the University of KwaZulu-Natal, South Africa, 2004; Associate Certificate, sustainable energy management, British Columbia Institute of Technology, Burnaby, Canada, 2011.

From 1994-1995, he was Engineering Inspector, Rainbow Energy Project at EASIGAS (Pty) Ltd, Cape Town; Senior Lecturer, University of Pretoria (1999-2001); Senior Lecturer, Department of Electrical Engineering, University of KwaZulu-Natal (UKZN), 2001–2006; Part-time Instructor, Graduate Engineering Program (Power & Energy), UKZN High Voltage DC Centre (2000-2008) a program co-offered by UKZN and Eskom - South Africa's Electric Utility. From 2005–2006, he was a Visiting Professor, Powertech Labs Inc., Surrey, BC, a world leading consortium in clean energy technologies, independent testing services, power system solutions and smart utility services. From 2007-2011 he was Energy Consultant in Surrey, BC, implementing energy efficiency (electricity/gas) measures, British Columbia provincial government's mandate on Climate Change. He has been an invited guest writer for the IEEE Power and Energy technical magazine as an Expert on Africa: "Energizing Africa's Emerging Economy", IEEE Power and Energy, Vol. 3, No 4, July/August 2005. He was Associate Professor of Electrical Engineering and Research Coordinator, University of Namibia (2012-2014); Director, Eskom Centre of Excellence in HVDC Engineering, UKZN (2014-2016). Currently, he is a Full Professor of Electrical Engineering, Durban University of Technology, South Africa. He is the author/co-author of over 150-refereed journal and conference papers. His research focus is on Grid integration of renewable energy using Smart Technologies and Innovation for Smart Cities.

Prof Davidson is a member, Western Canada Group of Chartered Engineers (WCGCE); the Institute of Engineering and Technology (IET Canada) British Columbia Chapter; a Chartered Engineer, C.Eng. United Kingdom. He is a Fellow of the South African Institute of Electrical Engineers and a registered professional engineer, P. Eng. (ECSA), South Africa.

Value Stream Mapping for Evaluation of Load Scheduling Possibilities in a District Heating Plant

Raivo Melsas, Argo Rosin and Imre Drovtar

***Abstract*— Demand side response enables cost optimization for energy systems and industrial consumers. In many countries, it is not widely used because of implementation complexity. One of the solutions for applying demand side response is industrial process scheduling according to the energy market needs. From the energy system point of view, process scheduling implies load scheduling. The aim of this paper is to provide a solution for load scheduling by implementing value stream mapping, which is a straightforward enough for production management. Decision makers in the industry should have a clear understanding about positive effect from load scheduling and its effect to production outcome and process availability. Value stream mapping is a well-known process optimization tool from lean production philosophy. The aim of value stream mapping is to shorten the lead time of industrial processes and to reduce the intermediate stock amounts. By complementing value stream map with process energy intensity and energy stored in intermediate stocks, we can promote load scheduling possibilities. Our methodology provides a tool that is understandable and traceable for industry-minded decision makers. Finally, we present a real life test example for the new methodology, which is based on the production process of a district heating plant.**

***Index Terms*— demand response, energy storage, load management, load scheduling, value stream mapping**

I. Introduction

Load scheduling (LS) as part of demand side response (DSR) must meet the needs of industry. One of the effects for the industry appears when load consumption is shifted from periods of high electricity price to those of low price. As a result, cost savings can be achieved by means of reduced consumer demand in high price periods. This requires better production planning, which is related to production management.

Previous DSR studies have resulted in the following: static Stackelberg game theory for voluntary load curtailment programs [1]; numerical calculation method for DSR when a battery energy storage system (BESS) is utilized [2]; solutions for DSR by means of automatic lighting [3]; DSR with micro-CHP systems [4]; an overview for DSR methods in high consumption industries and examples of market tools that support DSR [5]. In [6] an automated complex system for LS in industry is described, which takes into account stock restrictions, maintenance schedules, and crew management. All the necessary inputs are analyzed with a fuzzy/expert-based system combined with an optimization module. As a result, the system is able to identify whether and how much the industrial plant can participate in a DSR event. In [7] and [8] DSR is addressed as a part of the following main load shaping strategies:

a) *conservation - energy saving is achieved through static methods;*

b) *load growth - energy consumption is increased when an energy system has surplus energy production;*

c) *valley filling - load is increased through the off-peak periods or keeping stable consumption;*

d) *peak clipping - energy consumption is decreased in peak periods;*

e) *load shifting - peak consumption is shifted from peak periods to non-peak periods;*

f) *seasonal load reduction - annual energy peaks are reduced.*

LS is used mainly in “load shifting” strategy e; however, in some cases, “valley filling” strategy can be utilized as well. To use the LS, an industry must have the following one or several DSR options [8]: cooling equipment with cooling storage, heating equipment with heat storage, dual fuel systems that can operate either on electricity or on an alternative fuel, discretionary loads and process equipment that can be shifted during a short period or material handling equipment with storage possibilities (silos, stock, etc.). This paper focuses on the last option by looking at process as a whole in order to find LS solutions. In addition, it provides a method applicable in industry for outlining the possibilities with LS as a part of DSR by using value stream mapping (VSM). VSM is applicable in

This research was supported by the Estonian Centre of Excellence in Zero Energy and Resource Efficient Smart Buildings and Districts, ZEBE, grant 2014-2020.4.01.15-0016 funded by the European Regional Development Fund.

R. Melsas, A. Rosin and I. Drovtar are with the Department of Electrical Engineering, Tallinn University of Technology, Ehitajate tee 5, 19086 Tallinn, Estonia (e-mail: raivomelsas@gmail.com, argo.rosin@ttu.ee, imre.drovtar@gmail.com).

various ways. Originating from Toyota Production Systems [9], it was further elaborated and adjusted to find solutions for different problems in the production process. For example, VSM is used to solve quality problems [10]. This paper elaborates on VSM. Our proposal is to use it for indicating a possibility to shift an electrical load from a high price period to a low price period and utilize an intermediate stock for energy storage [11], [12], [13]. This paper will provide a straightforward solution for the industry in order to apply LS effectively and which is easily applicable.

II. II. ENERGY PRICE AS A DRIVER FOR LOAD SHIFTING

LS can yield an economic effect under rational consideration. Cost reduction can be achieved by taking advantage of energy price fluctuations during a day. It is reasonable to have demand response implemented in countries where an electricity pool exists and hourly based spot prices are known for a short period ahead. As a result, industries can plan their production according to the spot price. Fig. 1 shows an average 24-hour electricity market spot price in Estonia in 2014 [14]. As can be seen, electricity spot price is typically higher from 07:00 A.M. to 8:00 P.M. In general, there is at least 10-euro price difference during a day and a night. Considering the price peak and dip approximately 20-euro difference per MWh exists during a day. On average, price difference during a day is 15-euro MWh.

However the consideration above includes only electricity price; in addition, there are some fluctuations in grid service price as well. From 12:00 A.M. to 8:00 A.M. (11:00 P.M. to 7:00 A.M. in winter time), the grid service price is lower. This period is not overlapping 100% with a low spot price period. We will call this period (12:00 A.M. to 8:00 A.M.) as the Low Price Period (LPP) and the other period during a day as the High Price Period (HPP). Grid tariffs depend on grid connection voltage level and connection capacity (amps). In the following, we will describe one example to examine the daily price difference for the industry in Estonia.

At substantial electricity consumption, an industry is usually connected into a middle voltage (MV) grid. In that case, Estonian grid service price is 14.5 euros per MWh from 8:00 A.M. to 24:00 A.M. and during LPP 8.3 euros per MWh [15]. For some customers, no time difference is applied; the price for grid services is constant in time- 12 euros per MWh. Fig. 1 shows both the grid price and the spot price fluctuations.

In 2014, an average electricity spot price for LPP was 29.5 euros per MWh and with grid price fluctuations it amounted to 37.8 euros per MWh, which we call as the Low Price Period Price (LPPP). In 2014, an average HPP spot price was 40.9 and together with grid tariff, the average number was 55.1 euros per MWh, which we call as the High Price Period Price (HPPP). For clarity, 55.1 is an average found on hourly bases, i.e. spot price + grid price.

Based on the data provided, we can calculate potential savings for industry under LS. Potential cost saving is 31%, which is calculated by (1):

$$CS = \frac{HPPP - LPPP}{HPPP}. \quad (1)$$

In general, it can be concluded that grid tariff fluctuation has an important role in LS in Estonia, as the average difference in the spot price between HPP and LPP was 11.4 euros per MWh and grid tariff will add extra for the difference between HPPP and LPPP, according to [15], tariff depends on the grid connection parameters.

The shape of the electricity spot price in Fig. 1 can be considered as a typical shape of the daily demand of electricity as well; a similar shape of demand can be found in various places, e.g., even in South Africa [16]. Thus, DSR has a positive impact to overall efficiency to energy systems, not only to an industry itself.

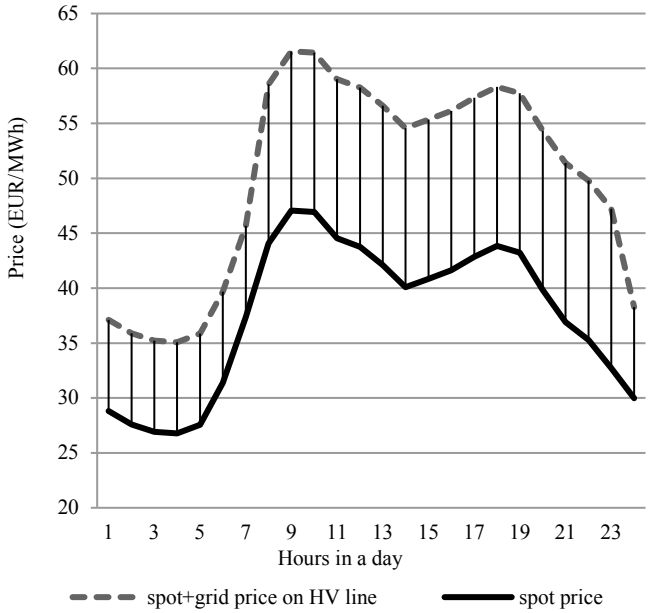

Fig. 1. Average Estonian 2014 electricity spot price during a day.

III. IMPROVEMENT OF VALUE STREAM MAPPING METHODOLOGY FOR EVALUATION OF LOAD SCHEDULING POSSIBILITIES

A. Load Scheduling at Intermediate Storage Use in Production

In the following, LS possibilities are examined for intermediate storage use as an energy saving unit, to enable shifting of energy intense production from HPP to LPP. In LS, it is important to understand energy intensive production units and their overall role in the production. Methods from lean philosophy [LP] can be used here. We propose to improve the value stream mapping (VSM) methodology with LS principles. Today LP is a leading production management philosophy. VSM is used to plan production as efficiently as reasonably possible. Energy intensity can be added in a process as additional information for a VSM, which will give a good overview about the possibilities in energy saving. Fig. 2 gives an overall picture of a typical VSM, elaborated with process energy intensity and amount of energy stored in the production intermediate storage.

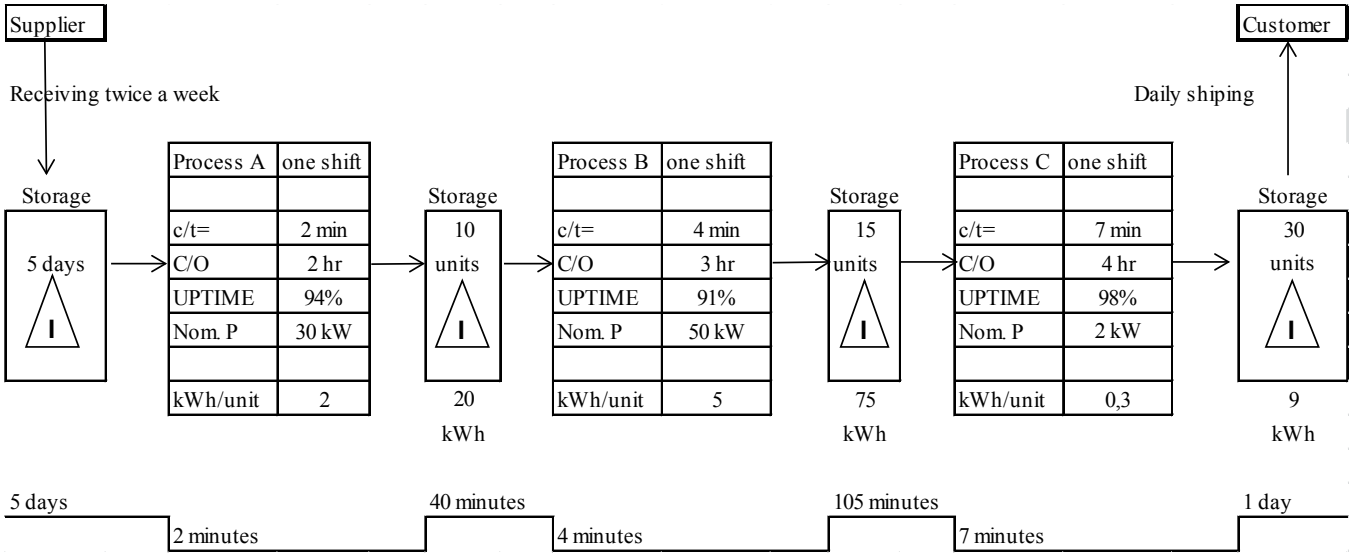

Fig. 2. VSM with energy consumption and storage overview.

As VSM gives an overview of the production planning and can additionally give information about energy intensity, the possibility of the LS should be studied in detail. From VSM, we will know if an energy intense process is at the same time a bottleneck in production. If it is not true, then the conclusion is that this process is not 100% utilized in time and LS can be implemented without increasing process capacity. Alternatively costs for increasing process capacity (CPC) need to be calculated.

Next, we focus on the storage. If production is shifted in time, storage volume can increase as compared to the state without LS utilized. Storage increase may need additional investments, which should also be considered as costs for storage (CS). Also, costs of the process (CP) itself for LS should be taken into account. As an example CP related to LS can be an increase in labor costs due to night shifts. Finally, if the costs related to LS are lower than a possible income from LS (ILS), the LS can be implemented in the industrial process. This criterion is given in the following (2):

$$CPC + CS + CP < ILS . \quad (2)$$

B. Methodology for LS with VSM.

The main initial goal of LP and VSM was to reduce lead time (L/T), i.e, the time it takes to move a produced piece all the way in the process or production from start until to the end. As a result, many costs or wastes, as defined in LP, will be reduced. As shown in (2), income from LS should be higher than costs related to it because LS can increase the intermediate stock and due to that it has a negative effect on the L/T as well. VSM is a tool that will help to find the processes which have a reasonable effect and income. To achieve that, cost saving potential must be estimated. In section II, we showed a possible gain from LS in Estonia. The next step is to define the energy consumption of the processes. It is useful to combine that with VSM. If a company already has VSM, then energy consumption should be added into the VSM. VSM will highlight important information to be considered for LS. Most importantly, the following information must be taken into account:

a) *Identify if the process is a bottleneck in production. If the process is a bottleneck, then load shifting is usually impossible without investment into the process output increase.*

b) *Process cycle time (C/T) is slower or faster than its next process C/T. C/T in VSM describes how often a part or a product is completed by a process. If the process C/T is slower than the process coming next, it is possible to increase intermediate stock at the end of the process coming after rather than at the end of the first process. In case the first process is faster than the next one, the LS applied will increase the intermediate stock.*

c) *Weather process uptime (UPTIME) is high or low, shows important information about process reliability. A low reliability process has a negative effect on LS.*

d) *If stock between processes is high or low, the reasons should be found out before applying load scheduling.*

e) *Change over time (C/O) is long or short. C/O is the time period for switching the process unit from one product to another. It can show also time for cold start of the process. C/O can highlight important information about the process start up time.*

The best way to start defining the energy consumption of a process is to make the consumer list. Consumer list should be based on processes described with VSM. The consumer list may be available in the facility electrical department. In that case, consumer list is usually based on the power cabinets and it has to be made process by process. If the consumer list is not available, it should be done from scratch. As the purpose is to find an initial energy intensive process, the consumer list can be composed without actual measurements. The consumer list should contain the following information: process name; device

label; rated power; $\cos_{\varphi}$; nominal current; nominal voltage and consumption type that can be either continuous, intermittent or stand by.

Upon completion of the consumer list, traditional VSM should be elaborated and total nominal loads in the process added. As a result, elaborated VSM will show which processes have sufficiently high energy intensity to gain benefits from LS and on the other hand, to estimate the particular potential to the process scheduling. After completing the estimation in conjunction with experts from production, the VSM should be elaborated further. Based on the measurements, energy intensity or the production unit is to be found. As the energy usage was previously estimated, measurements can be done in the production process where energy usage is estimated to be high or VSM shows that LS can be implemented without investing to process capacities or intermediate stocks.

As VSM describes product flow, the energy intensity should also be given per product or production unit. The unit energy consumption in the production process should be calculated based on the actual measurement. Fig. 2 shows a theoretical example of VSM together with data from the consumer list and energy intensity in the process. Energy intensity is energy consumption in each process to make one unit. As can be seen, process A C/T takes 2 minutes, i.e., one unit is completed during 2 minutes in the process. The total nominal power of the process is 30 kW and 2 kWh is consumed to make one unit. First intermediate stock capacity (after process A) is 10 pieces. It consists of 20kWh energy which is available for scheduling. Process B C/T is 4 minutes and the total nominal power in that process is 50 kW. As the second intermediate stock (after process B) capacity is 15 pieces, it has 75 kWh energy available for scheduling. Process C cycle time is 7 minutes, total nominal power is 2 kW and 0.3 kWh is consumed for making one unit. We can see that process A C/T is 2 times faster than process B and process C cycle time is 3.5 times faster than process A. As a result, we can conclude that the last process will dictate the whole process time and previous processes can be scheduled taking into account the possibilities of the last process. For that reason, we need to know how much time it takes to empty the intermediate stock before the slowest process, which we call buffer time (BT). In order to find BT, process C/T must be multiplied with an available intermediate stock capacity (ASC) (3) and (4).

$$ASC = MSC - SSC \,. \tag{3}$$

$$BT = C/T \cdot ASC \,. \tag{4}$$

ASC is a difference between maximum stock capacity (MSC) and safety stock capacity (SSC). SSC is to be defined by production management.

BT shows the maximum load scheduling period in the process. Neglecting safety stock capacity, in our example BT is 105 minutes. The total energy we can shift during 105 minutes is 95 kWh, which is the sum of stored energy in two intermediate stocks with 75 and 20 kWh accordingly.

IV. EXPERIMENTAL LOAD SCHEDULING ANALYSIS IN A DISTRICT HEATING PLANT WITH IMPROVED VSM METHODOLOGY

An example of the method above is described here. This example covers a district heating plant in Paide, Estonia. The company has one 8 MW woodchip boiler, several boilers fuelled with shale-oil and one CHP plant based on woodchips and with 8 MW thermal, 2 MW electrical output. Fig. 3 shows the process of the plant. Woodchip boiler stock (moving floor) is filled by a conveyor from the main storage (moving floor). The main storage is filled by the incoming tucks or a wheel loader. The company has 5-day storage available on site. Woodchip boiler stock can contain woodchips a day with boiler nominal load i.e. 180 m³. The conveyor between the main storage and the woodchip boiler stock has a maximum output of 50 m³/h. The conveyor from the woodchip boiler stock to the boiler has a strict limitation for processing output from the woodchip boiler. As it has no stock or daily silo available between the boiler and the conveyor, the output is 7.5 m³/h with the nominal boiler load. We start the cost reduction estimation from LS by modeling the process using VSM as a basis. One cubic meter of woodchips is taken here as one unit in VSM.

According to the conveyor output parameters, the total output time is 6 days and 15.2 minutes and the value creating time is 17.2 minutes (time when one cubic meter of woodchips is actually processed). Also, the VSM shows that the conveyor from the main to the boiler stock has excessive capacity and is able to process one cubic meter of woodchips approximately 6.67 times faster than the process bottleneck, i.e. woodchip boiler.

The boiler will process one cubic meter of woodchips into heat in 8 minutes. It can be concluded from VSM that there is a possibility of LS of the conveyor from the main storage to the boiler stock. It must be emphasized that we are dealing with a biomass conveyor; therefore, the following simplifications are used:

a) woodchip processing by a boiler is calculated based on the nominal load, and boiler efficiency parameter is 0.8;

b) woodchip energy intensity is approximated at 1.3 MW/m³, in real life it can be different, based on the fuel type and humidity level.

The next task is to estimate process energy intensity by making a consumer list behind the process. In our example, it is evident from VSM that the only process that can be scheduled is the process called “Conveyor from Main Stock to Boiler Stock”. Thus, we need to make a consumer list behind this process, which is given in Table I

Table I shows that the total nominal power behind the process is 73.5 kW. The consumer list is necessary to estimate of the process energy demand. It is possible that some consumer’s nominal power is much greater than the actual absorbed power. Therefore it is necessary to measure the process energy use.

TABLE I
CONSUMER LIST FOR CONVEYOR FROM MAIN STOCK TO BOILER STOCK

Description	Pn	Cos ϕ	In	Un	Consumption
Conv. Screen to dist. Conv.	15	0.8	46.9	0.4	Continuous
Distr. conveyor	7.5	0.8	23.4	0.4	Continuous
Floor to conveyor motor	4	0.8	8.6	0.4	Continuous
Floor to conveyor motor	4	0.8	8.6	0.4	Continuous
Hydro pack	15	0.85	28.9	0.4	Intermittent
Hydro pack	15	0.85	28.9	0.4	Intermittent
Screen	5.5	0.81	11.4	0.4	Continuous
Conv. floor to screen	7.5	0.8	23.4	0.4	Continuous

In our example, Fluke 1735 is used for measurements of the process energy use and current measurements for some continuous consumption. There is calculated absorbed power with the following (5).

$$P = 3 \cdot I_f \cdot U_f \cdot \cos_{\varphi}, \quad (5)$$

where P is absorbed power, If- phase current, Uf- phase voltage and $\cos_{\varphi}$ is power factor. By using absorbed power for a continuous load, energy consumption was estimated as well. Total energy consumption for processing 1 m³ of woodchips was 0.96 kWh. Complete VSM for the process examined is given in Fig. 3.

The VSM shows that by processing one cubic meter of woodchips there is consumed 0.96 kWh of electrical energy. As there is storage available with 180 m3 and SSC is 7.5 m3, ASC is 172.5 m3 using (3). By knowing process C/T behind the intermediate stock- it is 8 minutes per m3. There can be found out that BT is 23 hours by using (4).

We can conclude that BT is sufficiently long for considering LS from HPP to LPP given in section II. Paide boiler plant is connected to a grid at low voltage line, so the grid tariffs applicable will be different from those given in section II. HPPP for the current example is 83.4 euros per MWh with 43.5 euros per MWh grid tariff and LPPP is 55.2 euros per MWh with 25.7 euros per MWh grid tariff. Based on (1), we can calculate potential saving which is 33.8%.

As stored energy in the process is 0.166 MWh, by multiplying that with HPPP, the cost for the company will be 13.81 euros per day and saving from LS will be 4.67 euros per day.

In the previous example, the VSM process is not complicated; however, VSM is essential in case production is more complicated and processes are more complex and dependent on each other. In that case, VSM enables cost savings with LS. Moreover, LS is well understandable with VSM for staff involved in production management and planning.

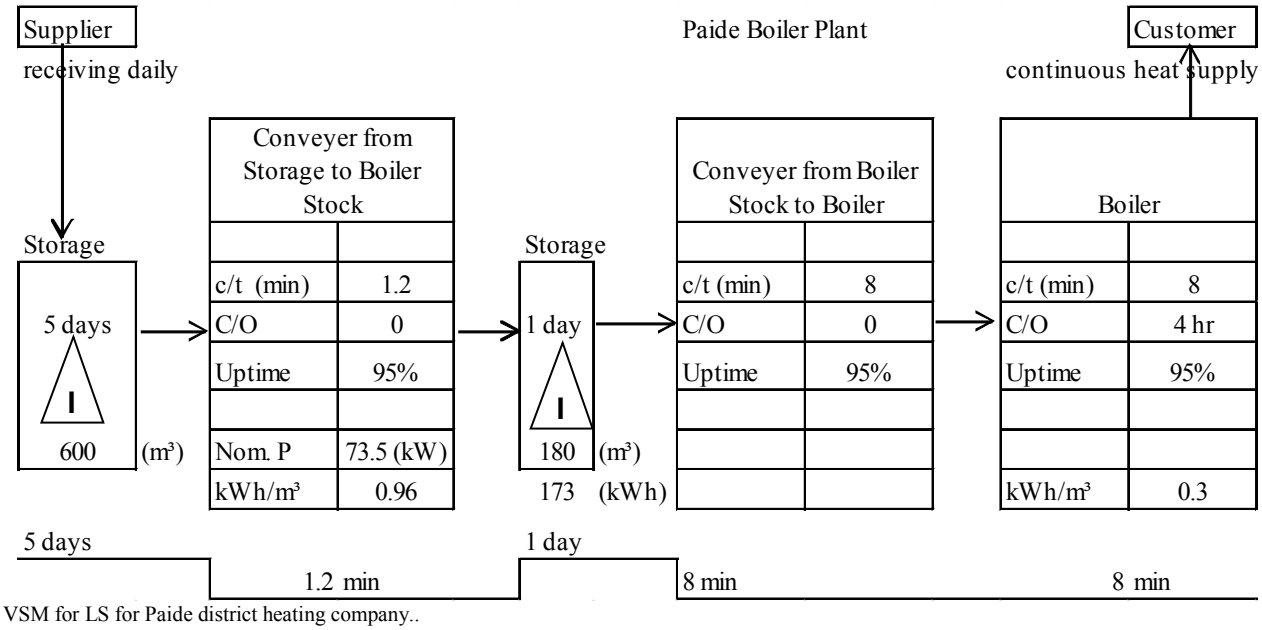

Fig. 3 VSM for LS for Paide district heating company..

V. CONCLUSION

Various aspects of DSR were studied. Focus was on the price difference in the electricity stock market in Estonia. If the loads are shifted from HPP to LPP LS will enable a cost reduction of 31%. The methodology based on VSM was introduced where cost savings were achieved with LS. Our analysis of experimental load scheduling was based on the district heating company in Estonia. The proposed methodology was found to be applicable as a straightforward tool to achieve cost savings. It can serve as first step for industry when implementing LS because of its simplicity. With minor costs, reduced time and lower complexity, a major cost saving can be achieved with simple solutions such as the method proposed.

REFERENCES

[1] P. Kontogiorgos and G. P. Papavassilopoulos, "Subsidized power interruption for reducing peaks in energy demand: A stackelberg game," Communications, Control and Signal Processing (ISCCSP), 2014 6th International Symposium on, Athens, 2014, pp. 421-424. doi: 10.1109/ISCCSP.2014.6877903

[2] G. Carpinelli, S. Khormali, F. Mottola and D. Proto, "Demand response and energy storage systems: An industrial application for reducing electricity costs. Part II: Numerical application," Power Electronics, Electrical Drives, Automation and Motion (SPEEDAM), 2014 International Symposium on, Ischia, 2014, pp. 1038-1042. doi: 10.1109/SPEEDAM.2014.6872040

[3] S. A. Raziei and H. Mohscnian-Had, "Optimal demand response capacity of automatic lighting control," Innovative Smart Grid Technologies (ISGT), 2013 IEEE PES, Washington, DC, 2013, pp. 1-6. doi: 10.1109/ISGT.2013.6497854

[4] M. Houwing, R. R. Negenborn and B. De Schutter, "Demand Response With Micro-CHP Systems," in Proceedings of the IEEE, vol. 99, no. 1, pp. 200-213, Jan. 2011. doi: 10.1109/JPROC.2010.2053831

[5] A. Rosin, I. Drovtar, S. Link, H. Hõimoja, H. Mõlder and T. Möller, "Analysis of large electricity consumers demand profiles to determine implementation of demand-side management measures", "Tarbimise juhtimine – suurtarbijate koormusgraafikute salvestamine ning analüüs juhtimise rakendamise võimaluste tuvastamiseks," Eleringi toimetised, pp. 1-57, 20 October 2014.

[6] S. Mohagheghi and N. Raji, "Dynamic demand response solution for industrial customers," Industry Applications Society Annual Meeting, 2013 IEEE, Lake Buena Vista, FL, 2013, pp. 1-9. doi: 10.1109/IAS.2013.6682583

[7] A. Mohamed and M. T. Khan, "A review of electrical energy management techniques:supply and consumer side (industries)," Journal of Energy in Southern Africa, vol. 20, no. 3, 2009.

[8] A. Kuhi Thalfeldt and P. Raesaar, "Possibilities and feasibility of demand-side management in the Estonian industrial sector," in 5 th International Symposium "Topical Problems in the Field of Electrical and Power Engineering", Kuressaare, 2008.

[9] T. Ohno, "Toyota production system: beyond large-scale production", Portland, 1988.

[10] B. Haefnera, A. Kraemera, T. Staussa and G. Lanzaa, "Quality value stream mapping," in 47th CIRP Conference on Manufacturing Systemss, Windsor, 2014.

[11] P. Uuemaa, J. Valtin, J. Kilter, A. Puusepp, I. Drovtar and A. Rosin, "Load control implementation in the energy intensive industry," Mediterranean Electrotechnical Conference (MELECON), 2014 17th IEEE, Beirut, 2014, pp. 213-218. doi: 10.1109/MELCON.2014.6820534

[12] I. Drovtar, P. Uuemaa, A. Rosin, J. Kilter and J. Valtin, "Using demand side management in energy-intensive industries for providing balancing power - The Estonian case study," Power and Energy Society General Meeting (PES), 2013 IEEE, Vancouver, BC, 2013, pp. 1-5. doi: 10.1109/PESMG.2013.6672418

[13] P. Uuemaa, J. Kilter, J. Valtin, I. Drovtar, A. Rosin and A. Puusepp, "Cost-effective optimization of load shifting in the industry by using intermediate storages," Innovative Smart Grid Technologies Europe (ISGT EUROPE), 2013 4th IEEE/PES, Lyngby, 2013, pp. 1-5. doi: 10.1109/ISGTEurope.2013.6695404

[14] AS, Nord Pool Spot, "Elspot_prices_2014_hourly_EUR," 2014. [Online]. Available: http://www.nordpoolspot.com/historical-market-data. [Accessed 20 June 2015].

[15] Elektrilevi OÜ, "Price list fo Elektrilevi from 01.04.2014", "Elektrilevi hinnakiri alates 01.04.2014," 1th April 2014. [Online]. Available: www.elektrlilevi.ee/hinnakiri. [Accessed 19th June 2015]

Description of Measurements on Biogas Stations

Ladislav Novosad, Zdenek Hradilek

***Abstract*—This paper focuses mainly on performance analysis for three biogas stations situated within the territory of the Czech Republic. This paper contains basic details of the individual biogas stations as well as description of their types. It also refers to the general description of the measurement gauge involved, with specifications of its potential use. The final part of this paper deals with the analysis of course data obtained, with special regard to voltage, current, active power and reactive power data.)**

***Index Terms*— biogas station; power analysis; measurement database; black out; co-generation units; distribution grid**

I. Introduction

The distribution networks (DN) have experienced the rise in volumes of electric power generated by renewable energy resources (RES) over the recent years. Vast majority of these resources work within the distribution network on decentralized basis and this practice brings a lot of new problems. Such problems are due to the very principle employed by certain resources. The dependency on weather conditions among photovoltaic and wind power plants would be a typical example. The question is how to ensure safe and stable operation or even development of such system. That is why one needs to know characteristics of particular RES, also including the biogas stations (BS). The reason above is therefore addressed by this paper with respect to operation of BS and provision of details referring to the variability of output produced over time.

II. Description of Measurement

These requirements were accommodated by several long-term measurements conducted right at biogas stations. These BS are situated at three various locations within the territory of Czech Republic, serving as both resources of electric power as well as heat. The generated heat is extracted from combustion products and cooling of the co-generation units by means of heat exchangers. It is then used for heating applied in BS technologies, fermenters, adjacent farm and office buildings. Nevertheless, most of the thermal energy is wasted, and conducted away to the surroundings through forced ventilation using electric fans and coolers. The utilization of thermal energy is not the primary aim of this article, and it is therefore not discussed further.

The measurement at each of the three biogas stations was conducted using the automatic digital measurement devices – the network analyzer BK ELCOM ENA 330 and Monitor distribution grids MDS-U(MDS10). This is a complete systems for monitoring and analysis of electric power quality. The devices was employed to record effective values of phase voltage and current in one-minute increments. The voltage readings were taken right from the bus bars inside the main distribution board of BS; monitoring of current was performed using flexible coils – AmpFLEX. The device then completed calculations of remaining values, as the active or reactive power, as well as the apparent power automatically and saved these details in its internal memory.

Fig. 1. Demonstration of a connection measurement equipment in the BS 1

The electric power generated by all three BSs is supplied to the main distribution board, which is linked with a transformer station rated for 0.4/22kV further connected to the 22kV distribution grid (DG).

The measurement of electric values also involved assessment of electric power quality in compliance with CSN EN 50160. The characteristics subject to assessment included mainly the magnitude and drops of voltage, the total harmonic distortion of voltage, flicker and voltage unbalance.

This research was partially supported by the SGS grant from VSB - Technical University of Ostrava (No. SP2016/95).

Fig. 2. Demonstration of a co-generation unit in the BS 1 biogas station

The network analyzer BK ENA 330 used in this case complies with the requirements focused on measurement equipment and the measurement procedure set forth by standards ČSN EN 50160, ČSN EN 61000-4-7, ČSN EN 61000-4-15 and ČSN EN 61000-4-30. [4]. This research was partially supported by the SGS grant from VSB - Technical University of Ostrava (No. SP2016/95).

A. Biogas station at location 1

The first measurement was conducted at the BS in location 1 (BS 1). The biogas station itself is situated within the premises of a piggery farming enterprise. The input raw material for the wet fermentation process is then represented mainly by pig's slurry and maize silage. This BS provides the installed electrical capacity of 1090 kW. Transformation of biogas into electric power is handled by four co-generation units. There are three identical compression ignition units delivering the output of 250 kWe and one spark ignition unit with the output of 340 kWe. (1 x KGJ: Agrogen type BGA 222 - 340 kWe and 3 x CGU: Schnell type ES 2507 - 250k We).

- The measurement was conducted in the following period: from 9.1.2014 to 24.2.2014 - 58 days in total

B. Biogas station at location 2

Another measured BS was the one in location 2 (BS 2). This station forms a part of the collective farm nearby; this is also the point for supply of the input raw materials for fermentation. The main input raw materials for wet fermentation at this BS is grass silage, wheat silage, maize silage, pig's or cow's slurry. This BS provides the installed electrical capacity of 1186 kWe. Conversion of biogas into electric power is handled by two co-generation units GE Jenbacher JGS 312 GS-B.LC with the electrical power of 549 kW and GE Jenbacher JGS 312 GS-B.LC with the electric power of 637 kW. [1]

- The measurement was conducted in the following period: from 20.8.2014 to 19.9.2014 - 31 days in total

C. Biogas station at location 3

The last measurement was performed at location 3 (BS 3). This BS also forms an immediate part of the collective farm enterprise dealing both with livestock and crops production. The extraction of biogas is also based on wet fermentation with the raw material represented by maize silage and farmyard slurry. These are supplied from the said collective farm enterprise. Electric power and heat are generated using three co-generation units (CGUs) made by Schnell, fitted with Scania combustion engines. The total installed electrical capacity of the BS is 750kW (2xKGJ with the electrical power of 265kW and 1xKGJ delivering the electrical power of 250kW).

- The measurement was conducted in the following period: from 20.8.2015 to 19.9.2015 - 31 days in total

III. CREATING A DATABASE OF MEASUREMENT

The method described above yielded large amounts of data. The initial processing of these data was done using software that comes with the measurement equipment. Comprehensive waveforms of individual variables depending on time were created with this software. Furthermore, the data were exported and processed using MS Office Excel 2007. STATGRAPHICS Centurion XV.II was subsequently used for the statistical evaluation. An example of a part of thus created database is shown in Fig. 3. [3]

Date	Time	Urms_1_avg	Urms_2_avg	Urms_3_avg	Urms_T_avg	Irms_1_avg	Irms_2_avg	Irms_3_avg	Irms_T_avg
03.09.2015	12:49:00.019	2,3884E+02	2,4051E+02	2,3949E+02	2,3961E+02	9,0427E+02	9,4752E+02	9,8417E+02	9,4588E+02
03.09.2015	12:50:00.025	2,3904E+02	2,4063E+02	2,3962E+02	2,3976E+02	9,2842E+02	9,6910E+02	1,0041E+03	9,6770E+02
03.09.2015	12:51:00.027	2,3888E+02	2,4059E+02	2,3920E+02	2,3956E+02	9,3943E+02	9,7975E+02	1,0112E+03	9,7723E+02
03.09.2015	12:52:00.027	2,3853E+02	2,4026E+02	2,3881E+02	2,3920E+02	9,4191E+02	9,8252E+02	1,0148E+03	9,8020E+02
03.09.2015	12:53:00.006	2,3863E+02	2,4040E+02	2,3891E+02	2,3931E+02	9,4101E+02	9,8167E+02	1,0149E+03	9,7964E+02
03.09.2015	12:54:00.195	2,3870E+02	2,4047E+02	2,3898E+02	2,3939E+02	9,5280E+02	9,9186E+02	1,0259E+03	9,9065E+02
03.09.2015	12:55:00.178	2,3862E+02	2,4040E+02	2,3890E+02	2,3931E+02	9,6789E+02	1,0064E+03	1,0407E+03	1,0054E+03
03.09.2015	12:56:00.167	2,3880E+02	2,4058E+02	2,3911E+02	2,3950E+02	9,7210E+02	1,0102E+03	1,0431E+03	1,0089E+03
03.09.2015	12:57:00.158	2,3833E+02	2,4014E+02	2,3867E+02	2,3905E+02	9,7522E+02	1,0114E+03	1,0453E+03	1,0110E+03
03.09.2015	12:58:00.164	2,3829E+02	2,4009E+02	2,3863E+02	2,3901E+02	9,7426E+02	1,0098E+03	1,0438E+03	1,0097E+03
03.09.2015	12:59:00.166	2,3867E+02	2,4049E+02	2,3902E+02	2,3939E+02	9,7380E+02	1,0094E+03	1,0435E+03	1,0093E+03
03.09.2015	13:00:00.149	2,3904E+02	2,4087E+02	2,3937E+02	2,3976E+02	9,6899E+02	1,0052E+03	1,0396E+03	1,0050E+03
03.09.2015	13:01:00.132	2,3922E+02	2,4103E+02	2,3951E+02	2,3992E+02	9,7022E+02	1,0078E+03	1,0413E+03	1,0069E+03

Fig. 3. Sample of database of measured data

IV. ASSESSMENT OF THE DATA MEASURED

The next part of this paper deals with the analysis of course data obtained, with special regard to voltage, current, active power and reactive power data. Figs 4 to 6 demonstrate the course of the entire active power (P) from the individual BSs measured. The total three-phase active power (P) is then equal to the sum of power ratings of individual phases (P1+P2+P3).

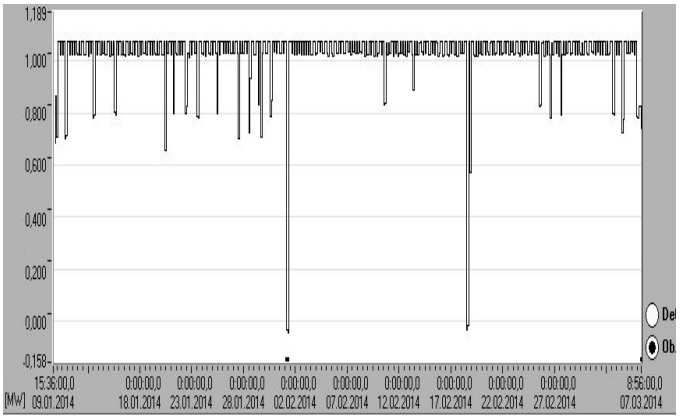

Fig. 4. Course of entire active power over the whole period observed at the location of BS 1

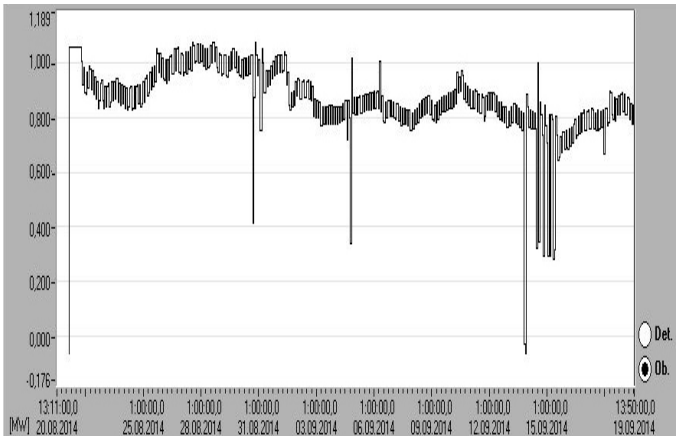

Fig. 5. Course of entire active power over the whole period observed at the location of BS 1

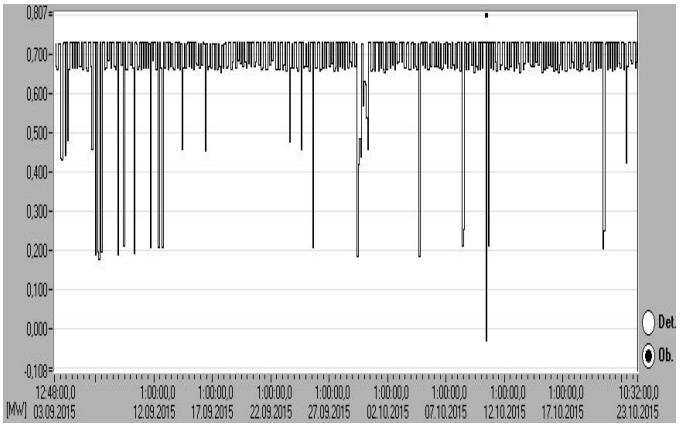

Fig. 6. Course of entire active power over the whole period observed at the location of BS 3

The graphs of active power and the chart depicted here also show that operation of all three BSs encountered black outs or drops of power supplied to the grid. All these BSs show basically the same nature of these drops of the power supplied or black outs, as the case may be. The total duration of these black outs or drops is almost negligible with respect to the total operation time, it ranges between approximately 3,5 and 73,7 hours, representing approx. 0,5 – 5,4 % of the total operation time of CGU in individual BSs. As far as this period is concerned, individual stations would suffer approx. 2,7-69 min. of total power black outs (approx. 0.004 – 0.084 % of the total operation time of individual BSs).

The stability of CGUs at individual biogas stations implies that the supply of electric power is stable and predictable. This is evident mainly during operation of BS 1 and BS 3. These two BSs operated in a fairly stable manner throughout the majority of measurement period, their active power ranged within values approximating the nominal values. The only unit showing larger fluctuation of the output active power was BS 2. However, this fluctuation was mainly due to the incorrect control of BS, i.e. the failure to obey procedures to feed the fermented material.

A. Total black out of the active power (P) supply

Each total black out resulted in a step change of the active power from the regular operating level to the zero supply values. All three biogas stations were disconnected from the grid upon the black out, so no values could be measured. The resumed operation then brought gradual rise of the supplied power up to the regular operating level. The average time to restoration of regular operation after the black out of all CGUs was below 10 minutes at each BS. However, total black outs of CGUs are a very rare phenomenon.

B. Total black out of the active power (P) supply

Another condition occurring during the operation more frequently than total black outs was the drop of supplied power, as mentioned above. As far as the nature of their course was concerned, these drops showed identical characteristics at all three BSs. These drops were characteristic for reduction of the active power of around 100-350kW. The apparent major cause of these drops was represented by shutdown of one or more CGUs for either operating (insufficient volume of biogas generated) or technical (failure/outage) cause. Since each of the BSs mentioned above is provided with a different number and type of co-generation units, the output power available during such drops actually differs.

The Table No. 1 below shows the basic statistical data describing operation of all three co-generation units, i.e. the data includes basic details about the power supply to the grid.

The entire measurement period showed significant fluctuations of grid voltage at all three BSs. The voltage course characteristics of this fluctuation were identical for all three stations and not affected by the operation of CGUs. For demonstration of the voltage course see Fig. 7.

The magnitude of voltage fluctuation was characterized by values from approx. 227V to 245V, i.e. with the total range of about 15.5V. The maximum and minimum deviations of voltage therefore did not exceed the limits defined for the relevant standard (± 10% Un); meaning values within the range from 207V to 253V.

TABLE I
BASIC INFORMATION OF CGUS OPERATION

Basic Information of CGUs Operation			
Basic Information on Power Supply	***BPS 1***	***BPS 2***	***BPS 3***
Total measurement period (h)	1361	693,1	1197,97
Total period of decreased power supply (h)	73,7	3,5	46
Total period of full power failures (h)	1,15	0,25	0.045
Trouble-Free Operation (no black out or power failures)	1287,3	689,6	1151.97
Full supply power failure	2	1	1

Further findings also revealed a certain imbalance of voltage between individual phases. The difference between voltage levels at particular phases amounted up to approx. 2V. This imbalance was then projected at all three BSs to a more or less extent. (Fig.8)

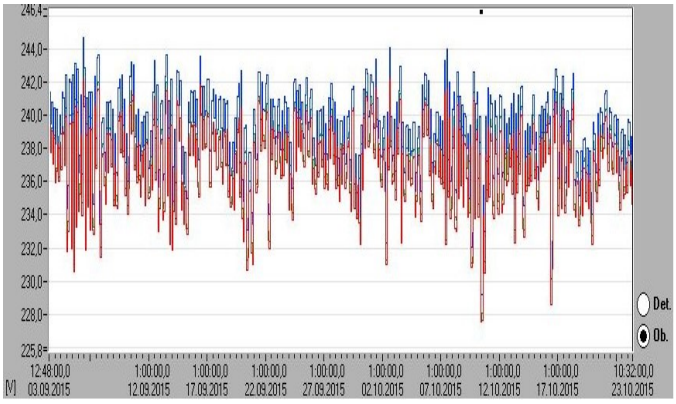

Fig. 7. Course of voltage at BS 3 (colors – individual phases)

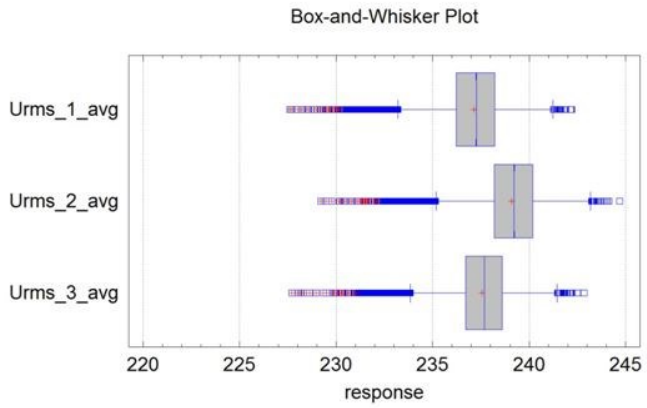

Fig. 8. Box plot of individual phase voltages

V. EVALUATION OF ELECTRIC POWER QUALITY

As already mentioned in the introductory part, each measurement conducted on particular BS was accompanied by evaluation of electric power quality in compliance with CSN EN 50160.

The outcomes of measurement then imply that the network parameters as the frequency, flicker and voltage unbalance complied with conditions given by the relevant standard and applicable to all three BSs subject to measurement. The spectra of harmonics of higher degree and currents were almost identical for all the BSs measured. Figs 9 and 10 show the sample spectrum of harmonic voltage of higher levels with designated permitted limits in accordance with CSN EN 50160 applicable to BS 2.

None of the limits were exceeded, the values approximating these limits are the fifth and seventh harmonics, which exceed a half of the limits permitted. Fig. 9 shows the spectrum of harmonic current of higher levels from the first (basic) up to the fiftieth harmonic. The only features visible throughout the entire spectrum are harmonics of lower levels, i.e. the second, the third, the fourth, the fifth, the sevenths and the eleventh one. Since the spectrum of higher degree harmonics show degrees above the spectrum of harmonic currents caused mainly by synchronous generators in co-generation units, these higher degrees of voltage are most likely dragged in form the superior 22 kV grid.

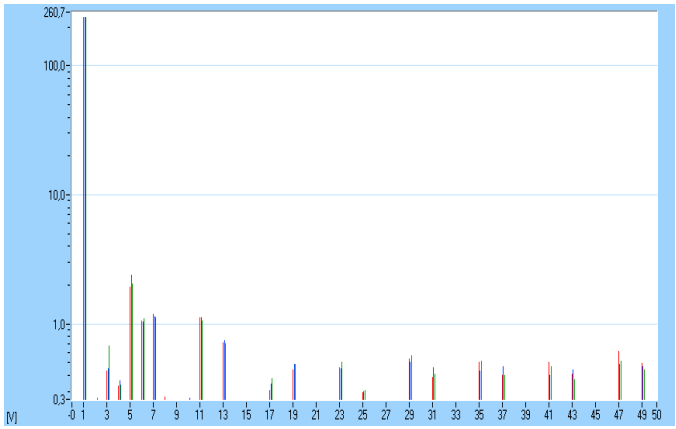

Fig. 9. Spectrum of harmonic voltage of higher levels with designated permitted limits in accordance with CSN EN 50160 – BPS2

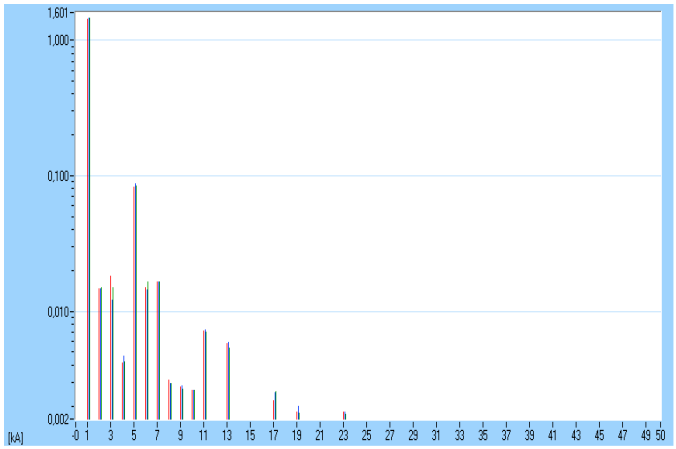

Fig. 10. Spectrum of harmonic current of higher levels with designated permitted limits in accordance with CSN EN 50160 – BS 2

VI. Evaluation of BS measurement results

As far as the operation of all three BSs is concerned, the measurement has proven these sources of electric power as strongly stable. As already mentioned above, these do not show any negative parameters with respect to the electric power quality either. The comparison relating to operation of individual BSs has not disclosed any significant differences. These stations were almost identical with respect to the nature of both their operation and their black outs. When compared to the remaining two BSs, the greatest differences were shown by BS 2.

The operation of all three CGUs shows drops or black outs of electric power. The apparently most frequent reason for full failures of all CGUs at a particular BS was the very configuration of CGU protection features, which mostly respond to extraordinary phenomena in the grid (voltage/undervoltage). These short-term changes could not be recorded owing to the measurement sampling characteristic (1 min).

However, there are more and more occasions with the drop of electric power supply to the grid during operation. The review of operating logs available for particular BSs clearly shows three potential causes of this operating condition. The apparently most frequent cause is the insufficient generation of biogas during the fermentation process or even its low quality. The other one would be regular technical attitudes to maintenance and unexpected black outs due to a technical problem.

The simplest method to reduce drops in electric power production would be to exclude falls caused by insufficient generation of biogas. This problem is associated with the technical procedures during fermentation but the option to store the biogas produced in particular. Storage of biogas produced, i.e. keeping its stock for periods of insufficient production, relates to the volume of gas tank. The vast majority of existing BSs within the territory of Czech Republic has been designed for uninterrupted operation, i.e. the biogas produced is consumed by CGUs almost immediately. In case the volume of biogas generated is excessive or if one or more CGUs have failed, the biogas cannot be stored and it must be combusted on the safety burner (flare), which seems highly uneconomical. This problem can be potentially resolved by construction of new gas tanks or even extension of storage space inside fermentation tanks. Biogas stored in these facilities could be then used to compensate for production lacks or higher demand for electric power or heat.

VII. Conclusion

The aim of this paper was to find reminiscence in the course of power supplied from individual BSs or even to explain the causes of black outs with the attempt to suggest a way for their further elimination.

The results obtained by measurement show the high reliability of electric power supply to the grid (the duration of black outs per BS is equal to approximately 0.0029 % of the operating hours). The supply of electric power from co-generation units combusting biogas can be therefore generally described as very stable and also easily predictable as a renewable energy resource. The greatest impact on power supply is seen at quality, that is the lack of biogas supplied (percentage of methane CH4 in biogas), strongly dependent on the quality of primary (organic) product.

This paper also serves as a source of information about stability of output from co-generation units for further research. The research will deal with cooperation among other renewable resources of electric power (solar or wind power plants) and present an opportunity for stabilization of the power supplied to 22kV grids. The last but not the least purpose of this paper is to contribute towards potential utilization of the BS for storage of electric power for its future re-use during emergency situations in the grid, for example black-outs.

References

[1] L. Novosad, Z. Hradilek, "Power Analysis of Co-Generation Units at Biogas Station", Proceedings of the 16th International Scientific Conference on Electric Power Engineering (EPE) 2015 Dlouhé Stráně, 2015, ISBN 978-1-4673-6788-2

[2] L. Novosad, Z. Hradilek, P. Moldřík, "Analysis of data measured in Tosanovice biogas station", ELNET 2015: 12th workshop : Ostrava, 24th November 2015, pp. 28-36

[3] M. Dummer, M. Litschmannova, "Statistika I.". *Statistika I*. VSB – Technical university of Ostrava, 1997, 80-7078-496-2

[4] Z. Hradílek, "*Elektroenergetika průmyslových a distribučních zařízení*," 1.vyd. VŠB – TU Ostrava. 2008. ISBN 978-80-7225-291-6.,p.315, 2008.

[5] L. Novosad, Z. Hradilek, "Analysis of Energy Balances Three Biogas Stations in Czech Republic", Proceedings of the 16th IEEE International Conference on Environment and Electrical Engineering, 2016

Long-Term Monitoring of Flicker and Some Other Parameters of Voltage Quality

Petr Krejci, Pavel Santarius, Radomir Gono, Zdenek Brunclik

***Abstract*—In 1997 cooperation began between the Faculty of Electrical Engineering and Computer Science and the power company CEZ on a joint project that involved monitoring selected voltage quality parameters. Over the course of several years measurements were carried out at 59 points of the distribution system at a low voltage (LV) level and their power supply nodes at medium voltage (MV) and high voltage (HV) levels, which constituted more than 100 measured points. The measurements continued until 2012 (with a one-year break in 2009) and with a total scope of five cycles of three-year measurements. The last phase of the measurements was focused, inter alia, on the evaluation of 15th and 21st voltage harmonics. From 2013, the cooperation focused again on monitoring flicker in localities with the occurrence of elevated levels of this voltage quality parameter. At these sites, the monitoring of flicker was carried out for two weeks in spring and autumn for a period of three years. The basis for evaluating the quality parameters is the standard EN 50160. In addition the results of annual continual monitoring for one selected locality on MV level will be presented in the paper. In addition the possibility of utilization of intelligent electrometers for monitoring of some quality parameters will be referred in the paper.**

Index Terms*— *flicker, unbalance, voltage harmonics, voltage quality.

I. Comprehensive Long-Term Monitoring of Some Parameters of the Voltage Quality in the Regional Power Engineering Company

As already mentioned, in 1997 cooperation began between the Faculty of Electrical Engineering and Computer Science and the power company CEZ on a joint project that involved monitoring selected voltage quality parameters. Among the main parameters to be monitored were selected harmonic voltages, flicker and voltage unbalance. Given the large number of measurement points, the measurements were divided into six partial stages (the whole range that was measured is shown in Fig. 1), in order to complete the entire measuring cycle within three years. After that period the measurements were repeated, and because they involved five three-year measurement cycles, the monitoring of these quality parameters lasted for 15 years. According to the requirements of the EN 50160 standard [1], the measurement of the voltage quality parameters was carried out for one week, with a measurement interval of 10 minutes. A diagram of the connection of the measuring points is shown in Fig. 2.

Fig. 1. Locality of Measurement

At single feeder points the measured data was evaluated in all phases and on all voltage levels:

- Selected voltage harmonics (3rd, 5th, 7th, 9th, 11th)
- Flicker
- Unbalance (N)

This research was partially supported by the SGS grant from VSB - Technical University of Ostrava (No. SP2016/95 and No. SP2016/146).

Petr Krejci, Pavel Santarius, Radomir Gono
- Faculty of Electrical Engineering and Computer Science
- VSB – Technical University of Ostrava, Ostrava, Czech Republic
- petr.krejci@vsb.cz, pavel.santarius@vsb.cz, radomir.gono@vsb,cz

Zdenek Brunclik
- CEZ Distribuce, a.s.,
- Czech Power Company (CEZ), Ostrava, Czech Republic
- zdenek.brunclik@cez.cz

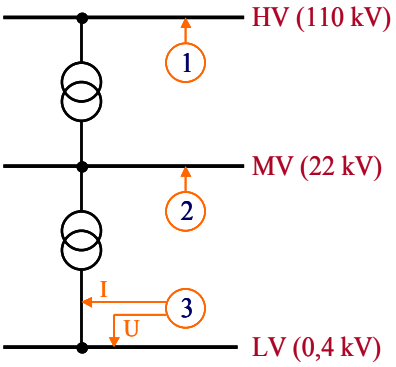

Fig. 2. Ideal connection diagram of measuring points

The results of this long-term measurement have been published continuously, e.g. [2]. This paper summarises the results and particularly the trends in the changes in the voltage quality parameters over the monitoring period of 15 years.

II. Conclusions – the trends of changes

Continuous results of the measurements have already been published several times, e.g. [2]. In the tables below the changes in the selected voltage quality parameters (selected harmonics, flicker and unbalance) in the LV, MV and HV network during the five monitoring cycles are summarised. An example of an evaluation of selected voltage quality parameters (fifth harmonic, flicker and unbalance) in the LV networks is shown in Fig. 3.

TABLE I. Trends of changes in the selected voltage quality parameters in the LV networks

	LV II.-I.	LV III.-II.	LV IV.-III.	LV V.-IV.
U_03 (%)	0.056	-0.016	-0.004	0.00
U_05 (%)	0.157	0.204	-0.334	-0.11
U_07 (%)	0.095	0.204	-0.017	-0.04
U_09 (%)	0.006	0.026	0.010	0.02
U_11 (%)	0.015	0.075	0.024	0.05
P_{st} (-)	0.157	-0.034	0.008	0.05
P_{lt} (-)	0.118	-0.005	-0.022	-0.05
N (%)	0.088	0.043	-0.066	-0.02

TABLE II. Trends of changes in the selected voltage quality parameters in the MV networks

	MV II.-I.	MV III-II.	MV IV-III.	MV V.-IV.
U_03 (%)	0.056	-0.026	-0.019	-0.02
U_05 (%)	0.335	0.181	-0.303	-0.14
U_07 (%)	0.111	0.193	-0.022	-0.09
U_09 (%)	-0.018	-0.009	-0.006	0.00
U_11 (%)	0.016	0.036	0.021	-0.01
P_{st} (-)	0.135	-0.093	0.048	-0.06
P_{lt} (-)	0.077	-0.079	0.022	-0.07
N (%)	0.135	-0.052	-0.058	-0.01

TABLE III. Trends of changes in the selected voltage quality parameters in the HV networks

	HV II.-I.	HV III-II.	HV IV-III.	HV V-IV.
U_03 (%)	0.183	0.089	-0.067	-0.045
U_05 (%)	0.065	0.106	-0.082	-0.057
U_07 (%)	0.040	0.073	-0.004	0.013
U_09 (%)	-0.050	-0.012	-0.002	-0.012
U_11 (%)	-0.001	0.001	0.022	-0.021
P_{st} (-)	0.113	-0.024	0.050	-0.091
P_{lt} (-)	0.131	-0.080	0.050	-0.103
N (%)	-0.017	0.169	-0.176	0.031

The most important conclusions:

a) as regards harmonics, the results are relatively positive; the values of individual harmonic components are significantly below the values of compatible levels and the fifth harmonic was the most considerable at all voltage levels. The extreme values were only found at one point in the LV network, where it exceeded the third harmonic in 1999 (10.7%) and in 2002 (12.6%) and the ninth harmonic in 2002 (2.1%). The probable reason for this was resonance in the LV network;

b) as for unbalance, the changes are also quite small. A small exceeding was only found at three points in the MV network;

c) as for flicker, the situation was worse. Exceeding the compatibility level was found at many measuring points and on all voltage levels;

d) the trends of changes in the selected voltage quality parameters during the years 1997 to 2012 do not show extreme swings or a long-term increase in the selected voltage quality parameters.

III. Measuring and evaluation of 15th and 21st harmonics

In the last monitoring cycle (2010-2012) the 15th and 21st voltage harmonics in the LV distribution network were measured and evaluated. The measuring and evaluation were performed by analysers with a measuring uncertainty of 0.1% of the first harmonic.

The compatibility level of 0.5% was not exceeded at any measurement point. The results of the evaluation of the 15th and 21st voltage harmonics in the LV distribution network are shown in Fig. 4.

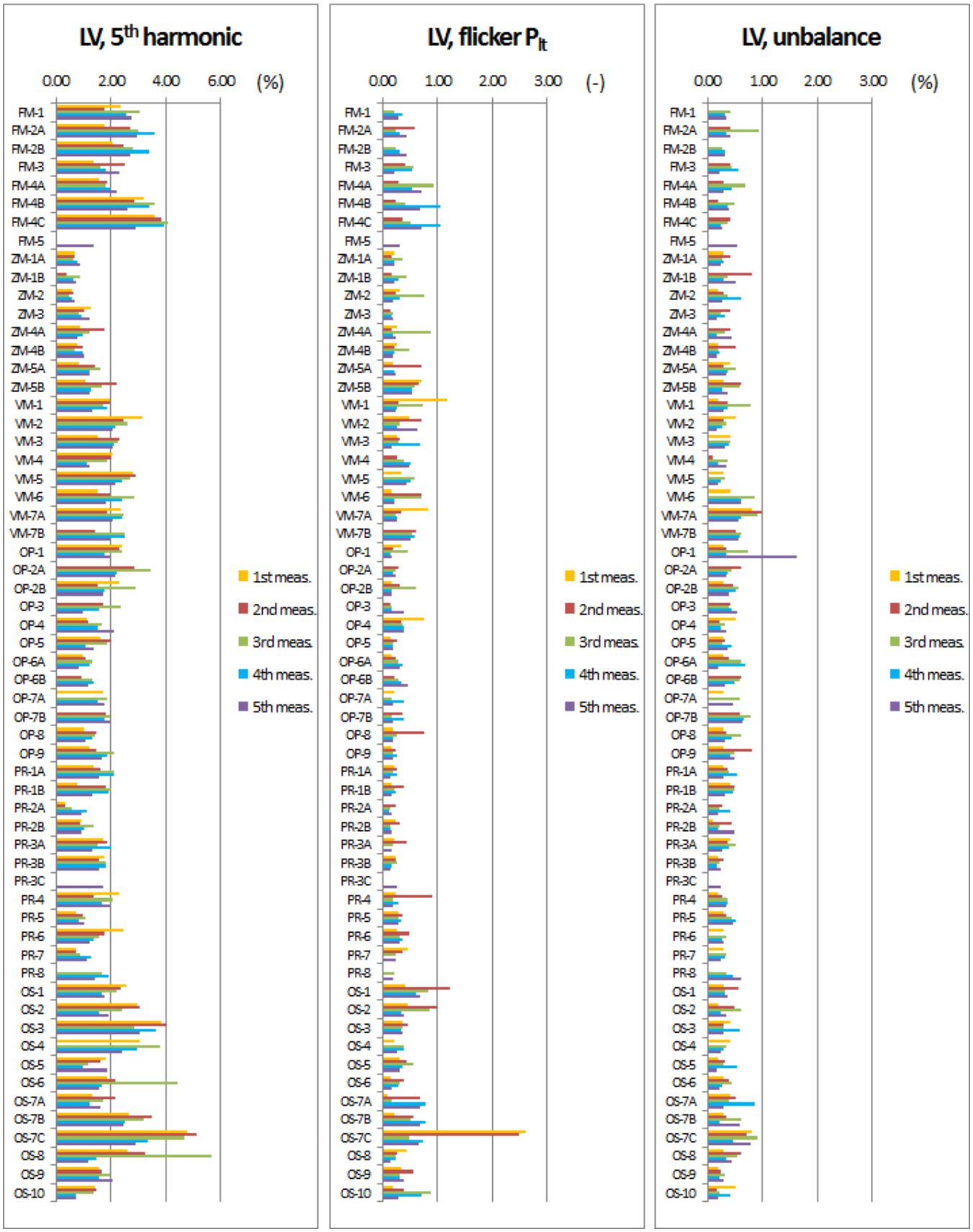

Fig. 3. Example of evaluation of selected voltage quality parameters (fifth harmonic, flicker and unbalance) in the LV networks

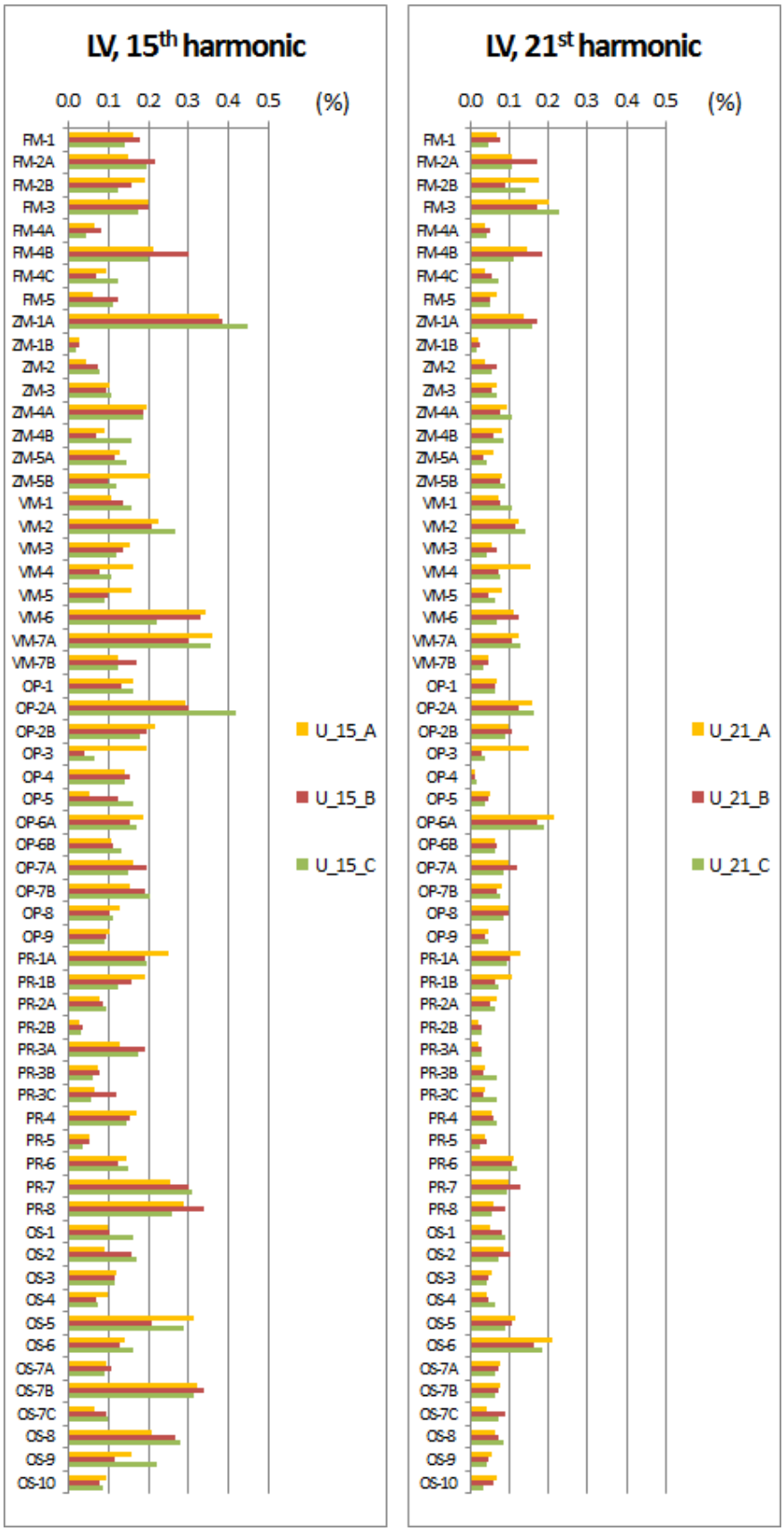

Fig. 4. The results of the measuring and evaluation of the 15th and 21st voltage harmonics in the LV distribution network

IV. LONG-TERM MEASURING OF FLICKER

In 2014 we started the long-term monitoring of flicker [3] at the feeding points at which a problem with compatibility limit violation of flicker was detected. The measuring was done during a two-week period in spring and in autumn. In the figures below examples of the evaluation of P_{st} and P_{lt} in the spring (Fig. 5) and autumn of 2014 (Fig. 6) are shown.

From the present results of the flicker monitoring it is possible to state that at some feeding points the values of P_{lt} were more than 1. The greatest value was 1.7.

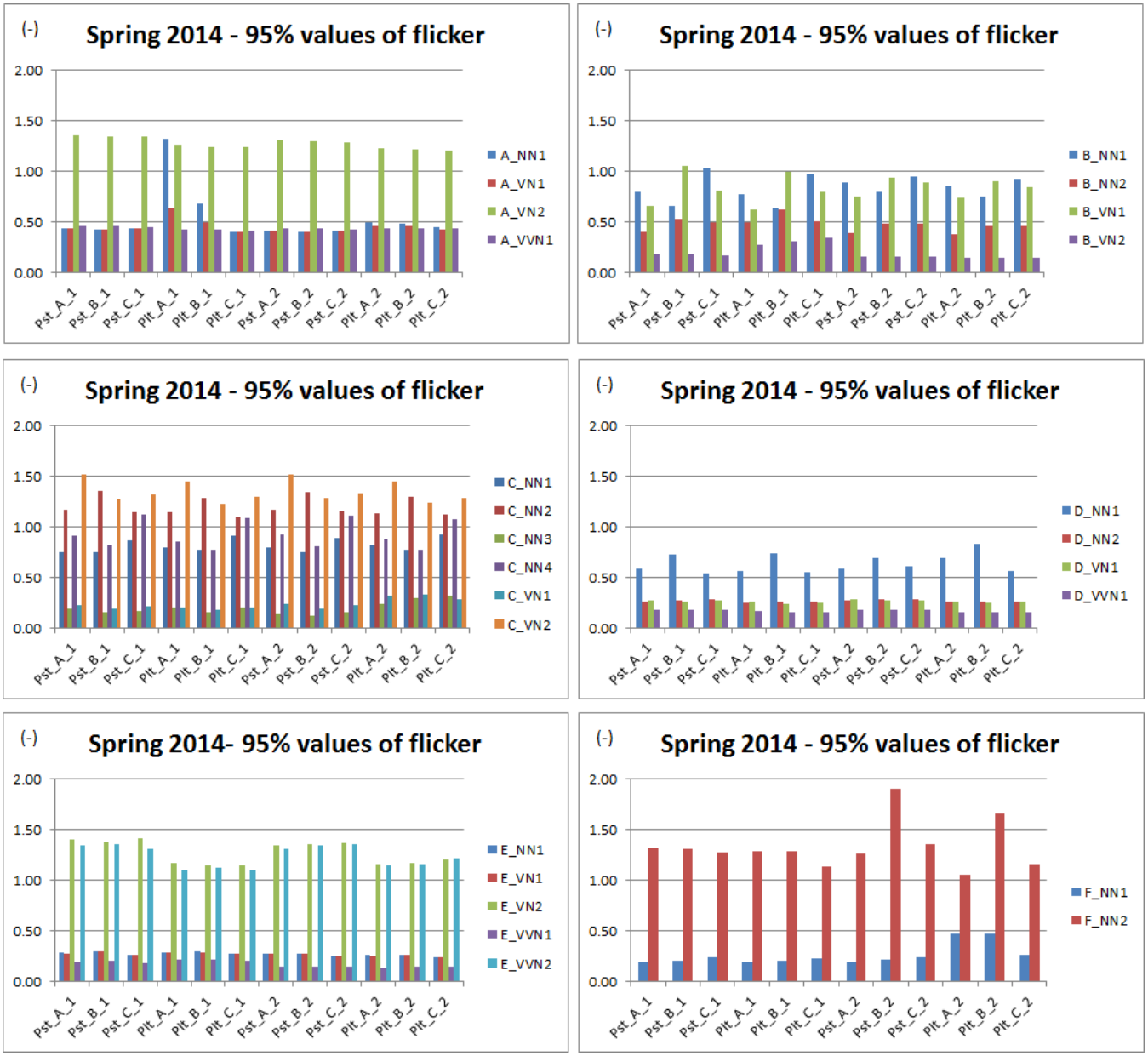

Fig. 5. The results of the measuring of flicker – Spring 2014

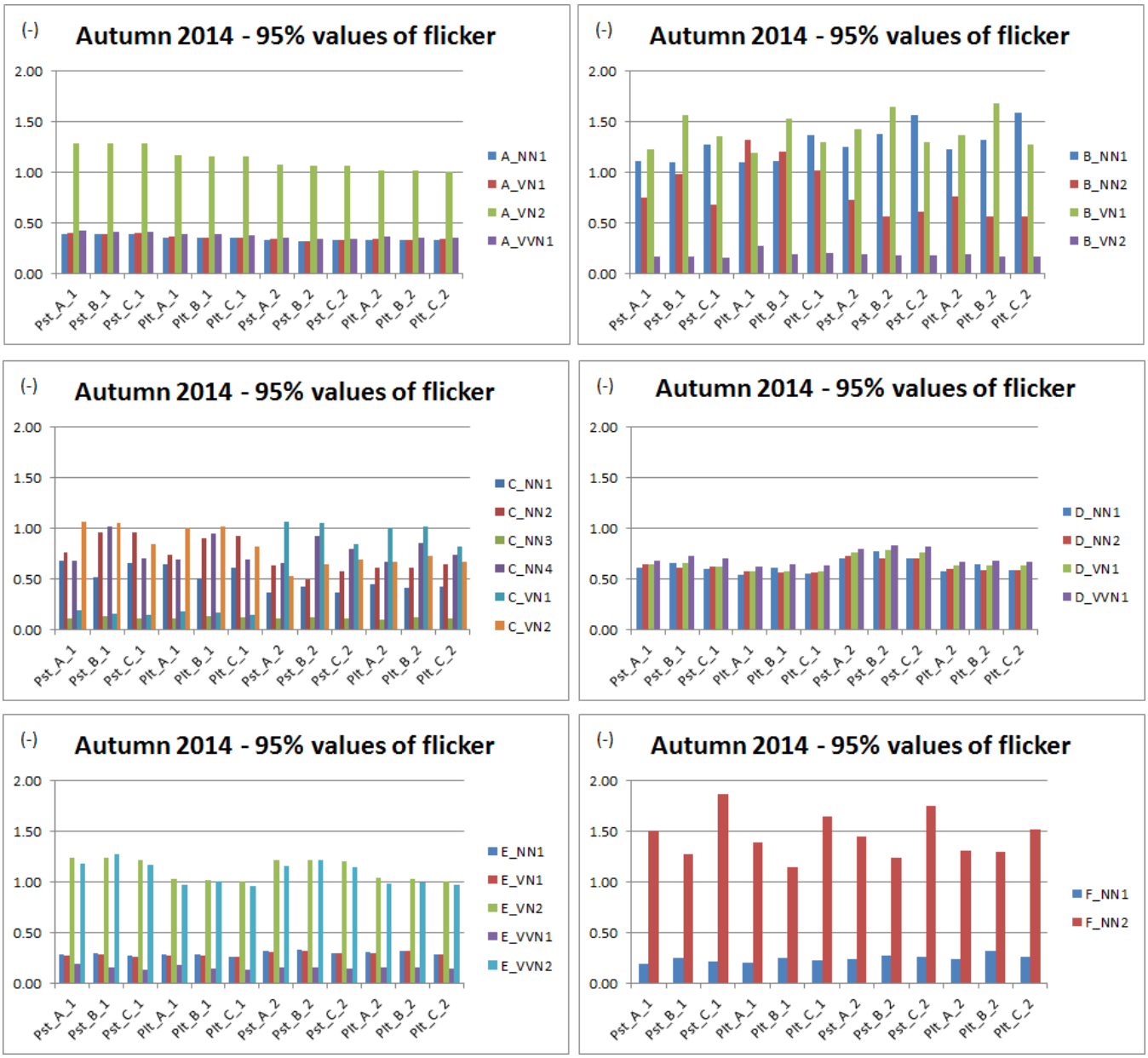

Fig. 6. The results of the measuring of flicker – Autumn 2014

V. QUALITY PARAMETERS MONITORING AT ALL TIMES

As of 2001, there are analysers QWave (manufactured by LEM) fitted to distribution points of 110 kV so as it is possible to register as much information on individual parameters of voltage quality and events in the distribution system, as possible. QWave Power measures, simultaneously, all voltage quality parameters and compares it with the limit values according to the CSN EN50160 standard, and furthermore, it also renders the current analysis. QWave Light is a simplified version, evaluating only current for its all guaranteed and indicative parameters.

The rules for operation of distribution networks (DN) contain Annex 3 (Quality of electrical power in the distribution system, manners of determination and evaluation). Based on these rules, there must be quality analyser of the electrical power supply fitted at all times, as of January 1, 2006, for all HV supply terminals, and as of January 1, 2007, for all supplies from DN 110 kV. The data acquired by these analysers are being continuously processed and archived. Ref. [4]

On the Fig. 7 you can see the illustration of the continuously monitoring power quality parameters at the selected place OS-8 MV distribution network. On the diagram there are also placed the results acquired by the cyclic monitoring at the same place as it was described in the previous part of the contribution. For example, you can see that the values of flicker acquired by the cyclic monitoring makes approximately one quarter of the maximal value acquired by the yearly monitoring.

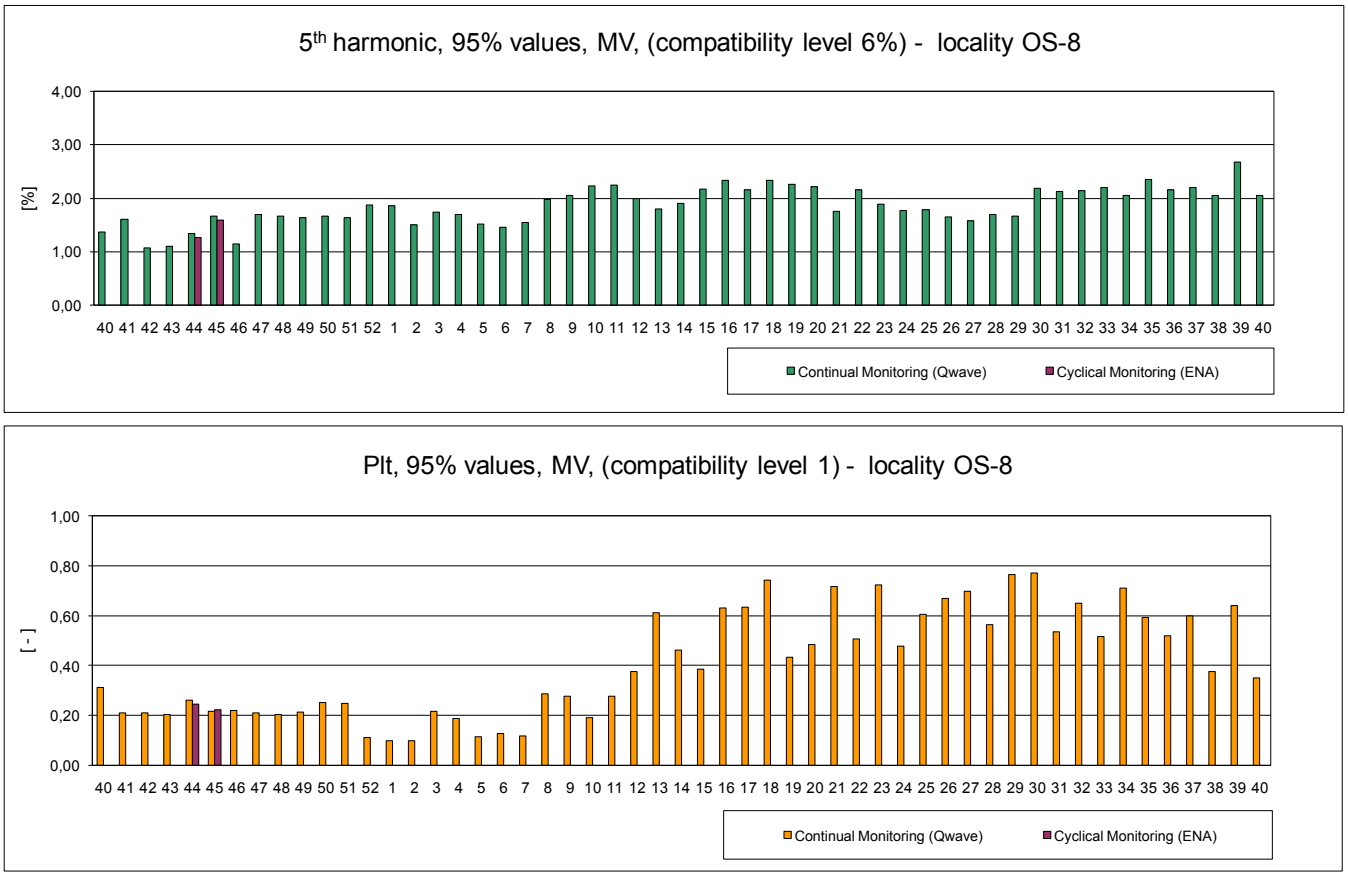

Fig. 7. 5th harmonic and flicker (P_{lt}) in MV network OS-8

VI. Use of Intelligent Electrometers for Monitoring of Quality Parameters

Characteristic parameters of voltage within low and high voltage networks are introduced in the standard ČSN EN 50160. The revised normative ČSN EN 50160 further defines parameters for very-high voltage networks.

Current intelligent electrometers usually provide data that is not in compliance with the normative mentioned above, but they afford relevant data for energy companies usable in operation.

As for usage in operation of distribution, the most crucial issues are long-term monitoring of voltage deviations and their evaluation in compliance with standard ČSN EN 50160. Further important values are overvoltage, falls and short-time blackouts typically with 1s sample period (thus quite not in accordance with ČSN EN 50160). Yet this data can give a power company relevant information, because events longer than 1 second still report about the conditions of distribution network and during the changes (usually rising) they indicate the error states. Unfortunately, these data are recorded as events, but the number or logged events are limited and set low.

Harmonics and THD, even evaluated until low frequencies only (till 10th or 25th harmonic multiple), can provide relevant information. For example, when the third harmonic element rises, it can indicate the problem of power transformer. A significant rise of any harmonic or THD indicates the problem with resonances in distribution network.

VII. Conclusions

Three PQ problems are summarised in the paper:

- the results of long-term (15 years) monitoring of selected voltage quality parameters and evaluation of trends in changes of these parameters; the most severe changes were registered for flicker;

- measurement and evaluation of the 15th and 21st voltage harmonics in the LV distribution network. The compatibility level of 0.5% was not exceeded at any measurement point;

- from the present results of the flicker monitoring it is possible to state that at some feeding points the values of Plt were more than 1. The greatest value was 1.7.

- the results from continuously monitoring of power quality parameters manifest that the measured values can differ during the year and therefore the continuously monitoring is well-founded.

- current intelligent electrometers usually provide data that is not in compliance with the normative mentioned above, but they afford relevant data for energy companies usable in operation.

ACKNOWLEDGMENT

This research was partially supported by the SGS grant from VSB – Technical University of Ostrava (No. SP2016/95 and No. SP2016/146).

REFERENCES

[1] EN 50160 Ed.3:2010 "Voltage characteristics of electricity supplied by public electricity networks".

[2] P. Krejci, P. Santarius, P. Bilík, R. Čumpelík "The Periodical and Continual PQ Monitoring of Selected Distribution Networks in Czech Republic," Electrical Power Quality and Utilisation 2011, Lisabon, 2011, pp. 1-6.

[3] M. Tesarova, M. Kaspirek "Evaluation of long-term voltage dip monitoring in the distribution system," International Scientific Symposium on Electrical Power Engineering 2011, Košice, 2013, pp.268-271.

[4] P. Krejci, P. Santarius, R. Hájovský, R. Velička, R. Čumpelík "Power Quality Monitoring in Selected Distribution Networks in Czech Republic," Electromagnetic Disturbances 2011, Bialystok, 2011, p. 145-148.

Optimal Management of a Virtual Power Plant

Dan Jigoria-Oprea, Gheorghe Vuc, Marcela Litcanu

***Abstract*— Deregulation of energy market led to the development of flexible and efficient framework for energy trading by energy companies in a competitive environment. Both deregulation and the concern towards environment issues increased the number of small and medium renewable power plants distributed in the network. The variability of renewable energy sources and the lack of their central monitoring led to new challenges concerning power system operation. The idea of aggregation for distributed energy sources led to the concept of virtual power plant, which determines a better control of production units but also a better visibility for the system operator. In this paper, the authors propose an optimal management solution which can offer a virtual power plant the capability to sell complete services, both for production and demand side management, by decreasing the necessary reserve for balance.**

***Index Terms*—energy market, optimal management, renewable energy sources, virtual power plant.**

I. INTRODUCTION

THE increased share of renewable energy sources in the electricity production brings issues concerning power balance in the power system. Generating electricity from renewable sources is influenced by weather conditions and by the availability of source – wind or sun. Using the power reserve of centralized sources is justified only form economic point of view. This reserve is used to compensate the shortage of energy determined by the unpredictable nature of renewable sources power generation. As a result, it seems more intelligent to transfer the balance load to another level of structure in the network. This structure should include different types of distributed resources, energy storage units and to have control and command rights.

All these can be combined in a structure like the virtual power plant (VPP) that can operate like a classical power plant. All operations for each unit can be programed in advance. The concept of VPP has already a history of over two decades, experimental projects being tested in several parts of the world [1-4].

For the Romanian Power System, using the VPP as a solution for the management of renewable energy is not applicable yet; the solution used now considers including the renewable energy sources (RES) in a large and diverse portfolio of a strong actor on the energy market.

II. MATHEMATIC MODEL

The optimization problem is actually a problem of maximizing the profit of the VPP [5], [6]. The aim is to maximize the profit for each and every one of the 24 hours:

$$profit = \sum_{t=1}^{24} \left(\lambda_t^{ISO} \cdot Bid_t + \lambda_t^{DR} \cdot R_t + \lambda_t^{VPP} \cdot D_t - E_t^{Disp} - y_t \cdot Start \right) \quad (1)$$

with constrains concerning:

- limits of the dispatchable generator:

$$E_t^{Disp} = a \cdot x_t + b \cdot G_t + c \cdot G_t^2 \quad (2)$$

$$x_t \cdot G^{\min} \le G_t \le x_t \cdot G^{\max} \quad (3)$$

$$-Ramp \le G_t - G_{t-1} \le Ramp \quad (4)$$

$$x_t - x_{t-1} \le y_t \quad (5)$$

- energy balance equation:

$$G_t + W_t + S_t \le D_t + Bid_t \quad (6)$$

- constrains concerning energy delivery:

$$\sum_{t=1}^{24} D_t = \sum_{t=1}^{24} \left(L_{it} - R_{it} \right) \quad (7)$$

$$D_t \ge 0.9 \cdot \sum_{t=1}^{N} \left(L_{it} - R_{it} \right) \quad (8)$$

$$D_t \le 1.1 \cdot \sum_{t=1}^{N} \left(L_{it} - R_{it} \right) \quad (9)$$

- demand response (DR) constrains:

This manuscript was submitted on 29 July 2016 and accepted on 18 September 2016.

D. Jigoria-Oprea is with the Power Systems Department at Politehnica University Timisoara, V. Parvan 2 Blvd., Timisoara, Timis, 300223, Romania (e-mail: dan.jigoria@upt.ro).

G. Vuc is with the Power Systems Department at Politehnica University Timisoara, V. Parvan 2 Blvd., Timisoara, Timis, 300223, Romania (e-mail: gheorghe.vuc@upt.ro).

M. Litcanu was with Politehnica University Timisoara. She is now with QMB ENERG SRL, Eduard Benes 6, Timisoara, Timis, Romania (e-mail: marcela.litcanu@upt.ro).

$$R_{it} = L_{it} \cdot \left(1 - \exp\left(-\alpha_{it} \cdot \left(\lambda_t^{DR} - \lambda_t^{VPP}\right)\right)\right) \quad (10)$$

$$\lambda_t^{VPP} \le \lambda_t^{DR} \le \lambda_t^{ISO} \quad (11)$$

$$\sum_{t=1}^{24} R_{it} > R^{\min} \quad (12)$$

where:

λ_t^{ISO} – forecasted price on the day-ahead market in the t period (€/MWh/h);

λ_t^{VPP} – contracted price inside the VPP during t period (€/MWh/h);

G^{max} – maximum production of dispatchable generator (MW);

G^{min} – minimum production of dispatchable generator (MW);

Ramp – maximum ramp rate of the dispatchable generator (MW/min);

Start –dispatchable generator starting costs (€);

W_t – forecasted wind production for t period (MW);

S_t – forecasted PV production for t period (MW);

L_{it} – forecasted load for consumer i for t period (MW);

D_t – forecasted demand for t period (MW);

α_{it} – elasticity price factor for consumer i in t period;

R^{min} – minimum acceptable level for total load reduction (MW);

E_t^{Disp} – generation costs for dispatchable generator during t period (€/MWh/h);

Gt – output of the dispatchable generator during t period (MW);

λ_t^{DR} – price for demand side reduction during t period (€/MW);

Profit – corresponding profit considering demand side reduction (€);

R_{it} – forecasted load reduction for consumer i during t period (MW);

Bid_t – hourly bid on energy market during t period (MW);

x_t – binary variable that indicate the state (operational/shut-down) of the dispatchable generator during t period;

y_t - binary variable that indicate if the dispatchable generator started during t period.

The objective function takes into consideration the VPP offers on the market, which can be positive or negative. Domestic consumers pay a fixed price according to bilateral agreements, λ_t^{VPP} equal to the levelized cost of energy (LCOE).

The constrains for the dispatchable generator (2-5) include the square cost function (2), minimum and maximum generation levels (3), ramp up/down limits (4) and starting elements (5). The energy balance constraint (6) imposes the balance between the dispatchable generator production, the renewable sources production and consumption. An excess of generated power or stored energy gives the sign of the demand side on the market. The energy delivery constrains grant the necessary power covering all the demand. Some deviations, positive or negative, are included in (8) and (9). Also, for the delivery constrains, the demand reduction using DR are subtracted from the entire demand quantity. This model also presents the minimum aggregated demand reduction which can be accepted by the VPP (12). The reductions are not accepted when the entire quantity is smaller than the minimum acceptable level.

III. Case Studies

All the presented case studies were conducted considering the entire Romanian Power System as a VPP, more exactly like a Bulk VPP (BVPP) [7], but with an arbitrary separation of each constituents of the VPP, in order to test and use all the integrated facilities of the *OptiMaCEV* application [6], including individual influence of each member of the BVPP.

The objective of the case studies was minimizing the financial losses (13) of the BVPP on the balancing market during 24 hours, losses which are determined by the errors between forecasted values for generation and real values of energy generation, errors which cannot be compensated by the DR.

$$FLoss = \sum_{t=1}^{24} \left(\Delta W_{prod} - \Delta W_{cons}\right)_t \cdot \Delta\lambda_t^{BM} \quad (13)$$

where:

$\Delta\lambda_t^{BM}$ is the difference of energy price between the balancing market and day-ahead market during t period (€/MW);

ΔW_{prod} – deviation of real energy production from forecasted value;

ΔW_{cons} – deviation of real energy consumption from forecasted value.

Several case studies were conducted for different characteristic days, from different seasons and with different structure of the history used for the forecast. The first case study is based on history data from 25-30 August 2014 and the focus day is 31 august. The second case study uses data from 5, 12, 19, 26 June, 3, 10 and 17 July and the focus day is 24 July.

All the case studies are using real data from 2014 in order to compare the forecast results to real evolution of consumption and generation for each considered source. Meanwhile, real market prices were used, both from the day-ahead market and balancing market. Values for load category elasticity factors were used from literature. The data used to model the VPP were obtained from the Romanian Transmission System Operator – Transelectrica [8]. To compute the deviations of the forecast for

each VPP component and the VPP imbalance, the real value of the consumption was used. The computation relations are:

$$Ab = \frac{V_{prod} - V_{real}}{W_{cons\_real}} \cdot 100[\%] \quad (14)$$

$$Dez = \frac{\Delta W_{prod} - \Delta W_{cons}}{W_{cons\_real}} \cdot 100[\%] \quad (15)$$

where:

Ab – corresponding deviation for the considered value (consumption, classical power plant production, etc.);

V_{prog} – forecasted value (consumption, classical generation, wind generation, PV generation, etc.);

V_{real} – real value for the considered time period (consumption, classical generation, wind generation, etc.);

W_{cons_real} – real consumption value;

Dez – value of unbalance for the VPP as the result of deviation of forecasted values from the real ones.

IV. Results and Discussions

A. Case Study #1

The results of interest for the forecasted (focus) day (on hourly intervals) are presented in Table 1.

The results for Case Study #1 show high values of deviation for all hourly intervals for the classical power plant generation (22%), while for PV the values are practically null. This is due to the fact that the installed power in these plants is smaller compared to other energy sources (also see (14)).

For the consumption component of the VPP, the deviations values are big. It is important to be noted that by aggregating the generation and consumption components in the VPP, the deviations per component are compensated and for all the VPP the maximum value of deviation is 21% and only for a few hourly intervals.

Another fact to note is that for 1 to 8 hour interval, the positive deviation of VPP is a "consumption excess" type and requires a reaction to decrease the value of the load. To minimize the unbalances of VPP, the R reaction of demand reduction (completely or partially), is used as necessary. Reducing the value of the unbalances have a positive influence for the VPP profit due to the fact that any unbalance must be covered using the balancing market, where prices are least favorable than on the day-ahead market.

The unbalance on VPP can reach the value 0 after considering the demand response for hourly interval 9, 11 and 16 to 20, because the demand response was greater or at least equal with the necessary needed to bring the unbalance to 0.

TABLE I
VPP Unbalance for Case Study #1 without and with DR

Hourly Interval	Classical Power Plant Deviation	Wind Deviation	PV Deviation	Consumption Deviation	Unbalance VPP	λ^{DR}	R	λ^{ISO}	Unbalance VPP with DR
1	8.2%	13.3%	0.0%	3.7%	17.8%	141.30	370.00	179.00	10.5%
2	11.8%	15.8%	0.0%	7.8%	19.7%	140.80	360.00	178.00	12.2%
3	9.8%	17.1%	0.0%	5.7%	21.2%	138.90	326.00	174.00	14.3%
4	12.2%	15.3%	0.0%	10.3%	17.2%	130.70	257.50	157.00	11.7%
5	12.7%	11.8%	0.0%	10.3%	14.2%	129.20	243.50	154.00	9.0%
6	12.0%	10.7%	0.0%	9.6%	13.1%	126.30	211.30	148.00	8.5%
7	18.0%	10.5%	0.0%	18.6%	9.8%	126.30	224.30	148.00	4.9%
8	8.2%	6.6%	-0.1%	8.0%	6.6%	126.80	249.70	149.00	2.0%
9	20.6%	5.5%	-0.6%	24.8%	0.7%	130.70	305.40	157.00	0.0%
10	22.6%	6.0%	-0.6%	30.4%	-2.4%	95.00	60.70	174.00	-2.4%
11	21.5%	7.4%	-0.4%	28.4%	0.0%	134.60	371.70	165.00	0.0%
12	20.0%	6.1%	0.0%	28.0%	-1.9%	95.00	64.50	168.00	-1.9%
13	17.4%	6.4%	0.2%	24.3%	-0.3%	95.00	63.00	157.00	-0.3%
14	19.7%	6.9%	0.2%	28.3%	-1.5%	95.00	65.40	154.00	-1.5%
15	20.8%	7.8%	-0.2%	29.7%	-1.4%	95.00	64.10	148.00	-1.4%
16	20.9%	7.2%	0.3%	27.5%	0.8%	121.80	213.40	139.00	0.0%
17	17.6%	7.9%	-0.5%	22.5%	2.5%	121.90	206.50	139.00	0.0%
18	2.8%	5.7%	-1.0%	3.7%	3.8%	129.20	295.00	154.00	0.0%
19	17.4%	6.6%	0.3%	22.4%	1.9%	134.60	367.60	165.00	0.0%
20	15.7%	4.0%	0.4%	19.4%	0.7%	135.90	422.60	174.00	0.0%
21	12.6%	2.4%	0.1%	17.6%	-2.6%	95.00	69.00	194.00	-2.6%
22	11.9%	2.7%	0.0%	16.9%	-2.4%	95.00	70.30	229.00	-2.4%
23	10.9%	2.3%	0.0%	14.9%	-1.7%	95.00	63.50	188.00	-1.7%
24	12.7%	4.0%	0.0%	15.9%	0.7%	141.80	425.00	180.00	0.0%

The balance price for the demand response, λ^{DR} for intervals 10 and 21-23 is smaller than the internal energy price for consumption, λ^{VPP}, and signals the necessity to stimulate the growth of internal consumption to reduce the unbalance. For all occurrences, the demand response was used to reduce the unbalance.

Another thing that is noted is the negative value of the deviation of VPP unbalance for interval 10, 12-15 and 21-23. This is a "low consumption" type, which means that is necessary a demand response in order to increase the consumption, a signal given even by the demand response balance price.

Regarding minimizing the financial losses, from Table 2 it can be seen very clearly that using DR reduces supplementary costs determined by acquiring or selling energy to the balancing market during unbalance hourly intervals. The economy is about 844398.9 RON from 1448759.3 to 604360.4 RON.

The presented results also emphasize the fact that deviation of VPP when using demand response is the one who better attenuates the individual unbalance of their components.

TABLE II
DR INFLUENCE ON FINANCIAL LOSSES FOR CASE STUDY #1

Hourly Interval	Unbalance Δ witihout DR	Unbalance Costs [RON/MWh]		Supplementary Cost	Unbalance influence without DR		Unbalance Δ with DR	DR	Supplementary Cost	Unbalance influence with DR	
	[MW]	Excess	Deficit	[RON]	[RON/MWh]	[%]	[RON]	[MW]	[RON	[RON/MWh]	[%]
1	-906.91	5.38	198.00	118450.91	23.25	14.5%	-536.91	-370.00	83011.4	16.29	10.18%
2	-950.73	39.57	243.49	92860.78	19.23	12.9%	-590.73	-360.00	64643.4	13.39	8.98%
3	-999.23	0.10	213.78	128521.93	27.30	18.3%	-673.23	-326.00	100244.5	21.29	14.29%
4	-801.29	0.10	214.62	64196.18	13.76	9.2%	-543.79	-257.50	80970.0	17.35	11.64%
5	-662.18	0.10	213.12	18747.80	4.01	2.7%	-418.68	-243.50	63178.8	13.52	8.95%
6	-605.25	0.10	221.68	1799.65	0.39	0.2%	-393.95	-211.30	66927.6	14.45	8.50%
7	-446.25	0.10	251.69	11680.67	2.57	1.3%	-221.95	-224.30	44028.3	9.69	4.88%
8	-360.72	0.10	258.83	14157.89	2.61	1.1%	-111.02	-249.70	25412.0	4.68	2.04%
9	-32.54	0.10	306.95	50763.69	10.38	4.1%	0.00	-32.54	0.0	0.00	0.00%
10	118.20	0.10	317.93	80914.05	16.38	7.0%	118.20	0.00	9920.8	2.01	0.86%
11	-2.37	0.10	310.29	63125.76	12.52	6.0%	0.00	-2.37	0.0	0.00	0.00%
12	97.05	0.10	290.83	54392.55	10.75	5.2%	97.05	0.00	8233.2	1.63	0.79%
13	14.49	0.10	292.78	36625.46	7.19	3.5%	14.49	0.00	1230.2	0.24	0.12%
14	76.41	0.10	304.85	58899.04	11.50	6.1%	76.41	0.00	8852.5	1.73	0.91%
15	67.90	0.10	299.80	53363.86	10.65	5.6%	67.90	0.00	7523.2	1.50	0.79%
16	-42.38	0.10	281.81	31384.22	6.22	3.3%	0.00	-42.38	0.0	0.00	0.00%
17	-127.81	0.10	278.55	19984.04	3.93	2.1%	0.00	-127.81	0.0	0.00	0.00%
18	-229.42	0.10	278.07	20381.66	3.38	1.8%	0.00	-229.42	0.0	0.00	0.00%
19	-101.35	0.10	260.70	61196.76	11.70	7.7%	0.00	-101.35	0.0	0.00	0.00%
20	-36.50	0.10	255.97	58790.76	10.89	5.9%	0.00	-36.50	0.0	0.00	0.00%
21	150.53	0.10	259.25	91217.77	15.47	8.6%	150.53	0.00	11929.4	2.02	1.12%
22	142.29	0.10	269.88	133859.31	22.16	14.9%	142.29	0.00	17200.5	2.85	1.91%
23	94.73	0.10	235.70	106233.32	19.13	16.1%	94.73	0.00	11054.5	1.99	1.67%
24	-37.83	0.10	232.78	77211.25	14.95	12.6%	0.00	-37.83	0.0	0.00	0.00%

B. Case Study #2

The results of interest for the forecasted (focus) day (on hourly intervals) are presented in Table 3.

The results for Case Study #2 show deviation values smaller than 10% for the majority of hourly intervals, while for the PV the values are practically null.

For the consumption component of the VPP the deviation values are also smaller (with a maximum value of 14.6%), the large values appearing only in three intervals. Again, by aggregating the generation and consumption components in the VPP, the deviations per component are compensated and for all the VPP the maximum value of deviation is 12% and only for a few hourly intervals.

The positive values for deviation during 3-7, 9-13 and 15-24 hourly intervals is a "consumption excess" type and requires a reaction to decrease the value of the load. To minimize the unbalances of VPP, the *R* reaction of demand reduction (completely or partially), is used as necessary. Also for this case, reducing the value of the unbalances have a positive influence for the VPP profit due to the fact that any unbalance must be covered using the balancing market, where prices are least favorable than on the day-ahead market.

For interval 2, 8 and 14, using DR the unbalance can be eliminated (the final value of the unbalance is 0) due to DR contribution – its availability was greater or at least equal with the necessary value to compensate the unbalance.

For this case study, only for the first hourly interval the deviation has a negative value – low consumption unbalance. This signals the fact that an increase of consumption reaction is needed.

TABLE III
VPP UNBALANCE FOR CASE STUDY #2 WITHOUT AND WITH DR

Hourly Interval	Classical Power Plant Deviation	Wind Deviation	PV Deviation	Consumption Deviation	Unbalance VPP	λ^{DR}	R	λ^{ISO}	Unbalance VPP with DR
1	0.2%	3.7%	0.0%	4.4%	-0.5%			149.0	-0.5%
2	0.0%	4.6%	0.0%	3.6%	1.0%	116.9	131.9	129.0	0.0%
3	-12.7%	3.9%	0.0%	-13.1%	4.3%	112.0	73.5	119.0	3.1%
4	2.4%	2.2%	0.0%	4.1%	0.6%	107.0	21.3	109.0	0.1%
5	0.0%	1.8%	0.0%	1.0%	0.8%	107.0	20.9	109.0	0.4%
6	-0.3%	5.2%	0.0%	0.7%	4.2%	109.3	44.7	113.6	3.3%
7	1.3%	4.9%	0.0%	3.1%	3.1%	116.9	131.7	129.0	0.7%
8	1.4%	3.4%	0.2%	1.7%	3.2%	129.2	288.3	154.0	0.0%
9	0.3%	5.0%	0.5%	-1.3%	7.1%	139.4	437.9	175.0	0.4%
10	-1.6%	6.2%	0.9%	-3.7%	9.2%	141.3	463.7	179.0	2.3%
11	0.3%	6.3%	0.8%	-0.8%	8.2%	141.3	479.1	179.0	1.1%
12	1.6%	7.2%	1.0%	1.0%	8.7%	141.3	489.3	179.0	1.5%
13	-10.1%	6.2%	-0.4%	-14.6%	10.3%	141.3	482.6	179.0	4.1%
14	3.8%	6.8%	-0.4%	3.8%	6.3%	141.3	507.9	179.0	0.0%
15	-0.1%	5.7%	-1.1%	-1.9%	6.3%	136.5	417.7	169.0	0.2%
16	1.6%	5.1%	-0.1%	0.4%	6.3%	131.1	344	158.0	1.1%
17	-0.3%	8.5%	-0.4%	-2.3%	10.0%	131.1	340.2	158.0	4.9%
18	0.2%	10.6%	-0.4%	-1.2%	11.5%	136.5	408.5	169.0	5.4%
19	-0.3%	10.5%	-0.1%	-1.5%	11.7%	136.5	403.2	169.0	5.5%
20	0.2%	9.3%	-0.2%	-0.9%	10.2%	136.5	405.7	169.0	4.0%
21	5.7%	10.3%	0.0%	6.3%	9.8%	136.5	441	169.0	3.2%
22	2.7%	8.6%	0.0%	2.0%	9.3%	136.5	438.8	169.0	2.9%
23	-9.5%	5.7%	0.0%	-14.3%	10.6%	129.2	321.3	154.0	6.5%
24	2.5%	8.6%	0.0%	2.7%	8.4%	129.2	299.9	154.0	3.5%

TABLE IV
DR INFLUENCE ON FINANCIAL LOSSES FOR CASE STUDY #2

Hourly Interval	Unbalance Δ witihout DR	Unbalance Costs [RON/MWh]		Supplementary Cost	Unbalance influence without DR		Unbalance Δ with DR	DR	Supplementary Cost	Unbalance influence with DR	
	[MW]	Excess	Deficit	[RON]	[RON/MWh]	[%]	[RON]	[MW]	[RON	[RON/MWh]	[%]
1	29.4	30	344	4369.5	32.74	16.8%	29.38	0.00	4369.5	0.78	0.40%
2	-51.4	34.26	356.78	7858.5	32.25	17.2%	0.00	-51.36	0.0	0.00	0.00%
3	-262.5	75.79	394	24435.9	27.99	16.6%	-188.97	-73.50	17593.0	2.90	1.72%
4	-28.8	50.22	384	3448.8	41.21	24.2%	-7.50	-21.30	897.7	0.18	0.10%
5	-42.0	77.04	390	4026.3	40.32	23.3%	-21.10	-20.90	2022.8	0.39	0.23%
6	-217.3	67.4	390	26899.0	26.65	13.9%	-172.60	-44.70	21365.6	4.12	2.16%
7	-168.8	67.51	400	23682.3	29.36	14.1%	-37.11	-131.70	5206.2	0.97	0.47%
8	-187.2	78.1	431	30863.5	29.69	12.2%	0.00	-187.15	0.0	0.00	0.00%
9	-460.8	30	407	101829.6	16.29	6.5%	-22.87	-437.90	5053.7	0.78	0.31%
10	-616.7	30	415	136285.6	9.73	3.9%	-152.98	-463.70	33807.9	5.05	2.01%
11	-551.8	30	413	118630.7	9.98	4.1%	-72.67	-479.10	15624.2	2.33	0.95%
12	-588.9	30	408	122490.1	6.82	2.9%	-99.59	-489.30	20715.7	3.08	1.29%
13	-806.7	30	400.28	169403.4	1.23	0.5%	-324.12	-482.60	68062.2	8.67	3.61%
14	-430.4	30	401	83920.1	9.66	4.3%	0.00	-430.36	0.0	0.00	0.00%
15	-431.9	30	380	81626.1	6.66	3.0%	-14.18	-417.70	2680.8	0.39	0.18%
16	-415.7	30	382	73169.7	6.10	3.0%	-71.74	-344.00	12625.7	1.91	0.93%
17	-670.3	30	378	117976.4	2.42	1.2%	-330.12	-340.20	58101.2	8.67	4.21%
18	-764.0	30	381	148974.0	4.79	2.1%	-355.47	-408.50	69316.5	10.48	4.66%
19	-765.0	30	388	152235.1	1.42	0.6%	-361.80	-403.20	71998.3	10.98	4.80%
20	-669.6	30	399	140612.3	6.08	2.5%	-263.91	-405.70	55419.3	8.46	3.52%
21	-651.0	30	405	143865.5	8.57	3.4%	-209.98	-441.00	46404.5	6.99	2.78%
22	-636.8	30	413	140731.2	10.11	4.0%	-197.99	-438.80	43756.4	6.36	2.53%
23	-826.0	30	411	161060.4	2.92	1.3%	-504.65	-321.30	98406.9	12.62	5.61%
24	-512.9	30	333	92329.3	3.72	1.8%	-213.04	-299.90	38347.3	6.31	3.01%

Regarding minimizing the financial losses, from Table 4 it can be seen very clearly that using DR reduces supplementary costs determined by acquiring or selling energy to the balancing market during unbalance hourly intervals. The economy is about 1418947.9 RON from 2110723.3 to 691775.4 RON.

V. CONCLUSION

Implementing the concept of VPP, determine the growth of power system benefits, due to using more efficient the distributed generation units, hence a greater operation efficiency. In this case, distributed generation can become more visible, can have a better access to energy markets and also can maximize the opportunities regarding incomes from selling the energy and reducing the environment pollution by using fewer classical power plants. The VPP can be considered an observable instrument for optimal solving of renewable energy sources integration and the case studies presented emphasize this aspect.

The results from the case studies prove that including the original elements in the VPP management - meaning considering the level of BVPP and the level of additional optimization by minimizing the financial losses due to acquiring energy from the balancing market, is justified and leads to better performance for the VPP.

Even more, it is again confirmed the fact that the VPP can be the favorable element in the power grid evolution towards "smart grid".

REFERENCES

[1] L. Nikonowicz, J. Milewski, (2012). Virtual Power Plants – general review: structure, application and optimization, *Journal of Power Technologies. 92 (3)*, pp. 135-149.

[2] P. Andersen, B. Poulsen, M. Decker, C. Traeholt, J. Ostergaard, "Evaluation of a generic virtual power plant framework using service oriented architecture", *2nd IEEE International Conference on Power Energy (PECon 08)*, Johor Baharu, Malaysia, December 1-3, 2008, pp. 1212-1217.

[3] G. Kaestle, "Virtual Power Plants as real CHP-clusters: a new approach to coordinate the feeding in the low voltage grid", *2nd International Conference on Integration of Renewable and Distributed Energy* Resources, Napa, CA, USA, 4-8 December, 2006.

[4] S. You, *Developing Virtual Power Plant for optimized distributed energy resources operation and integration*, PhD. Thesis, Department of Electrical Engineering, Technical University of Denmark, September 2010.

[5] A. Mnatsakanyan, S. Kennedy, "Optimal demand response bidding and pricing mechanism: Application for a virtual power plant", *1st IEEE Conference on Technologies for Sustainability (SusTech)*, Portland, OR, USA, 1 – 2 august 2013, pp. 167-174,.

[6] L. Marcela, *Virtual power plant management optimization OptiMaCEV*, PhD. thesis, Ed. Politehnica, Timisoara, Romania, 2015 (in romanian).

[7] R.A. Ahangar, A. Sheykholeslami (2014). Bulk Virtual Power Plant, a Novel Concept for Improving Frequency control and Stability in Presence of Large Scale RES, *International Journal of Mechatronics, Electrical and Computer Technology*, *4 (10)*, pp. 1017-1044.

[8] CNTEE Transelectrica S.A., Romanian Trasmission System Operator, Productie, Consum, Sold. Available: http://www.transelectrica.ro

Dan Jigoria-Oprea (M'08) was born in Caransebes, Romania on the 31st of October 1983. He received the B.S. (2007) and PhD. (2010) in power systems engineering from Politehnica University Timisoara, Romania.

From 2007 to 2010 he was a PhD. Student and Research Assistant at the Power Systems Department of Politehnica University Timisoara. From 2010 to 2012 was a Teaching Assistant and since 2012 is an Assistant Professor/Lecturer at the Power Systems Department of Politehnica University Timisoara. He is the author of over 45 articles, 5 books and member in 10 research contracts. His research interests include power systems optimization and operation, renewable energy sources integration and energy market.

Mr Jigoria-Oprea is also a member of SIER, the Romanian Society of Power Systems Engineers.

Gheorghe Vuc (M'05) was born in Timisoara, Romania, in 1958. He received the B.S. (1984) and the Ph.D. degree (1998) in power systems engineering from Politehnica University Timisoara, Romania.

From 1984 to 1990 he was operational engineer at Romanian TSO (Transelectrica).

From 1990 to 1998 he was a PhD. Student and Assistant Professor at the Power Systems Department of Politehnica University Timisoara. From 1998 to 2006 was a Lecturer and since 2006 is an Associate Professor at the Power Systems Department of Politehnica University Timisoara. He is the author of over 68 articles, 4 books and member in 12 research contracts. His research interests include power systems optimization and operation, renewable energy sources integration and energy market.

Mr. Vuc is also a member of SIER, the Romanian Society of Power Systems Engineers.

Marcela Litcanu was born in Otelu Rosu, Romania on the 30th September 1986, received the PhD. in power systems engineering from Politehnica University Timisoara, Romania, in 2015. Previously, she recieved a bachelor and master degree in Engineering and Management from Faculty Of Management In Production And Transportation, at Politehnica University of Timisoara.

From 2011 to 2015, he was a Research Assistant and PhD. Student with the Power Systems Department at Politehnica University of Timisoara. Currently, she is with QMB Energy SRL from Timisoara, Romania. She is an author of 8 articles. Her research interest includes energy market and power system operation.

Degree of Fault Tolerance as a Comprehensive Parameter for Reliability Evaluation of Fault Tolerant Electric Traction Drives

Igor Bolvashenkov and Hans-Georg Herzog

***Abstract* – This paper describes a new approach and methodology of quantitative assessment of the fault tolerance of electric power drive consisting of the multi-phase traction electric motor and multilevel electric inverter. It is suggested to consider such traction drive as a system with several degraded states. As a comprehensive parameter for evaluating of the fault tolerance, it is proposed to use the criterion of degree of the fault tolerance. For the approbation of the proposed method, the authors carried out research and obtained results of its practical application for evaluating the fault tolerance of the power train of an electrical helicopter.**

Keywords: reliability, degree of fault tolerance, multi-phase electric motor, multilevel inverter, traction vehicle drive.

I. Introduction

With the constant growth of complexity of modern engineering systems it becomes more complicated to achieve the required level of sustainable and safety operation. The task of implementing the specified requirements is closely related to the problem of the most accurate assessment of indicators of sustainable operation of the system, shown in Fig.1. Particularly important is to assess the required reliability and security for the safety-critical systems correctly. In safety-critical applications such as vehicle propulsion systems, the fault tolerance of all the equipment is obligatory. According to the plans for the electrification of various types of vehicles based on the electric energy generated by renewable sources, the tasks of a quantitative estimation of fault tolerance in creating of the safety-critical systems have now become very topical.

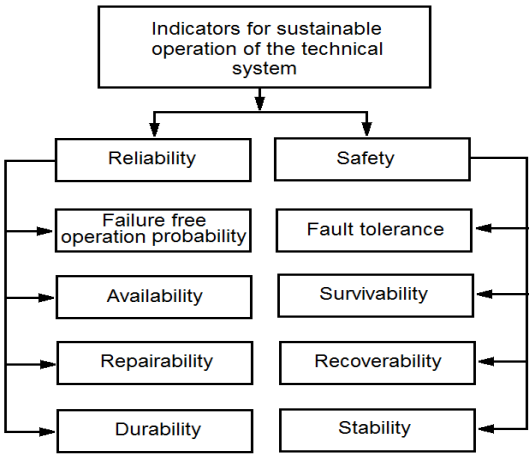

Fig.1. Indicators for sustainable operation

One of the most important requirements for the vehicle's propulsion system is the level of fault tolerance. In other words, the vehicle's propulsion system should operate and continue its sustainable functioning even if one or more of its components have failed.

To implement this requirement, all components included in the system should be fault tolerant. As an example of practical use of the proposed method the fault tolerance of a two main parts of the vehicle's propulsion system - traction multi-phase permanent magnet synchronous motor (PSM) of electrical helicopter and electric inverter in conventional and multilevel versions were evaluated. In this case, according to the specified requirements of a safe flight of the designed electrical helicopter, the total failure rate for the entire traction drive of designed electrical helicopter should be less than 10^{-9}/h [1].

Due to the constant need of traction electrical machines for special application, there are many publications describing the comparison or analysis of different fault tolerant electric machines and electric inverter topologies for different vehicle applications [1]-[7] and [8]-[12]. Thus, it should be noted that the authors generally have studied various aspects of the fault tolerance, and in most cases only a qualitative assessment was performed. For example in [1] a qualitative method for the fault tolerance evaluation is proposed, which results are given in Table I.

TABLE I. Comparative Evaluation of the Fault Tolerance [1]

Phase number / **Parameter**	**5 Phase**	**6 Phase**	**7 Phase**	**9 Phase**
Overload capacity	8	9	9.5	10
Partial load mode	7	9	8	10
Torque ripple	7	8	10	9
Total	22	26	27.5	29

Modern methods for determining the degree of fault tolerance of electrical machines, power electronics, and the computer network topology are presented in [13]-[15] and [28]-[31]. The proposed methods have one typical common

disadvantage - the lack of universality. Each of them allows solving a local specific problem for a particular object.

The authors have proposed a new universal approach and developed the methodology of assessing the degree of fault tolerance (DOFT) of safety-critical systems as a whole, as well as the DOFT of their components.

II. Approach and Methodology

A. Degree of Fault Tolerance

Considering the definition of the fault tolerance of a technical system as an ability to maintain the required functional level of the system in case of one or more failures of its components, DOFT can be defined as the amount of time which the system may remain in a degraded state without irreversible changes in its functionality. Mathematically, in general form this can be written by (1):

$$DOFT_i = \frac{W_R}{W_N} \cdot \frac{\Delta t_i}{\Delta t_N} \quad (1)$$

where W_R and W_N – reduced and nominal values of performance of technical system; Δt_i , Δt_N – respectively, duration of functioning after i-number of failures and without failure.

As the value of the performance W can be considered the productivity, power, energy, quantity of information, etc. The value of Δt_i is defined by overload capability of the system after i-number of failures.

In the case when the required level of W_R has been predetermined by project requirements, it is useful to determine DOFT for each corresponding level of performance in accordance with (2):

$$DOFT_{R\,i}\left(W_R\right) = \frac{\Delta t_i}{\Delta t_N} \quad (2)$$

Δt_N is determined depending on the type of electric vehicles and is largely depending on the specifics of its operation (aircraft, ships, trains, cars). For example, for the electric helicopter 30 minutes are needed for sustainable and safety completion of its function "search and rescue". Δt_i is determined by the overload capacity of system and its thermal stability. Δt_i indicates the duration time during which the system may operate in a critical failure mode without irreversible changes in the quality and functional inability to further use.

Based on the considerations above, the procedure for determining the DOFT is following:

- Determination of all possible failures on the basis of Fault-Tree Analysis (or Failure Mode and Effects Analysis);
- Classification of all failures on critical dangerous and non-dangerous failures;
- Definition of opportunities and complexity (if recovery is possible) of the failure elimination;
- Definition of development and the consequences of each non-repairable failure (if the recovery is not possible);
- Evaluation of degree of reduction of the system's functionality;
- Estimation of an acceptable level of performance reducing in accordance with the requirements;
- Evaluation of the ratio between the performance and demand for each failure operational mode;
- In the cases when the demand is greater than the required performance, the analysis and evaluation of system's overloading state is carried out, and the value of Δt_i is calculated for the appropriate level of performance reduction;
- Based on the calculated data the DOFT can be computed.

On the Figure 2 and Figure 3 the values of DOFT, respectively of traction multi-phase electric motor and electric power inverter are equal to the area below the degradation curves. The "grey" area above the curve of the degradation of 9-phase motor is equal to probability of the transition of this motor in the next degraded state following the critical failure.

The number of "steps" in Fig.2 corresponds to the number of degraded states of the electric machine after each critical failure until the moment of time when the motor losses completely their functional ability. For multi-phase electric motor, this corresponds to the next critical phase failure. Thus, multi-phase traction motor can be regarded as multi-state-system, which will be given special attention in the section II.B.

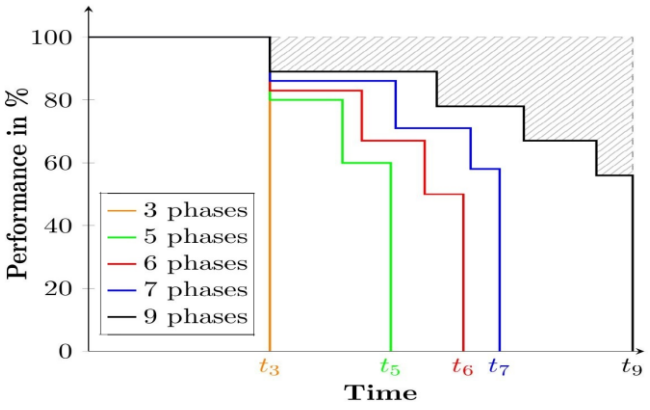

Fig.2. Graphical *DOFT* representation of different multi-phase motors as multi-state systems

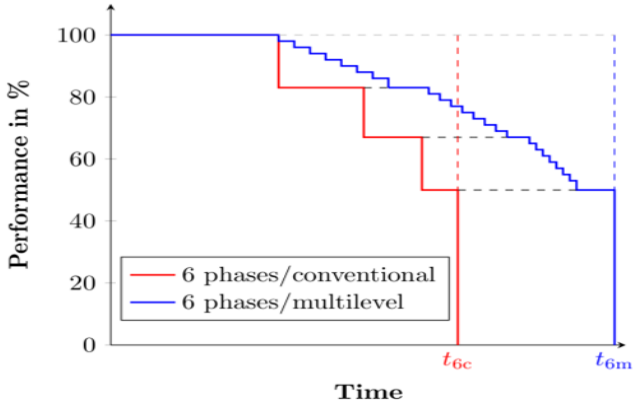

Fig.3. Graphical *DOFT* representation of conventional vs multilevel inverter as multi-state systems

Quantitative assessment of the total duration of the electric motor operations in all degraded states allows a quantitative comparative analysis of various possible topologies and design of the machine, considering their lifetime.

Figure 3 is a graphical representation of the qualitative comparison's results of the DOFT of conventional and multilevel inverter for 6-phase traction motors. The figure shows that DOFT of the multilevel inverter is much superior to the conventional version.

Additionally to the critical failures, the effect of small (non-critical) failures on the fault tolerance value of traction electric motor and electric power inverter, leading to partial or temporary loss of system functionality, can also be investigated using DOFT, as can be seen in Figure 4.

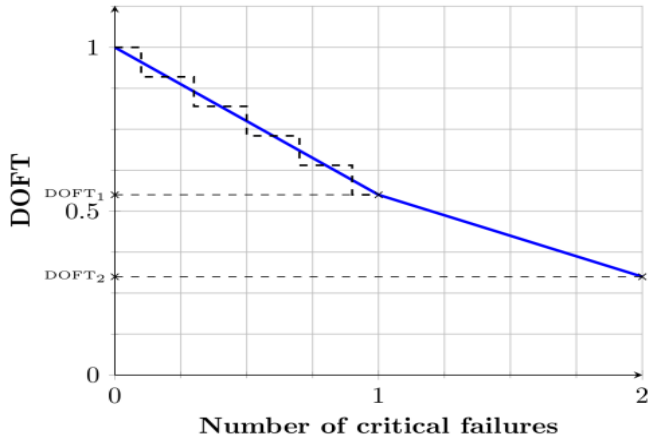

Fig.4. Graphical *DOFT* representation of different types of failure

A distinctive feature of the proposed methodology of quantitative assessment of technical systems in comparison with existing techniques is its universality, i.e. the possibility of its use for different types of technical systems. As an example of its practical use, figure 5 shows the evaluation of the fault tolerance and transition probabilities of electric helicopter traction drive with multi-phase motors and multilevel inverters.

B. MSS Markov Models and Transition Probabilities

Considering the above requirements on the probability of total failure of electrical helicopter, as well as statistical data on the reliability of traction electric motor and electric inverter it was determined that the optimal model for an analysis of fault tolerance in such conditions is a MSS Markov Model (MSS-MM), with K states, as shown in general form in Fig.5. Theoretical base of this method is well known and described in [16]-[18] and examples of application in [25]-[27].

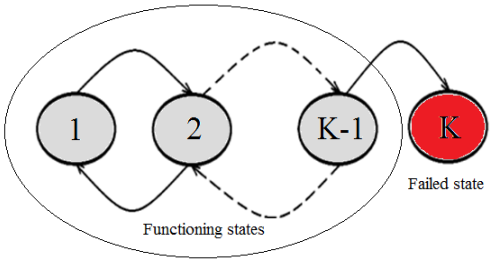

Fig.5. Multi-State Markov model of electric traction drive [16]

The first state corresponds to a completely failure-free operation of the system. The second and other states (before state *K*) are the states of degradation and correspond to failure cases – phase open-circuit failure, respectively, of the one, two or more phases. The state *K* of the model corresponds to the completely failed system when the helicopter's drive completely loses the ability to operate. Thus, every following state of the degradation corresponds to one critical failure with a corresponding partial functionality loss of the traction drive.

At the same time, the number of the degraded state of the MSS-MM determined in accordance with the requirements of the project on the fault tolerance defines the technical capabilities of the system to continue functioning with reduced performance level as a result of the critical failure.

The most important and most difficult point for simulations using Markov models is to determine the transition probabilities and the number of states with a reduced level of functionality.

The values of the transition probabilities $\lambda_1, \lambda_2,...\lambda_K$ are derived from the results of calculations of Degree of Fault Tolerance (*DOFT*) for the states 1, 2 and *K* respectively:

$$\lambda_{Ri} = 1 - DOFT_{Ri} \tag{3}$$

Here *R* is the value of reduced performance level according to the project requirements and *i* - number of critical failures. The values of transition probabilities are affected by a large number of different factors, from design and environmental parameters to the using types of maintenance strategies, monitoring, and diagnostics.

As can be seen from (3), for the calculation of the transition probabilities the main importance is the correct calculation of *DOFT* for a given project required performance levels. Application cases of proposed methodology for the estimation reliability features of electric traction drive of helicopter will be presented in the next section.

III. Fault Tolerant Electric Traction Drive

A. Electric Traction Drive

The power part of the traction drive of electric vehicles includes a source of electrical energy (battery, fuel cell, etc.), an electric energy converter/inverter, and a traction electric motor, as can be seen from Figure 6. In the present study, the electric power source was not considered, but will be considered at the next stage of research.

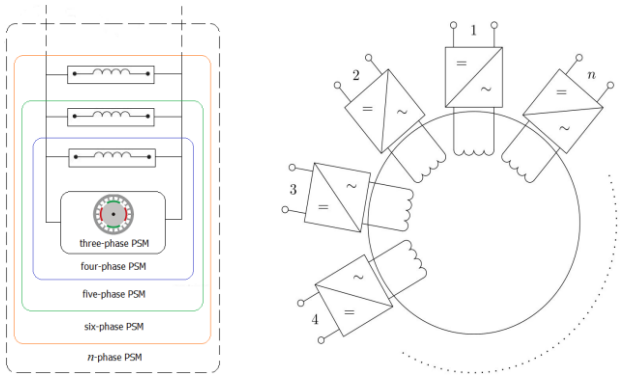

(a) (b)

Fig.6. Schematic graphical system definition for a multi-phase traction motor (a) and for the whole traction drive (b)

B. Critical Failures

In the paper [6] has been demonstrated that the vast majority of elements failures of the system "power inverter-traction electric motor" can be reduced to four basic types of failures of electric traction drive:

- open-circuit and short-circuit of the electric motor's phase;
- open-circuit and short-circuit of the inverter submodule.

In the development of an electric motor scheme is usually provided such a connection of the each inverter submodule with the protection system, which disconnects the electrical circuit of the failed submodule. This solution allows the failure "short-circuit" of the inverter's submodule to lead to the failure "open-circuit" of submodule.

The failure type "phase short-circuit" of electric motor can be reduced to the failure of "phase open-circuit" based on special design options of the stator winding performance, improve the quality of insulation materials and advanced production technology.

Excluding the possibility of failure type "short-circuit" on the basis of their reducing to the failures of the type "open-circuit" is one way to keep a functionality of multi-phase electric motors in failure cases. Thus, in the simulation of functioning of electrical traction drive in failure conditions, as the critical failures will be considered the motor's "phase open-circuit" and inverter's "submodule open-circuit".

C. Multi-Phase Electric Motor

The results of a previous study by the authors [1] indicate that for the 3-phase PSM the specified requirements on the reliability for the entire power drive of a designed helicopter is not achievable without a functional and/or structural redundancy, and/or other activities that improve the indicators of reliability to the required value.

One way to create the fault tolerant traction electric motors of high reliability is to increase the number of motor phases without changing the value of the motor's power. This allows to reduce the current value in each phase's open winding and to perform the power electronics unit integrally fabricated.

Based on the diversity of various schemes, connection methods of power supplies and inverters as well as switching algorithms of the stator phases of electric motor, it is possible to implement the system using automatically changed structures and parameters, resp., depending on the purpose and functioning conditions.

At the same time, independent performance of each phase's switching channels provides increased reliability of the electric machine based on the principle of functional redundancy.

Unlike an electrical machine with a small number of phases in which the majority of critical elements failures leads to a complete failure of the machine, the multi-phase electrical machine remains in operation up to a certain level of degradation and a corresponding change in the output characteristics. This allows realizing so called functional redundancy.

Thus, on the one hand, increasing the number of phases of the electric motor reduces the impact of each failure in power electronics control channel or in the phase of the motor, on the characteristics of the whole traction drive.

On the other hand, increasing the number of phases leads to an increase of the failure probability in one of phases. In this context, it is necessary to find an optimal compromise solution, based on the design requirements, the possibility of redundancy, and the reliability indices of the electrical machine and power electronics.

On the basis of the known values for the failure probability of each phase of the electric motor the optimal number of phases can be calculated, at which the required reliability and fault tolerance indicators of electric motor can be implemented, taking into account the possibility of one or more critical failures. The use of this redundancy method has its own features that must be considered in the study of physical processes and the design of the traction electric drive as a whole.

As shown in [1] the optimal electric machine for the safety-critical electric drives, considering system approach techniques, is a multi-phase PSM with distributed stator windings and internal v-shaped arrangement of permanent magnets on the rotor. For a detailed study 5-, 6-, 7- and 9-phase PSM were selected.

For the traction electric motor of the helicopter considering high requirements on the drive safety and fault tolerance, the overload capability in the fail operational modes is especially important. In such operating conditions, a stable operation for a specified time on the modes of reduced power without critical asymmetry of PSM's parameters is also extremely important.

Considering a normal, i.e. failure-free, operational mode, the electric motor can endure a short-term overload because the thermal capacity is sufficiently large, whereas for failure cases the situation is changing dramatically. As known from operating experience, the largest numbers of operational failures are caused by technological overloads [19] - [21].

Most of the total failures of traction electric motors (more than 80%) occur because of stator windings faults and bearings failures, so that these components play a crucial role in the overall reliability value of the motor. Their lifetime and fault tolerance significantly affect the operating temperature, developed inside the motor. The overheating causes quickly deterioration of the motor winding insulation and bearing.

The causes for overheating of electrical machines can be technological overload of the motor as well as the occurrence of different failure modes. The main of them are the various types of short circuits, unbalanced work at the loss of one or several phases, jamming of the rotor of electric machine. Technological overload leads to an increase in temperature of the motor windings to a higher level, a gradual deterioration and finally to its total failure.

In the case of a short circuit in the stator windings, the current value exceeds the nominal value to a multiple. Thus, the rate of rise of the stator winding temperature reaches 7-10°C per second and after 10-15 seconds the motor temperature is out of limits.

The unbalanced mode (phase loss) occurs in the case of burned out fuse in the phase, wire breakage, faults in contacts or in the case of protection operation. Thus there is a redistribution of the currents, the magnitude of current in the remaining phase's increases, which leads to overheating and total failure of the electrical machine.

According to recent research [20], long-term operation of the electric motor with an overcurrent by only 5% of the nominal reduces its lifetime by 10 times.

Most of the overcurrent failures of electric motors are associated primarily with damages inside the motor, leading to an asymmetric overcurrent and, as a consequence, to overheating. The main types of failures that lead to dangerous overheating of the stator windings and to a total failure of the electric motor (without system of protection) are the short circuit faults:

- between turns;
- between coils;
- between phases;
- between wires and the housing of the motor.

Their effects are described in detail in the literature. These effects lead to dramatic increasing of the current in one or more phases of the motor and ultimately to the motor's overheating. At an effective system of protection against emergency situations, each of the above-discussed failures can be reduced to an embodiment of the loss of failed phases (or automatic shutdown).

When it is required to maintain the load at a given level, which is a common requirement for safety-critical systems, such as a helicopter traction drive, it is necessary to increase the phase currents in the remaining phases of the electric motor. This will result in a certain level of the motor's overheating and severely limited, in terms of reliability, duration of operation in this mode of load.

For the traction drives of the electric helicopter the given levels of maintain load in the failed operation are: 65% of the nominal load (long time operation) and 85% of the nominal load (short time operation).

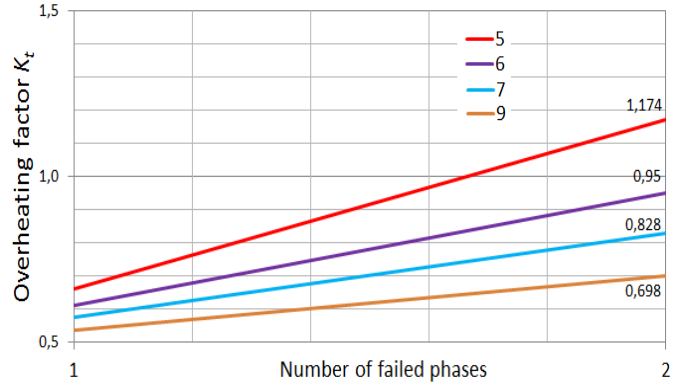

(a)

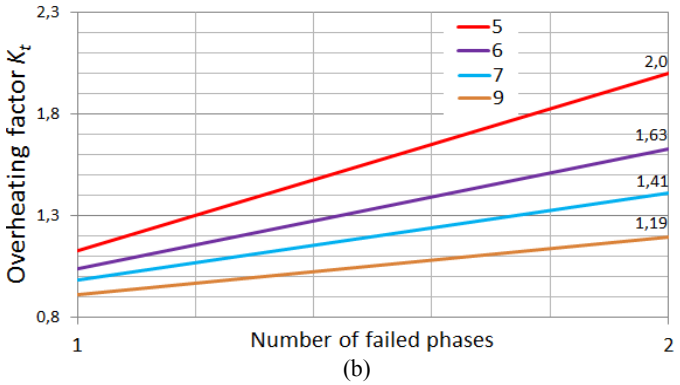

(b)

Fig.7. Overheating at the phase loss, (a) - 65%, (b) - 85% of nominal load

To estimate the level of overheating of the windings of multi-phase traction motors and respective conclusions on its thermal stability in the case of failure in one or two phases, it is proposed to use the overheating factor K_T, which shows how many times the motor windings temperature exceeds the nominal value:

$$K_T = \frac{T_i}{T_N} \tag{3}$$

where T_i and T_N –, respectively, describe the windings temperature in failed operational mode in i-phases and in the nominal failure-free operational mode. Overheating factor is graphically presented in Fig.7.

Table II shows the results of a preliminary assessment of the overload capability of multi-phase traction motors in case of an open-circuit failure of one or two phases.

TABLE II. COMPARISON OF OVERLOAD CAPABILITY

Phase number	**5**		**6**		**7**		**9**	
Fault number	1	2	1	2	1	2	1	2
Load level								
100%	0	0	0	0	0	0	+	0
85%	+	0	+	0	++	0	++	+
75%	++	0	++	+	++	+	++	++
65%	++	+	++	++	++	++	++	++
50%	++	++	++	++	++	++	++	++

Table II has the following designations:

++ - there is no overload;

\+ - overload is less than 15%;

0 - overload is greater than 15%.

The main goal of the preliminary analysis of the presence (or absence) of overload modes of a traction electric motor at various critical failures, is to find the critical points in terms of thermal stability and overload capacity.

Conditional separation of considering multi-phase motors on the level of overload capability into three groups was carried out based on the analysis of the thermal stability of the motor windings for different thermal load conditions.

From the operating experience of electrical machines with appropriate power [20] it is known that when the phase current has insignificant excess (10-15% of the nominal value), the electric motor can be operated a certain time without critical deterioration of insulation of the stator windings. Therefore, such failure operational overloads modes can be considered as partially acceptable. Considering the low rates of overload capability and thermal stability of the 5-phase traction motor, as can be seen from Fig.7, this version was excluded from further analysis.

When current overloads are larger than the above mentioned values, this operational mode has been regarded as critical.

The consequences of the large overload in failure operational mode are overcurrent and overheating of PSM, which lead to a reduction of reliability indices and decrease lifetime of the motor, as can be seen in Fig.8.

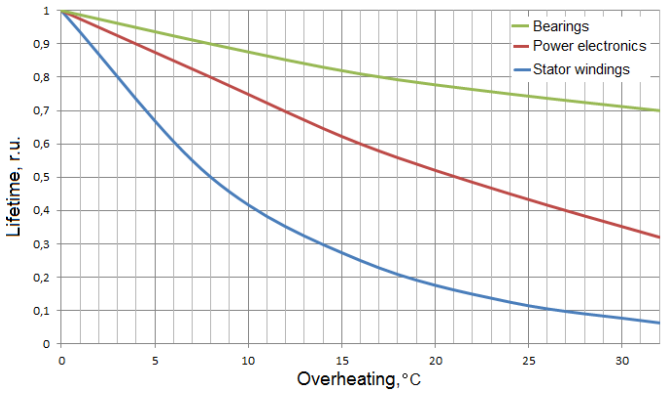

Fig.8. Lifetime of the parts of electric drive [22]

The main characteristic of the load modes of PSM for evaluation of DOFT is the thermal characteristics, estimated by formulas [20]:

$$t_N = \{ln\, K^2 - ln\,(K^2 - 1)\}/(A/C) \qquad (4)$$

where t_N – describes the time of achievement of acceptable motor temperature value, K – the rate of exceeding the nominal value of the phase current, A – the heat irradiation of the motor, and C – the thermal capacity of the electrical machine.

Figure 9 shows graphically the results of calculating the thermal behavior of the electric motor in overload conditions, as a result of one or two critical failures considering thermal stability of the stator windings. The values of N_{deg} and N_{nom} in Fig.9 correspond to the values of traction drive performance (driving power) in degraded and nominal modes, respectively.

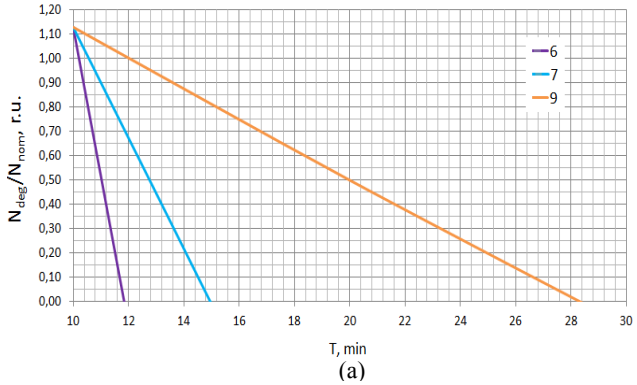

(a)

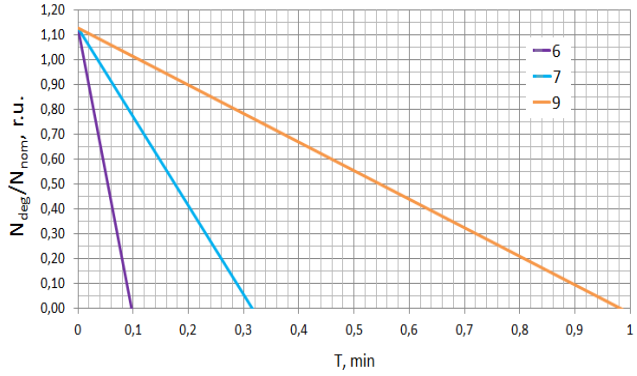

(b)

Fig.9. The duration of the safe motor operation at 113% load at a one (a) and two (b) critical failures

On the basis of the analysis of the thermal behavior of the motor the values Δt_i for the different versions of the traction motor and the various failure modes can be determined. Based on the value Δt_i, the transition probabilities of Markov Models were calculated.

Schedule of DOFT at 65%, 85% and 113% of nominal load, on the number of critical dangerous failures is shown in Fig.10, a, b, c, respectively.

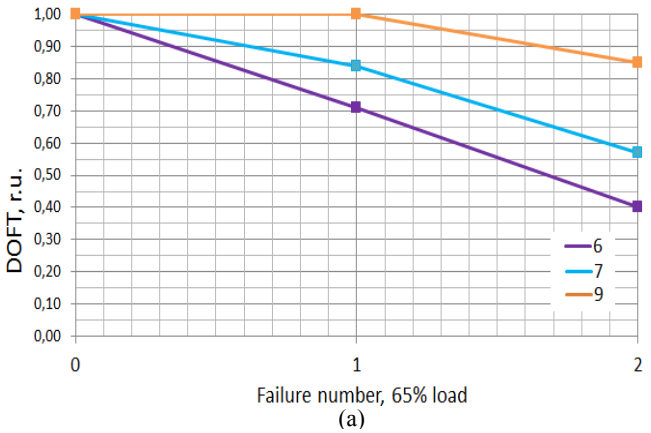

(a)

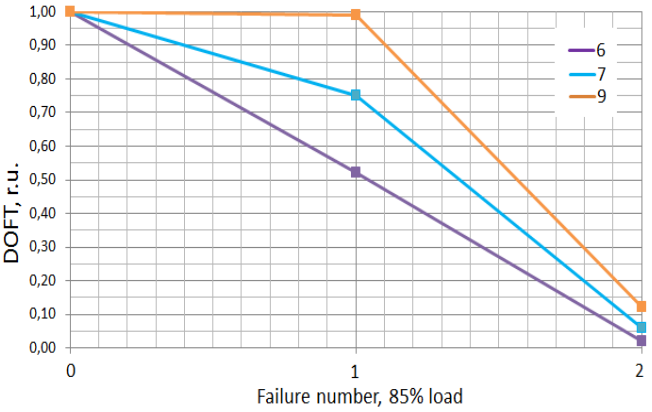

(b)

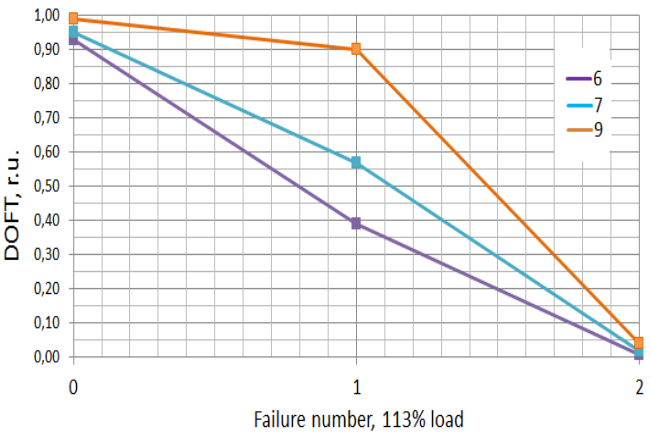

(c)

Fig.10. DOFT of multi-phase PSM in fail operations, (a) - 65%, (b) - 85% and (c) – 113% of nominal load

Based on the constructed graphs a comparative analysis of DOFT for considered variants of the electric motors can be carried out quite easily. However, according to the authors, more informative and convenient for practical use are the dependencies of DOFT on the value of a given load maintenance level, as shown in Fig.11. Thus, it is possible to assess the compliance of parameters of fault tolerance for each compared alternative to design requirements.

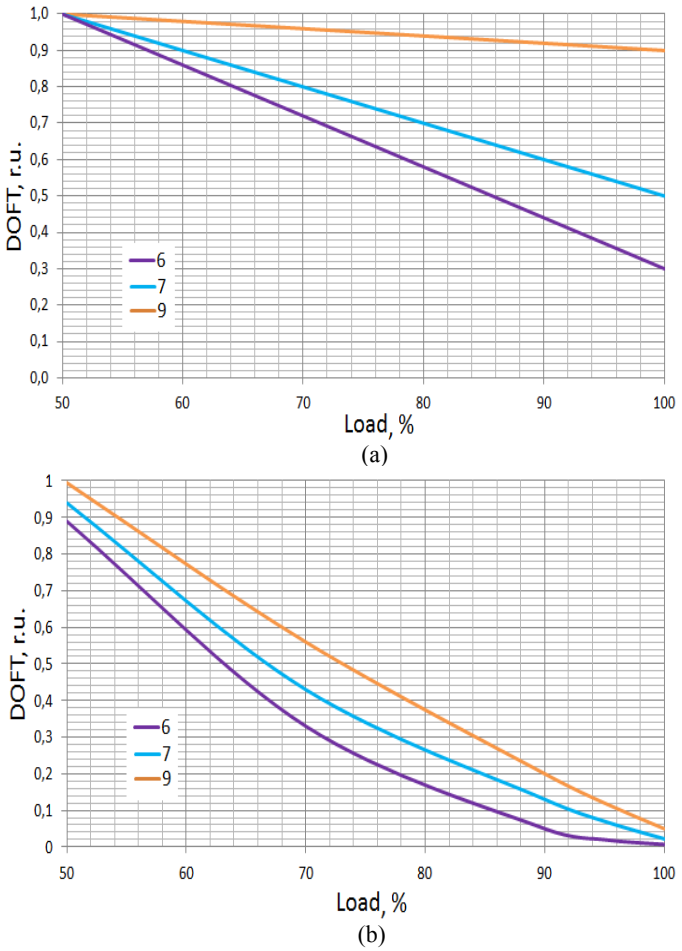

Fig.11. DOFT of a given load level in fail operations, (a) – one failed phase, (b) – two failed phases

D. *Electric Inverter*

Considering the current developments in the field of power electronics, for the comparative analysis of the fault tolerance has been considered two options of electrical power inverter: conventional and multilevel. Voltage Source Inverter (VSI) is the most commonly used power converter between the series-parallel-configured batteries and the electric motor in electrical mobility applications.

It is well known that multilevel inverters offer several advantages compared to their two-level counterparts [12]: smaller power filters, smaller voltage ratings for semiconductors, lower switching frequencies and less power losses. They offer also more modularity and are more reliable.

Currently, mainly three types of electric multilevel inverters are used: Neutral Point Clamping (NPC), Flying Capacitors (FC), and Cascaded H-Bridge (CHB). Considering [8], [10], [11], and [12], CHB inverters need the lowest number of components. NPC and FC inverters need more components than CHB and have less modularity, due to the central storage unit.

Thus, CHB inverters are constructed on a series connection of single-phase inverters supplied by isolated DC electric energy sources. This kind of inverters gives a high modularity degree and consequently high reliability and fault tolerance. An approach based on the full inverter's power control could optimize the implementation and the reliability of the inverter while offering optimized operational behavior.

It should also be noted that CHB is an interesting inverter's topology for the electrical vehicle because of its possibility to work with unbalanced or faulty DC sources. This in turn can increase the life time of battery packs and the autonomy of the vehicle. In the case of using CHB inverters with appropriate control strategies, state of charge unbalances can be managed as well as state of health allowing to optimize the access to the electrical energy and electric vehicle autonomy.

Based on the reqired design parameters of the traction drive of electric helicopter, the preferred inverter option is a topology 17-Level CHB inverter. So, in each phase there are 8 submodules, as shown in Fig.12.

Figure 12 shows the basic topology of one phase of a CHB using batteries on the DC side. Each battery module is connected to a H-bridge with 4 MOSFETs. The use of MOSFETs enhances the efficiency of the CHB inverter, because of the low conduction losses.

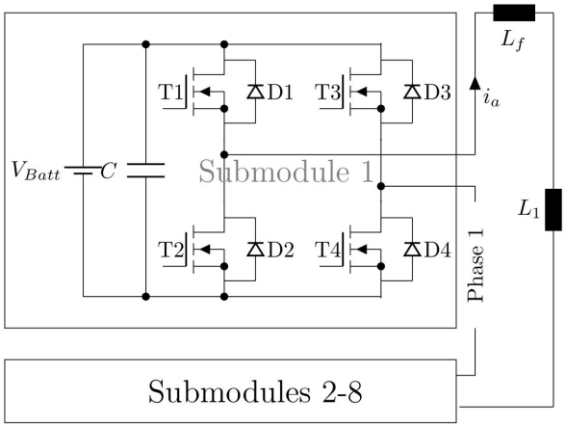

Fig.12. One submodule of the proposed 17-level CHB inverter

For the fault tolerant operation in failure case either the inverter module must be shut down or switched to a possibly existing redundant inverter leg/module. Each of these modes leads to a rapid increase of the current at the emergency site and an overload of the semiconductors. At overload, power losses occur in the p-n-transition and its temperature increases dramatically, due to the low heat capacity. In the case of exceeding a certain critical temperature of p-n-transition, the semiconductor device fails. Hence, overheating temperature is the main parameter characterizing the overload capability of semiconductor devices, as it is shown in Fig.8.

The graph presented in Fig.13 has been plotted based on the data regarding the standard overload capability of the power electronics.

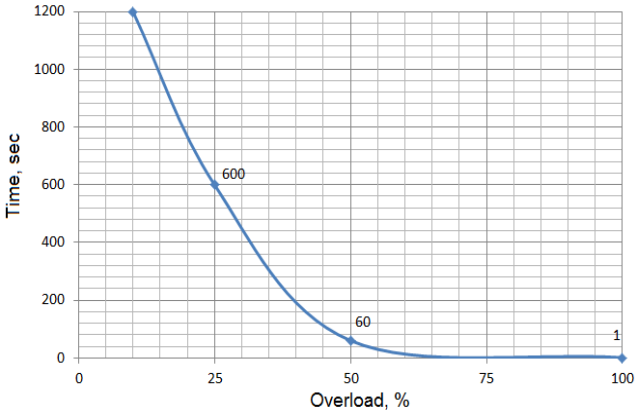

Fig.13. Overload capacity of inverter

Based on the analysis of the thermal modes of inverters in the failure cases, critical operational point considering the thermal stability of semiconductor devices have been identified as shown in Table III and Table IV.

TABLE III. OVERLOAD OF CONVENTIONAL INVERTER IN FAILURE MODES

Phase number	6			7			9		
Fault number	1	2	3	1	2	3	1	2	3
Load level									
113%	+	MF	MF	++	+	MF	+++	+++	++
85%	+++	+	MF	+++	+++	+	+++	+++	+++
65%	+++	+++	MF	+++	+++	+++	+++	+++	+++

TABLE IV. OVERLOAD OF MULTILEVEL INVERTER IN FAILURE MODES

Phase number	6			7			9		
Fault number	1	2	3	1	2	3	1	2	3
Load level									
113%	+	PhF	PhF	++	+	PhF	+++	+++	++
85%	+++	++	+	+++	+++	++	+++	+++	+++
65%	+++	+++	+++	+++	+++	+++	+++	+++	+++

Table III and IV have the following designations:

+ + + - overload is less than 10 %;
++ - overload is less than 25 %;
+ - overload is less than 40%;
MF - motor failure;
PhF - phase failure.

Qualitative analysis of the data presented in the Tables shows that the 17-level inverter significantly exceeds the level of fault tolerance of the inverter with a conventional topology.

IV. SIMULATION RESULTS ON THE MARKOV MODEL

For more accurate assessment of fault tolerance of each comparable traction motor and electric inverter, and for compliance (or non-compliance) with design requirements, MSS Markov Models of reliability were built, which theoretical base is described in [16] and [17].

To construct such models the multi-phase PSM as well as the multilevel inverter can be considered as a system with a loaded functional redundancy and consequently, with an appropriate reserve of fault tolerance. The transition probabilities for MSS Markov Models were calculated using the above mentioned DOFT method.

As was discussed above, the phase open-circuit failure has been considered as the main dangerous failure for electric motor's stator, i.e. it is the most severe kind of failure, to which less dangerous failures can be summarized. For the electric inverter, the MOSFET's submodule open-circuit failure was considered to be the worst case.

Considering the above requirements on the fault tolerance of safety-critical drives as well as statistical data on the reliability of the multi-phase PSM and electric power inverter from [1], [23], [24], and [27], it was determined that the optimal model structure for the analysis of fault tolerance in such conditions is a MSS Markov Models with four states for traction motor and five states for electric power inverter, respectively, as shown in Fig.14 and Fig.15.

The number of states of the MSS Markov Model is determined by the probability of failure-free operation of the system in the failure-free mode and fault tolerance requirements established by the design documentation.

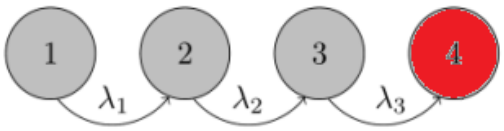

Fig.14. Multi-State Markov model of traction multi-phase PSM

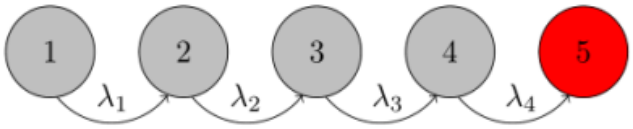

Fig.15. Multi-State Markov model of multilevel inverter

The first state corresponds to a completely failure-free operation of the motor and inverter. The second and third states of the motor and the second, third, and fourth of the inverter are the states of degradation and correspond to failure cases. For the electric motor this means phase open-circuit failure of one and two phases, respectively.

The fourth state of the motor's model (Fig.14) corresponds to the completely failed electric motor when the helicopter's drive completely loses the ability to operate. Thus, every following state of the degradation corresponds to one emergency phase loss with a corresponding loss of the part of functionality of the motor.

The fifth state of the inverter's model (Fig.15) corresponds to the completely failed conventional inverter when the traction motor does not receive the necessary power for a safe flight. Thus, every following state of the degradation corresponds to the worst case – a loss of an inverter's submodule. For the multilevel CHB inverter the fifth state of the model means the loss of one complete phase of the electric motor.

The proposed assessment approach for transition probabilities in the MSS Markov reliability model is well formalized and suitable for practical application in reliability engineering to assess fault tolerance indices of multi-phase traction motors considering the aging process under the influence of operating conditions.

Regarding the design requirements on fault tolerance of an electric helicopter, the reliability of the traction electric motor at reduced power of 65% or 85% of the nominal value as well as at 113% of nominal value was analyzed using the MSS MM. Corresponding graph for 6-, 7- and 9-phase PSM at the 113% load level are presented in Fig.16. The horizontal axis indicates operational time in hours and vertical axis - probability of total failure of traction motor.

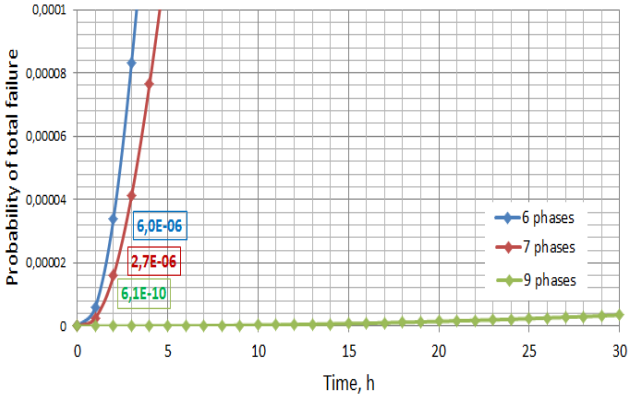

Fig.16. Probability function of total failure of PSM at the 113% load

TABLE III. PROBABILITIES OF COMPLETE FAILURE OF PSM

Phase number	**6**	**7**	**9**
65% nominal load	$2.85 \cdot 10^{-11}$	$2.38 \cdot 10^{-12}$	$6.80 \cdot 10^{-16}$
85% nominal load	$8.19 \cdot 10^{-9}$	$1.27 \cdot 10^{-10}$	$5.42 \cdot 10^{-12}$
113% nominal load	$6.00 \cdot 10^{-6}$	$2.71 \cdot 10^{-6}$	$6.10 \cdot 10^{-10}$

The simulation results of two consecutive critically dangerous failures allow of quantifying the reliability indices degree of the fault tolerant multi-phase electric motor, which is one important part in the traction drive of electric helicopters, and of estimating the compliance of calculated values with design requirements.

The obtained results confirm the results of the studies presented in [5] and [6], that 7-phase electric traction motors can be operated after the loss of two phases during a limited time, at nominal load (limitation because of thermal stability), and for a long time with a reduced load.

For the simulation the worst case and critically dangerous variant of failure has been considered, i.e. the submodule failures occur in the same phase. In case of a simulation of a not safety-critical failure, as well as the possibility of partial recovery of the power drive's operating ability in the degraded state, the value of the fault tolerance will be significantly higher.

Regarding the design requirements on fault tolerance, the reliability of the inverter was analyzed using the above MSS Markov Models, in case of emergency reducing the power to 113% of the nominal value. The corresponding graphs for a different number of phases and inverter topologies are presented in Fig.17 and Fig. 18, respectively.

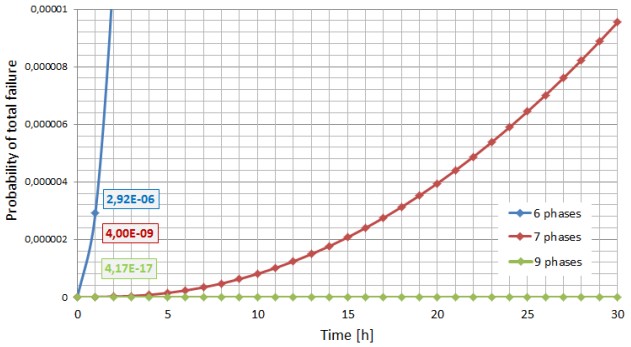

Fig.17. Probability function of a total motor failure with conventional inverter at the 113% load

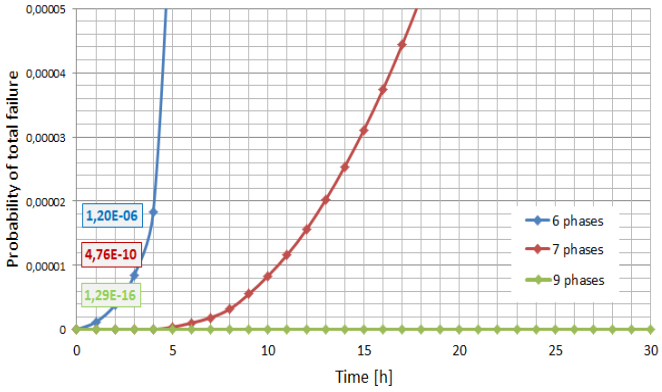

Fig.18. Probability function of a total failure of one motor phase with multilevel inverter at the 113% load

The results of the probability calculations of a failure-free operation of the electric inverter during one operational hour at 113% of nominal load for two inverter's topologies are summarized in Table IV.

TABLE IV. PROBABILITIES OF COMPLETE FAILURE OF INVERTER

Phase number / **Topology**	**6**	**7**	**9**
B6 (Motor total failure)	$2.9 \cdot 10^{-6}$	$4.0 \cdot 10^{-9}$	$4.2 \cdot 10^{-17}$
CHB (Phase total failure)	$1.2 \cdot 10^{-6}$	$4.8 \cdot 10^{-10}$	$1.3 \cdot 10^{-16}$

The results of simulation of three consecutive critically dangerous failures allow quantifying the degree of fault tolerance of a 17-level inverter, which is one of the important parts of the traction drive of helicopters. The 7- and 9-phase options have shown the maximum compliance with the requirements relating to the safety-critical drives.

V. CONCLUSION

The paper presents a new approach and methodology for assessing the degree of fault tolerance of a safety-critical technical system, such as a vehicle's electric traction drive. The suggested assessment of the reliability of fault tolerant topologies of electric traction drives is well formalized and suitable for practical application in reliability engineering to assess fault tolerance indices of multi-phase traction motors as well as an electric power inverter, considering the aging process under the influence of operating conditions.

As an example of practical use of the proposed method the fault tolerance of two important parts of a vehicle's electric propulsion system - traction motor and electric inverter - were evaluated.

Results of comparative analysis allow to conclude that for given project requirements on the level of reliability and fault tolerance of helicopter's electric traction drive in the real flying conditions only 9-phase motors in combination with 17-level inverters completely fulfill the design requirements without any restriction.

More broadly, the proposed method can be used as a universal tool for evaluation and optimization of the degree of fault tolerance in safety-critical technical systems, considering all the possibilities of its increasing, such as redundancy, monitoring, predictive control and type of maintenance strategy.

REFERENCES

[1] I. Bolvashenkov, J. Kammermann, S. Willerich and H.-G. Herzog, "Comparative Study of Reliability and Fault Tolerance of Multi-Phase Permanent Magnet Synchronous Motors for Safety-Critical Drive Trains", in Proceedings of the International Conference on Renewable Energies and Power Quality (ICREPQ'16), 4 th to 6th May, Madrid, Spain, 2016, pp.1-6.

[2] E. Levi, "Multiphase Electric Machines for Variable-Speed Applications", IEEE Transactions on Industrial Electronics, Vol.55, No 5, 2008, pp.1893-1909.

[3] M. Villani, M. Tursini, G. Fabri and L. Castellini, "Multi-Phase Permanent Magnet Motor Drives for Fault-Tolerant Applications", In Proc. of IEEE International Electric Machines & Drives Conference (IEMDC), 5-18 May 2011, Niagara Falls, Canada, 2011, pp.1351-1356.

[4] F. Scuiller, J.-F. Charpentier and E. Semail, "Multi-Star Multi-Phase Winding for a High Power Naval Propulsion Machine with Low Ripple Torques and High Fault Tolerant Ability", In Proc. of the IEEE Vehicle Power and Propulsion Conference (VPPC), 1-3 Sept. 2010, Lille, France, 2010, pp.1-5.

[5] E. Semail, X. Kestelyn and F. Locment, "Fault Tolerant Multiphase Electrical Drives: the Impact of Design", European Physical Journal - Applied Physics (EPJAP), Vol.43, Iss.2, 2008, pp.159-162.

[6] P.G. Vigrianov, "Assessment the impact of different failures on the power characteristics of the low power 7-phase permanent magnet synchronous motors", Moscow, Journal "Questions to Electromechanics", Moscow, Vol.128, Iss.3, 2012, pp.3-7. (in Russian)

[7] D. Fodorean, M. Ruba, L. Szabo and A. Miraoui, "Comparison of the main types of fault-tolerant electrical drives used in vehicle applications", In Proc. of International Symposium on Power Electronics, Electrical Drives, Automation and Motion, (SPEEDAM), June 11-13, Ischia, Italy, 2008, pp. 895-900.

[8] O. Josefsson, T. Thiringer, S. Lundmark and H. Zelaya, "Evaluation and comparison of a two-level and a multilevel inverter for an EV using a modulized battery topology", In Proc.of IEEE 38th Annual Conference on Industrial Electronics Society (IECON), Oct. 25-28, Montreal, Canada, 2012, pp. 2949-2956.

[9] A. V. Brazhnikov and I. R. Belozyorov,"Prospects for Use of Multiphase Phase-Pole-Controlled AC Inverter Drives in Traction Systems", European Journal of Natural History, Russia, Vol.2, 2011, pp.47-49.

[10] B. Sarrazin, N. Rouger, J. P. Ferrieux and J. C. Crebier, "Cascaded Inverters for electric vehicles: Towards a better management of traction chain from the battery to the motor?", In Proc. of IEEE International Symposium on Industrial Electronics, June 27-30, Gdansk, Poland, 2011, pp. 153-158.

[11] S. Fazel, S. Bernet, D. Krug and K. Jalili, "Design and Comparison of 4-kV Neutral-Point-Clamped, Flying-Capacitor, and Series-Connected H-Bridge Multilevel Converters", IEEE Transactions on Industry Applications, Vol.43, No.4, Jul.-Aug. 2007, pp. 1032-1040.

[12] M. Malinowski, K. Gopakumar, J. Rodriguez and M. Perez, "A Survey on Cascaded Multilevel Inverters", IEEE Transaction on Industrial Electronics, Vol. 57, No. 7, July 2010, pp. 2197-2206.

[13] B. A. Welchko, T. A. Lipo, T. M. Jahns and S. E. Schulz, "Fault Tolerant Three-Phase AC Motor Drive Topologies: A Comparison of Features, Cost, and Limitations", In: IEEE Transactions on Power Electronics, Vol.19, No 4, 2004, pp.1108-1116.

[14] U. De Pra, D. Baert and H. Kuyken, "Analysis of the Degree of Reliability of a Redundant Modular Inverter Structure", In Proc. of IEEE 12th International Telecommunications Energy Conference, 04-08 Oct. 1998, San Francisco, CA, 1998, pp.543- 548.

[15] S. Krivoi, M. Hajder, P. Dymora and M. Mazurek, "The Matrix Method of Determining the Fault Tolerance Degree of a Computer Network Topology", Sofia, Bulgaria, Publisher: ITHEA, Vol.13, No 3, 2006, pp.221-227.

[16] A. Lisnianski, I. Frenkel and Y. Ding, "Multi-state System Reliability Analysis and Optimization for Engineers and Industrial Managers", Berlin, New York, Springer, 2010, 393 p.

[17] B. Natvig, "Multi-state systems reliability theory with applications", John Wiley & Sons, New York, 2011, 232 p.

[18] I. Bolvashenkov and H.-G. Herzog, "Use of Stochastic Models for Operational Efficiency Analysis of Multi Power Source Traction Drives", In Proc. of IEEE of International Symposium on Stochastic Models in Reliability Engineering, Life Science and Operations Management (SMRLO'16), 15-18 Feb. 2016, Beer Sheva, Israel, 2016, pp.124-130.

[19] D. Hann,"A combined electromagnetic and thermal optimisation of an aerospace electric motor", Int. Conference on Electrical Machines, ICEM, 6-8 Sept. 2010, Rome, Italy, 2010, pp.1-6.

[20] M. M. Katzman, "Electrical machines", Akademia, Moscow, Russia, 2001, 463 p. (in Russian)

[21] S. Mahdavi, T. Herold and K. Hameyer, "Thermal modeling as a tool to determine the overload capability of electrical machines", International Conference on Electrical Machines and Systems (ICEMS), 26-29 Oct. 2013, Busan, Korea, 2013, pp.454–458.

[22] I. Bolvashenkov and H.-G. Herzog, "Approach to Predictive Evaluation of the Reliability of Electric Drive Train Based on a Stochastic Model", In Proc. of IEEE 5th International Conference on Clean Electric Power (ICCEP'15), 16-18 June 2015, Taormina, Italy, 2015, pp.1-7.

[23] E. Lauger, "Reliability in electrical and electronic components and systems", North - Holland Publ. Co., Amsterdam, 1982, 1171p.

[24] N. P. Ermolin and I. P. Zerichin, "Zuverlässigkeit elektrischer Maschinen", Berlin, Verlag Technik, 1981, 227 p. (in German)

[25] A. H. Ranjbar, M. Kiani and B. Fahimi, "Dynamic Markov Model for Reliability Evaluation of Power Electronic Systems", In Proc. of IEEE International Conference on Power Engineering, Energy and Electrical Drives (POWERENG), Malaga, Spain, May 2011, pp.1-6.

[26] M. Molaei, H. Oraee and M. Fotuhi-Firuzabad, "Markov Model of Drive-Motor Systems for Reliability Calculation", In Proc. of IEEE International Symposium on Industrial Electronics, 9-13 July 2006, Montreal, Canada, pp.2286-2291.

[27] T. Geyer and S. Schroder, "Reliability Considerations and Fault-Handling Strategies for Multi-MW Modular Drive Systems", In: IEEE Transactions on Industry Applications, Vol.46, No.6, Nov.-Dec. 2010, pp. 2442-2451.

[28] K. S. Trivedi, "Probability and Statistics with Reliability, Queuing, and Computer Science Applications", Second edition, Wiley, 2002, 848 p.

[29] S. J. Bavuso, J. B. Dugan, K. S. Trivedi, E. M. Rothmann and W. E. Smith, "Analysis of Typical Fault-Tolerant Architectures using HARP", In: IEEE Transactions on Reliability, Vol.R-36, Iss.2, June 1987, pp.176-185.

[30] N. Muellner and O. Thee, "The Degree of Masking Fault Tolerance vs. Temporal Redundancy", In: IEEE Workshops of International Conference on Advanced Information Networking and Applications (WAINA), 22-25 March 2011, Biopolis, Singapore, 2011, pp.21-28.

[31] R. Ubar, S. Devadze, M. Jenihhin, J. Raik, G. Jervan and P. Ellervee, "Hierarchical Calculation of Malicious Faults for Evaluating the Fault-Tolerance", In Proc. of 4th IEEE International Symposium on Electronic Design, Test & Applications (DELTA), 23-25 Jan. 2008, Hong Kong, 2008, pp.222-227.

Igor Bolvashenkov, Dr.-Eng., Senior researcher, Institute of Energy Conversion Technology, Technical University of Munich (TUM), Munich, Germany.

Igor Bolvashenkov obtained his diploma (1981) and doctoral degree (1989) in Electrical Engineering from Admiral Makarov State University of Maritime and Inland Shipping, Leningrad, USSR. From 1987 till 1993 he worked as Associate Professor at the Murmansk State Technical University, Russia. Since 2004 he works at the Institute of Energy Conversion Technology of Technical University of Munich (TUM), Germany.

He has specialized in development and simulation of electric propulsion safety-critical systems for ships, cars, aircraft with analysis of their reliability, survivability, and fault tolerance.

He published more than 75 scientific articles, book chapters and patents in the fields of development of traction drives for the various type of electric vehicle and system analysis of efficiency, reliability and fault tolerance.

Hans-Georg Herzog, Prof. Dr.-Eng., Institute of Energy Conversion Technology, Technical University of Munich (TUM), Munich, Germany.

Hans-Georg Herzog holds a diploma and a doctoral degree (with distinction) from Technical University of Munich (TUM). After his time as a research associate, he joined Robert Bosch GmbH, Leinfelden-Echterdingen, Germany. Since 2002, he is Head of the Institute of Energy Conversion Technology at TUM.

His main research interests are energy efficiency of hybrid-electric, full-electric vehicles and electric aircrafts, reliability of drive trains and their components, energy and power management and advanced design methods for electrical machines

Hans-Georg Herzog is Senior member of IEEE and member of VDI and VDE.

Pattern Recognition Methods for Detecting Voltage Sag Disturbances and Electromagnetic Interference in Smart Grids

Turgay Yalcin, Muammer Ozdemir

Abstract— **Identification of system disturbances, detection of them guarantees smart grids power quality (PQ) system reliability and provides long lasting life of the power system. The key goal of this study is to find the best accuracy of identification algorithm for non-stationary, non-linear power quality disturbances such as voltage sag, electromagnetic interference in smart grids. PQube, power quality and energy monitor, was used to acquire these distortions. Ensemble Empirical Mode Decomposition is used for electromagnetic interference reduction with first intrinsic mode function. Hilbert Huang Transform is used for generating instantaneous amplitude and instantaneous frequency feature of real time voltage sag power signal. Outputs of Hilbert Huang Transform is intrinsic mode functions (IMFs), instantaneous frequency (IF), and instantaneous amplitude (IA). Characteristic features are obtained from first IMFs, IF, and IA. The six features—, the mean, standard deviation,skewness, kurtosis of both IF and IA are then calculated. These features are normalized along with the inputs classifiers. The proposed power system monitoring system is able to detect power system voltage sag disturbances and capable of recognize electromagnetic interference component. In this study based on experimental studies, Hilbert Huang Transform based pattern recognition technique was used to investigate power signal to diagnose voltage sag and in power grid. Support Vector Machines and C4.5 Decision Tree were operated and their achievements were matched for precision and CPU timing. According to the analysis, decision tree algorithm without dimensionality reduction produces the best solution.**

Index Terms— C4.5 decision trees, electromagnetic interference, feature extraction, hilbert huang transform, power quality disturbance, smart grids, support vector machines

I. INTRODUCTION

Smart grids have been constructed structure where a number of control devices are used to provide reliability, stability and efficiency in the power generation, transmission and distribution. To enhance forecasting faults and risks in addition to ensuring protection against any possible internal and external threats, the new generation, smart grids, will be supplied with communication facilities and real time measurement techniques [1, 2]. The smart grid design is mainly based on restructuring the power industry and optimizing its resources. Smart Grids could optimize transfer capability of transmission and distribution networks to meet the demands for higher quality and more reliable power supply [1, 2]. The main benefits of the Smart Grid technologies include**:** minimized shutdown of the distributed generation in overload conditions, power quality improvement, improved voltage profile, coordinated restoring of the power system avoid to grid blackout [1,2,3,4].

A. Voltage Sag

Voltage sags are short-duration (less than 1 sec) reduction in voltage magnitude. This kind of disturbance is presently one of main power quality problems (Figure 1b.). Momentary increase of current has many origins in power systems such as energizing of transformers, short circuits, earth faults and starting of induction motors [5, 6].

B. Electromagnetic Interference (EMI)

Electromagnetic interference (EMI), side-effect results of the power conversion and control devices processes, can emerge in a wide frequency range from the basic harmonic and inter-harmonics of the mains frequency. A rise in switching frequencies gives rise to the high energy obstruction, created by the realization of the energy conversion processes, to be shifted in frequency range approximately operated (9 kHz-30 MHz) EMI range. Moreover, a new growing power quality problem especially (2 kHz-150 kHz) threatened the smart grid power quality [7]. EMI normalized voltage signal (L1-N / phase A) generated with arbitrary function generator Tektronix AFG3022C is shown in Figure 1c [2, 6].

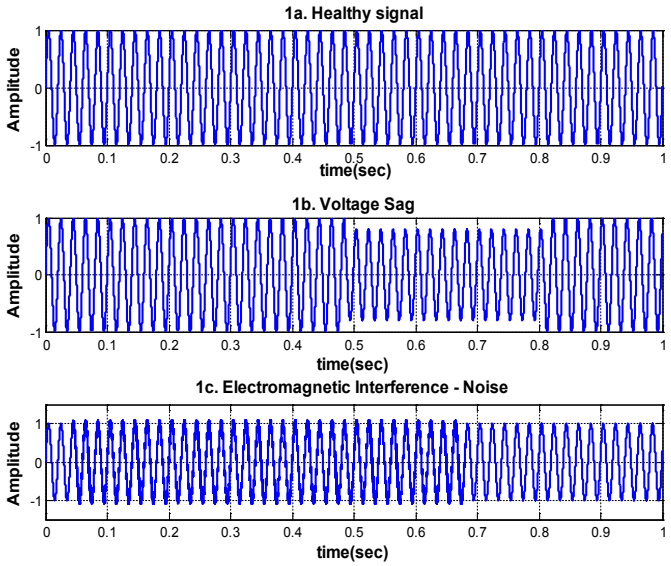

Fig. 1. Healthy signal (1a), normalized voltage sag (1b) and EMI normalized voltage signal (1c) (L1-N / phase A) generated with Tektronix AFG3022C

This scientific study is supported by TUBITAK. (Project Number: 114E919)
T. Yalcin is with the Ondokuz Mayis University, Department of Electrical & Electronic Engineering, 55139, Samsun, TURKEY (e-mail: turgay.yalcin@omu.edu.tr). M. Ozdemir is with the Ondokuz Mayis University, Department of Electrical & Electronic Engineering, 55139, Samsun, TURKEY (e-mail: ozdemirm@omu.edu.tr).

Hilbert Huang Transform method used for recognizing and identifying real time power quality disturbances have described in Section II.

II. FEATURE EXTRACTION

A. Emprical Mode Decomposition (EMD)

The algorithm [8, 9, 10] includes the steps:

i. Determine all the extrema of the signal, *s(t)*.
ii. Find the upper and lower envelope constructed in step (i). (Interpolation of the extrema analyses with the cubic spline)
iii. Then, find the subtraction signal and the mean function of the upper and lower envelope (mean(t)), $dif(t) = s(t) - mean(t)$.
iv. Only when the iteration stops, $dif(t)$ becomes first imf $c_1(t)$; or else, branch to step (i) change $s(t)$ with $dif(t)$.
v. Find the residue signal, $res(t) = s(t) - c_1(t)$.
vi. Continue the operation from steps (i) to (vi) to attain second IMF, $c_2(t)$. Achieve $c_n(t)$, continue steps (i) – (vi) after *n* iterations. The routine is broken when the last imf (residual signal $res(t)$) is acquired as a monotonic function.

This routine called *sifting process. Finally,* we get residue $res(t)$, gathering of *m* IMF, from $c_1(t)$ to $c_n(t)$. The targeted signal can be expressed as:

$$s(t) = \sum_{i=1}^{m} c_i(t) + res(t) \tag{1}$$

we can regard $res(t)$ as $c_{m+1}(t)$ [11, 12,13].

C. Feature Generation: Hilbert-Huang Transform (HHT)

HHT [13, 14, 15] enables the real time signal $X(t)$ into the time frequency domain by merging EEMD with the Hilbert transform (Fig. 3.). *The Hilbert transform* is then implemented for each IMF component $\boldsymbol{C_j}$ generated with sifting process which is explained in Section III.A.

$$v_j(t) = \frac{1}{\pi} \int_{-\infty}^{+\infty} \frac{c_j(\tau)}{t-\tau} d\tau \tag{3}$$

$c_j(t)$ *is* real part and $v_j(t)$ is imaginary part of an analytic signal $z_j(t)$:

$$z_j(t) = c_j(t) + j v_j(t) \tag{4}$$

B. Ensemble Emprical Mode Decomposition (EEMD)

The EEMD algorithm (Fig. 2.) steps are hearunder:

i. Add noise, $wn(t)$, to target signal $s_1(t)$. $s_2(t) = s_1(t) + wn(t)$.
ii. Used EMD algorithm for decomposing the final signal $s_2(t)$.
iii. Continue steps (i) and (ii) till the trial numbers. When new imf combination $C_{ij}(t)$ is succeeded, predict the ensemble mean of the last imf. The aimed output:

$$EEMD[c_j(t)] = \sum_{i=1}^{tn} c_{ij}(t) \tag{2}$$

tn: trial numbers, *i:* iteration number and *j:* imf scale [13,14].

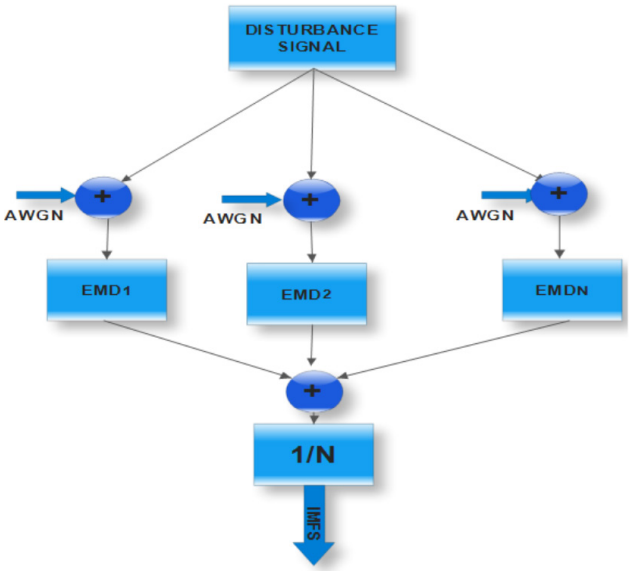

Fig. 2. The representation of the EEMD algorithm

$$z_j(t) = A_j(t) \exp(j w_j(t)) \tag{5}$$

Amplitude and *phase* expressed with equation (6) and (7):

$$A_j(t) = \sqrt{c_j(t)^2 + v_j(t)^2} \tag{6}$$

$$\theta_j(t) = \arctan\left(\frac{v_j(t)}{c_j(t)}\right) \tag{7}$$

Thus, the *instantaneous frequency* $w_j(t)$ was given by:

$$w_j(t) = \frac{d\theta_j(t)}{dt} \tag{8}$$

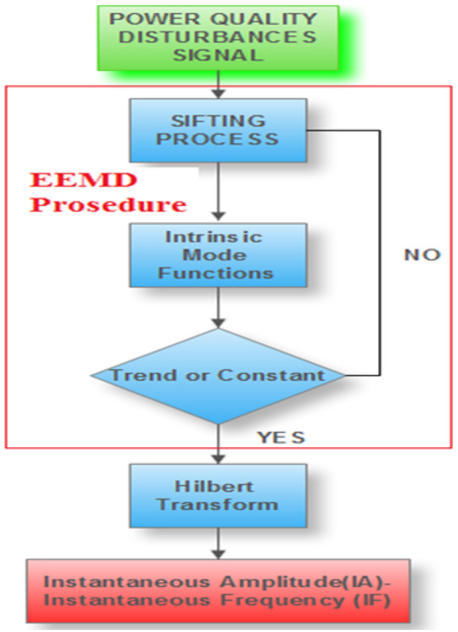

Fig. 3. Main steps of the feature generation routine with HHT

III. Experiment Set Up

In this part of the study, PQube was installed to acquire measurements, firstly in basic electricity laboratory for one phase (L1-N) records. Secondly it was utilized in computer laboratory for three phases (L1-N, L2-N, L3-N) records which its loads are computers. HHT is used in signal processing part of the study for generation of Instantaneous Amplitude (IA) and Instantaneous Frequency (IF) features. They respectively generated for real time values from PQube one phase in basic electricity laboratory, three phases in computer laboratory for computers.

A. Real Time Basic Electricity Laboratory Measurements

One phase (L1-N) voltage sag (Fig. 4.) event history which recorded by PQube is shown in Table I.

TABLE I

EVENT HISTORY (ONE PHASE)

Event_Type	Voltage Sag
Event_Magnitude	60.44%
Event_Duration_In_Seconds	0.110
Trigger_Date	2015/11/08
Trigger_Time	T 03:05:51.687
Trigger_Channel	L1-N
Trigger_Threshold	90.0% of nominal
Trigger_Sample_Number	257
Samples_Per_Cycle	128
Microseconds_Per_Sample	156.398

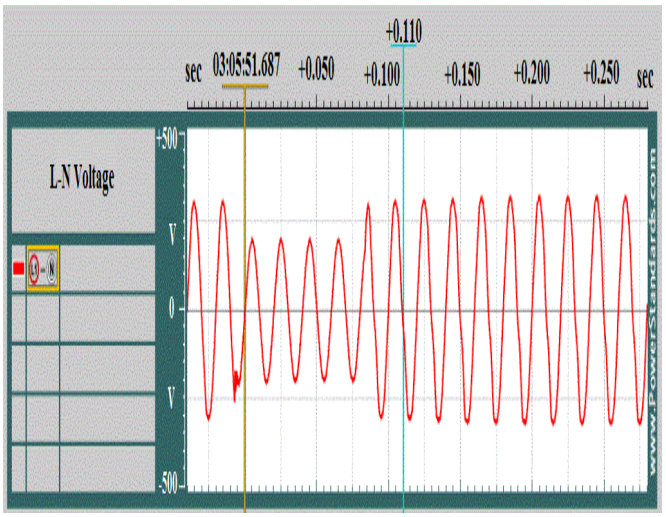

Fig. 4. Power Quality Monitor with PQube voltage sag condition of signal (2015/11/08)

Fig. 5. illustrates that first component imf1 the noise (lowest magnitude and highest frequency signal) on the line (L1-N). Lower order of imfs means high frequency and oscillation higher order otherwise.

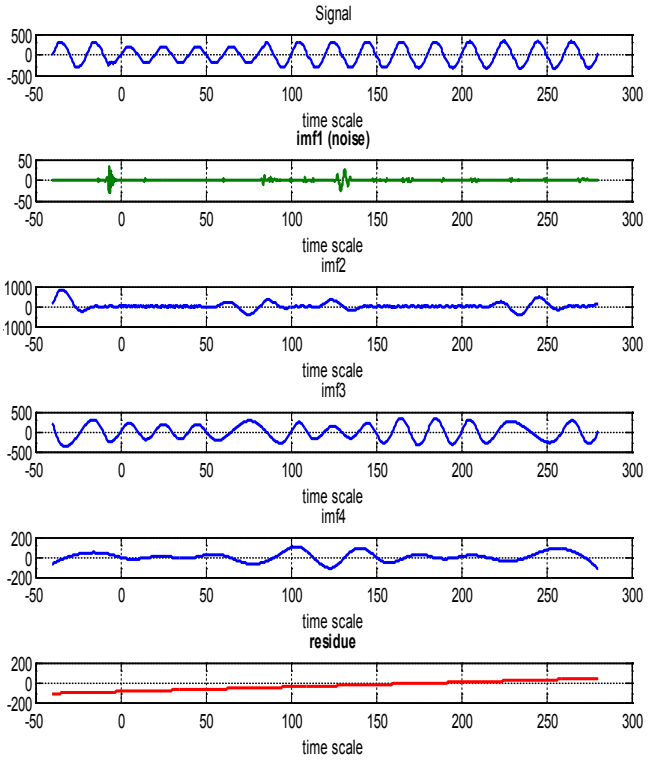

Fig. 5. IMFs for a voltage sag signal processed with EEMD

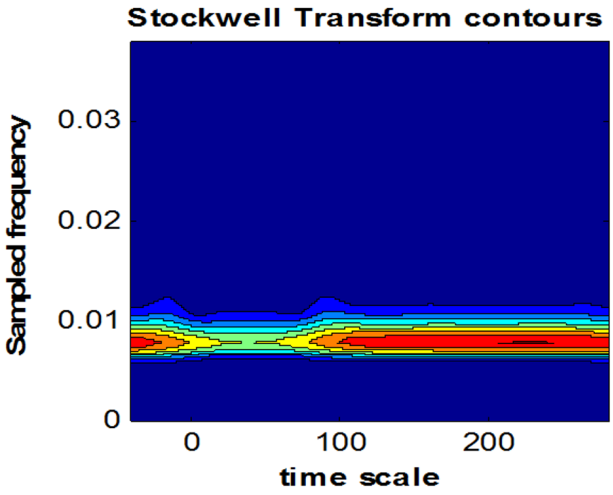

Fig. 6. Stockwell Transform (ST) contours

The Stockwell Transform (ST) is developed method related with the Gabor Transform (GT) and Wavelet Transform (WT). Several works have used ST for the analysis of PQ disturbance because it allows location in time, real and imaginary components of the spectrum [16, 17, 18, 19]. Fig. 6. shows that ST can produce proper features for detecting voltage sag. Table II shows the main advantages and disadvantages of two signal processing methods (HHT, ST).

Table II

COMPARISON OF TWO FEATURE EXTRACTION METHOD FOR PQ DISTURBANCES [25, 28]

	HHT	ST
Advantages	Appropriate for feature extraction of non-linear non-stationary signal, generates perpendicular imfs whereby instantaneous amplitude and phase can be easily assessed	Maintain time and frequency representation. Good time-frequency resolution
Disadvantages	For narrow band conditions is limited, end effects	Does not accomplish real-time requirement based on block processing, false harmonics measurement owing to dependency of frequency window width.

B. Real time Computer Laboratory measurements

For 3 phases (L1-N, L2-N, L3-N) real time processing the first intrinsic mode function is removed with the addition (superposition) of remain components to reconstruct the analyzed signal (Equ. 1.). Respectively, fig. 7. and fig. 8. show that after removing noise component normal and voltage sag cases.

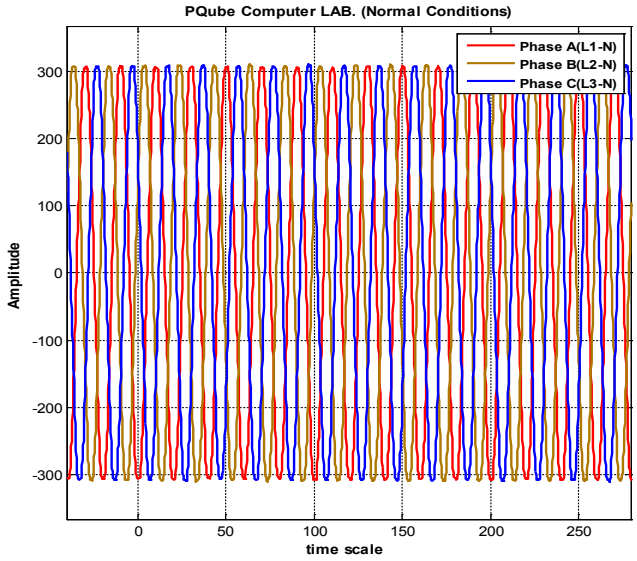

Fig. 7. After removing first imf normal condition of signal

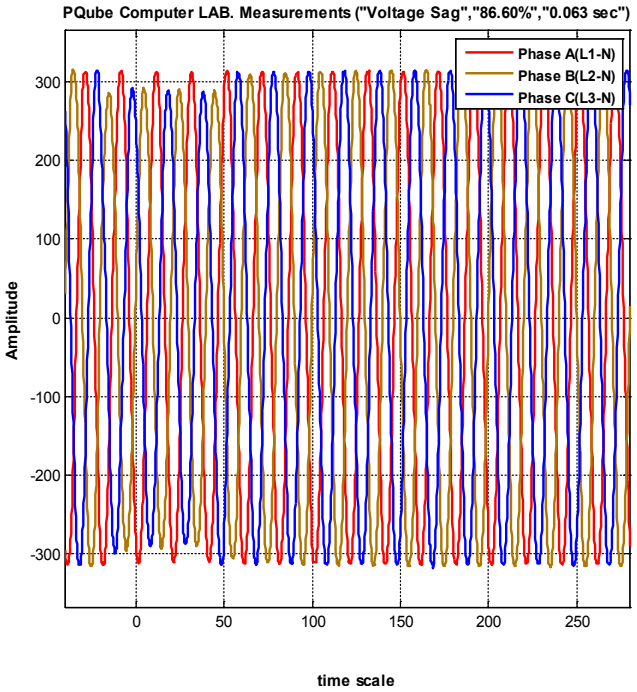

Fig. 8. After removing first imf voltage sag condition of signal

Fig 8. illustrates real time computer laboratory measures that after reconstructing the voltage sag (rate: 86.60%-duration: 0.063 sec) signal, namely the first imf removing from the noisy component. In addition, voltage sag occurred on phase B-C as a result of this case different load types and number of computers on line. This is main vision of this scientific work to identify the fault on active different load types.

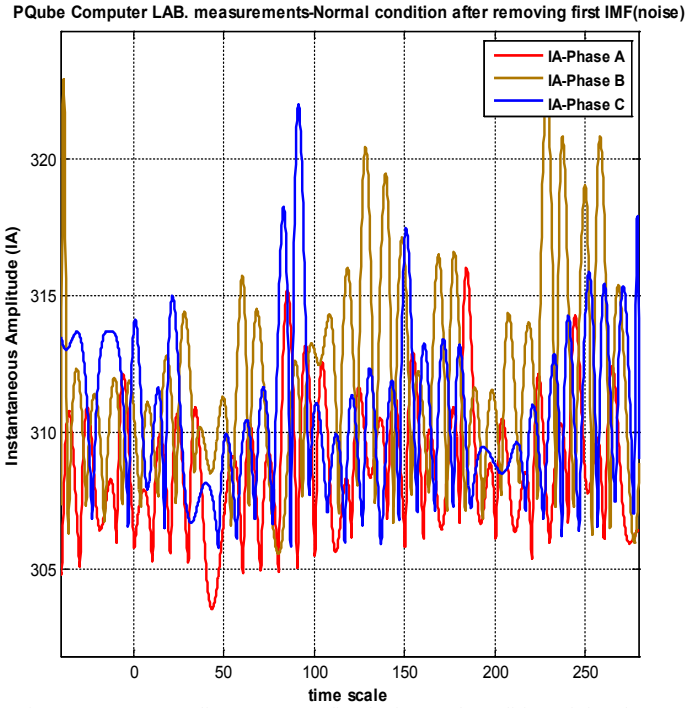

Fig. 9. IA corresponding to remove first imf normal condition of signal

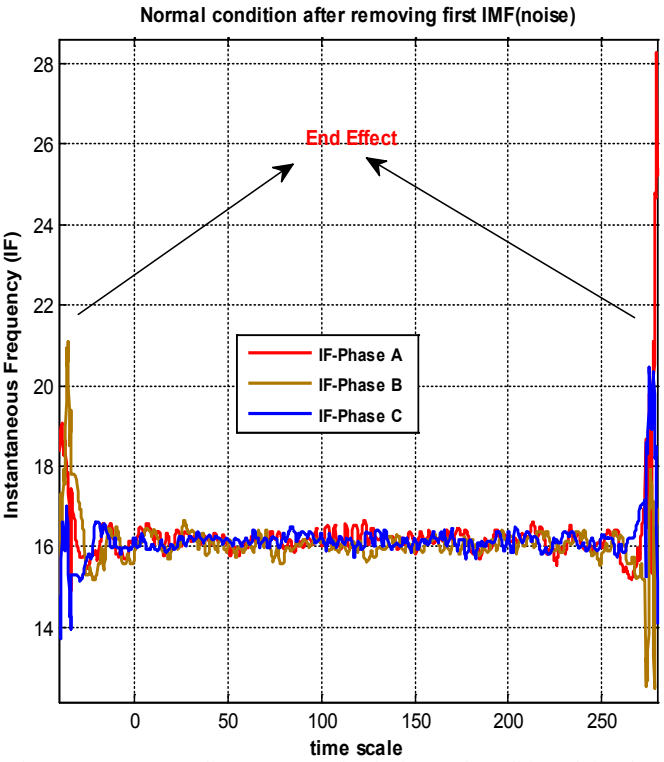

Fig. 10. IF corresponding to remove first imf normal condition of signal

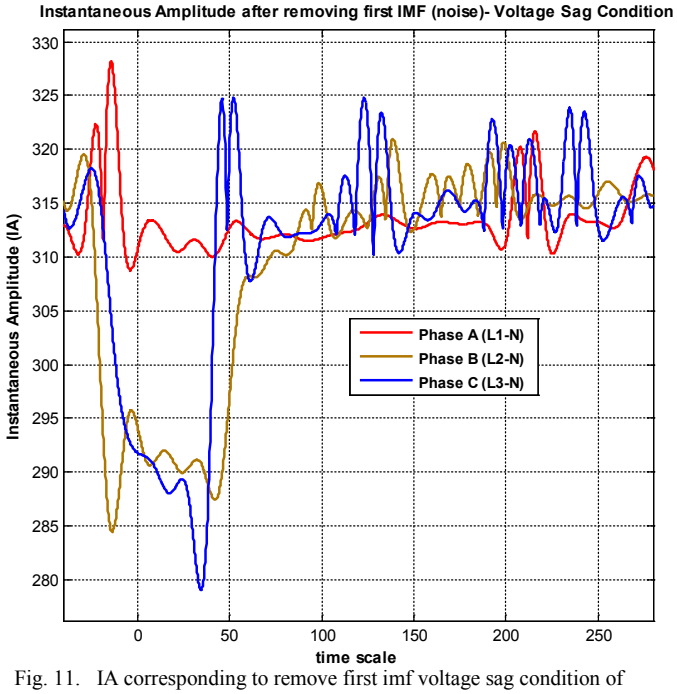

Fig. 11. IA corresponding to remove first imf voltage sag condition of signal

The results show explicitly different pattern in Fig. 9.- normal condition as for Fig. 11. – voltage sag condition. Also it is clearly shown in fig. 11. voltage sag on two phases (L2-N, L3-N). This information will be used for evaluating active loads types and risk management of the grid.

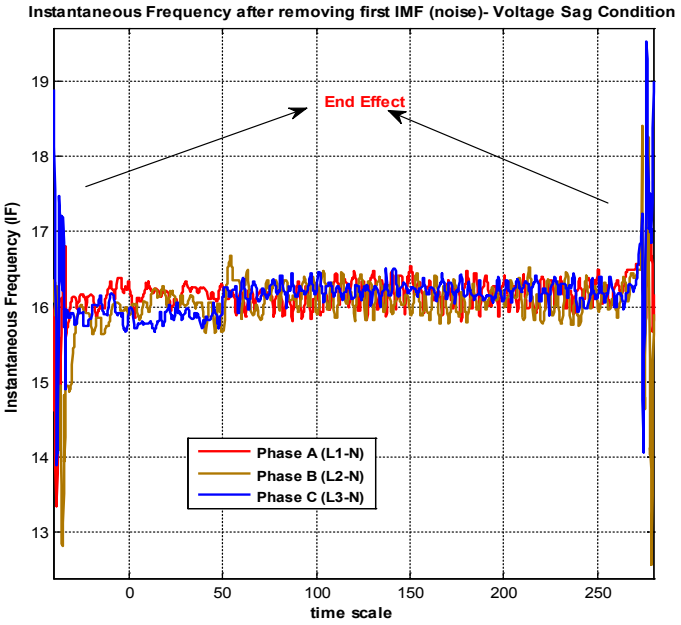

Fig. 12. IF corresponding to remove first imfs voltage sag condition of signal

IF signal can use for separation for two cases but there is end effect problem that have to be solved. This is another future work of the study. When cubic spline fitting is computationally demanding, generates distortions near the end points. This is a technical problem that causes data

failures and peaks at the beginning and at the end of the signal. This fault will be investigated on HHT (Fig. 10. - 11.).

C. Feature Selection

For diagnosis of disturbances, extracted features are produced from firstly EEMD method so as to classify the voltage sags in grid. After reconstruction signal without noisy part, first imf pre-processing stage. Second stage IA and IF) are generated by means of HHT. The statistical analysis and classification for identification power quality disturbances. The following features were extracted: mean, standard deviation, skewness of IA and IF. Selecting appropriate features of voltage sag events are highly crucial for diagnosis of the disturbance. The primary schematic model consists of four steps as shown in Fig. 13.

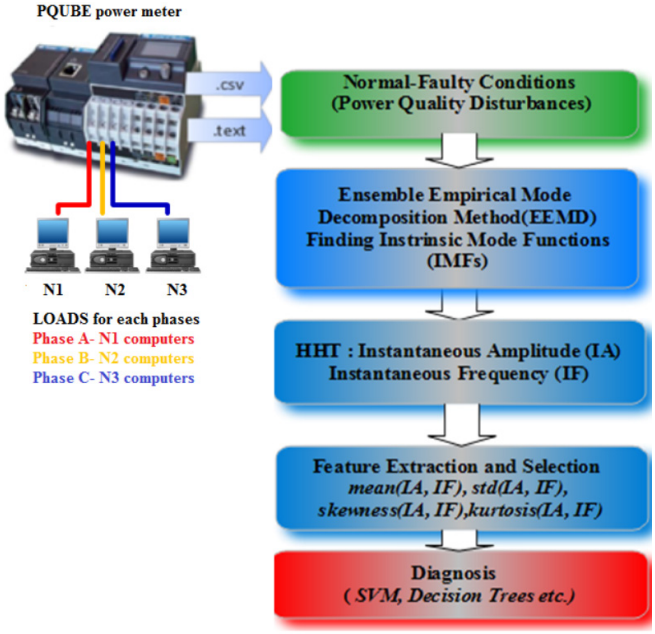

Fig. 13. Schematic model of identification of PQ disturbance

IV. PQ DISTURBANCES CLASSIFICATION TECHNIQUES

A. Support vector machine

Support Vector Machine (SVM) methods, which are developed by Vapnik, whereby statistical learning technique being the basis contributes a novel machine learning method. SVMs are linked supervised learning methods used for classification and regression [20, 21, 25, 28].

B. Decision Trees

Decision trees are methods that utilize divide-and-conquer approaches as structure learning by induction [22, 23]. The C4.5 algorithm was developed by Qinlan, contains the generation of a tree whereby a training set, finding the information gain criterion to find the finest attribute/feature to be used at each node. Furthermore, the algorithm applies the post pruning approach to diminish the size of the tree and prohibit over fitting. C4.5 is a technique for approximating discrete-valued functions that is powerful tool to noisy data and suitable for learning distinctive statements [23, 24, 25, 26, 27, 28].

V. PERFORMANCES OF CLASSIFICATION ALGORITHMS AND DISCUSSIONS

To figure out the performance of the proposed power quality classification algorithm, a total number of 30 PQube Analyzer real time disturbances data were used. The PQ signals are divided into two categories; 20 of them were used for training and 10 of them were used for testing the proposed algorithm with shuffling the data.

In the light of Table III., it is concluded that for sigmoid kernel degree 0.01 with dimensionality reduction with Singular Value Decomposition (SVD) described in [29] is better result in terms of CPU time (3.56 sec), and for polynomial kernel d=3, is also better result CPU time (3.58) in non linear classification SVM. Decision Tree algorithm has the precision of 100% and CPU time of 4.10 sec. Eventually, C4.5 Decision tree based method is the best and gives more proper outcomes than the SVM technique without SVD. (Note: the most proper and robust classifiers for each data set are showed by Red font in Table III).

TABLE III

PERFORMANCES OF DISTURBANCE DIAGNOSE ALGORITHMS

Classifier	Precision	Time (sec)
SVM-Linear	50%	2.35
SVM-poly d=2	100%	3.75
SVM-poly d=2 preprocessing SVD (r=2)	100%	3.59
SVM-poly d=3	90%	1.91
SVM-poly d=3 preprocessing SVD (r=3)	100%	3.58
SVM-poly d=3 preprocessing SVD (r=2)	60%	1.06
SVM-RBF sigma =0.01	50%	0.36
SVM-RBF sigma =0.01 preprocessing SVD (r=3)	**100%**	**3.56**
SVM-RBF sigma =1	50%	0.40
SVM-RBF sigma =1 preprocessing SVD (r=3)	50%	0.36
DecisionTree C4.5	**100%**	**4.10**
DecisionTree C4.5 preprocessing SVD (r=3)	**100%**	**4.0606**

VI. CONCLUSION

In this real time analysis, EEMD-HHT signal processing system was used for generation features of different characteristics IA and IF for normal condition and voltage sag

cases. The technique reported in this study clearly accomplishes generation of features different for normal – voltage sag cases aiming that identification of smart grid faults. Simulations results have illustrated the capability and validity of the HHT. This study shows that the proposed approach can be easily used for detecting electromagnetic interference on non-stationary signals. Results of the experiments will be conduct for relation on three phases between computer numbers and voltage disturbances for future studies. In PQ Diagnosis part of the study, SVM and Decision Tree (C4.5) were operated and their results were match for precision and CPU time. In consequence of precision and timing criteria, without dimensionality reduction with SVD, SVM-RBF (sigma =0.01) algorithm presented the best solution. Results from the simulations clarify that the proposed method is effective in detecting non-stationary PQ signal. For analyzing the real time power quality disturbance signals and classifying them, Matlab ™ Toolboxes are used for simulations.

ACKNOWLEDGEMENT

This scientific study is supported by TUBITAK. (Project Number: 114E919)

REFERENCES

[1] J. Momoh, "Smart Grid: Fundamentals of Design and Analysis", First Edition, Institute of Electrical and Electronics Engineers, 2012.

[2] R. Smolenski, "Conducted Electromagnetic Interference (EMI) in Smart Grids", Springer -Verlag London, 2012.

[3] S. Borlase "Smart Grids: Infrastructure, Technology, and Solutions" , CRC press, 2012.

[4] Report to NIST on the Smart Grids Interoperability Standarts Roadmap, EPRI, 2009.

[5] M. H. J. Bollen and I. Y. H. Guo, "Signal Processing of Power Quality Disturbances", New York: Wiley, 2006.

[6] P. F. Ribeiro, C.A. Duque, P. M. Silveria, and A. S. Cerqueira, " Power Systems Signal Processing for Smart Grids". Chichester, UK: John Wiley & Sons, Inc., 2013.

[7] A. McEachern, "Practical Power Quality: An Update, Large Customer Conference", Power Standards Lab, November 25, 2015.

[8] K.-M. Chang,"Arrhythmia ECG Noise Reduction by Ensemble Empirical Mode Decomposition", *Sensors*, *10*, 2010, pp. 6063 - 6080.

[9] N.E. Huang, Z. Shen., S.R. Long, M.L. Wu, H.H. Shih, Q. Zheng, N.C. Yen, C.C. Tung, H.H. Liu, "The empirical mode decomposition and Hilbert spectrum for nonlinear and non-stationary time series analysis", Proc. Roy. Soc. London A, Vol. 454, 1998, pp. 903–995.

[10]Z. Wu, N.E. Huang, "A study of the characteristics of white noise using the Empirical Mode Decomposition method," Proc. Roy. Soc. London A, 2002.

[11] S. Baykut, T. Akgül, S. Ergintav, "EMD – Based Analysis and Denoising of GPS Data", IEEE 17th Signal Processing and Communications Applications Conference, Antalya, 2009.

[12] T.Yalcin, O.Ozgonenel, "Feature vector extraction by using empirical mode decomposition from power quality disturbances", IEEE SIU, Fethiye, Mugla, 2012.

[13] O.Ozgonenel, T. Yalcin, I. Guney, U. Kurt, "A New Classification for Power Quality Events in Distribution System", Electric Power System Research (EPSR), 95, 2013, pp. 192-199.

[14] Z.Wu, N.E. Huang, "Ensemble empirical mode decomposition: a noise-assisted data analysis method", *Adv. Adapt. Data. Anal.*, 1, 2009, pp.1–41.

[15] Z. Wang, Q. Zhu, J. Kiely, R. Luxton, "Hilbert Huang transform impedance measurement data for cellular toxicity monitoring" International Conference on Networking, Sensing and Control, 2009, pp. 767-772.

[16] M. Uyar, S.Yildirim, M.T. Gencoglu, "An effective wavelet-based feature extraction method for classification of power quality disturbance signals", Electr. Power Syst. Res, 78, (10), 2008, pp. 1747–1755.

[17] T. Nguyen, Y. Liao, "Power quality disturbance classification utilizing S-transform and binary feature matrix method", Electr. Power Syst. Res., 79, (4), 2009, pp. 569–575

[18] C.N. Bhende, S. Mishra, B.K. Panigrahi, "Detection and classification of power quality disturbances using S-transform and modular neural network", Electr. Power Syst. Res., 78, (1), 2008, pp. 122 –128.

[19] S. Suja, , J. Jerome, "Pattern recognition of power signal disturbances using S transform and TT transform", Int. J. Power Energy Syst., 32, (1), 2010, pp. 37–53.

[20] B. Biswal, PK. Dash, S. Mishra, "A hybrid ant colony optimization technique for power signal pattern classification", Expert Syst Appl,38, 2011, pp. 6368–75.

[21] K. K. Hoong, S. P. Lam, C. Y. Chung. "An output regulation based unified power quality conditioner with Kalman filters.", IEEE Trans Ind Electron, 59 (November (11)), 2012, pp. 4248–62.

[22] I. H.Witten, E. Frank, "*Data Mining: Pratical Machine Learning Tools and Techniques*.", San Mateo, CA, USA: Morgan Kaufmann, 2005.

[23] M. T. Hagan, M. B. Menhaj, "Training feedforward networks with the Marquardt algorithm," *IEEE Trans. Neural Netw.*, , Nov., vol. 5, no. 6, 1994, pp. 989– 993.

[24] R. J. Quinlan, "*C4.5: Programs for Machine Learning"*, San Mateo, CA, USA, Morgan Kaufmann, vol. 1, 1993.

[25] S.Mishra, T. Nagwani, "A Review on Detection and Classification Methods for Power Quality Disturbances", International Journal of Engineering Science and Computing, Volume 6, Issue No. 3, 2016.

[26] F. A. S. Borges, R. A. S. Fernandes, I. N. Silva, C. B. S. Silva, "Feature Extraction and Power Quality Disturbances Classification Using Smart Meters Signals", IEEE Transactions on Industrial Informatics, Vol. 12, No. 2, 2016.

[27] Ozgonenel O., Thomas D. W. P., Yalcin T., "Superiority of decision tree classifier on complicated cases for power system protection" , 11th International Conference on Developments in Power Systems Protection, Birmingham, UK, 2012, pp. 134–134.

[28] Mahela O. P. , Shaik A. G. , Gupta N., "A critical review of detection and classification of power quality events", Renewable and Sustainable Energy Reviews, Volume 41, 2015, pp. 495–505.

[29] B. Schölkopf, A. Smola, K. Müller, "Nonlinear component analysis as a kernel eigenvalue problem", Neural Computation, 10, 1998, pp. 1299–1319.

Turgay Yalçın received the B.Sc. Erciyes University (EU), Kayseri, Turkey in 2006 and M.Sc. degrees in electrical engineering from Ondokuz Mayıs University (OMU), Samsun, Turkey, in 2010 and he is currently pursuing the Ph.D. degree in electrical engineering from Ondokuz Mayıs University (OMU).

Currently, he is an research assistant with the Department of Electrical and Electronics Engineering, Ondokuz Mayıs University (OMU), Samsun, Turkey from 2007. His areas of interest are Identification of Power Quality Disturbances, Signal Processing Methods and Machine Learning Algorithms.

Muammer Özdemir received the B.Sc. and M.Sc. degrees in electrical engineering from Black Sea Technical University (KTÜ), Trabzon, Turkey, in 1988 and 1991, respectively, and the Ph.D. degree in electrical engineering from The University of Texas at Austin (UT), Austin, TX, USA, in 2002.

Currently, he is an Assistant Professor with the Department of Electrical and Electronics Engineering, Ondokuz Mayıs University (OMU), Samsun, Turkey. His areas of interest are power systems harmonics, power quality, and power system analysis.

Optimizing Signal Behavior of Femtocells for Improved Network

O. A. Akinlabi and Meera K. Joseph, University of Johannesburg, South Africa

***Abstract*— The high demand for network coverage in an indoor setting brought about the acceptance of femtocell technology as a solution using the backhaul connectivity in the existing network. The quality of signal, voice calling, Internet, security and data are improved through the use femtocell at the indoor environment. Here the service provider attempts to reduce their operation cost by presenting self-organizing mechanisms for optimization of the network. The remarkable part is that, femtocells improves coverage, enhances the data rate at the indoor environment. Therefore, the challenges of the femtocell also known as interference deteriorates the capacity and quality performance of the whole cellular network. In this paper we simulate the bit error rate against signal behaviour at the indoor environment and we also simulate the transmitting power over signal for both macrocells and femtocells. We focus on the transmitting power that might cause interference within the cellular network.**

***Index Terms*— Femtocells, Macrocells, Signal behavior, Transmitting Power.**

I. Introduction

Most users of mobile network demand a quality performance of service such as voice calling, data, Internet and better signal within an indoor environment. The failure of macrocell in order to achieve the above mentioned has brought about femtocell technology. However, the deployment of femtocell has drawn the attention of researchers, academics and experts in telecommunication industry over macrocell for improved coverage and security purposes.

Thus, mobile network has become one of the daily use of the human race, such as Internet, educational resource for learners, social media, advertising and business purposes. These mobile network supports voice calling and reduced the need for travel. Though the signal experience poor reception, and alteration of calls because of the high demand of number of Macro base station site from the service providers cannot be met due to the cost of operation.

A study was carried out by the Femtoforum that confirmed an increase in voice calling and data used in an indoor environment [1]. The deployment of femtocell technology is favorable over macrocell at the indoor environment for coverage and system capacity in a low cost manner. Femtocells focuses on the quality of voice calling, data and improved signal coverage in an indoor environment for all mobile users.

In line with [1], femtocell guarantees improved coverage, capacity over the Internet backhaul with full operating capacity under the licensed spectrum at a low price for the end users. Femtocells are small base station in an indoor environment, set up by the end user and connected through the Internet, access to the mobile provide [2]-[6].

Thus femtocell supports at least four to five users at the indoor environment and is applied to residential, enterprise, hot spot and metro. The values of communication such as voice calling over networks, quality of service are linked to economic stability a country. The significance of femtocells in mobile network is that it enhance quality service and improve coverage network. Figure 1, illustrates the application of femtocell in a home setting and connections to the mobile provider through the broadband access.

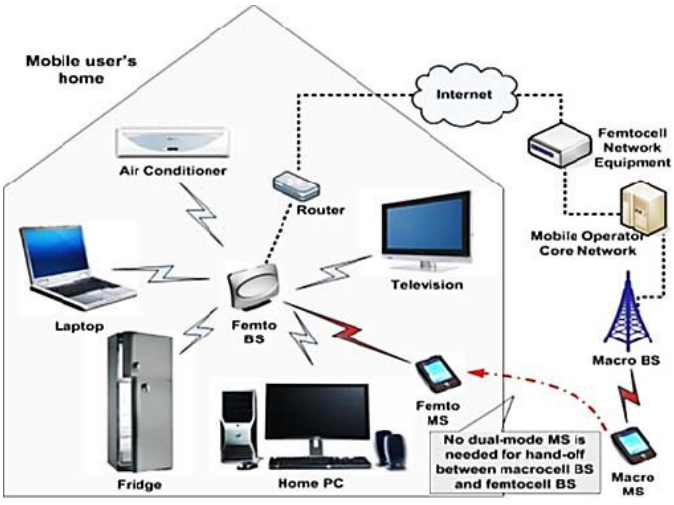

Fig. 1: Femtocell in a home setting [7]

This manuscript was submitted in July 21, 2016 for review, accepted on 15 October 2016. This work was supported in part by the University of Johannesburg, Johannesburg, South Africa. Department of Electrical and Electronic Engineering Sciences.

O. A. Akinlabi is a doctoral student at the Department of Electrical and Electronic Engineering Science, University of Johannesburg, Johannesburg, South Africa, SA (e-mail: akinlabiakindeji@gmail.com).

Dr. Meera K. Joseph, is Senior Lecturer, at the School of Electrical Engineering, University of Johannesburg, Johannesburg, South Africa and she leads the ICT4D research group (e-mail: meeraj@uj.ac.za).

The value of femtocell has contributed to the fast growth of economies and increase in mobile revenue for service providers. The market report launch by Femtoforum on femtocell has shown that it increases mobile revenue [1]. In fact, it cuts down operational cost, infrastructure and maintenance cost for mobile provide. More so, it performs certain functions of which macrocell may not perform such as it guaranteed good connectivity, home security, remote control of home appliance and quality of voice experience.

Apart of all this, it lessens the traffic load over macrocell and increase the performance of the mobile provider. Femtocell utilised the broadband for connection through the existing macrocell network for quality of voice calling, media and video streaming in which this cannot cause any problem when the provider of such broadband differs. The problem arises when they are using the same license band for the same purpose. The technical challenge is caused due to the use of the same licensed band with the existing spectrum of macrocell and ad hoc deployment of femtocell which led to interference management. But they are needed for mobile to deploy femtocell successfully for improved coverage at the indoor environment at low cost. However, the deployment of femtocells, still provides a better coverage in the network

The network traffic grew widely over the last decade due to the profitable rate flat launch by Femtoforum [1], and such request should be met by new mobile communication systems, as well as increasing the revenue. Hence, the achievement of the wireless network will depend on the providing a broadband access for mobile user, where costs per bit error rate are low [8].

Often, mobile traffic is highly demanding in homes and office environment and according to [9], more than 80% of the mobile traffic is used in an indoor environment. The new technology will offer solution for home and office, where there will be an improved reception of signals in an indoor and these promotes cost effective for the network users. The target of service provider is to satisfy the need for the high demand of mobile data in an indoor environment and also to offer an added value able service.

Mobile operator benefits mostly from these new technology known as femtocell in such a way that the operator has enough saving on coverage and profit, no more electricity bills and no time wasting on problems. Finally, it provides broadband access point in order for a connection with a satellite backhaul, for instance, inside an airplane, complex, shopping mall, train and warship respectively. These access points are modelled to be linked to the business model.

This paper is organized as follows. Related work on interference in femtocell section II. Femtocell over macrocell were explained in section III. In section IV, brief notes on the problem statement. The notation and system analysis were discussed in section V. Results based on simulations as carried out in section VI. The conclusions are drawn in VII.

II. RELATED WORK ON INTERFERENCE IN FEMTOCELL

The related work centered on the deployment of femtocell technology and interference as a main challenge in order to achieve the desired quality of service, good voice calling and network coverage in an indoor environment. Femtocell deployment used to achieve good connectivity to mobile users and improvement of signal behavior in an indoor environment.

The approach in [7] has practical problems due to the architecture networks constrained by number of height of radio and power emission antenna. It is more difficult to analyse the system topologies with feasible transmitter location and to find out the optimal network.

The work in [8] [9] [10] aims the optimal transmitter antenna configuration. Siomina *et al.* [11], offers a simulated annealing due to the central algorithm used in optimizing the channel level of the power and antenna angle. The Universal Mobile Telecommunications System (UMTS) networks in such a manner that the total channel level of the power is brought down.

As pointed out in [7], Fagen *et al.* carried out an algorithm that is capable to count on for the ability stage of each cell in the network in parliamentary procedure to maximize the area coverage as well as mitigate interference within a desired signal in the coverage area. In [12] the optimization of femtocell network is performed under interference in an indoor coverage using power scheme to mitigate the cause of interference among femtocell BSs is presented.

Another proposed scheme in [13] and [14], whereby a distributed utility is offered based on the SINR method at the Femtocell Access Point (FAP). FAP sets up connections to the core network over the subscriber's broadband connection and end users can enjoy improved network capacity. With the above mentioned method they provide a better output and an error estimation of SINR and intricacy of implementing the algorithm for the strength of the network.

The decentralized approach strategies that allow the Femtocell Access Point's to sense the channel and self-organize, in conditions of resource allocation and the topology of the network systems, this give a framework on game theory approach to design decentralized mechanisms for optimization and resource allocation among each femtocell user. Recently, game theory has been employed as a powerful too, which is used for the systematic analyses of the resource allocation strategies among the radio nodes [11] have been proposed for cognitive radio.

The work presented in [20] focus on the signal strength of the deployment of femtocell over macrocell where they are poor reception of signals for indoor users. It proved that the signal of the femtocell is improved over macrocell but the limitation of the study is that it does not emphasis on the transmitting

power to avoid interference that reduces the functioning capacity of femtocell technology.

III. FEMTOCELL OVER MACROCELL

Thus, femtocell technology aimed is to cognitive abilities for the purpose of mobile communication, traffic loading, capacity, and coverage optimization over others mobile cellular network at the indoor [2]. Wi-Fi network is generally applicable mostly to all cellular service providers due to the strength of the signal, but the femtocell technology is much better off in terms of improved signal strength, security purpose, and voice calling service at home or office environment. However, the received signal strength gets improved due to the functionality of femtocell technology as a base station in an indoor environment. A macrocell transmit in a wide range with high transmission power that cover up to about 20miles radius due to a base station.

NO.	Table 1: Femtocell and other cellular networks		
	Table column subhead	*Femtocell*	*Macrocell*
1	Data Rate	45Mbps	Non
2	Installation	Customer	Operator
3	Rent of Site	No Site Rentage	Rentage of Site
4	Operating Frequency	2,6GHz	5GHz
5	Power Ranges	10dBm	25dBm
5	Primary Service	Quality of voice calling, Multi-media, Video and security	Data and voice calling

In table 1, we provide the dissimilarity between both technologies used for communication transmission [13]. In order to mitigate interference femtocell must transmit at a lower power. What really distinguished femtocell technology is the valued added service introduced by the mobile provider for end users at the home or office environment. It is a service that a mobile provider is always enthusiastic to integrate as much as possible.

IV. PROBLEM STATEMENT

Femtocell technology has immensely improved signal strength of the mobile network, but there are challenges that need to be controlled by the mobile provider due to the fact that it shares the same spectrum with the existing network. There are two cases of interference in two tier architecture networks such as co-tier and cross-tier interference. Mostly this is caused by unwanted transmitting signal within the frequency band, which gives rise to interference. Hence, the absence of interference mitigation will interfere in the quality of femtocell deployment within the network. Other challenges that faced deployment of femtocell were mobility movement and handover, self-organization, access mode and synchronization and timing etc. Our focus is on interference which is caused by the high transmitting power of Femtocell Access Point of the users. This should be the main concern for the mobile operators.

V. NOTATION AND SYSTEM ANALYSIS

Here we present the system notation, and parameter for network performance results. Our primary concern is to achieve an improved signal and quality of service. The estimation of SINR [14] is highly important, which is expressed as (1):

$$Sinr = \frac{g_{fbs} p_{fbs}}{\sigma + \sum p_{fbs} + \sum p_{mbs}} \qquad (1)$$

p_{fbs} ……Transmitting power of the femto base station

p_{mbs} …… Transmitting power of the macrocell base station

g_{fbs} …… Channel gain

σ …….. Noise.

In this paper, we used the path loss model [15]. These path loss models are approximations of the instability of signal behavior in an indoor environment. Therefore, the path loss is given [15] in the equation (2):

$$\begin{aligned} PL(dB) &= \max(15.3 + 37.6 Log_{10}(d)), 38.4 \\ &+ 20 Log_{10}(d) + 0.7 d_{2D,indoor} \\ &+ 18.3 n^{\left(\frac{n+2}{n+1}\right) - 0.46} + qL_{iw} + L_{ow1} + qL_{ow2} \end{aligned} \qquad (2)$$

Where, *PL* is the path loss model

n ---- Number of penetration floors

q ---- Number of walls in the flats

L_{iw} ------ Penetration Loss of the wall that different the apartment

$0.7 d_{2D,indoor}$ ------ Penetration Loss by the walls inside the flats

d ----- Distance between transmitter and receiver in meter

L_{ow} --------- Penetration Loss of outdoor wall

L_{ow} and L_{iw} are set to 20dB and 5dB respectively.

Then, we presumed that the capacity saved as the network throughput [16], mathematically it is given as (3):

$$T = \beta \log_2(1 + \sin r) \qquad (3)$$

Where T is the throughput and sinr is the signal. Here, a number of femtocells are selected to be used in the indoor environment with equal service provider in this area and one outdoor macrocell. Each femtocell act well as defined in the experiment, the parameters for the system analysis are shown in Table 2 and some of the above equations as presented in [20].

Nos	Table 2: Simulators Parameters	
1	Parameters	Values
2	Scenario size	350x350
3	Macrocell Base station	1
4	Femtocell as a Base Station	1
5	Bandwidth	5MHz
6	Noise	-174dBm/Hz
7	Macro Tx Power	43dBm
8	Femto Tx Power	10dBm

The system simulation uses MATLAB as a model of operation to analysis the signal behavior of femtocell over macrocell in an indoor environment. The real life network model takes a series of events to achieve the main objective of the goal of the application of a femtocell.

VI. RESULTS

In this section, we observed the simulation results of deployment of femtocell for improved signal and quality of voice calling. We consider the parameters and equation in section V. The simulation results prove the signal of both femto cells and macro cells in a cellular network for better performance in an indoor environment.

Based on the result, figure 4 illustrates the deployment of femtocell in the residential area. Here we indicate the randomness of femtocell in a network, while the colors indicate subscriber and nonsubscriber of femtocell network. Here, the FAP is randomly scattered around the area.

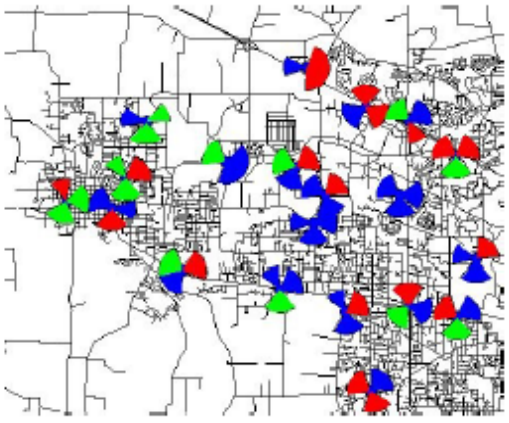

Fig 4: Deployment of femtocell network in residential area

With the simulation result shown in figure 5, bit error rate against the signal. We considered the bit error rate at the indoor environment, this is the major parameter in data transmission and communication system. From the result, we observed that the bit error rate is low and this promotes voice calling. The system throughput is obtained by a reduction of bit error rate.

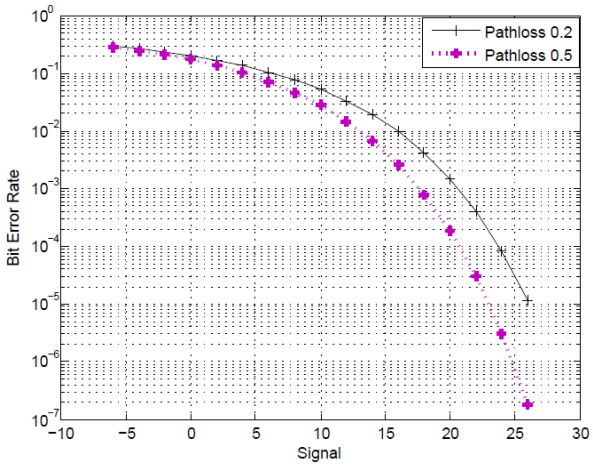

Fig. 5: Relationship between BER against the signal

In figure 6 we illustrate the throughput of both femtocell and macrocell against signal in order achieve a better signal strength at the indoor environment. With the results it was observed that the throughput of femtocell improved coverage in an indoor environment which promotes quality of service, performance for femtocell user.

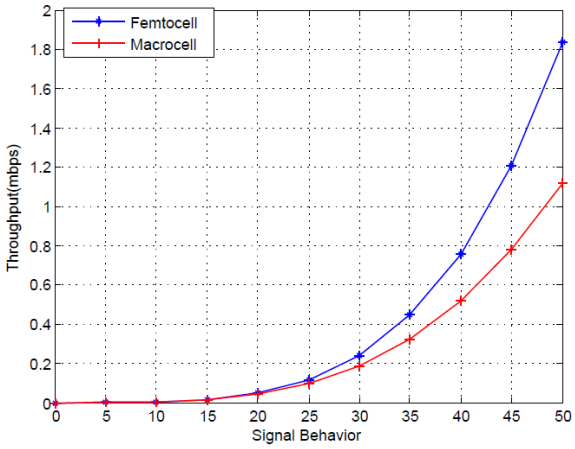

Fig 6: Signal behavior of femtocell over macrocells in an indoor environment

Although similar simulations as in Figure 5 and Figure 6 were presented in [20], in this paper we also illustrate the iteration of transmitting power against a signal behavior for both femtocell and macrocell as illustrated in Figure 7. This enables us to benchmark the transmitting power of both femtocell and macrocell in order to access an improved signal. Thus, this also shows that the power consumption is low compared to the macrocell. However, the measures for excellent performance, and quality signal, that can be used as a benchmark for femtocell deployment.

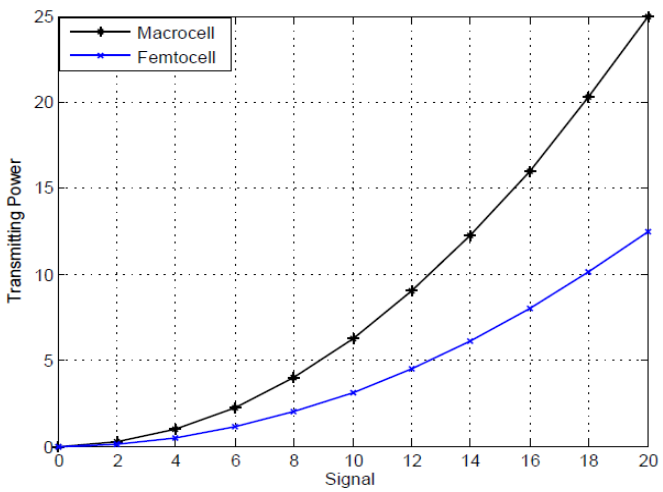

Fig 7: Iteration of transmitting power over signal behavior

VII. CONCLUSIONS

In the past, macrocell have been the only means used for communication, data, media and many more at the indoor and outdoor environment. But due to poor reception of signals at the indoor environment femtocell was introduced. However, it has improved the reception of signals, particularly places like urban and rural environment.

It is observed that the signal performance is achieved through the deployment of femtocell technology over macrocells. The deployment of femtocells over the existing macrocell has brought efficiency and profitable solution for mobile operators. However, the cost implication of femtocell is much less than building a macrocell site, paying rent and electricity bills which is undertaken by the mobile provider. Thus, Femtocell has attracted the attention of service providers due to the valuable service and decrease of related energy consumption. Femtocells utilize the broadband connection which may be used for other applications such as video streaming. There can be associated problems when the provider of the broadband service differs from the mobile network provider. There will be cost drawbacks considering the installation in certain residential areas.

The performance capacity is attained since of the femtocell served as the Base Station (BSs) to the users in an indoor environment. The deployment of femtocell will continue to play a vital role in the market for mobile operator's network. Further work will be that of cost function implementation over power transmitting for all Femto users in the cellular network. This will allow to reduce interference within the users since the transmitting power is bench on 10-15dB for better signal used.

REFERENCES

[1] Femtocell forum http:// www.femtoforum.org.com Accessed 20 October 2015

[2] 3GPP work items on Self-Organizing Networks. (Accessed 15 August 2015). [Online]. Available: http://www.3gpp.org/ftp/Information

[3]] D. L. Perez, G. D. la Roche, A. Valcarce, A. Juttner, and J. Zhang, "Interference avoidance and dynamic frequency planning for WiMAX femtocells networks," 11th IEEE Singapore International Conference on Communication Systems, pp. 1579–1584, 19-21 Nov. 2008.

[4] M. Yavuz, F. Meshkati, S. Nanda, A. Pokhariyal, N. Johnson, B. Roghothaman, and A. Richardson, "Interference management and performance analysis of umts/hspa+ femtocells," IEEE Commun. Mag., vol. 47, no. 9, pp. 102–109, Sep. 2009.

[5] H. Claussen, "Performance of macro and co channel femtocells in a hierarchical cell structure," IEEE 18th International Symposium on Personal, Indoor and Mobile Radio Communications, pp. 1–5, 3-7 Sep. 2007.

[6] R. Baines, "The need for WiMAX Pico cell and femtocells," WiMax London, pp. 1–36, 25-26 April 2007.

[7] Femtocell Base Station compared to Macrocell Base Station:Available online http://www.analog.com/library/analogdialogue/archives/42-12/AD42_12_FIG-01.jpg

[8] T. Giles, J. Markendahl, J. Zander, P. Zetterberg, P. Karlsson, G. Malmgren, J. Nilsson, " Cost drivers and deployment scenarios for future broadband wireless networks- key research problems and directions for research" IEEE 59th Vehicular Technol. Conference, VTC 2004- Spring 4, 2042-2046 (2004) 17-19 May 2004, Milan (Italy).

[9] Fagen, P.A. Vicharelli, J. Weitzen, "AutomatedWireless Coverage Optimization With Controlled Overlap," *IEEE Transactions on VehicularTechnology*, vol. 57, no. 4, pp. 2395–2403, Jul 2008.

[10] Y. Sun, F. Gunnarsson, K. Hiltunen, "CPICH Power Settings in Irregular WCDMA Macro Cellular Networks," in *Proc. PIMRC*, Beijing, China, Sep 2003, pp. 1176–1180.

[11] M. Garcia-Lozano, S. Ruiz, J.J. Olmos, "UMTS Optimum Cell Load Balancing for Inhomogeneous Traffic Patterns," in *Proc. IEEE VTC*, Los Angeles, CA, USA, Sep 2004, pp. 909–913.

[12] K. Valkealahti, A. H¨oglund, J. Parkkinen, A. Hamalainen, "WCDMA Common Pilot Power Control for Load and Coverage Balancing," in *Proc. PIMRC*, Lisbon, Portugal, Sep 2002, pp. 1412–1416.

[13] I. Siomina, P. V¨arbrand, D. Yuan, "Automated Optimization of Service Coverage and Base Station Antenna Configuration in UMTS Networks," *IEEE Wireless Communications*, vol. 13, no. 6, pp. 16–25, Dec 2006.

[14] Kwanghun Han, Youngkyu Choi, Dongmyoung Kim, Minsoo Na, Sunghyun Choi, Kiyoung Han, "Optimization of femtocell network configuration under interference constraints," *7th International Symposium on Modelling and Optimization in Mobile, Ad Hoc, and Wireless Networks,* pp. 1-7, 23-27 Jun. 2009.

[15] V. Chandrasekhar, J.G. Andrews, T. Muharemovic, Zukang Shen, A. Gatherer, "Power control n two-tier femtocell networks," , *IEEE Transactions on Wireless Communications*, vol. 8, no. 8, pp. 4316-4328, Aug. 2009.

[16] V. Chandrasekhar, J.G. Andrews, S. Zukang, T. Muharemovic, A. Gatherer, "Distributed Power Control in Femtocell-Underlay Cellular Networks," *IEEE Global Telecommunications Conference,* pp.1-6, Nov. 30-Dec. 4 2009.

[17] D Lo´pez-Pe´rez, A Valcarce, A´ kos Lada´nyi, G de la Roche, and J Zhang, "Femtocell versus Wi-Fi: A Survey and Comparison of Architecture and Performance", IEEE Wireless Communications, Vol. pp no. 916-920, 2009. 13

[18] P. Lee, T. Lee, J. Jeong, and J. Shin, "Interference Management in Lte Femtocell Systems Using Fractional Frequency Reuse," in Advanced Communication Technology (ICACT), 2010 The 12th International Conference on, vol. 2, Feb. 2010, pp. 1047 –1051.

[19] B. S. L. Castro, I. R. Gomes, F. C. J. Ribeiro, G. P. S. Cavalcarite, "COST231-Hatta and SUI Models Performance using a LMS Tuning Algorithm on 5.86Hz in Amazon Region Cities" Proc. Of IEEE. EUCAP-2010. ISBN: 978-847653-472-4, pp. 1-3, Jul. 2010.

[20] O.A. Akinlabi, M.K. Joseph "Signal behaviour in an indoor environment; Femtocell over Macrocell" 16th IEEE International Conference on Environment and Electrical Engineering, pp, 7-10 June 2016. Florence, Italy.

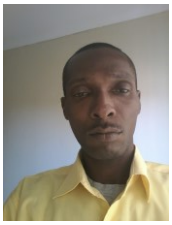

Akinlabi Olaniyi Akindeji was born in Surulere, Lagos State, Nigeria, and West Africa country in 1978. He received the B.Tech in Electrical and Electronic Engineering from Rivers State Polytechnic, Rivers state, Nigeria and his M.Tech. Degree in Electrical Engineering from the University of Johannesburg (UJ) in 2014. The author become a member of SAIEE in 2013. He is currently enrolled for DPhil Electrical and Electronic Engineering at UJ. For academic excellence, he has the best paper award from IMECS 2014. He has many research papers to his credit already. His research interest focuses on Information and Communications Technology and power distribution and generation and femtocells.

Meera K. Joseph received the degrees of DPhil. Engineering Management from the University of Johannesburg (UJ) in 2013, and M.C.A in 1997 from the Bangalore University. She works as a Senior Lecturer at UJ and is a Professional Member of IITPSA. Many post graduate students completed under her supervision and she has many IEEE international conference papers, Journal papers and book chapters to her credit. She runs the ICT4D research group in the School of Electrical, UJ. Her research interests include Information and Communication Technology for Development (ICT4D), smart grids, Femtocells, cloud computing and wireless networks.

A Methodology for Long-Term Analysis of Innovative Signalling Systems on Regional Rail Lines

Luca D'Acierno, Marilisa Botte, Claudia Di Salvo, Chiara Caropreso, and Bruno Montella

***Abstract*—A rail system may be considered a useful tool for reducing vehicular flows on a road system (i.e. cars and trucks), especially in high-density contexts such as urban and metropolitan areas where greenhouse gas emissions need to be abated. In particular, since travellers maximise their own utility, variations in mobility choices can be induced only by significantly improving the level-of-service of public transport. Our specific proposal is to identify the economic and environmental effects of implementing an innovative signalling system (which would reduce passenger waiting times) by performing a cost-benefit analysis based on a feasibility threshold approach. Hence, it is necessary to calculate long-term benefits and compare them with intervention costs. In this context, a key factor to be considered is travel demand estimation in current and future conditions. This approach was tested on a regional rail line in southern Italy to show the feasibility and utility of the proposed methodology.**

***Index Terms*—Microscopic rail system simulation, operational cost definition, public transport management, signalling system, travel demand estimation.**

I. Introduction

ACCORDING to the European Commission [1], 23.2% of greenhouse gas emissions in 2014 were produced by the transport sector, of which road transport accounted for 72.8%. The development of actions to promote sustainable transportation systems and to reduce vehicular flows on the road system (i.e. cars and trucks) could therefore significantly abate the sector's emission contributions.

In this context, adoption of a public transport system based on the use of a rail technology which makes railways the high-performing mobility backbone represents a sound choice: besides being environmental friendly, rail systems are high-performing (high travel speeds and low headways), competitive (lower unit costs per seat-km or carried passenger-km) and they are able to ensure a high degree of safety thanks to the presence of signalling, control and train protection systems.

Obviously, the attractiveness of public transport can be enhanced only by improving service quality and minimising user discomfort. Indeed, since according to the assumptions of rational decision-maker each user tends to choose the alternative of maximum utility (i.e. minimum disutility), the goal is to minimise user generalised costs, which represent the weighted sum of times and monetary costs spent by passengers during their trips. Such costs may be split into: access and egress times, waiting times, travel times, transfer times and ticket costs.

The measures for reducing user generalised cost may be classified according to three main categories: infrastructural measures (new lines or modification of existing lines), fleet improvement (partial or complete replacement of rolling stock) and signalling system modification (replacement or upgrade of trackside and on-board equipment).

Obviously, each kind of intervention affects a specific component of the user generalised cost. Indeed, under the assumption that timetables and all public transport services are integrated and optimised:

- access and egress times depend on the location of stops and stations;
- waiting times depend on the headway between two successive convoys allowed by the travel speed and signalling system adopted;
- travel times depend on rolling stock performance and infrastructure characteristics;
- transfer times depend on the layout of stations, platforms and rolling stock;
- ticket costs depend on pricing policies adopted by administrations.

Clearly, an infrastructural intervention requires high funding availability and may be unfeasible in densely populated contexts. However, in certain cases, it could be essential.

Likewise, the adoption of policies based on replacing existing fleets or reducing fare levels entails increases in national or regional subsidies, which would be difficult to

This paper was partly supported under research project FERSAT grant no. PON03PE_00159_4 (Italian Ministry of Education, Universities and Research).

L. D'Acierno (corresponding author), M. Botte, C. Caropreso and B. Montella are with the Department of Civil, Architectural and Environmental Engineering, Federico II University of Naples, via Claudio 21, Naples, 80125 Italy (email: luca.dacierno@unina.it; marilisa.botte@unina.it; chiara.caropreso@yahoo.it; bruno.montella@unina.it).

C. Di Salvo is with GE Oil&Gas, via Cassano 77, Casavatore (Naples), 80020 Italy (email: claudia.disalvo@ge.com).

achieve in the current economic climate.

Hence the interventions on which to focus concern implementation of innovative signalling systems whose effect is an increase in service frequencies of a rail system and a consequent reduction in passenger waiting times. Moreover, such measures have been made very topical by recent European Union policy whose aim is to create a single European standard for rail networks.

The necessity of the presence of a signalling system lies in the fact that, since the friction between a train wheel (made of steel) and a rail track (also made of steel) imposes stopping distances of several hundred metres (sometimes kilometres), a system solely based on driver visibility is impossible to create. In particular, the safety of a rail system is based on two main aspects: spacing between convoys and train integrity. The former consists in technologically imposing, by means of a signalling system, a minimum distance between two successive trains so that, in the case of the first train slowing or stopping, the following train is able to react and stop safely. The latter consists in verifying the completeness of the train composition while it is in operation.

There are several types of signalling systems currently in use. However, as mentioned above, in order to make rail networks interoperable, the European Union has promoted the development of the *European Rail Traffic Management System* (ERTMS) [2]. In particular, *European Train Control Systems* (ETCS), which represent the signalling, control and train protection systems designed to harmonise all European safety systems, can be implemented on four levels: from Level 0 (when an ETCS-compliant rolling stock interacts with a line that is non-ETCS compliant) to Level 3 (when the infrastructure loses any safety and verification function). The higher the implementation level, the higher is the network performance in terms of maximum speed and minimum headway between two successive convoys. In terms of real applications, only Level 2 has been applied in actual railways because on-board train integrity verification is still under research and development (see, for instance, [3]).

In this context, the Italian Ministry of Education, Universities and Research (MIUR) has funded the research project FERSAT whose aim is to develop a rail signalling system based on satellite technologies in order to apply ETCS Level 3. In this regard, we analysed the effects of different rail signalling systems in the case of a regional rail line by performing a cost-benefit analysis. However, since the proposed signalling system is based on the ETCS Level 3 paradigm, the achieved results may be easily exported in the case of conventional rail lines, also in the presence of complex nodes.

A key factor to be taken into account for carrying out such an analysis is estimation of travel demand in terms of potential or expected passengers with related characteristics (i.e. starting and arrival stations, adopted time slot, trip duration, etc.). Indeed, such information is essential for any kind of assessment related to transportation systems. This has generated an extensive literature on the estimation and forecasting methodologies of travel demand, which is summarised below.

In general, estimation of current and future demand can be performed by [4]: direct estimation, disaggregated estimation and aggregated estimation. The first approach, indicated in the literature as direct estimation (see, for instance, [5]–[7]), can be adopted to determine only 'present' travel demand. It is based on the application of sampling theory in the case of mobility choices. The main limits of this methodology consist in the vast amount of information to be collected and the inability to predict future developments due to transportation network or socio-economic variations.

The second approach, known as disaggregated estimation (see, for instance, [8]–[11]), consists in specifying (i.e. providing the functional form and related variables), calibrating (i.e. determining numerical values of model parameters) and validating (i.e. verifying the ability of the model to reproduce original data) a model by means of appropriate data. These data express disaggregate information related to a sample of individuals, where the size and sample characteristics generally differ from those used in the first approach. This methodology allows mobility choices to be simulated in current conditions (based on the ability to reproduce sampling data) and in the case of future conditions (based on the ability to simulate user reactions to transportation network or socio-economic variations). The above disaggregated approach is referred to in the literature as the *Revealed Preference* (RP) approach [4] since it is based on the use of data related to real behaviour of travellers. In the last decades (see, for instance, [12] and [13]), the *Stated Preference* (SP) approach has been developed, based on the statements of travellers about their appropriately described and designed preferences in hypothetical scenarios. With the use of this second approach the prediction abilities of the calibrated demand models can be improved.

Finally, the last approach, known as aggregated estimation (see, for instance, [14]–[16]), is based on modifying demand model results after correcting them by means of traffic counts (i.e. vehicular or passenger flows). The aim of this approach is to identify an Origin-Destination (OD) matrix which is closest to its estimation by model and, once it is assigned to the network, generates flows closest to the counting data.

Therefore we propose a methodology based on the use of different data sources (censuses, historical data, forecasts, counts, etc.) to estimate travel demand in a wide time period (several decades), so as to perform a cost benefit analysis based on a feasibility threshold approach. Specifically, this assessment concerns the economic and environmental effects of implementing an innovative signalling system, even combined with infrastructural measures which, as we will see, in some cases become imperative in order to make any kind of further intervention effective.

The paper is organised as follows: Section 2 describes the main features of the proposed methodology by focusing on travel demand estimation and investigated performance indexes; Section 3 verifies the usefulness of the proposed approach by applying it in the case of a real regional line; finally, conclusions and research prospects are summarised in Section 4.

II. The Proposed Methodology

A cost-benefit analysis to estimate economic and environmental utility in modifying the current signalling system on a regional rail line requires the simulation of effects of interactions between all components of a rail system, namely: infrastructure, signalling system, rolling stock, timetable and travel demand. As shown by ([17]–[18]), it is possible to simulate in detail the main aspects of a rail system by resorting to a combination of three kinds of models: a *service model* for simulating train movements depending on infrastructure, signalling system, rolling stock, planned timetable and travel demand ([19]–[24]); a *supply model* for simulating performance of all transportation systems in the area depending on passenger flows ([4]); a *travel demand model* for simulating user choices in terms of mobility selections (departure time, modal choice, starting and arrival stations) and platform behaviour (choices of runs, coaches and entering doors). Details on demand estimation and related interactions with supply models can be found in [25]–[27].

In particular, the whole simulation of the rail system can be performed by using commercial microsimulation software (OpenTrack® software [21]) appropriately integrated with ad-hoc tools.

As already shown, the main contribution of a new signalling system is reduced passenger waiting times: reduction in headways allows an increase in the number of convoys per hour. Moreover, in certain cases, a different signalling system may also increase travel speeds if they are not limited by infrastructural conditions or close distance between stations.

In light of the above considerations and since our purpose is to implement the methodology by means of a feasibility threshold approach, in the following we do not provide any technological detail concerning the new signalling system, but we characterise it only in terms of maximum achievable performance and maximum level of costs provided.

In particular, in order to evaluate and compare different intervention scenarios within the cost-benefit analysis, it is necessary to simulate effects on travel demand explicitly (by taking into account its variability in a long time horizon) and establish certain evaluation criteria.

The proposed procedure for estimating passenger flows in current and future conditions and the data sources used are set out below, together with the performance indexes adopted.

A. Travel Demand Estimation

Defining travel demand may be considered of primary importance for evaluating effects of any intervention on transportation systems. However, whatever the methodology adopted, the following requirements have to be met:

- accurate reproduction of the current situation;
- prediction of future conditions arising at least from demographic changes and/or different performance of transportation systems;
- travel demand must be considered a random variable and hence not only average values but also their distribution must be analysed.

This implies that the model has to be elastic at least at the level of modal choice (in the case of transportation system variations) and trip generation (in the case of demographic changes).

Hence, in order to meet these conditions, we propose a methodology based on the use of different Italian data sources, even if generalisations to different contexts may easily be obtained. In particular, the suggested procedure can be divided into seven steps.

The first phase consists in using data from the national census ([28]) which provide revealed information (i.e. related to behaviour actually occurring in the days prior to the survey) concerning mobility choices in terms of origin, destination, daily time period and transport mode. It is worth noting that census data concern systematic trips (i.e. for work or school purposes) during the average working day and origins and destinations are expressed in terms of municipalities. Likewise, daily times are indicated as the morning peak hour (7.30-9.29) and the rest of the day. Moreover, although trips are generally bidirectional (i.e. from home to the workplace and return), these data provide only outward trips. In order to satisfy the third requirement (i.e. a wide distribution of considered values) and increase our dataset, we propose to analyse data from at least two decades (i.e. data from the 2001 and 2011 Italian censuses).

The second phase consists in extending information by means of data from mobility observatories (such as [29]). Indeed, information such as total daily trips, rates of trips during morning peak hours, rates of trip chains (i.e. trips with intermediate destinations) and regional modal split needs to be collected. Indeed, by combining such data, we may generate non-systematic trips during the average working day classified by origin and destination municipality, time period and transport mode used.

In the third phase, by using historical data from the resident population ([30]), previous data may be extended from the census period to a successive period by considering the trip generation model as elastic and adopting a variation rate equal to population variation (i.e. a variation in α% of population in municipality A provides a variation in α% of all trips generated in A).

The following phase consists in generating travel demand matrices related to all-day trips where the origin and destination are the stations of the rail line in question. This means that two sub-phases may be identified: the first for obtaining round trips from outward trips in the case of all-day trips; the second for transforming trips expressed in terms of origin and destination municipalities into origin and destination stations. Obviously, the second sub-phase requires the definition of a regional network model in order to implement a minimum path approach for associating each municipality to each station with suitable assumptions if there are two or more stations in a municipality.

The fifth phase consists in correcting origin-destination matrices associated to rail mode (r) by using turnstile counts, as widely shown in the literature by [14]–[16].

The sixth phase consists in the temporal extension to one or more analysis periods of corrected matrices. In particular, the new matrices may be obtained by considering (real or

estimated) demographic variations as in the case of the third phase.

In order to make demand elastic at least at modal choice level, it is possible to specify, calibrate and validate a suitable choice model by adopting traditional methodology proposed in the literature (see, for instance, [4]). In particular, it is necessary to:

- specify a utility formulation and a probability choice model;
- calibrate the values of parameters by solving an optimisation problem;
- validate results by means of suitable statistical tests.

The following phase consists in determining hourly matrices consistent with the corrected matrices and data on daily variation in travel demand.

It is worth noting that the above-mentioned procedure makes use of all methodologies previously described for estimating and forecasting travel demand by properly integrating them with each other in a comprehensive theoretical framework. Indeed, recourse to data from national census represents direct estimation of travel demand. In addition, considering three different levels of demographic variation allows us to meet the requirement of stochasticity.

The fifth phase makes use of data from turnstile counts in order to correct the initial Origin-Destination matrices so as to reproduce surveyed flows. Hence, this step addresses the issue of aggregate estimation of travel demand.

Finally, the sixth phase includes both forecasting techniques of travel demand (by means of the temporal extension to future analysis periods of corrected matrices) and its disaggregated estimation (by means of the specification, calibration and validation of a suitable modal choice model).

B. Performance Indexes

Regarding performance indexes, in order to analyse effects of each intervention scenario, we propose the adoption of an objective function which jointly considers the costs of public administration, passengers and society:

$$OFV = NOC + PGC + EC \tag{1}$$

The first term is represented by the *Net Operational Cost* (*NOC*) which is equal to the part of operational costs not covered by ticket revenues. It can be expressed as follows:

$$NOC = TOC - TR \tag{2}$$

where *TOC* is the total operational cost of the rail system and *TR* is the ticket revenues.

National and regional governments are often inclined to finance public transport in order to improve the mass-transit level-of-service and reduce related fares (i.e. increase user utility). Obviously, there are some regulations for funding public transport. In particular, in Italy, there is a contractual rate (indicated as standard cost) at which the government pays the service company according to transport supply, and a constraint on service effectiveness expressed in terms of the ratio between ticket revenues and operational costs.

Hence, by adopting a standard cost approach, the term *TOC* can be expressed as:

$$TOC = C_{train\text{-}km} \cdot train\text{ - }km \tag{3}$$

with:

$$train\text{ - }km = \sum_i \sum_{\Delta t} L_i \cdot \varphi_{i,\Delta t} \cdot T_{\Delta t} \tag{4}$$

$$\sum_{\Delta t} T_{\Delta t} = 8{,}760 \text{ hours} = 1 \text{ year} \tag{5}$$

where $C_{train\text{-}km}$ is the standard cost (expressed in Euros per *train-km*); *train-km* is the unit of measurement adopted to quantify the supply service; L_i is the length (expressed in kilometres) of line i; $\varphi_{i,\Delta t}$ is the service frequency (expressed in trains per hour) of line i during time interval Δt; $T_{\Delta t}$ is duration (expressed in hours) of time interval Δt.

Ticket Revenues (*TR*), which depend on fare policies and user choices, can be expressed as follows [31]:

$$TR = \sum_j \sum_l \sum_{\Delta t} \left(tc_j / n_{l,j} \right) \cdot f_{l,\Delta t} \tag{6}$$

where tc_j is the revenue associated to ticket type j; $n_{l,j}$ is the number of trips made by user category l by using ticket j; $f_{l,\Delta t}$ is the passenger flow of category l during time interval Δt.

The second term is the *Passenger Generalised Cost* (*PGC*), which can be expressed as follows:

$$PGC = RPG + MTPC + RC \tag{7}$$

where *RPG* is passenger cost on the analysed rail system, *MTPC* is passenger cost on mass-transit systems except the analysed rail system and *RC* is user cost on the road system. In particular:

$$RPG = T_{ae} + T_w + T_{ob} + T_t + C_m \tag{8}$$

$$MTPC = T_{ae} + T_w + T_{ob} + T_t + C_m \tag{9}$$

$$RC = T_{ob} + T_w + C_m \tag{10}$$

where T_{ae} is the access and egress time, T_w is the waiting time, T_{ob} is the on-board time, T_t is the transfer time and C_m is the monetary cost.

In the case of the road system, the on-board and waiting times represent, respectively, times spent travelling along road links and waiting at intersections or searching for parking. However, details on the formulation of the above times can be found in [4] and [32].

Finally, the third term is the *Environmental Cost* (*EC*)

associated to the whole transportation system. It can be formulated as proposed by [32], that is:

$$EC = ec_{km} \cdot \sum_{\Delta t} \sum_{a} fc_{a,\Delta t} \cdot L_a \qquad (11)$$

where ec_{km} is the environmental cost (expressed in Euros per kilometre) associated to each vehicle in the road system (i.e. car or truck), $fc_{a,\Delta t}$ is the traffic flow associated to road link a during time interval Δt, and L_a is the length (expressed in kilometres) of road link a.

In particular, the implementation of different signalling systems allows different headways to be adopted between two successive trains, which results in an increase in service frequencies. Hence, it is possible to have an increase in total operational costs (TOC), a reduction in passenger waiting times (T_w), an increase in passenger flows on the rail system (which allows an increase in ticket revenues TR) and a reduction in traffic flows on the road system (which allows a reduction in environmental costs). Obviously, it is necessary to verify quantitatively any compensation between increases and reductions.

III. Application in the Case of a Regional Rail Line

In order to verify the feasibility and the utility of the proposed approach, we applied it to the Naples–Sorrento regional rail line serving the metropolitan area of Naples in southern Italy (see Fig. 1). The line connects the regional capital (i.e. Naples) with the Sorrento peninsula, where the city of Sorrento represents the line terminus.

The line can be decomposed into a first part, 24.5 km long, between Naples and Moregine, based on a double-track framework and a second part, 17.0 km long, between Moregine and Sorrento, based on a single-track framework.

Moreover, in Barra and Torre Annunziata there are the junctions respectively for Sarno and Poggiomarino. Hence, between Naples and Torre Annunziata there is the overlap among the different lines.

Since the average distance between successive stations is about 1.2 km and the maximum acceleration and deceleration is fixed by comfort conditions (i.e. higher values may cause standing passengers to fall over), increases in the maximum speed of lines do not provide significant reductions in travel times. Hence, improvements due to signalling systems are mainly related to reductions in headways between two successive rail convoys which mean reductions in passenger waiting times.

However, it should be pointed out that in the current framework of the line, the existence of a single-track section represents the real bottleneck of the line operation for any possible improvement. Hence, although in a highly populated area such as the analysed contexts (where the average density is 2,631 inhabitants/km^2) any infrastructural intervention may require considerable funds, doubling the line, which would cost about € 300-800M, represents a major intervention for optimising the benefits of a new signalling system.

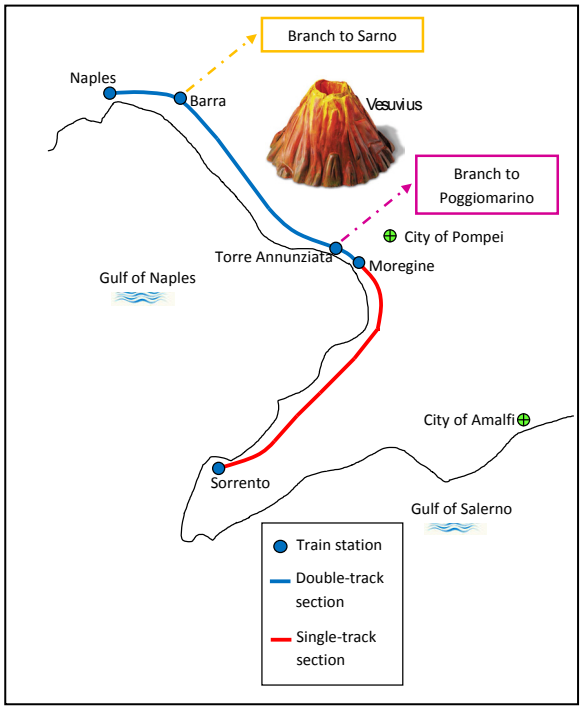

Fig. 1. General framework of the Naples–Sorrento regional rail line.

TABLE I
Scenarios Analysed

Scenario	Description
1	Current infrastructure; current signalling system; current timetable.
2	Current infrastructure; current signalling system; current timetable for overlapping lines; maximising frequency for Naples–Sorrento line.
3	Current infrastructure; current signalling system; maximising frequency for Naples–Sorrento line, considering it a priority over other overlapping lines.
4	Current signalling system; doubling of Moregine–Sorrento section; current timetable for overlapping lines; maximising frequency for Naples–Sorrento line.
5	Current signalling system; doubling of Moregine–Sorrento section; maximising frequency for Naples–Sorrento line, considering it a priority over other overlapping lines.
6	Doubling of Moregine–Sorrento section; innovative signalling system which allows a 4 minute headway to be achieved between two successive rail convoys; maximising frequency for Naples–Sorrento line, considering it a priority over other overlapping lines.
7	Doubling of Moregine–Sorrento section; innovative signalling system which allows a 3 minute headway to be achieved between two successive rail convoys; maximising frequency for Naples–Sorrento line, considering it a priority over other overlapping lines.
8	Doubling of Moregine–Sorrento section; innovative signalling system which allows a 2 minute headway to be achieved between two successive rail convoys; maximising frequency for Naples–Sorrento line, considering it a priority over other overlapping lines.

In the above context, we considered the current situation of the line (Scenario 1) and seven additional scenarios of increasing complexity in terms of technological and monetary

effort. Details of the scenarios analysed are summarised in Table I.

TABLE II
OBJECTIVE FUNCTION VALUES (OFVS) – YEAR 2016

Scenario	Objective Function Value		
	Minimum	Average	Maximum
1	21,612,206	26,001,375	30,390,544
2	21,562,321	25,966,660	30,371,000
3	21,556,056	25,962,951	30,369,845
4	21,350,117	25,822,162	30,294,208
5	21,181,881	25,694,677	30,207,474
6	21,005,063	25,557,593	30,110,123
7	20,363,535	25,030,696	29,697,858
8	18,136,387	22,935,558	27,734,729

TABLE III
OBJECTIVE FUNCTION VALUES (OFVS) – YEAR 2026

Scenario	Objective Function Value		
	Minimum	Average	Maximum
1	20,902,096	25,470,409	30,150,743
2	20,857,177	25,438,469	30,132,151
3	20,851,346	25,434,976	30,131,060
4	20,659,078	25,301,345	30,057,672
5	20,499,187	25,178,209	29,972,295
6	20,330,619	25,045,435	29,876,295
7	19,716,293	24,533,087	29,468,742
8	17,574,679	22,488,373	27,524,045

TABLE IV
OBJECTIVE FUNCTION VALUES (OFVS) – YEAR 2036

Scenario	Objective Function Value		
	Minimum	Average	Maximum
1	19,878,911	24,640,361	29,653,055
2	19,841,150	24,612,758	29,636,438
3	19,835,943	24,609,605	29,635,479
4	19,663,374	24,487,163	29,566,759
5	19,515,507	24,370,825	29,484,199
6	19,358,826	24,244,789	29,391,002
7	18,783,695	23,755,185	28,993,229
8	16,765,324	21,789,297	27,086,785

TABLE V
OBJECTIVE FUNCTION VALUES (OFVS) – YEAR 2046

Scenario	Objective Function Value		
	Minimum	Average	Maximum
1	18,535,015	23,484,308	28,845,225
2	18,506,654	23,462,747	28,831,814
3	18,502,268	23,460,065	28,831,068
4	18,355,572	23,353,207	28,769,925
5	18,223,498	23,246,337	28,691,938
6	18,082,430	23,129,687	28,603,290
7	17,558,779	22,671,758	28,221,393
8	15,702,281	20,815,657	26,377,041

TABLE VI
OBJECTIVE FUNCTION VALUES (OFVS) – YEAR 2056

Scenario	Objective Function Value		
	Minimum	Average	Maximum
1	16,869,305	21,984,231	27,695,675
2	16,852,596	21,970,508	27,686,826
3	16,849,226	21,968,439	27,686,385
4	16,734,599	21,881,802	27,636,024
5	16,622,100	21,787,218	27,564,543
6	16,500,384	21,682,746	27,482,370
7	16,040,541	21,265,919	27,123,063
8	14,384,679	19,552,276	25,367,067

The simulation outcome in terms of objective function values in the analysed time period, detailed for minimum, average and maximum levels of demographic variation, is set out below (Tables II–VI).

TABLE VII
OBJECTIVE FUNCTION VARIATIONS – YEAR 2016

Scenario	Objective Function Variation		
	Minimum	Average	Maximum
1	–	–	–
2	-0.06%	-0.14%	-0.23%
3	-0.07%	-0.16%	-0.26%
4	-0.32%	-0.74%	-1.21%
5	-0.60%	-1.26%	-1.99%
6	-0.92%	-1.81%	-2.81%
7	-2.28%	-3.93%	-5.78%
8	-8.74%	-12.20%	-16.08%

TABLE VIII
OBJECTIVE FUNCTION VARIATIONS – YEAR 2026

Scenario	Objective Function Variation		
	Minimum	Average	Maximum
1	–	–	–
2	-0.06%	-0.13%	-0.21%
3	-0.07%	-0.15%	-0.24%
4	-0.31%	-0.71%	-1.16%
5	-0.59%	-1.22%	-1.93%
6	-0.91%	-1.77%	-2.73%
7	-2.26%	-3.87%	-5.67%
8	-8.71%	-12.11%	-15.92%

TABLE IX
OBJECTIVE FUNCTION VARIATIONS – YEAR 2036

Scenario	Objective Function Variation		
	Minimum	Average	Maximum
1	–	–	–
2	-0.06%	-0.12%	-0.19%
3	-0.06%	-0.13%	-0.22%
4	-0.29%	-0.67%	-1.08%
5	-0.57%	-1.16%	-1.83%
6	-0.88%	-1.70%	-2.62%
7	-2.23%	-3.78%	-5.51%
8	-8.65%	-11.96%	-15.66%

TABLE X
OBJECTIVE FUNCTION VARIATIONS – YEAR 2046

Scenario	Objective Function Variation		
	Minimum	Average	Maximum
1	–	–	–
2	-0.05%	-0.10%	-0.15%
3	-0.05%	-0.11%	-0.18%
4	-0.26%	-0.60%	-0.97%
5	-0.53%	-1.08%	-1.68%
6	-0.84%	-1.60%	-2.44%
7	-2.16%	-3.63%	-5.27%
8	-8.56%	-11.73%	-15.28%

TABLE XI
OBJECTIVE FUNCTION VARIATIONS – YEAR 2056

Scenario	Objective Function Variation		
	Minimum	Average	Maximum
1	–	–	–
2	-0.03%	-0.06%	-0.10%
3	-0.03%	-0.07%	-0.12%
4	-0.22%	-0.49%	-0.80%
5	-0.47%	-0.95%	-1.47%
6	-0.77%	-1.44%	-2.19%
7	-2.07%	-3.42%	-4.91%
8	-8.41%	-11.40%	-14.73%

Furthermore, variations in the objective function value with

respect to the non-intervention scenario (i.e. Scenario 1) are reported in Tables VII–XI.

Our numerical results point to a common conclusion: it is indispensable to double the line in order to fully exploit the advantages provided by the innovative signalling system. Indeed, as can be seen, in the current infrastructural configuration of the line (i.e. with a section with a single-track framework) timetable optimisation (i.e. Scenarios 2 and 3) provides improvements which are at most equal to 0.26% in 2016. Then they drop to 0.12% in 2056. Moreover, also complete replacement of the signalling system provides results similar to those of Scenario 3, since the major limitation is related to the single-track section. Hence, although doubling the line (Scenarios 4 and 5) provides maximum improvements lower than 2.0% over the whole examined period, it represents an intervention required to reduce the current minimum headway between two successive rail convoys. Indeed, a new configuration of the line, based on a fully double-track framework, confers benefits from an innovative signalling system (Scenarios 6, 7 and 8) in terms of a reduction in minimum headways, providing maximum improvements between 16.08% and 14.73%.

The trend of objective function value variations, during the tested period, in the case of an average rate of demographic change, is shown in Fig. 2.

Leaving aside the slightly decreasing pattern, simply due to a reduction in demographic terms, the graph shows, once again, the importance of the doubling intervention in order to take full advantage of implementing the innovative signalling system. Indeed, although the gap between scenarios 2 and 3 (represented respectively by the black and green line) and scenarios 4 and 5 (represented respectively by the red and blue line) appears limited, without the infrastructural intervention of the doubling of the line it would be impracticable to obtain the benefits provided by scenarios 6, 7 and 8 (represented respectively by the orange, brown and dark green line) which show a far higher gap with respect to the other scenarios.

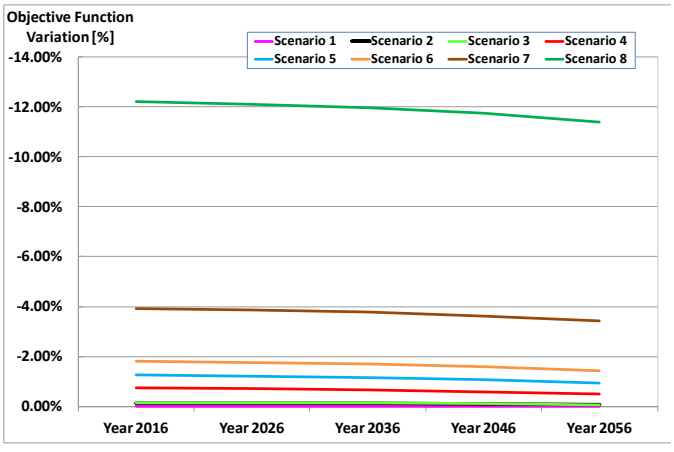

Fig. 2. Variation of objective function value in average conditions during the analysed time period (2016-2056).

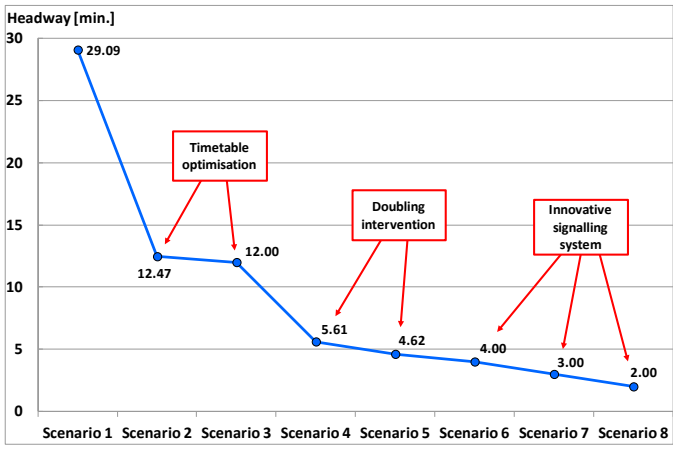

Fig. 3. Simulation results in terms of headway for each scenario analysed.

TABLE XII
NUMBER OF CONVOYS REQUIRED

Scenario	Convoys required	Additional convoys
1	10	0
2	19	9
3	20	10
4	40	30
5	49	39
6	56	46
7	74	64
8	110	100

Fig. 3 shows the effects of each intervention scenario in terms of the headway between two successive convoys. As can be seen, thanks to timetable optimisation, the headway can be reduced from 29 to 12 minutes, with a reduction of more than 50%; whereas by doubling the line, we can regain only around 7 minutes. However, this infrastructural intervention is essential in order to reduce headways between two successive convoys to as low as 2 minutes.

Obviously, in order to ensure such low headways, it is necessary to put in place an appropriate fleet in terms of number of available convoys per rail service: the lower the headway, the higher the number of trains needed (Table XII).

Hence, besides the above-mentioned costs, additional resources are required to acquire a suitable number of vehicles.

IV. CONCLUSIONS AND RESEARCH PROSPECTS

The paper proposed a methodology for evaluating economic and environmental effects related to implementing an innovative signalling system by performing a cost-benefit analysis based on a feasibility threshold approach. The application in the case of a real regional rail line shows the usefulness of the proposed procedure and points out that, in the considered context, the main limitation to network improvements is represented by the single-track section. Hence, the replacement of the existing signalling system may be successfully implemented only if combined with doubling of the line.

The costs of infrastructure improvements are clearly high (€ 300-800M). Yet it is worth noting that they have the same order of magnitude as benefits achievable after just one year.

A key role in the proposed procedure is represented by the estimation and forecasting techniques for travel demand which is a fundamental factor to consider for evaluating the effects of any intervention in the case of transportation systems. In particular, the suggested methodology makes use of data from Italian sources.

Hence, in terms of future research, we propose to apply the described approach in other contexts both on other Italian railways (in order to verify the correctness of the procedure and, in particular, the reliability of the adopted data sets in different network configurations) and other non-Italian railways (in order to test the methodology in the case of different data sources).

Finally, the main limitation of the proposed approach in the case of more complex rail networks is related to the excessively high number of solutions to be analysed and related computation times. However, recently [33] and [34] have proposed some methodologies based on the use of heuristic and/or meta-heuristic algorithms in order to solve these kinds of problems by reducing computational efforts.

REFERENCES

[1] European Commission, *Climate Action: Reducing emissions from transport*. Available: http://ec.europa.eu/clima/policies/transport/index_en.htm (last access: September 2016).

[2] J. Pachl, *Railway operation and control*. VTD Rail Publishing, Mountlake Terrace (WA), USA, 2009.

[3] Shift2Rail Joint Undertaking, *Multi-Annual Action Plan*. European Union: Brussels, Belgium, 2015.

[4] E. Cascetta, *Transportation systems analysis: models and applications*. Springer, New York (NY), USA, 2009.

[5] M. J. Smith, "The existence, uniqueness and stability of traffic equilibria," *Transportation Research Part B*, vol. 13, no. 4, pp. 295–304, 1979.

[6] W. Brog and E. Ampt, "State of the art in the collection of travel behaviour data," in *Travel Behaviour for the 1980's*, Special Report 201, National Research Council, Washington (DC), USA, 1982.

[7] J. de D. Ortuzar and L. G. Willumsen, *Modelling Transport*, 4th ed., John Wiley and Sons Ltd., Chichester, United Kingdom, 2011.

[8] T. A. Domencich and D. McFadden, *Urban travel demand: a behavioural analysis*. American Elsevier, New York (NY), USA, 1975.

[9] J. Horowitz, "Identification and diagnosis of specification errors in the Multinominal Logit Model," *Transportation Research Part B*, vol. 15, no. 5, pp. 345–360, 1981.

[10] C. F. Manski and D. McFadden, *Structural Analysis of discrete data with econometric applications*. The MIT Press, Cambridge (MA), USA, 1981.

[11] M. Ben-Akiva and S. R. Lerman, *Discrete choice analysis: Theory and application to travel demand*. The MIT Press, Cambridge (MA), USA, 1985.

[12] M. Ben-Akiva and T. Morikawa, "Estimation of switching models from revealed preference and stated intention," *Transportation Research Part A*, vol. 24, no. 6, pp. 485–495, 1990.

[13] J. de D. Ortuzar, "Stated Preference in travel demand modelling," in *Proc. WCTR 1992*, Lyon, France, 1992.

[14] H. -P. Lo and C. -P. Chan, "Simultaneous estimation of an origin-destination matrix and link choice proportions using traffic counts," *Transportation Research Part A*, vol. 37, no. 9, pp. 771–788, 2003.

[15] E. Cascetta, A. Papola, V. Marzano, F. Simonelli and I. Vitiello, "Quasi-dynamic estimation of o-d flows from traffic counts: Formulation, statistical validation and performance analysis on real data," *Transportation Research Part B*, vol. 55, pp. 171–187, 2013.

[16] C. -C. Lu, X. Zhou and K. Zhang, "Dynamic origin-destination demand flow estimation under congested traffic conditions," *Transportation Research Part C*, vol. 34, pp. 16–37, 2013.

[17] L. D'Acierno, M. Gallo, B. Montella and A. Placido, "The definition of a model framework for managing rail systems in the case of breakdowns," in *Proc. IEEE ITSC 2013*, The Hague, The Netherlands, pp. 1059-1064, 2013.

[18] L. D'Acierno, A. Placido, M. Botte and B. Montella, "A methodological approach for managing rail disruptions with different perspectives," *International Journal of Mathematical Models and Methods in Applied Sciences*, vol. 10, pp. 80–86, 2016.

[19] R. Prinz, B. Sewcyk and M. Kettner, "NEMO: Network Evaluation Model for the Austrian railroad (ÖBB)," *Eisenbahntechnische Rundschau*, vol. 50, no. 3, pp. 117–121, 2001.

[20] M. Kettner and B. Sewcyk, "A model for transportation planning and railway network evaluation," in *Proc. WCITS 2002*, Chicago (IL), USA, 2002.

[21] A. Nash and D. Huerlimann, "Railroad simulation using OpenTrack," *Computers in Railways*, vol. 9, pp. 45–54, 2004.

[22] T. Siefer and A. Radtke, "Railway simulation: key for better operation and optimal use of infrastructure," in *Proc. 1st International Seminar on Railway Operations Modelling and Analysis*, Delft, The Netherlands, 2005.

[23] M. Marinov and J. Viegas, "A mesoscopic simulation modelling methodology for analyzing and evaluating freight train operations in a rail network," *Simulation Modelling Practice and Theory*, vol. 19, no. 1, pp. 516–539, 2011.

[24] E. Quaglietta, "A microscopic simulation model for supporting the design of railway systems: Development and applications," Ph.D. dissertation, Federico II University of Naples, Naples, Italy, 2011.

[25] G.E. Cantarella, "A general fixed-point approach to multimodal multi-user equilibrium assignment with elastic demand," *Transportation Science*, vol. 31, no. 2, pp. 107–128, 1997.

[26] S. Nguyen, S. Pallottino and M. Gendreau, "Implicit enumeration of hyperpaths in a logit model for transit networks," *Transportation Science*, vol. 32, no. 1, pp. 54–64, 1998.

[27] M. Ercolani, A. Placido, L. D'Acierno and B. Montella, "The use of microsimulation models for the planning and management of metro systems," *WIT Transactions on the Built Environment*, vol. 135, pp. 509–521, 2014.

[28] Istituto Nazionale di Statistica – ISTAT (Italian National Institute of Statistics). Population and housing census. Available: http://www.istat.it/it/censimento-popolazione (last access: September 2016).

[29] Osservatorio sui comportamenti di mobilità degli italiani – AudiMob (Observatory on the Italian mobility behaviour). Regional mobility statistics. Available: http://www.isfort.it/sito/statistiche/Audimob.htm (last access: September 2016).

[30] Istituto Nazionale di Statistica – ISTAT (Italian National Institute of Statistics). Resident population. Available: http://www.istat.it/it/popolazione (last access: September 2016).

[31] B. Montella, L. D'Acierno and M. Gallo, "A multimodal approach for determining optimal public transport fares," *Journal of Applied Sciences*, vol. 14, no. 21, pp. 2767–2781, 2014.

[32] M. Gallo, B. Montella and L. D'Acierno, "The transit network design problem with elastic demand and internalisation of external costs: An application to rail frequency optimisation," *Transportation Research Part C*, vol. 19, no. 6, pp. 1276–1305, 2011.

[33] L. D'Acierno, M. Gallo and B. Montella, "Application of metaheuristics to large-scale transportation problems," *Lecture Notes in Computer Science*, vol. 8353, pp. 215–222, 2014.

[34] M. Botte, C. Di Salvo, A. Placido, B. Montella and L. D'Acierno, "A Neighbourhood Search Algorithm for determining optimal intervention strategies in the case of metro system failures," *International Journal of Transport Development and Integration*, vol. 1, no. 1, pp. 63–73, 2017.

Luca D'Acierno is Associate Professor at Federico II University of Naples, Italy. He holds an MSc degree in Civil Engineering (2000) and a PhD in Road Infrastructures and Transportation Systems (2003), both from Federico II University of Naples, Italy. His research interests include public transport planning and design, rail system analysis and management, multimodal transportation network design, transportation network assignment, pricing policy analysis, and probe vehicle use. He has authored more than 130 papers in peer-reviewed journals and conference proceedings.

Marilisa Botte is a PhD student in Civil System Engineering at Federico II University of Naples, Italy, having completed her MSc in Hydraulics and Transportation Systems Engineering (2014) at the same university. Her research interests include rail system analysis and management, and travel demand estimation. She has authored 15 papers in peer-reviewed journals and conference proceedings.

Claudia Di Salvo is Materials Planner at GE Oil&Gas (Italy) and research collaborator at Federico II University of Naples. She holds an MSc degree in Civil and Environmental Engineering (2012), and has completed postgraduate training for experts in Digital Pattern techniques (2014), both at Federico II University of Naples, Italy. Her research interests include signalling system analysis, long-term travel demand estimation and rail system simulation. Moreover, she has authored five papers in peer-reviewed journals and conference proceedings.

Chiara Caropreso is a scholarship holder at the Department of Civil, Architectural and Environmental Engineering, Federico II University of Naples where she was awarded an MSc degree in Hydraulics and Transportation Systems Engineering in 2016. Her research interests include rail system simulation and long-term travel demand estimation. Moreover, she has authored two papers in conference proceedings.

Bruno Montella is Full Professor at Federico II University of Naples, Italy. He holds an MSc degree in Transportation Engineering (1973) from the same university. His research interests include transit system analysis and management, multimodal transportation network design and optimisation, and public transport quality. He has authored more than 170 papers in peer-reviewed journals and conference proceedings.